UNIVERSITÀ DEGLI STUDI DI ROMA "TOR VERGATA"

FACOLTA' DI INGEGNERIA

DOTTORATO DI RICERCA IN

Ingegneria delle Telecomunicazioni e Microelettronica

XXII CICLO DEL CORSO DI DOTTORATO

Stability investigation for high power amplifier stages at microwave and millimeter-wave frequencies

Maciej Jankowski

A.A. 2009/2010

Tutor: Prof. Ernesto Limiti

Coordinatore: Prof. Giuseppe Bianchi

INDEX

ACKNOWLEDGEMENTS

The work detailed in this thesis would not have been possible without the generous contributions of a few individuals. Therefore, I would like to express my appreciation for their support and voluntary help.

For the invaluable advice, discussion and essential criticism, as well as support beyond scientific relation I would like to express my gratitude for Professor Ernesto Limiti.

Also, I am deeply grateful to Krzysztof Madziar for planting the idea of the PhD in Rome in my head and helping me to put my first steps myself on the Italian soil. Moreover, a big "Thank You" to Professor Bogdan Galwas and Krzysztof Nyka for their valuable support.

Further, to Luca for a helping hand while dealing with Italian speaking reality, hectoliters of "real coffee" and patience to my daring experiments with the language. Rocco, Elisa, Marco, Flavio, Fabrizio, Francesco for showing Italian hospitability.

In addition, I offer my sincere thanks to Professor Franco Gianini, Professor Paolo Colantonio, Nathalie Nostro, Lucio Scucchia, Antonio Nanni, Mauro Ferrari, Sergio Arena, Tommaso Cavanna, Walter Ciccognani and all the people involved in the creation of a friendly atmosphere of MiMEG.

Also, I am deeply grateful to Valerio and Santina for their friendship, support and all the help.

I offer my sincerest thanks to my parents and in-laws for their support.

Last but not least; Thank You Anna for ingraining in me the importance to pursuit one's dreams.

ABSTRACT

Constant development of the telecommunication systems led to a situation, when more and more advanced technologies, standards and higher frequency bands are adopted each year to satisfy the consumers' needs. At the same time, the economic part of any new solution requires to be cost effective. These two different points of reference result in the contradictory requirements for the systems and their elements. Therefore, the balance between the performances and technology advancements needs to be accompanied by reasonable cost. The integrated circuit approach adopted to many electronic circuits seems to follow the balance path while that allows to obtain very good results introducing many advantages on both, economic and technology sides. However, the designer's situation is far more complex than a pursuit to reach the performance goals with the simultaneous cost effective solution. Among the existing inevitable rules and requirements to any project, the stability pays extremely important role. Therefore, in order to succeed in any amplifier design it is vital to understand the importance of the stability matter. Consequently, in the 1st chapter of my thesis I described the basic stability concept together with the time and frequency domain based stability tests. In that very part of the research, for the sake of introducing the stability issue in a more familiar field of the microwave engineering, the commonly used circuit descriptions along with the frequency domain stability test methods applicable to them are demonstrated. Afterward, the particular problem of the odd mode instability is displayed, revealing the shortcomings of the classic and over trusted tests. The critical situation of not detected instability affects particular group of PA, making the designers' actions a gamble.

Then, various approaches to the problem of the contradictory requirements imposed at the power amplifiers designs allow to find different compromises. Among them a power combining approach serves a crucial role. Consequently, in the 2nd chapter I emphasized the power combining's importance, along with a specificity of the Integrated Circuit approach to it. The presented result is especially prone to the previously mentioned Odd mode instabilities so that assistance and guidance in solving this particular stability problem have become the goal of this work.

Thus, two potentially useful methods that detect odd mode instabilities have been chosen and investigated in the chapter 3. Ideas of the tests along with possible CAD implementations were drafted with the outcome of the analysis of the simple odd mode unstable amplifier.

In the chapter 4 we focus on the CAD implementation of the Freitag method in case of the ideal corporate amplifier. Symmetry of such a structure permits great simplification when implementing the test. The example PA structures are stabilized by the means of the Freitag method. Later, they are compared with the Ohtomo test results. Inconsistency is noticed and the dedicated PA examples are applied to study its origin through the Time Domain simulation results. The end result lets to comprehend the limitations of the original method thus, the method gets improved and positively verified. Moreover, the automation of the procedure is defined.

Furthermore, due to the contradictions of the Power Amplifier's nature, as well as the condition of its small signal test, the Freitag method is extended to the Large-Signal/Small-Signal operation in the chapter 5. More, the example circuit has been tested with the extended method, then the parametric odd mode instability has been detected. Eventually, the results are successfully verified by the means of the Time domain simulation.

Ultimately, in the chapter 6, the dilemma of non ideal symmetry of the amplifier bisections is discussed. As a consequence, modification of the method was proposed and the generalized method was tested. In the end, the results were confronted with the Ohtomo tests, revealing full agreement between methods.

1 STABILITY PROBLEM IN ELECTRONIC CIRCUITS

1.1 Introduction to stability

It is perfectly understandable why designers pay special attention to the stability of designed circuits. Any unwanted oscillations occurring in circuit can be responsible for harmful behaviours like generation of spurs signals, pushing active devices into large-signal modes and deterioration of performances. Finally, oscillations may even damage active devices. Unwanted behaviour of the circuit in the design and laboratory testing phase is as frequent as arduous case. Nevertheless, in that stage it is yet a simple task to remove the oscillations if their source is found. On the other hand, if the oscillations occur at a production phase it will increase time and cost of a manufacturing product. But if they occur while the product is already on the market that makes it the worst case scenario. From this point of view, it is essential in the design process to be able to determine if the circuit is or is not stable. Stability in this case is understood as circuit immunity for causing spurious oscillations. If the circuit is unstable, the signal at any point of circuit can increase without any limits. This is possible only in case of ideal linear circuits. In real life, circuits nonlinearities limit the maximum signal level and either set it into a steady state oscillation or stop it completely. But in most cases, the oscillation starts with a small signal, therefore linear conditions and in the end it leads to nonlinear work of system.

This situation gives an opportunity to eliminate several problems, even with the simplifying assumption of the linear and small signal regime. To achieve this, a robust design tool is needed. Such a tool will provide knowledge about ability of circuit as to oscillate in wide frequency range and different terminations. Possession of such a tool became more and more important for saving time and money in the design flow. Therefore, a short introduction to stability problems is given in a form of a review through basic stability concepts, definitions and finally through approaches of the stability test in general, and in the particular case of the microwave circuits. Stability tests will be considered with attention to their shortcomings and major idea of usefulness in CAD design reality.

1.1.1 Stability concept

While considering the stability concept, an intuitive example of a ball on the surface is often applied [1]. The ball which is free to roll on the surface could be placed in different points. For the presented fragment of the surface a particular set of points was chosen and marked on the figure with letters: A, E, F, G. Also ,there was marked the set of points between B and D, and an example point C. Each of those points is so called “equilibrium point” of the presented system.

In the space within which the possible instantaneous states of the system may be described- so called “state space”, the equilibrium point is a point where the state of the system is not changing through time in the absence of inputs and disturbances. If the system is in the equilibrium point – and if there is no input or disturbance, it will remain there. While observing Figure 1 it is possible to ascribe intuitively stability properties to each mentioned equilibrium point. Infinitesimally disturbance which is to move the ball from its original position in case of points A and F will cause it to diverge from these points. In case of points E and G it could be expected that the ball will

eventually return to its original position after the disturbing action. If only a displacement action will be held in point C, the ball will remain in new position.

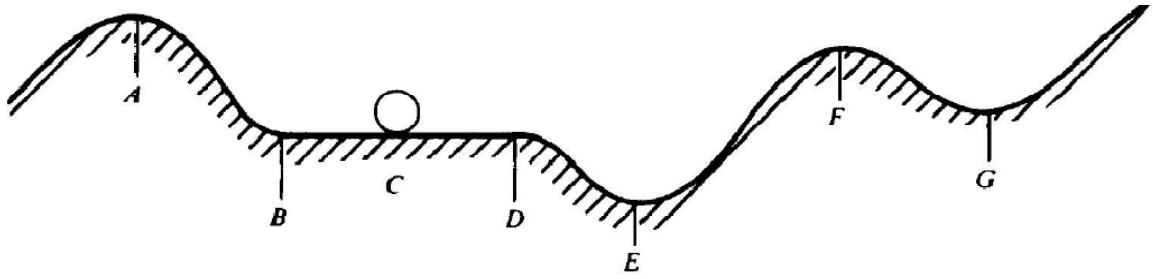

Figure 1 The example of the ball and surface system.

These naturally distinguished three different behaviours due to the presence of infinitively small disturbance will classify equilibrium points as: not stable, stable and neutrally stable. Moreover, it is intuitively justified to ascribe another property to the stability considered in the following way: its locality. It happens due to infinitively small value of disturbance used in the considerations. If ball will be displaced from the point G to the left, behind the point F, it will never return to its original position. Thus, depending on the value of the displacement different conclusions may be made. Such a matter should rise awareness before one labels system as a stable or not. As we observe in this simple example, the stability of the system is not a general feature of the system itself. It is rather the property related to different equilibrium points or to the steady state solutions, related to the value and character of disturbance. Then, it could be made a conclusion, that stability problem deals with questions of system state in the presence of perturbation. What will be the response of the system after the perturbation was applied in the case of the equilibrium point? Will the system return to its original equilibrium? Or will it never return to its original equilibrium, will it remain close to it? Or maybe it will diverge from the equilibrium state with time? Same type of questions can be asked regarding the steady state solution. Fortunately, previously introduced linear assumptions of the initial phase of the design may be applied here. While the system under consideration is linear, the origin of the state space is the equilibrium point. In case any of the eigenvalues of the system matrix is equal to zero, an infinitive amount of equilibrium points exist, which corresponds to the example equilibrium points between B and D on the Figure 1. But if otherwise, the equilibrium point is an isolated one and at the same time this is the only equilibrium point of the system, what greatly simplifies the stability problem.

1.1.2 Stability definitions

Taking into consideration drafted ideas based on the system of the ball and the surface it is possible to present few definition of the stability. In literature exists a variety of different definitions but in this consideration two of them are of greatest importance.

$$\frac{dx(t)}{dt} = f(x,0,t), \quad x(t_0) = x_0 \tag{1.}$$

For the linear system without input signals (1.), it is assumed that there exists a unique solution as follows:

$$x(t, x_0, t_0) = \Phi(t, t_0) \cdot x_0$$

(2.)

While the origin is an equilibrium point it is stable: if for every $\varepsilon > 0$, there exist a $\delta(\varepsilon) > 0$ such that, if $\|x_0\| < \delta$ then $\|\Phi(t,t_0) \cdot x_0\| < \varepsilon$ for every $t \geq t_0$. Stability defined in this way is so called stability in sense of Lyapunow (abbreviation - i.s.L.). This kind of stability ensures that system state will be kept with a ε in norm, while perturbation will be less than δ in norm.

$$\forall t \geq t_0, \forall \varepsilon > 0, \exists \delta(\varepsilon) > 0, \|x_0\| < \delta \Rightarrow \|\Phi(t,t_0) \cdot x_0\| < \varepsilon$$

(3.)

Taking into consideration that:

$$\|\Phi(t,t_0) \cdot x_0\| \leq \|\Phi(t,t_0)\| \cdot \|x_0\|$$

Definition can be rephrased to:

$$\forall t \geq t_0, \forall \varepsilon > 0, \exists N(t_0) > 0, \|x_0\| < \frac{\varepsilon}{N(t_0)} \Rightarrow \|\Phi(t,t_0)\| \leq N(t_0)$$

Equilibrium is asymptotically stable if it is stable in the sense of the Lyapunow (i.s.L.) and there exists number $\delta'(t_0) > 0$ such that whenever $\|x_0\| < \delta'$ solution in time satisfies $\lim_{t\to\infty} \|\Phi(t,t_0) \cdot x_0\| = 0$. Which means that the solution will return to the equilibrium point after the infinitive time.

$$\forall t \geq t_0, \exists \delta'(t_0) > 0, \|x_0\| < \delta' \Rightarrow \lim_{t\to\infty} \|\Phi(t,t_0) \cdot x_0\| = 0$$

(4.)

Important observation can be made that the asymptotic stability of the linear system does not depend on the x_0. Thus, if linear system is asymptotically stable it is globally asymptotical stable. Therefore the definition can be rephrased again to:

$$\lim_{t\to\infty} \|\Phi(t,t_0)\| = 0$$

1.1.3 State space representation

Lets apply this definition of stability to the formalized description of the system called the “state space representation”.

$$\frac{dx(t)}{dt} = A \cdot x(t) + B \cdot u(t)$$
$$y(t) = C \cdot x(t) + D \cdot u(t)$$

(5.)

It is often used general mathematical model of physical system where input signals u(t), output signals y(t) and state variables are related by first order differential equations. These variables are expressed as vectors and equations are written in the matrix form, therefore A, B, C, D are matrixes. State variable vector is defined as the smallest set of variables which describes the state of the system at any given time. It is assumed that the considered system is linear time invariant.

The time invariance manifests itself in the system description with matrixes A, B, C, D being constant in respect of the time. A general solution of such a system to any particular steady excitation is composed of a linear superposition of transient and steady state responses (6.).
The transient response depends on the initial state of the system, while the steady state response involves the input signals but not the initial state.

$$\begin{aligned} x(t) &= e^{At} \cdot x_0 + \int_0^t e^{A(t-\tau)} \cdot B \cdot u(\tau) \cdot d\tau \qquad x_0 = x(t=0) \\ y(t) &= C \cdot x(t) + D \cdot u(t) \end{aligned} \tag{6.}$$

Response of the system for zero input condition called “free” or “natural response” is investigated with previously described stability definitions.

$$\begin{aligned} x(t) &= e^{At} \cdot x_0 \\ y(t) &= C \cdot e^{At} \cdot x_0 \end{aligned} \qquad x_0 = x(t=0) \quad and \quad u(t) = 0 \tag{7.}$$

System will be stable if:

$$\forall t \geq t_0, \forall \varepsilon > 0, \exists \delta(\varepsilon) > 0, \|x_0\| < \delta \Rightarrow \left\| e^{At} \cdot x_0 \right\| < \varepsilon \tag{8.}$$

System will be asymptotical stable if additionally:

$$\lim_{t \to \infty} \left\| e^{At} \right\| = 0 \tag{9.}$$

Norm of the solution is rather cumbersome therefore the properties of the A matrix are investigated. It will be assumed that n independent eigenvectors ξ_i and eigenvalues λ_i were founded for matrix A. Since this set of eigenvectors is linearly independent it can determine the basis for the new state space Σ, and at any given time t, state x(t) can be expressed as:

$$x(t) = q_1(t) \cdot \xi_1 + q_2(t) \cdot \xi_2 + \dots q_n(t) \cdot \xi_n \tag{10.}$$

Same time product of matrix B and input signal vector can be expressed as:

$$B \cdot u(t) \in \Sigma \quad \rightarrow \quad B \cdot u(t) = \beta_1 \cdot \xi_1 + \beta_2 \cdot \xi_2 + \dots + \beta_n \cdot \xi_n \tag{11.}$$

Applying (10.)and (11.) to the system description (5.):

$$\frac{dx(t)}{dt} = A \cdot x(t) + B \cdot u(t)$$
$$\frac{dq_1(t)}{dt} \cdot \xi_1 + \frac{dq_2(t)}{dt} \cdot \xi_2 + \cdots + \frac{dq_n(t)}{dt} \cdot \xi_n =$$
$$= q_1 \cdot A \cdot \xi_1 + q_2 \cdot A \cdot \xi_2 + \cdots + q_n \cdot A \cdot \xi + \beta_1 \cdot \xi_1 + \beta_2 \cdot \xi_2 + \cdots + \beta_n \cdot \xi$$

(12.)

And recalling the relationship:

$$A \cdot \xi_i = \lambda_i \cdot \xi_i$$

(13.)

After reorganization system can be described as:

$$\left(\frac{dq_1(t)}{dt} - \lambda_1 \cdot q_1 - \beta_1\right) \cdot \xi_1 + \left(\frac{dq_2(t)}{dt} - \lambda_2 \cdot q_2 - \beta_2\right) \cdot \xi_2 + \cdots + \left(\frac{dq_n(t)}{dt} - \lambda_n \cdot q_n - \beta_n\right) \cdot \xi_n = 0$$

(14.)

While set of eigenvectors ξ_i is linearly independent this leads to n independent equations:

$$\frac{dq_1(t)}{dt} = \lambda_1 \cdot q_1 + \beta_1 \quad for \quad i = 1,2,\cdots,n$$

(15.)

Which demonstrates that while A possesses the full set of eigenvectors, the system is completely described by a set of n uncoupled equations to which solutions are as follows:

$$q_i(t) = e^{\lambda_i t} \cdot q_{i,0} + \int_0^t e^{\lambda_i (t-\tau)} \cdot \beta_i \cdot u(\tau) \cdot d\tau$$

(16.)

By recalling the definition of the state vector (10.) it is possible to notice that the solution is a sum of so called n system modes. With this interpretation it is easy to obtain a more convenient form of the previous equation with the use of so called modal matrix (17.). This matrix is created as a row matrix with each element corresponding to one of eigenvectors.

$$M = [\xi_1, \xi_2 \ldots \xi_n]$$

(17.)

$$x(t) = M \cdot q(t)$$

(18.)

While M is constant due to the time invariance of the system:

$$\frac{dx(t)}{dt} = M \cdot \frac{dq(t)}{dt}$$

(19.)

Therefore, :

$$M \cdot \frac{dq(t)}{dt} = A \cdot M \cdot q(t) + B \cdot u(t)$$

(20.)

With simplifying notation for the elements of the final equation:

$$J = M^{-1} \cdot A \cdot M$$
$$B_n = M^{-1} \cdot B$$
$$C_n = C \cdot M$$

(21.)

It can be rephrased as:

$$\frac{dq(t)}{dt} = M^{-1} \cdot A \cdot M \cdot q(t) + M^{-1} \cdot B \cdot u(t) \quad \rightarrow \quad \frac{dq(t)}{dt} = J \cdot q(t) + B_n \cdot u(t)$$
$$y = C \cdot M \cdot q(t) + D \cdot u(t) \qquad\qquad y = C_n \cdot q(t) + D \cdot u(t)$$

(22.)

Finally, if the exponent function will be represented as infinitive series:

$$e^{At} = \mathrm{I} + A \cdot t + A^2 \cdot \frac{t^2}{2!} + A^3 \cdot \frac{t^3}{3!} + \cdots$$

(23.)

Joining (21.) and (23.) it is possible to see that:

$$M^{-1} \cdot e^{At} \cdot M = M^{-1} \cdot \mathrm{I} \cdot M + M^{-1} \cdot A \cdot M \cdot t + M^{-1} \cdot A \cdot M \cdot M^{-1} \cdot A \cdot M \cdot \frac{t^2}{2!} + \cdots =$$
$$= \mathrm{I} + J \cdot t + J^2 \cdot \frac{t^2}{2!} + \cdots = e^{Jt}$$

(24.)

This leads to a final conclusion that previously obtained zero input response can be presented in a new form:

$$x(t) = e^{At} \cdot x_0 = M \cdot e^{Jt} \cdot M^{-1} \cdot x_0 = M \cdot \begin{bmatrix} e^{\lambda_1 t} & 0 & \cdots & 0 \\ 0 & e^{\lambda_2 t} & \cdots & 0 \\ \vdots & \vdots & \ddots & \vdots \\ 0 & 0 & \cdots & e^{\lambda_n t} \end{bmatrix} \cdot M^{-1} \cdot x_0$$

(25.)

Therefore it is possible to present the system state using the system modes:

$$x(t) = e^{At} \cdot x_0 = M \cdot e^{Jt} \cdot M^{-1} \cdot x_0$$
$$q(t) = e^{Jt} \cdot q_0 = \begin{bmatrix} e^{\lambda_1 t} \cdot q_{0,1} \\ e^{\lambda_2 t} \cdot q_{0,2} \\ \vdots \\ e^{\lambda_n t} \cdot q_{0,n} \end{bmatrix}$$

(26.)

While eigenvalues are in general complex numbers $\lambda_i=\sigma_i+j\omega_i$ it is possible to describe the state of any of n system mode as:

$$q_i(t) = e^{\lambda_i t} \cdot q_{0,i} = e^{(\sigma_i + j\omega_i)t} \cdot q_{0,i} = e^{\sigma_i t} \cdot e^{j\omega_i t} \cdot q_{0,i}$$

(27.)

Clearly, the first exponential element of the final product will be responsible of the amplitude evolution of the mode in time. Therefore, the real parts of the eigenvalues are indicative of the stability properties of the system. The results of this analysis allow the interpretation of the previous stability definitions with use of the matrix A eigenvectors. Three different possibilities emerge than as follows:

- Asymptotical stable system if all eigenvalues λ_i of the A matrix have a negative real part $\mathrm{Re}(\lambda_i) < 0 \quad i = 1,2,\cdots,n$
- Stable i.s.L. system if no one of λ_i eigenvalues of the A matrix have a positive real part $\mathrm{Re}(\lambda_i) \le 0 \quad i = 1,2,\cdots,n$
- Strongly unstable system if any of λ_i eigenvalues of the A matrix have a positive real part $\mathrm{Re}(\lambda_i) > 0 \quad i = 1,2,\cdots,n$

A practical example of analysis will be presented with a very simple example: RC circuit – Figure 2.

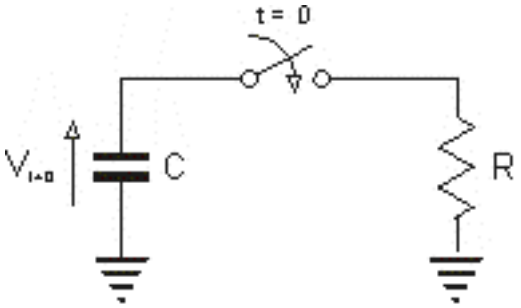

Figure 2 Example of the simple RC circuit.

The circuit state is represented with the voltage V(t) and described with the following equations:

$$-C\frac{dV(t)}{dt} = \frac{V(t)}{R}$$
$$V(t=0) = V_0$$

(28.)

When the system state description is used:

$$\begin{array}{l|l} \dfrac{dV(t)}{dt} = \dfrac{1}{-RC}V(t) & \dfrac{dx(t)}{dt} = A \cdot x(t) \\ V_0 = V(t=0) & x_0 = x(t=0) \\ V(t) = V_0 e^{-\left(\frac{1}{RC}\right)t} & x(t) = e^{At} \cdot x_0 \end{array}$$

(29.)

While this equation is scalar, its stability analysis simplifies. For scalar value of the A, eigenvalue is just a value of the scalar element. Moreover, the norm of solution will be just absolute value of the solution. Therefore, it is easy to observe that the circuit stability depends on the product of the R and C circuit elements' values. Assuming C as a real and positive we can differentiate three different possibilities.

Positive resistance, R >0 therefore:

$$\lim_{t \to \infty} e^{-\left(\frac{1}{RC}\right)t} = 0$$

(30.)

Circuit is asymptotically stable when it is returning to its equilibrium with time – Figure 3.

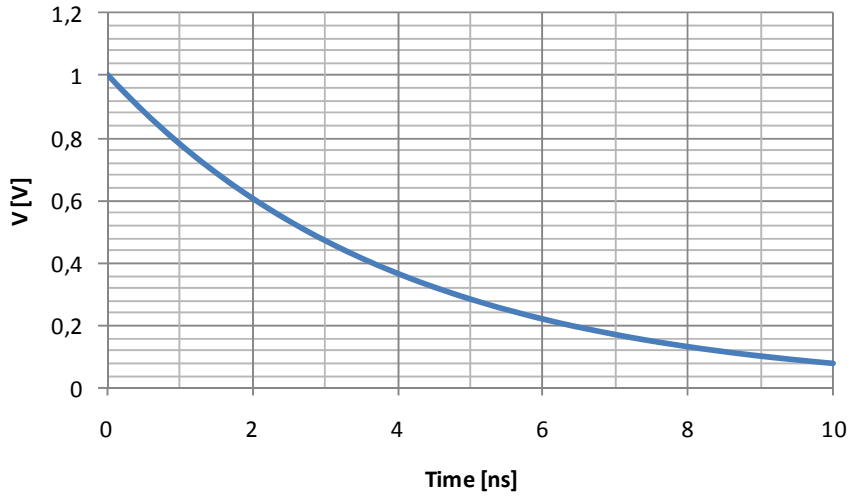

Figure 3 Evolution of voltage V [V] after t=0 while R>0.

Open circuit, R =∞ therefore:

$$\forall t \geq t_0, \forall \varepsilon > 0, \exists \delta(\varepsilon) > 0, |V_0| < \delta \Rightarrow \lim_{t \to \infty} \left| e^{-\left(\frac{1}{RC}\right)t} \cdot V_0 \right| < \varepsilon,$$

(31.)

State of the system will be always equal to zero state, thus if zero sate is limited, the resulting state of the system will be limited – Figure 4. For this reason the circuit will be stable i.s.L. system.

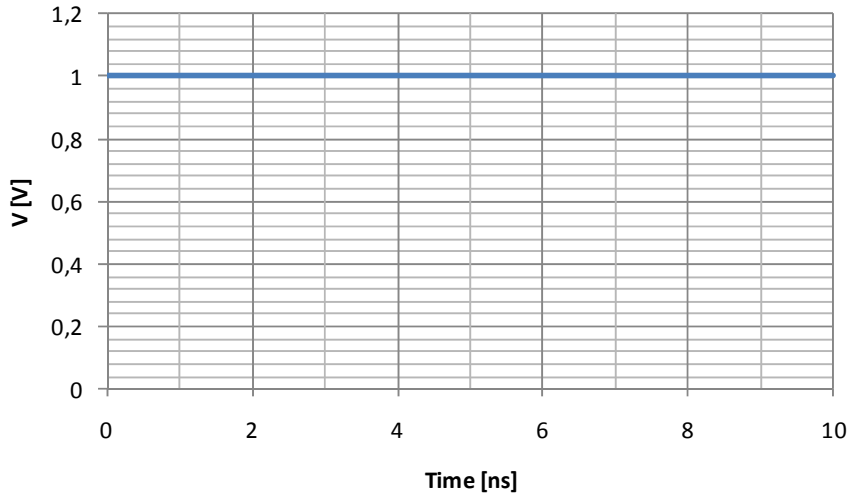

Figure 4 Evolution of voltage V [V] after t=0 while R=∞.

Negative resistance, R<0 resulting in unstable system, while the system state is diverging from the equilibrium point – Figure 5.

$$\forall V_0 \neq 0, \forall RC < 0, \lim_{t\to\infty} \left| V_0 e^{-\left(\frac{1}{RC}\right)t} \right| = \infty \tag{32.}$$

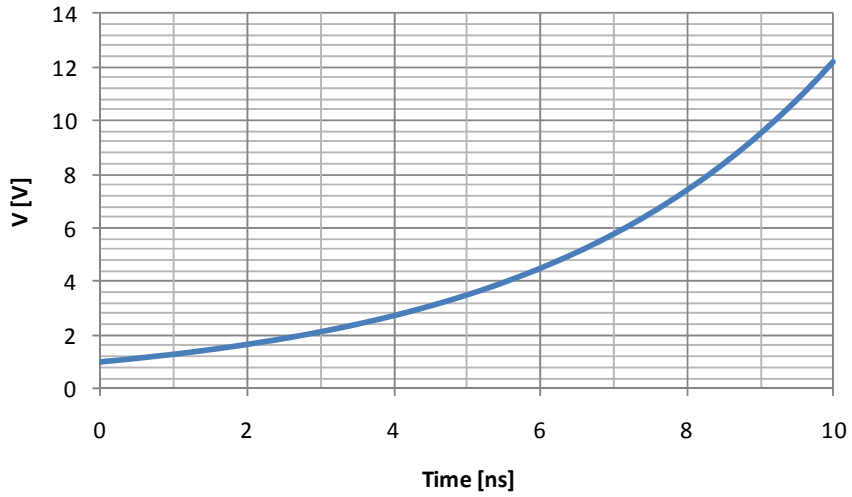

Figure 5 Evolution of voltage V [V] after t=0 while R<0.

The results of this simple analysis are in agreement with the results of the simulations made with usage of Time Domain CAD. Unfortunately, it is not too convenient to describe the electronic circuits using differential equations. While they are powerful in their ability to describe behaviour of the systems, they are also difficult to solve in the case of not well established solutions. Once again, the properties of the linear time invariant system are of a great help when allowing the usage of Laplace transform.

1.1.4 Laplace transform

Laplace transform is one of the best known mathematical tool commonly used by engineers. Thanks to applying the Laplace transform the ordinary differential equations are converted to easily solvable algebraic equations. Laplace is integral transformation that maps original functions f(t) in the time domain into the image functions F(s) in the s domain- called complex frequency domain. While transformation is defined as:

$$F(s)=\mathrm{L}\{f(t)\}=\int_0^{\infty} f(t)\cdot e^{-s\cdot t}\cdot dt \tag{33.}$$

The complex frequency is defined as a complex variable s = σ+jω. The transformation is defined for positive time. Another useful property of Laplace transform is that many relationship and operations over image functions are simpler than over the original functions. It is easily recognizable when the properties of Laplace are given:
Linearity of Laplace transformation:

$$\mathrm{L}\{a\cdot f_1(t)+b\cdot f_2(t)\}=a\cdot F_1(s)+b\cdot F_2(s) \tag{34.}$$

Laplace transform of the derivative:

$$\mathrm{L}\left\{\frac{df(t)}{dt}\right\}=s\cdot F(s)-f(0^+)$$
$$\mathrm{L}\left\{\frac{d^n f(t)}{dt^n}\right\}=s^n\cdot F(s)-\sum_{k=0}^{n-1} s^{n-k-1}\cdot f^{(k)}(0^+) \tag{35.}$$

Laplace transform of the integration:

$$\mathrm{L}\left\{\int_{-\infty}^{t} f(t)\cdot dt\right\}=\frac{F(s)}{s}+\frac{1}{s}\int_{-\infty}^{0^-} f(t)\cdot dt \tag{36.}$$

Laplace transform of the convolution:

$$\mathrm{L}\{f_1(t)*f_2(t)\}=\mathrm{L}\left\{\int_0^t f_1(\tau)\cdot f_2(t-\tau)d\tau\right\}=F_1(s)\cdot F_2(s) \tag{37.}$$

Knowing some basic properties it is possible to apply Laplace transformation to the space state representation of the system (5.) .

$$L\left\{\frac{dx(t)}{dt}=A\cdot x(t)+B\cdot u(t)\right\}\rightarrow s\cdot X(s)-x(0)=A\cdot X(s)+B\cdot U(s)$$
$$X(s)=\left[s\cdot I-A\right]^{-1}\cdot x(0)+\left[s\cdot I-A\right]^{-1}\cdot B\cdot U(s) \tag{38.}$$

If exponential function will be represented as the infinitive series it is possible to calculate its transformation:

$$e^{At} = I + A \cdot t + A^2 \cdot\cdot \frac{t^2}{2!} + \cdots$$
$$\mathrm{L}\left\{e^{At}\right\} = \mathrm{L}\left\{I + A \cdot t + A^2 \cdot\cdot \frac{t^2}{2!} + \cdots\right\} = I\frac{1}{s} + A \cdot \frac{1}{s^2} + A^2 \cdot \frac{1}{s^3} + \cdots = \left[s \cdot I - A\right]^{-1}$$

(39.)

Therefore the solution can be easily obtained:

$$X(s) = \left[s \cdot I - A\right]^{-1} \cdot x(0) + \left[s \cdot I - A\right]^{-1} \cdot B \cdot U(s)$$
$$x(t) = L^{-1}\left\{X(s)\right\} = e^{At} \cdot x_0 + \int_0^t e^{A(t-\tau)} \cdot B \cdot u(\tau) d\tau$$

(40.)

The resulting equation is identical to, (6.), although than it was presented without any proof. Additional exercise can be performed with the previous RC circuit example.

$$-C\frac{dV(t)}{dt} = \frac{V(t)}{R} \quad \rightarrow \quad L\left\{C\frac{dV(t)}{dt} + \frac{V(t)}{R} = 0\right\}$$
$$C \cdot s \cdot V(s) - C \cdot V(0^+) + \frac{V(s)}{R} = 0$$
$$V(s) = \frac{C \cdot V(0^+)}{s \cdot C + \frac{1}{R}} = \frac{V(0^+)}{s + \frac{1}{RC}}$$
$$V(t) = V(0^+) \cdot e^{-\left(\frac{1}{RC}\right)t} \quad \leftarrow \quad V(t) = L^{-1}\left\{V(s)\right\} = L^{-1}\left\{\frac{V(0^+)}{s + \frac{1}{RC}}\right\}$$

(41.)

The result obtained is exactly the same as the one before (29.). Laplace transformation and the complex frequency domain in presented examples serves only as a tool allowing to solve differential equation more efficiently. This is due to transformation of ordinary linear differential equations to simple algebraic ones. Moreover, the usefulness of the complex frequency domain is not restricted only for that transformation. In case of the distributed elements ubiquitous in the microwave circuits, the time domain is very inconvenient. In contrast, the natural and accurate models of such elements are available in the frequency domain. Hence, it is very convenient to describe and solve the stability problems directly in there.

1.1.5 The complex frequency domain

Thus, the idea to describe and solve the stability problems directly in the complex frequency domain will be conducted with the usage of the system state representation. As a starting point, the equation describing the system will be transformed from the time domain to a complex frequency domain.

$$L\left\{\frac{dx(t)}{dt} = A\cdot x(t) + B\cdot u(t)\right\} \rightarrow s\cdot X(s) - x(0) = A\cdot X(s) + B\cdot U(s)$$

(42.)

Then for the zero input response the previously defined relationships are applied: (18.), (21.):

$$\begin{aligned} &s\cdot X(s) - X_0 = A\cdot X(s)\\ &(s\cdot \mathrm{I} - A)\cdot M\cdot Q(s) = M\cdot Q_0\\ &M^{-1}\cdot(s\cdot \mathrm{I} - A)\cdot M\cdot Q(s) = Q_0 \quad \rightarrow\\ &(s\cdot \mathrm{I} - M^{-1}\cdot A\cdot M)\cdot Q(s) = Q_0\\ &(s\cdot \mathrm{I} - J)\cdot Q(s) = Q_0 \end{aligned} \quad \rightarrow \quad \begin{bmatrix} s-\lambda_{11} & 0 & \cdots & 0\\ 0 & s-\lambda_{22} & \cdots & 0\\ \vdots & \vdots & \ddots & \vdots\\ 0 & 0 & \cdots & s-\lambda_{nn} \end{bmatrix}\cdot\begin{bmatrix} Q_1(s)\\ Q_2(s)\\ \vdots\\ Q_n(s) \end{bmatrix} = \begin{bmatrix} Q_{1,0}\\ Q_{2,0}\\ \vdots\\ Q_{n,0} \end{bmatrix}$$

(43.)

To solve this set of n linear equation the Cramer's rule is invoked:

$$W\cdot y = z \quad \rightarrow \quad y_i = \frac{\det(W_i)}{\det(W)} \quad M_i = \left[\begin{array}{ccc|c|ccc} w_{11} & w_{12} & \cdots & z_1 & \cdots & w_{1n}\\ w_{21} & w_{22} & \cdots & z_1 & \cdots & w_{2n}\\ \vdots & \vdots & & \vdots & \ddots & \vdots\\ w_{n1} & w_{n2} & \cdots & z_1 & \cdots & w_{nn} \end{array}\right]$$

$\uparrow i^{th}$ column

$$Q_i(s) = \frac{\det\{(s\cdot \mathrm{I} - J)_i\}}{\det(s\cdot \mathrm{I} - J)}$$

(44.)

A careful investigation of (44.) leads to the subsequent observation:

$$Q_i(s) = \frac{\det\{(s\cdot \mathrm{I} - J)_i\}}{\det(s\cdot \mathrm{I} - J)} = \frac{(s-\lambda_1)\cdots(s-\lambda_2)\cdot Q_{i,0}\cdot(s-\lambda_{n-1})\cdots(s-\lambda_n)}{(s-\lambda_1)\cdots(s-\lambda_2)\cdot(s-\lambda_i)\cdot(s-\lambda_{n-1})\cdots(s-\lambda_n)} = \frac{Q_{i,0}}{(s-\lambda_i)}$$

(45.)

Once again, the recalling relation (18.) state of the system can be described as:

$$\begin{aligned} X_i(s) &= \sum_{j=1}^{n} M_{i,j}\cdot Q_j(s) = \sum_{j=1}^{n} M_{i,j}\cdot\frac{Q_{j,0}}{(s-\lambda_j)}\\ X_i(t) &= \sum_{j=1}^{n} M_{i,j}\cdot Q_{j,0}\cdot e^{\lambda_j t} = \sum_{j=1}^{n} M_{i,j}\cdot Q_{j,0}\cdot e^{j\varpi_j t}\cdot e^{\sigma_j t} \end{aligned}$$

(46.)

Clearly and as it was already stated: the real parts of matrix A eigenvalues will be responsible for the stability of the system. However, knowing the result it is possible to stop before the end of the analysis and deduce that the zeros of the determinant of the matrix $(s\cdot \mathrm{I} - J)$ are equal indication of the stability. These zeros are eigenvalues of J. Whereas A and J are similar matrixes, their eigenvalues and determinants are equal:

$$J = M^{-1} \cdot A \cdot M \quad \rightarrow \quad \det(J) = \det(M^{-1} \cdot A \cdot M) = \det^{-1}(M) \cdot \det(A) \cdot \det(M) = \det(A)$$

(47.)

So it is also true:

$$(s \cdot I - J) = M^{-1} \cdot (s \cdot I - A) \cdot M \quad \rightarrow \quad \det(s \cdot I - J) = \det(s \cdot I - A)$$

(48.)

As the description of the circuit state is:

$$(s \cdot \mathrm{I} - A) \cdot X(s) = X_0$$

(49.)

Zeros of the denominator of the $(s \cdot \mathrm{I} - A)$ are eigenvalues of A and they are referred as natural frequencies of the system or poles of the system. In agreement with the previous definition of stability, the system will be unstable if any of the natural frequencies have a positive real part. Such a result shows that it is likely to resolve the stability issue directly in the complex frequency domain.
Alas, due to the complexity of the system, the space state representation is not preferred by the engineers in this domain. Consequently, it is more convenient to use existing notations ubiquitously used in designs like admittance or impedance matrix description. As a result, by means of the previously defined properties of Laplace transform, the basic circuit elements description will be transformed to the complex frequency domain:

$$\mathrm{L}\{i(t) = G \cdot v(t)\} \Rightarrow i(s) = G \cdot v(s)$$
$$\mathrm{L}\left\{i(t) = C\frac{dv(t)}{dt}\right\} \Rightarrow i(s) = C \cdot s \cdot v(s) + C \cdot v(0^+)$$
$$\mathrm{L}\left\{i(t) = \frac{1}{L}\int_0^t v(t)dt\right\} \Rightarrow i(s) = \frac{1}{L} \cdot \frac{v(s)}{s}$$

(50.)

Moreover, the transmission lines are expressed by:

$$\mathrm{Y}_{12} = \mathrm{Y}_{21} = \mathrm{Y}_0 \mathrm{ctgh}(\gamma l) \text{ and } \mathrm{Y}_{11} = \mathrm{Y}_{22} = \mathrm{Y}_0 \mathrm{csch}(\gamma l)$$
$$\text{Where: } \mathrm{Y}_0 = \sqrt{\frac{\mathrm{G}+\mathrm{sC}}{\mathrm{R}+\mathrm{sL}}} \text{ and } \gamma = \sqrt{(\mathrm{G}+\mathrm{sC})(\mathrm{R}+\mathrm{sL})}$$

(51.)

G,C,R,L are: shunt conductance, shunt capacitance, series resistance and series inductance per length of the line, where *l* is the line length.
Then, via the admittance representation we can describe dynamic response of the circuit as the vector equation:

$$\mathbf{Y}(s) \cdot \mathbf{V}(s) - \mathbf{I}(s) = 0$$
$$\mathbf{Y}(s) \cdot \mathbf{V}(s) = \mathbf{I}(s)$$

(52.)

where: Y(s) - is *n* x *n* system matrix and V(s) is system state vector *1* x *n* and I(s) is *1* x *n* vector of excitations of *n* node circuit. Zero input response is described as:

$$\mathbf{Y}(s)\cdot\mathbf{V}(s)=0 \tag{53.}$$

Two different solutions are possible. Trivial one when state vector is simply zero and non trivial, when the system matrix is singular. In the latter case equation is true for non zero state vector and this is possible if the determinant of the system matrix is equal to zero.

$$\mathrm{V}(s)\neq 0 \Rightarrow \det\{\mathrm{Y}(s)\}=0 \tag{54.}$$

Equations (49.) and (53.) are similar and as stated before the zeros of the determinant of the matrix description of the system are natural frequencies or poles of the system. This plain observation allows applying the zeros of the determinant in stability analysis exactly in the same way as eigenvalues of matrix A.

The previous practical example is now modified according to the used notation. The switch is now closed and an input port is introduced.

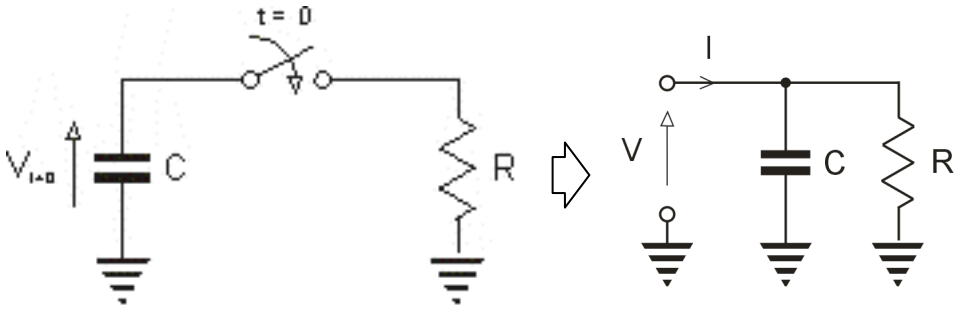

Figure 6 Example of the simple RC circuit modified to a new description.

The matrix description can be omitted, while each matrix consists of one element only. The system is described with equation:

$$\mathrm{Y}(s)=\frac{s+\dfrac{1}{RC}}{C} \tag{55.}$$

As a result, the zeros of the determinant are simply zeros of the Y(s) element:

$$\det\{\mathrm{Y}(s)\}=\mathrm{Y}(s)$$
$$\det\{\mathrm{Y}(s)\}=0 \Leftrightarrow s=-\left(\frac{1}{RC}\right) \tag{56.}$$

Such a result is in agreement with all the previous analysis for this example.

1.2 High frequency circuits stability

Evaluation of the zeros of the circuit determinant presented in paragraph 1.1.5 is a direct and comprehensive way to determine the stability. Regrettably, it is very laborious for larger networks. Moreover, with use of the determinant, circuits stability can be assured only for one set of the source-load termination value. Occasionally, often at low frequency applications the circuit needs to be stable only for a range of possible termination. Unfortunately high frequency circuits need to operate in difficult conditions of changeable source-load terminations. Obviously their performances do not need to be maintained in case of source-load termination deviation from assumed range, but their stability need to be assured for any passive source-load termination. Moreover high frequency electronic introduce different concepts of the circuit description and measurement techniques that reflect its specific therefore stability test need to be able to operate with them. Furthermore, with nowadays importance of CAD tools, the stability tests need to be easily integrated with existing CAD environments. Also it is very convenient to have an opportunity for inclusion of the stability tests in the optimization routines, which save time in the search for an optimal design. Such demanding and a particular design oriented requirements rules out test as laborious as the determinant. More efficient methods are required than. One of the ways leading to efficiency is simplicity, what in case of the stability analysis involves a transition from the state variable description to the two-port representation of the circuit.

1.2.1 Description of the two port network

In most popular cases we are interested to describe the designed circuit in a way which is most natural and simple. That is, to employ only input and output terminals and describe interactions between the quantities at the terminals as the linear dependence. In order to achieve precision in the terminology the term port is used a name for pair of terminals on the input and output. For typical applications like filters, amplifiers, phase shifters two ports are needed to represent circuit behaviour. It is not entirely spot on because the real circuits are not only nonlinear but their behaviour is also dependent on many, not only electrical variables, often with memory effects. Nevertheless, for most passive circuit and linear region of work of the active devices this representation is extremely useful in terms of the basic design process or as a starting point.

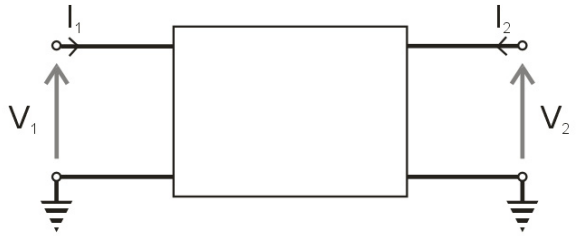

Figure 7 Linear two-port circuit.

Assuming linear, time invariant and memoryless two-port network shown in Figure 7; there have been gathered the most significant two port circuit descriptions below:
The admittance matrix Y:

$$I = \begin{bmatrix} I_1 \\ I_2 \end{bmatrix} = \begin{bmatrix} y_{11} & y_{12} \\ y_{21} & y_{22} \end{bmatrix} \cdot \begin{bmatrix} V_1 \\ V_2 \end{bmatrix} = Y \cdot V \quad , \tag{57.}$$

where elements of Y matrix are determined by the equation:

$$y_{ji} = \left. \frac{I_j}{V_i} \right|_{V_k = 0, \quad k \neq i} \tag{58.}$$

Term V_k=0 means that any port other than the input one will be terminated by short.
The impedance matrix Z:

$$V = \begin{bmatrix} V_1 \\ V_2 \end{bmatrix} = \begin{bmatrix} z_{11} & z_{12} \\ z_{21} & z_{22} \end{bmatrix} \cdot \begin{bmatrix} I_1 \\ I_2 \end{bmatrix} = Z \cdot I \tag{59.}$$

where the elements of Z matrix are determined by the equation:

$$z_{ji} = \left. \frac{U_j}{I_i} \right|_{I_k = 0, \quad k \neq i} \tag{60.}$$

Term I_k=0 means that any other port than the input one will be terminated by open.
Transmission matrix ABCD:

$$\begin{bmatrix} V_1 \\ I_1 \end{bmatrix} = \begin{bmatrix} A & B \\ C & D \end{bmatrix} \cdot \begin{bmatrix} V_2 \\ -I_2 \end{bmatrix}, \text{ where elements are determined by } \begin{matrix} A = \left. \frac{V_1}{V_2} \right|_{-I_{2=0}}, & B = \left. \frac{V_1}{-I_2} \right|_{V_{2=0}} \\ B = \left. \frac{I_1}{V_2} \right|_{-I_{2=0}}, & D = \left. \frac{I_1}{-I_2} \right|_{V_{2=0}} \end{matrix} . \tag{61.}$$

These forms of description are very useful but somehow abstract in the microwave circuits. This is due to the fact that the voltage or current measurements are difficult or unattainable unless a clearly defined terminal pair is available. Also, a pure short or open circuit are very difficult to obtain except for the narrowband solutions. Besides, the active devices are often prone to short and open terminations becoming unstable in these conditions. For that reason, the equivalent voltage and the current waves concept were introduced. Voltage and current in the point z are described by means of equivalent voltage and current incident (V+,I+) and reflected (V-,I-) waves - (62.). For this description the reference plain is also defined at z=0 providing a phase reference.

$$\begin{aligned} V(z) &= V^+ \cdot e^{-j\beta z} + V^- \cdot e^{j\beta z} \\ I(z) &= I^+ \cdot e^{-j\beta z} - I^- \cdot e^{j\beta z} \end{aligned} \tag{62.}$$

The above definitions extend possible descriptions for the natural microwaves concepts of the incident, as well as for reflected and transmitted waves. The reflection and transmission coefficients related to them are, according to the microwave measurements, natural quantities. They may be defined as ratio of voltage waves due to:

$$\Gamma_j = \left.\frac{V_i^-}{V_i^+}\right|_{V_k=0,\quad k\neq i}, \quad T_{ji} = \left.\frac{V_j^-}{V_i^+}\right|_{V_k=0,\quad k\neq i}$$

(63.)

This in turn means, that the reflection coefficient at terminal *i*, is a ratio of reflected wave to the incident voltage one, when any other incident waves equals to zero. The transmission coefficient from port *i* to *j* is than the ratio of transmitted wave to port *j* to the incident wave at port *i,* with all the other incident waves equal to zero. With the use of relations between the current, voltage and characteristic the impedance at reference plane z=0 (62.) leads to:

$$V^+ = \frac{1}{2}\left(V + Z\cdot I\right)$$
$$V^- = \frac{1}{2}\left(V - Z\cdot I\right)$$

(64.)

If the normalisation with the terminal impedance $Z_{0,i}$ is performed, the final description of the incident a_i and reflected b_i wave at the terminal i is obtained:

$$a_i = \frac{V_i + Z_{0,i}\cdot I_i}{2\cdot\sqrt{Z_{0,i}}}, \quad b_i = \frac{V_i - Z_{0,i}\cdot I_i}{2\cdot\sqrt{Z_{0,i}}}$$

(65.)

This particular form - (65.) - is very useful as it may be treated as normalized voltage or current and at the same time square of it is proportional to the wave power. By applying these quantities in order to describe the microwave network presented in Figure 8 the result in form of the definition of the scattering matrix S (66.) is achieved:

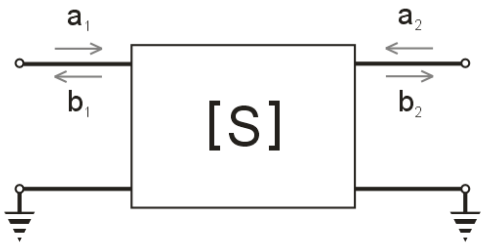

Figure 8 Linear two-port circuit described in terms of S parameters.

$$[b] = \begin{bmatrix} b_1 \\ b_2 \end{bmatrix} = \begin{bmatrix} S_{11} & S_{12} \\ S_{21} & S_{22} \end{bmatrix} \cdot \begin{bmatrix} a_1 \\ a_2 \end{bmatrix} = [S]\cdot[a],$$ and their elements; $$S_{ij} = \left.\frac{b_i}{a_j}\right|_{a_k=0\quad k\neq i}$$

(66.)

Term a_k=0 means that any port other than the input one needs to be terminated with the characteristic impedance Z_0 leading to Γ_k=0. This, in consequence leads to $a_k = b_k * \Gamma_k$ =0. In other words, we need to close each port with a match, in order to avoid reflection from load impedance. What is more, the input port needs to be connected to the source with a characteristic impedance $Z_{0,k}$. Obviously, the diagonal elements of the S matrix, for which the subscript numbers are equal, are also equal to the reflection coefficients, $S_{ii}=\Gamma_i$. Other elements are the transmission coefficients with subscript numbers indicating interacting ports and direction, $S_{ji}=T_{ji}$. The utility of S parameters matrix is connected with a straightforward and intuitive wave description of the circuit together with the nature of s parameters reflecting the real measurements.

1.2.2 Simple two-port stability tests for the linear two ports

With the circuit characterized the same way as in one of the previously mentioned matrix we can now refer back to the stability analysis and the simplified approach presented by Rollett in [3].
An equivalent statement to the stability based on the determinant of the system is: "(…) the real part of the immittance looking in at only one of the two ports remains positive with arbitrary passive terminations at the other, provided also that the characteristic frequencies of the two-port with ideal terminations (infinite immittances, i.e., open or short circuits, as appropriate) lie in the left half-plane".
This definition depicts unconditional stability of the circuit reduced to the two-port and represented by the matrix as shown in Figure 9. It may be expressed with the use of the reflection coefficient with what follows:

$$\begin{aligned} &\forall \Gamma_L \quad |\Gamma_L| \le 1 \Rightarrow |\Gamma_{in}| < 1 \\ &\forall \Gamma_S \quad |\Gamma_S| \le 1 \Rightarrow |\Gamma_{out}| < 1 \end{aligned} \tag{67.}$$

where Γ_S denotes the source reflection coefficient, Γ_L is the load reflection coefficient, Γ_{in} input reflection coefficient, and Γ_{out} output reflection coefficient.

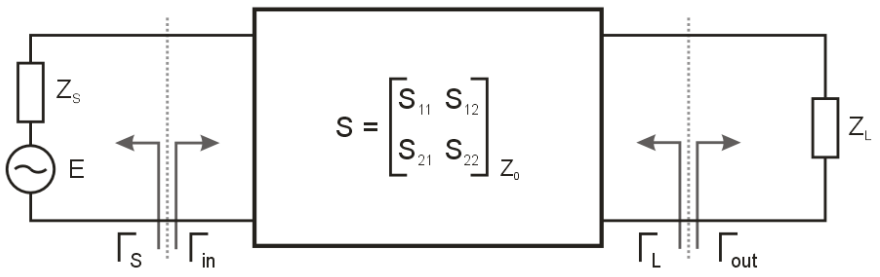

Figure 9 Two port described by S matrix with the denoted four reflection coefficients used in stability analysis.

Definition of the circuit stability given by Rollett is very intuitive. The term 'unconditional' in Rollett's case refers to the circuit which is stable for any source and the load passive termination. Alas, this approach requires the designer to check all the possible terminations on each side of the circuit, due to the previously mentioned rules and given equations for Γ_{in} and Γ_{out} - (68.). Besides, this test needs to be done for each frequency not limiting the calculations only to the band of interest, but should be performed for the whole band, where two-port is not a passive circuit.

$$\left|\Gamma_{in}\right| = \left| s_{11} + \frac{s_{21} \cdot s_{12} \cdot \Gamma_L}{1 - s_{22} \cdot \Gamma_L} \right|$$
$$\left|\Gamma_{out}\right| = \left| s_{22} + \frac{s_{21} \cdot s_{12} \cdot \Gamma_S}{1 - s_{11} \cdot \Gamma_S} \right|$$

(68.)

Basing on such described Γ_{in} , Γ_{out} and recalling the terms of stability, three kinds of impedance could be differentiated. For the two-port explained here with S matrix, they will be called and described as follows:

- impedances leading to stability - Z_{ls} - value of impedance causes Γ on other side to be less than one,
- leading to instability and - Z_{li} - value of impedance causes Γ on other side to be higher than one,
- borderline - Z_b - value of impedance causes Γ on other side to be the equal one,

,where Γ is reflection coefficient looking into the circuit port, on other side of the circuit than the connected impedance. Three groups in each side of the circuits can be distinct by checking previously defined Γ_{in} , Γ_{out}. Adding another subscript, the source and load side is differentiated. All the cases were collected together bellow:

$$\begin{aligned} &Z_{\mathrm{L}} = Z_{\mathrm{L\,ls}} \Rightarrow \left|\Gamma_{\mathrm{in}}\right| < 1 \qquad Z_{\mathrm{S}} = Z_{\mathrm{S\,ls}} \Rightarrow \left|\Gamma_{\mathrm{out}}\right| < 1 \\ &Z_{\mathrm{L}} = Z_{\mathrm{L\,b}} \Rightarrow \left|\Gamma_{\mathrm{in}}\right| = 1 \qquad Z_{\mathrm{S}} = Z_{\mathrm{S\,b}} \Rightarrow \left|\Gamma_{\mathrm{out}}\right| = 1 \\ &Z_{\mathrm{L}} = Z_{\mathrm{L\,li}} \Rightarrow \left|\Gamma_{\mathrm{in}}\right| > 1 \qquad Z_{\mathrm{S}} = Z_{\mathrm{S\,li}} \Rightarrow \left|\Gamma_{\mathrm{out}}\right| > 1 \end{aligned}$$

(69.)

While each group will be plotted on the Smith Chart they will create two regions separated by the circle for each side of the circuit. If the circuit is unconditionally stable, the Unity Smith chart will be free of impedances different than Z_{ls}. If there is not any point on either side denoting Z_{li} or Z_b in the Unity Smith Chart, it means that the passive impedance leading to the instability not exists in there.
A circle created from the points representing all $Z_{S\,b}$ will be named the source stability circle. Solving (68.) Γ_{out} for Γ_S leads to expression for the circle centre position C_S and a radius r_S.

$$C_S = \frac{\left(s_{11} - s_{22}^{*}\Delta\right)^{*}}{\left|s_{11}\right|^2 - \left|\Delta\right|^2}, \quad r_S = \frac{\left|s_{21}s_{12}\right|}{\left|s_{11}\right|^2 - \left|\Delta\right|^2}$$

(70.)

Graphical representation of the source stability circle was shown in Figure 10. A circle created from the points representing all $Z_{L\,b}$ will be called the load stability circle. Same procedure leads to a description of the centre position C_L and radius r_L for the load stability circle.

$$C_L = \frac{\left(s_{22} - s_{11}^{*}\Delta\right)^{*}}{\left|s_{11}\right|^2 - \left|\Delta\right|^2}, \quad r_L = \frac{\left|s_{21}s_{12}\right|}{\left|s_{22}\right|^2 - \left|\Delta\right|^2}$$

(71.)

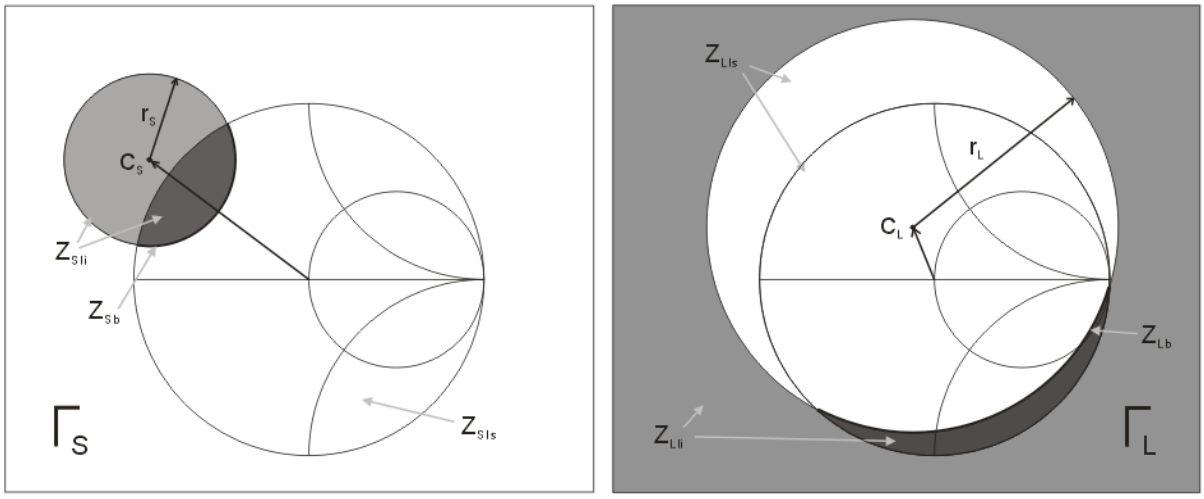

Figure 10 Graphical representation of the source and the load stability circle examples.

Interpretation of the circles is simple and intuitive, however each one of them can carry two possible solutions. The region of the impedances leading to the stability might be inside or outside the circle. This difference between that solutions is shown in Figure 10. The source stability circle internal points are set of impedance leading to instability in contrast to the set of the impedances leading to stability in case of the load stability circle. Due to gain full knowledge about the character of the impedances inside the stability circle, an additional test of the membership on one arbitrary chosen passive impedance needs to be performed. The reached information gives a full picture and allows to name the areas leading to instability or stability.

The circles are a very useful design tool in case when the unconditional stability of the circuit is not mandatory. They could be also very supportive in the search for the solution to stabilize the circuit denoting a forbidden area of impedances. This method however, is still not simple enough, as it requires a graphical inspection or checking three parameters for each side of the circuit.

Rollett in [3] resolved this problem by defining parameter k called the stability k-factor. It is determined as follows:

$$k = \frac{2\rho_{11}\rho_{22} - \mathrm{Re}(\gamma_{12}\gamma_{21})}{\left|\gamma_{12}\gamma_{21}\right|}, \tag{72.}$$

where $\rho_{11} = \mathrm{Re}(\gamma_{11})$ and γ will be used for any of the z, y, h, g of the two-port parameters.

Usage of the defined k-factor criterion for unconditional stability may be written down as:

$$k \geq 1 \quad \text{provided} \quad \rho_{11}, \rho_{22} \geq 0 \tag{73.}$$

Then, the criterion may be expressed in terms of S parameters as follows:

$$k = \frac{1 - \left|S_{11}\right|^2 - \left|S_{22}\right|^2 + \left|\Delta_S\right|^2}{2\left|S_{12}\right|\left|S_{21}\right|} \geq 1 \quad \text{where} \quad \left|\Delta_S\right| = \left|S_{22}S_{11} - S_{12}S_{21}\right| \tag{74.}$$

Provided that any of the following:

$$B_1 = 1 + |S_{11}|^2 - |S_{22}|^2 - |\Delta_S|^2 > 0$$
$$B_2 = 1 - |S_{11}|^2 + |S_{22}|^2 - |\Delta_S|^2 > 0$$
$$|\Delta_S| < 1$$
$$1 - |S_{11}|^2 > |S_{12}S_{21}|$$
$$1 - |S_{22}|^2 > |S_{12}S_{21}|$$

(75.)

If the circuit satisfies condition $k \geq 1$ with any of the additional conditions (75.) it is unconditionally stable. According to the definition it implies that for any passive termination at one port, positive immittance is observed at the other port.

Even simpler test was based on geometrical approach and mapping functions between the pairs of reflection coefficients Γ_{out}, Γ_S and Γ_{in}, Γ_L. Edwards *et al*. in [4] defined the conditions for the unconditional stability of the two port linear circuit described with S parameter matrix in the following way:

$$\mu \equiv \frac{1 - |S_{11}|^2}{|S_{22} - S_{11}^* \Delta| + |S_{12}S_{21}|} > 1 \quad \text{or} \quad \mu' \equiv \frac{1 - |S_{22}|^2}{|S_{11} - S_{22}^* \Delta| + |S_{12}S_{21}|} > 1$$

(76.)

At this point, the described μ factor and companion μ' factor possesses very intuitive meaning. It presents the distance between the unstable region and the centre of the Smith Chart. Then, it is achievable to use μ or μ' as a measure of stability, as the higher the value, the farther lay instability region on the complex plane.

1.2.3 Problems with the simple two-port stability tests

The above, relatively simple methods were quickly accepted and extensively used in a design process. Unfortunately, many designers forgot that proviso which needs to be fulfilled is priori to them . As it was described by Rollett: the system must be stable for one specific set of passive terminations. Traditionally, this condition used to be neglected though, as the designers based their designs on devices S parameters from the measurement data. This in consequence implied that proviso was fulfilled, as the proper measurements were possible only in a stable circuit. Nowadays, the designers tend to use devices models instead of the measurement results and what is more, the designed circuits became more and more complex. These facts lead back to the importance of the proviso.

In [6], [5] the examples of the circuits which pass test for K and Δ or μ may be found, but they are unstable. Double-checking of the proviso shows that the network has poles in Right Half of the Complex Plane - so the test is invalid. A simple T structure presented in the Figure 11 is one of such examples.

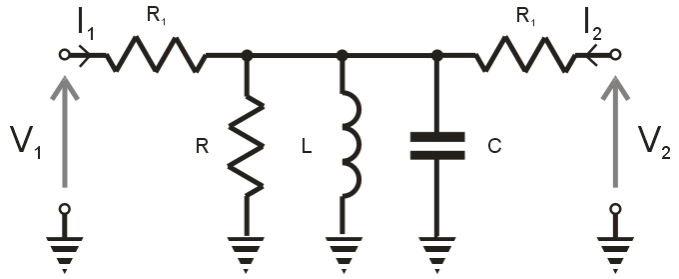

Figure 11 Simple T structure to test k-factor.

To test its behaviour L and C components will be chosen to resonate at 1 GHz and R_1 and resistors will be fixed to 10 Ω. With the usage of ADS environment, k and B_1 factors are plotted as a function of resistor R value, at the resonance frequency.

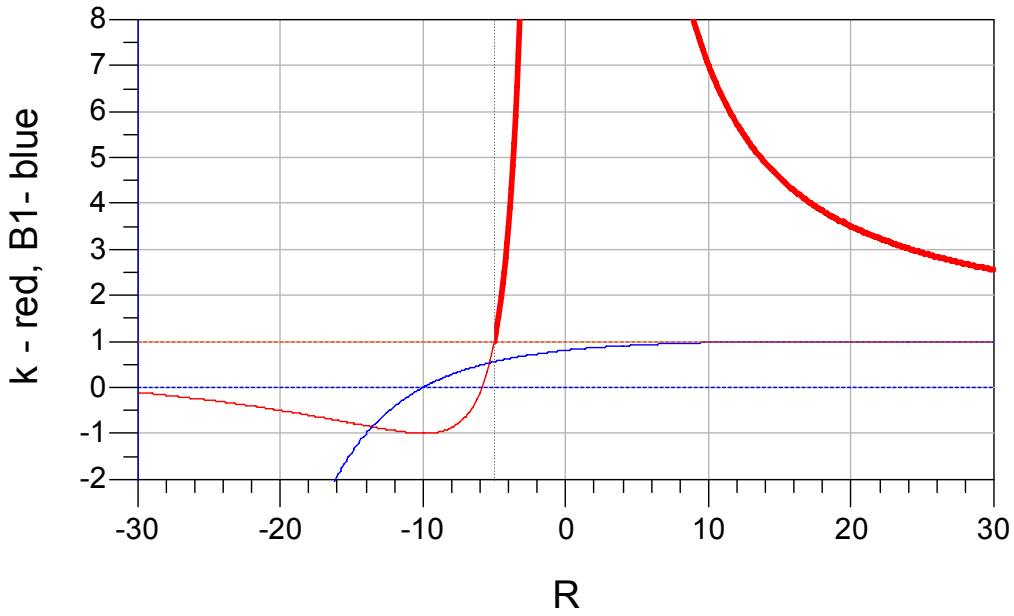

Figure 12 Rollett's k-factor and B1 for simple T network from Figure 11 as function of resistance R.

From the Figure 12, it is seen clearly, that the circuit is stable when R>-5 Ω and when conditions (74.) and (75.) are fulfilled.

To verify that result, Z matrix description of the circuit will be used:

$$[Z(s)] = \frac{1}{s^2 + \frac{1}{R \cdot C}s + \frac{1}{L \cdot C}} \cdot \begin{bmatrix} R_1 \cdot s^2 + \frac{(R_1 + R)}{R \cdot C}s + \frac{R_1}{L \cdot C} & \frac{s}{C} \\ \frac{s}{C} & R_1 \cdot s^2 + \frac{(R_1 + R)}{R \cdot C}s + \frac{R_1}{L \cdot C} \end{bmatrix} \tag{77.}$$

It is also easy to monitor that the common element for [Z] matrix is the source of problems in case of the stability analysis. A detailed investigation of that element denominator (78.) reveals two zeros – s_1 and s_2. These zeros automatically become the poles of all matrix elements. Their value is dependent on R, L and C values. With the assumption of constant value of L and C and the R value changing from -50 Ω to 50 - the evolution of the poles position on S-plane is presented in Figure 13.

$$\frac{1}{s^2+s\frac{1}{R\cdot C}+\frac{1}{L\cdot C}}=\frac{1}{(s-s_1)(s-s_2)}=\frac{1}{\left(s-\frac{-L+\sqrt{L^2-4\cdot C\cdot R^2\cdot L}}{2\cdot C\cdot R\cdot L}\right)\left(s+\frac{L+\sqrt{L^2-4\cdot C\cdot R^2\cdot L}}{2\cdot C\cdot R\cdot L}\right)} \quad (78.)$$

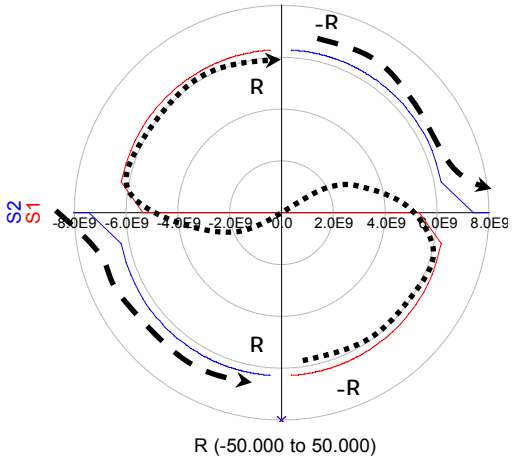

Figure 13 Position of Z matrix common element poles for different R values.

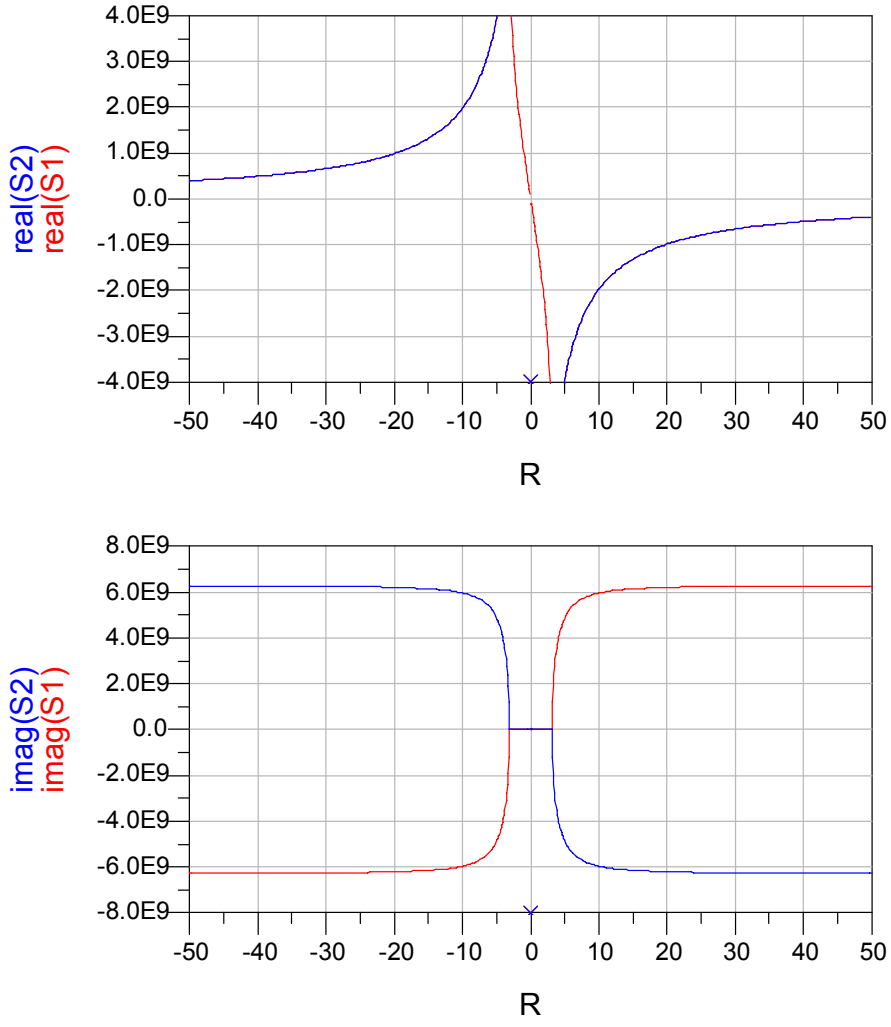

Figure 14 The real and the imaginary part of Z matrix common element poles values (s1, s2).

For an easy interpretation of the results, the imaginary and the real part of the poles were presented separately in Figure 14. By recalling that any Right Half Complex Plane pole in the circuit description may break the proviso, it is justified that in such a case the circuit will be unstable for R<0. Such a conclusion questions the validity of k-factor test without a priori provision check.
Next example is shown in Figure 15. If Z_0 is equal to the reference impedance, the circuit is matched and the reflection coefficients are equal zero.

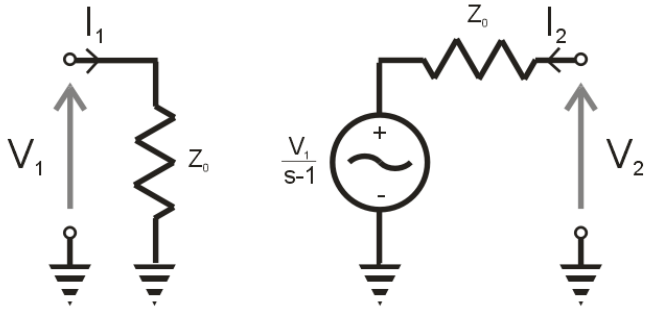

Figure 15 Unilateral two-port.

S matrix representing circuit is as follows:

$$[S(s)] = \begin{bmatrix} 0 & 0 \\ \dfrac{1}{2\cdot(s-1)} & 0 \end{bmatrix} \tag{79.}$$

Clearly, the circuit will pass k-factor test as being unstable. Again, the validity of k factor as a standalone test is proven to be wrong, by underlying the importance of proviso in the stability tests.

1.2.4 Problem of a reduced network representation

The two port representation of the circuit was presented here as a response to the stability test simplification requirement. Obviously, the stability issue was not a major force leading to its creation, but its existence simplifies the stability problems. The two port representation's intuitive meaning and availability in CAD environments together with linear stability tests like k or μ factors shapes design reality nowadays. Such a situation may be hazardous as k or μ factors became most available tests whilst there are no common tools to check the proviso. As it was shown in the example from Figure 11., the simple k-factor test gives misleading information about the stability. By carefully investigating a matrix description it can be found that the circuit is unstable despite *k*>1 and B_1>0. However, in actual complex designs most nodes of circuit are treated as internals. Now and then there exists only two port representation of the complex circuit. A question arises than: does the reduced representation of the circuit give enough knowledge to assure of stability? This dilemma will be approached with the use of example parallel amplifier circuit presented in Figure 16.

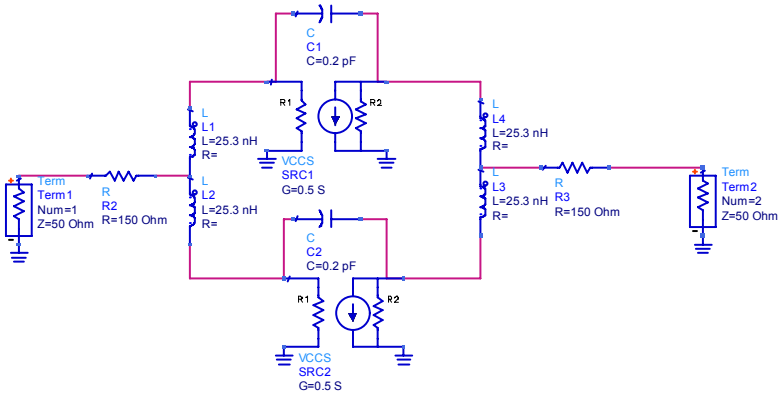

Figure 16 Parallel amplifier example circuit.

In the above simplified example of an amplifier the two controlled current sources represent active devices with parasitic capacitance C and resistances R_1 and R_2. Input and output combining structures are created with the usage of two inductors L and a common resistor R. Two port Z matrix representation of circuit presents as follows:

$$Z=\begin{bmatrix} \frac{1}{2}\cdot\frac{1}{g+\frac{1}{R_1}+\frac{1-\frac{g}{s\cdot C}}{R_2+\frac{1}{s\cdot C}}}+\frac{s\cdot L}{2}+R & \frac{1}{2}\cdot\frac{R_1}{1+R_1\cdot\left(\frac{1}{R_2}+g\right)+\frac{1}{R_2\cdot s\cdot C}} \\ \frac{1}{2}\cdot\frac{1-\frac{g}{s\cdot C}}{\left(1+\frac{1}{R_2\cdot s\cdot C}\right)\cdot\left(g+\frac{1}{R_1}+\frac{1-\frac{g}{s\cdot C}}{R_2+\frac{1}{s\cdot C}}\right)} & \frac{1}{2}\cdot\frac{R_1-\frac{1}{s\cdot C}}{1+R_1\cdot\left(\frac{1}{R_2}+g\right)+\frac{1}{R_2\cdot s\cdot C}}+\frac{s\cdot L}{2}+R \end{bmatrix} \tag{80.}$$

All matrix elements share common pole:

$$s=-\frac{1}{C\cdot\left(R_1+g\cdot R_1\cdot R_2+R_2\right)} \tag{81.}$$

Evidently, positive and finite values of R1 and R2 will shift the pole to LHCP. Therefore, the proviso is fulfilled and matrix can be used in k-factor test. For value of the circuit elements are as follows: R=150Ω, R_1=R_2=1kΩ, L=25.3nH, C=0.2pF g=0.5S, K-factor is computed and presented in Figure 17. The circuit is unconditionally stable while k>1 and B1>0 for all frequencies.

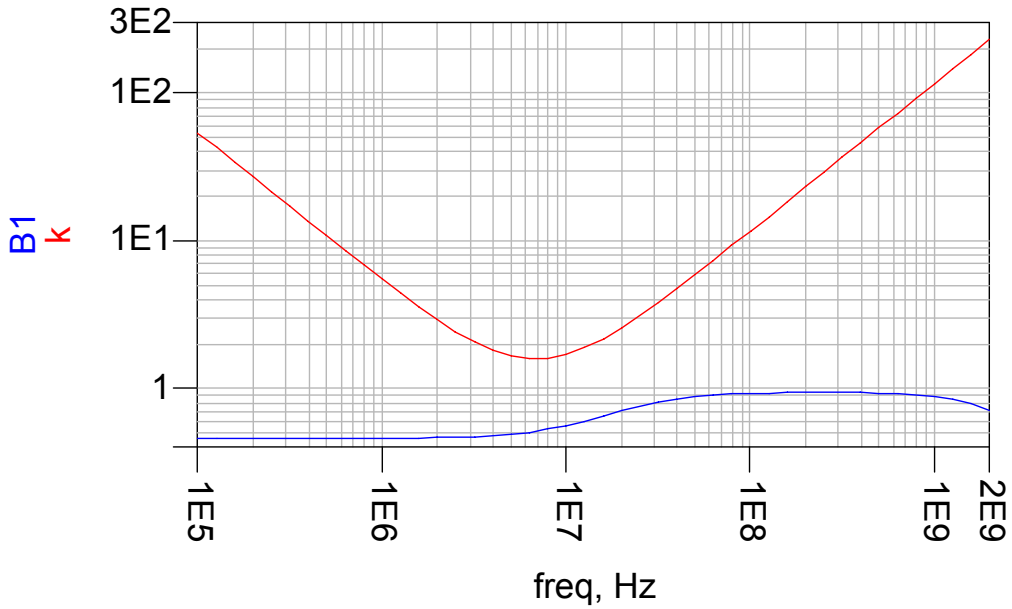

Figure 17 K-factor and B1 coefficient of example parallel amplifier.

Following this particular result, the empirical experiment is performed in CAD environment - Figure 18. With exploiting the time domain, the simulator response for voltage pulse is computed.

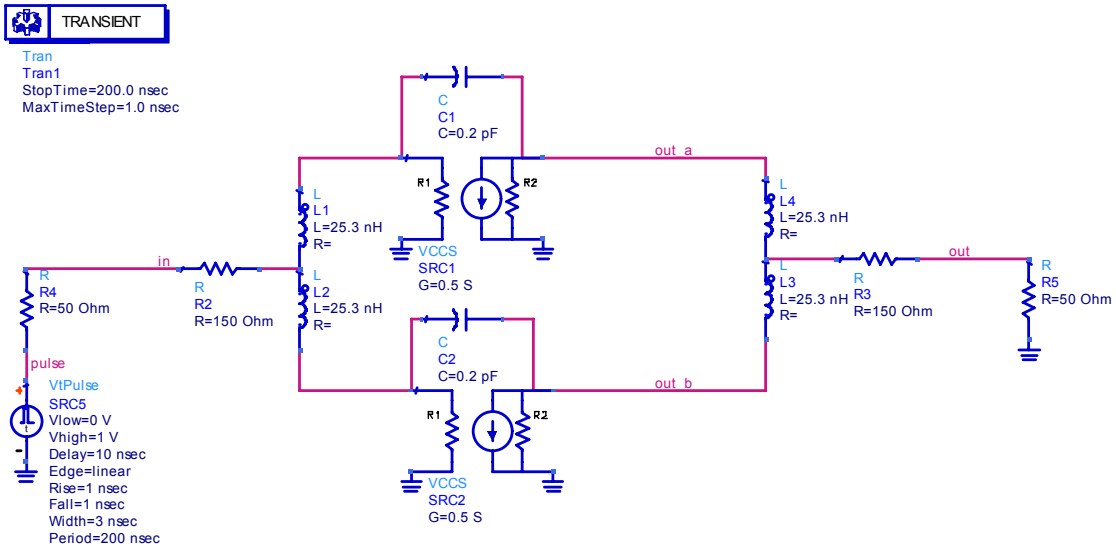

Figure 18 Time domain simulation setup of the example parallel amplifier.

Limited output for limited input excitation is not unexpected, while asymptotical stability of the system implies BIBO stability. The curves presented in the Figure 19 seem to confirm it as well. Sadly, the time domain simulator is crashing without visible reason at t=121.713 ns.

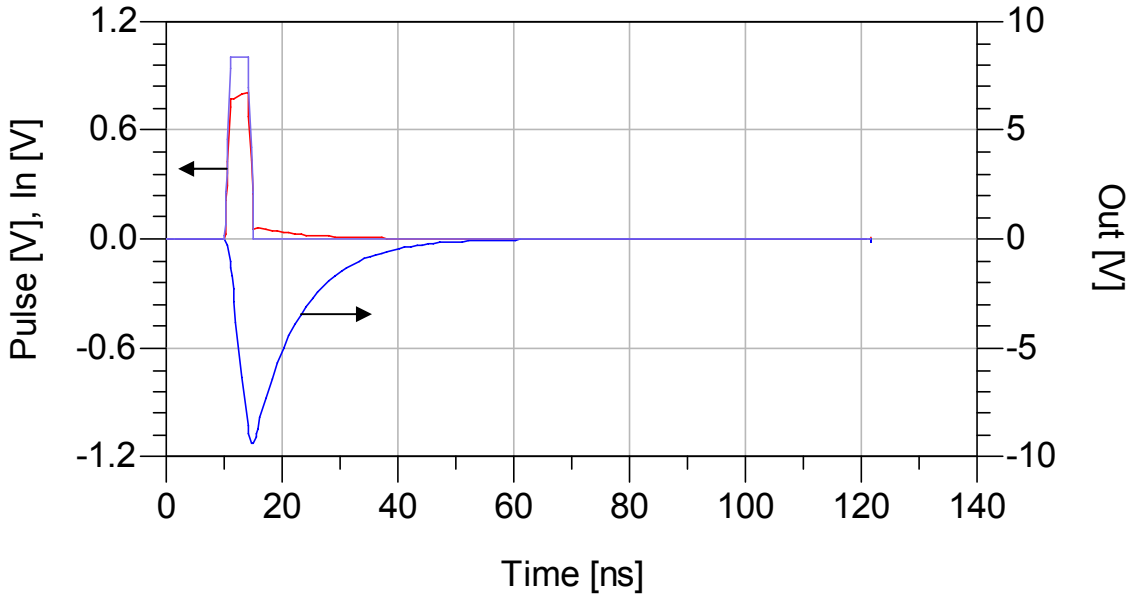

Figure 19 Time domain simulation results of the example parallel amplifier.

Not even inspection of input and output signals reveals any reason. Then, internal voltages are investigated.

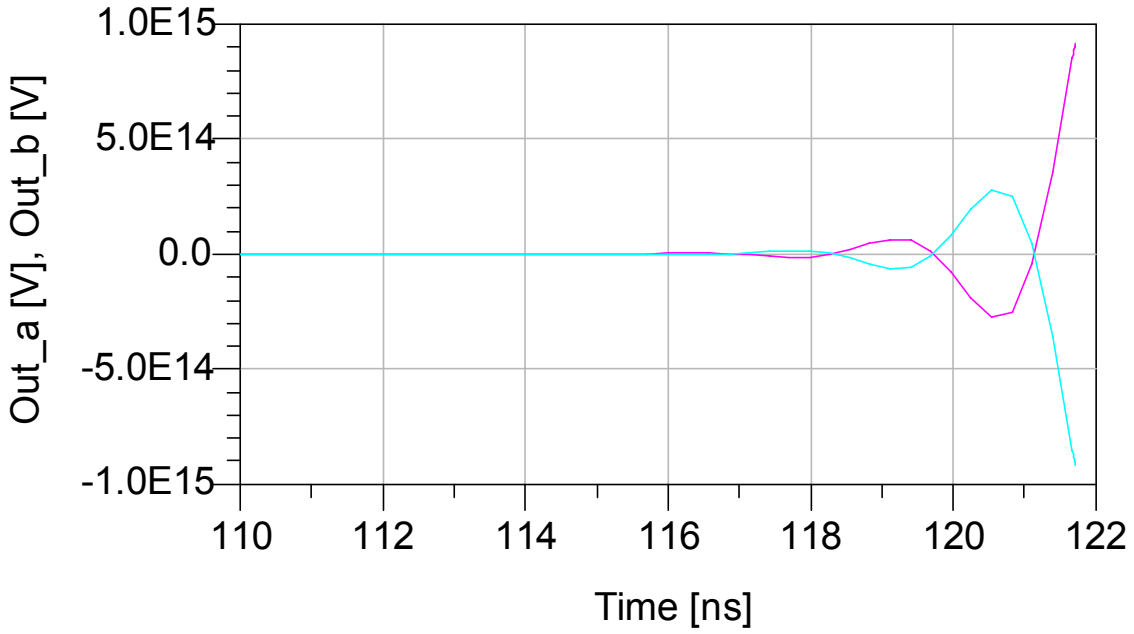

Figure 20 Internal voltages of example parallel amplifier.

So, inspection of the voltage curves from Figure 20 finally exposes the cause of the simulator crash. While circuit is linear, instability grounds internal voltages to grow outside numerical range of the simulator. Moreover, the nature of this instability justifies lack of symptoms at input and output of the circuit. While voltages at branch *a* and *b* are of the same value and of the opposite phase, there is no contribution to output or input voltage. In ideal symmetrical and linear circuit this internal oscillation is invisible from the input and output terminals. It is also not detectable in two port representation of the circuit as it was already demonstrated using k-factor test. Therefore, the previous question concerning the amount of information enough to assure stability guides us to

another class of circuits for which two port representation is misleading when stability properties are brought up. A simple experiment shows the source of this error. As it was demonstrated by Platzker and W. Struble in [2] original and reduced network, the determinant carries different amount of information about the circuit properties. If original circuit is described as follows:

$$\begin{bmatrix} Y_{11} & Y_{12} \\ Y_{21} & Y_{22} \end{bmatrix} \cdot \begin{bmatrix} V_1 \\ V_2 \end{bmatrix} = \begin{bmatrix} I_1 \\ 0 \end{bmatrix} \tag{82.}$$

, where Y_{11}, Y_{12}, Y_{21} and Y_{22} elements are sub-matrices and V_1, V_2 and I_1 are the column vectors of the appropriate dimensions. Y_{22} can be eliminated by a direct substitution and the representation of the reduced circuit is obtained as:

$$\left[Y_{11} - Y_{12} \cdot Y_{22}^{-1} \cdot Y_{21}\right] \cdot \left[V_1\right] = \left[I_1\right] \tag{83.}$$

The determinants of the original and reduced circuits can be obtained:

$$\begin{aligned} &\det\left[Y_{11} - Y_{12} \cdot Y_{22}^{-1} \cdot Y_{21}\right] \cdot \det\left[Y_{22}\right] && \text{- for the original circuit} \\ &\det\left[Y_{11} - Y_{12} \cdot Y_{22}^{-1} \cdot Y_{21}\right] && \text{- for the reduced one.} \end{aligned} \tag{84.}$$

The difference between the two above determinants is clear and the impact on the stability analysis could be summarized into the three cases:

- The determinant of the sub-network has no zeros in the Right Half Complex Plane. Any network pole can originate only from zeros of the determinant of the reduced network and can be detected.
- The determinant of the sub-network Y_{22} contains all the Right Half Complex Plane zeros of the original network determinant. The determinant of the reduced network will have no zeros or poles in the Right Half Complex Plane and its analysis will not give us true information about the stability of the original circuit.
- Both determinants have zeros in Right Half Complex Plane. In this case, only partial information about stability can be obtained from analysis of a reduced network.

When the two-port representation of the circuit belongs to the second class of the circuits system poles, they are not observable via two port parameters. In such a case the positive result from the classical two port stability methods give no certainty about the unconditional stability of the network. It can be observed in case of the example parallel amplifier presented before. If determinant of the circuit terminated with 50Ω terminations is tested with numerical methods, three zeros are found:

$$\begin{aligned} s_1 &\cong -1.221 \cdot 10^8 \\ s_2 &\cong -1.483 \cdot 10^{10} \\ s_3 &\cong -1.682 \cdot 10^{10} \end{aligned} \tag{85.}$$

If additional two ports will be introduced in a way presented in Figure 21, the circuit will be described with the equation (86.):

$$Y = \begin{bmatrix} Y_{11} & 0 & Y_{13} & Y_{13} \\ 0 & Y_{22} & Y_{23} & Y_{23} \\ Y_{21} & Y_{32} & Y_{33} & Y_{34} \\ Y_{21} & Y_{32} & Y_{34} & Y_{33} \end{bmatrix}$$

$$Y_{11} = \frac{1}{R + \frac{s \cdot L}{2}}$$

$$Y_{13} = -\frac{1}{R} \cdot \frac{\frac{s \cdot L \cdot R}{s \cdot L + R}}{s \cdot L + \frac{s \cdot L \cdot R}{s \cdot L + R}}$$

$$Y_{21} = -\frac{1}{2 \cdot R + s \cdot L}$$

$$Y_{22} = \frac{1}{R + \frac{s \cdot L}{2} + \frac{R_2}{2 + 2 \cdot s \cdot R_2 \cdot C}}$$

$$Y_{23} = -\frac{\left(s \cdot L + \frac{R_2}{1 + s \cdot R_2 \cdot C}\right) \cdot \left(1 - \frac{g}{s \cdot C}\right)}{\left(R + s \cdot L + \frac{R_2}{1 + s \cdot R_2 \cdot C}\right) \cdot \left(s \cdot L + \frac{R \cdot \left(s \cdot L + \frac{R_2}{1 + s \cdot R_2 \cdot C}\right)}{R + s \cdot L + \frac{R_2}{1 + s \cdot R_2 \cdot C}}\right) \cdot \left(1 + \frac{1}{s \cdot R_2 \cdot C} + s \cdot C \cdot \left(s \cdot L + \frac{R \cdot \left(s \cdot L + \frac{R_2}{1 + s \cdot R_2 \cdot C}\right)}{R + s \cdot L + \frac{R_2}{1 + s \cdot R_2 \cdot C}}\right)\right)}$$

$$Y_{32} = -s \cdot C \cdot \left(1 - \frac{R + \frac{s \cdot L}{2}}{R + \frac{s \cdot L}{2} + \frac{R_2}{2 + 2 \cdot s \cdot R_2 \cdot C}}\right)$$

$$Y_{33} = \frac{1}{R_1} + g + \frac{1}{s \cdot L + \frac{s \cdot L \cdot R}{s \cdot L + R}} + \frac{\left(\frac{1}{R_2} + \frac{1}{s \cdot L + \frac{R \cdot \left(s \cdot L + \frac{R_2}{1 + s \cdot R_2 \cdot C}\right)}{R + s \cdot L + \frac{R_2}{1 + s \cdot R_2 \cdot C}}}\right) \cdot \left(1 - \frac{g}{s \cdot C}\right)}{1 + \frac{1}{s \cdot R_2 \cdot C} + s \cdot C \cdot \left(s \cdot L + \frac{R \cdot \left(s \cdot L + \frac{R_2}{1 + s \cdot R_2 \cdot C}\right)}{R + s \cdot L + \frac{R_2}{1 + s \cdot R_2 \cdot C}}\right)}$$

$$Y_{34} = -\frac{1}{s\cdot L}\cdot\frac{\frac{s\cdot L\cdot R}{s\cdot L+R}}{s\cdot L+\frac{s\cdot L\cdot R}{s\cdot L+R}} - \frac{\frac{R_2}{1+s\cdot R_2\cdot C}}{s\cdot L+\frac{R_2}{1+s\cdot R_2\cdot C}}\cdot\frac{\frac{R\cdot\left(s\cdot L+\frac{R_2}{1+s\cdot R_2\cdot C}\right)}{R+s\cdot L+\frac{R_2}{1+s\cdot R_2\cdot C}}}{s\cdot L+\frac{R\cdot\left(s\cdot L+\frac{R_2}{1+s\cdot R_2\cdot C}\right)}{R+s\cdot L+\frac{R_2}{1+s\cdot R_2\cdot C}}}\cdot\frac{1-\frac{g}{s\cdot C}}{1+\frac{1}{s\cdot R_2\cdot C}+\frac{1}{s\cdot C\cdot\left(s\cdot L+\frac{R\cdot\left(s\cdot L+\frac{R_2}{1+s\cdot R_2\cdot C}\right)}{R+s\cdot L+\frac{R_2}{1+s\cdot R_2\cdot C}}\right)}}$$

(86.)

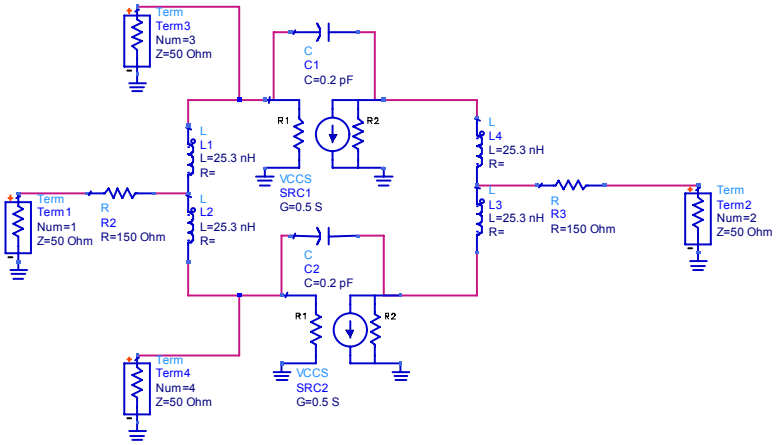

Figure 21 Example parallel amplifier as a four port network.

For the numerically computed zeros of the determinant of the four port description a right half complex plane conjugate pair of zeros is revealed.

$$\det\left(\begin{bmatrix} Y_{11}+Y_0 & 0 & Y_{13} & Y_{13} \\ 0 & Y_{22}+Y_0 & Y_{23} & Y_{23} \\ Y_{21} & Y_{32} & Y_{33} & Y_{34} \\ Y_{21} & Y_{32} & Y_{34} & Y_{33} \end{bmatrix}\right) \rightarrow s_1 \cong 1.139\cdot 10^9 \pm 2.25\cdot 10^9$$

(87.)

The same conjugate zero pair could be discovered while the matrix (88.) is checked. This matrix is equivalent of Y_{22} element from equation (82.) and contains elements of four port description of the example parallel amplifier - (86.).

$$Y = \left[\begin{array}{cc|cc} Y_{11}+Y & 0 & Y_{13} & Y_{13} \\ 0 & Y_{22}+Y_0 & Y_{23} & Y_{23} \\ \hline Y_{21} & Y_{32} & Y_{33} & Y_{34} \\ Y_{21} & Y_{32} & Y_{34} & Y_{33} \end{array}\right] = \left[\begin{array}{c|c} Y'_{11} & Y'_{12} \\ \hline Y'_{21} & Y'_{22} \end{array}\right]$$

$$\det\left(Y'_{22}\right) = \det\left(\begin{bmatrix} Y_{33} & Y_{34} \\ Y_{34} & Y_{33} \end{bmatrix}\right) = 0 \rightarrow s_1 \cong 1.139 \cdot 10^9 \pm 2.25 \cdot 10^9 \quad (88.)$$

This result indicates the second possibility , for that reason two port representation will not give us true information about the stability of the original circuit. It is quite a disturbing discovery as the amplifier used as an example is representative of a general group of the multi-device parallel amplifiers. These amplifiers are an important group, especially in the integrated circuits environment. The idea behind the paralleling smaller amplifiers is to introduce a compromise linking more complicated structure and loses of additional combiners versus higher: output power, gain and bandwidth performances of a single smaller power stage. However, as it was presented, these amplifiers are susceptible to particular instability called Odd mode oscillations.

1.2.5 Odd mode oscillations

In general, in the circuit of *n* parallel combined devices can exist *n* modes of operation. The stability analysis with K and Δ or μ factors addresses only one particular mode of the circuit, thus amplifiers can still oscillate in others in spite of fulfilling the requirements of the previously mentioned factors. The typical, two port representation of simplified circuit of the parallel combined amplifier was supplemented with internal branch currents and presented in Figure 22.

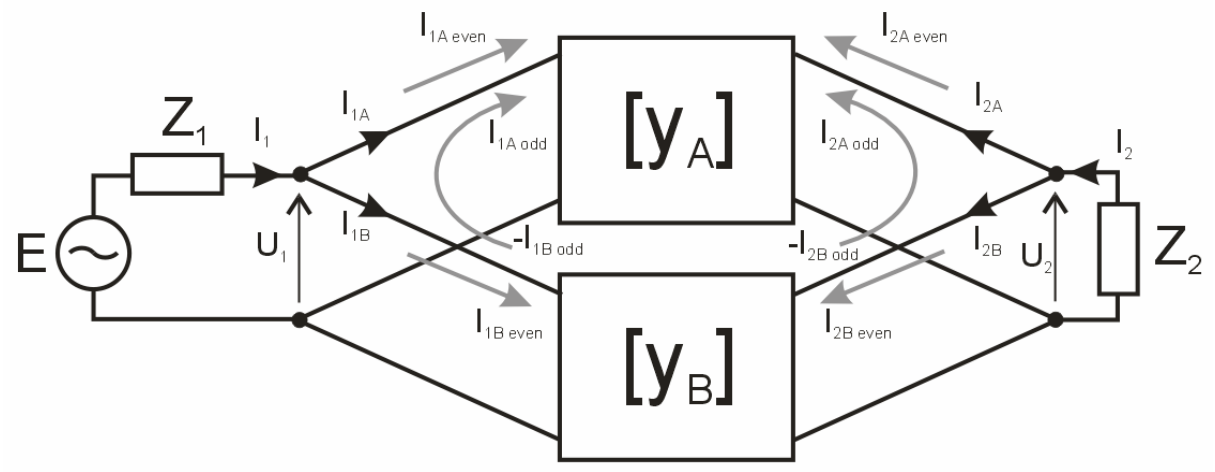

Figure 22 Parallel amplifier example with marked odd and even mode currents.

The voltage in each branch at input and output is the same. In contrast, the input and output branch currents may not be equal. This situation is described with following equations for input terminal. Same equations could be used to describe output currents.

$$I_1 = I_{A1} + I_{B1}$$
$$\begin{matrix} I_{A1} = I_{A1,even} + I_{A1,odd} \\ I_{B1} = I_{B1,even} + I_{B1,odd} \end{matrix} \rightarrow I_{B1,odd} = -I_{A1,odd} \rightarrow \begin{matrix} I_{A1} = I_{A1,even} + I_{A1,odd} \\ I_{B1} = I_{B1,even} - I_{A1,odd} \end{matrix}$$
$$I_1 = I_{A1,even} + I_{A1,odd} + I_{B1,even} - I_{A1,odd} = I_{A1,even} + I_{B1,even} = I_{1,even}$$

(89.)

It is clear form (89.) that *odd* component of the internal currents I_{A1} and I_{B1} is not observable from the input terminal of the amplifier. The input current is related only to the *even* component. This is the base of the failure for the standard two-port network stability tests. They are related only to *even* component which is in general the only one of *n* super-positioned current components in the circuit. This is exactly same situation as in case of the state space representation stability analysis with use of the system modes. In this situation system modes will be called 'modes of operation'. In case when each amplifier is excited by a desired mode in phase and with the same signal amplitude it is called the Even mode. In contrast, unintentional modes characterized by the opposite phase among parallel branches are called Odd modes. In a truly linear circuit the odd modes instabilities lead to oscillations which are not observable from the circuit terminals which was demonstrated with the previous example. But in case of the real circuits the oscillations will mix with the even mode on nonlinearities and will become detectable as spurs signals. Such behaviour leads to deterioration of the amplifier performance and eventually shows the way to catastrophic failures of the active devices.

Another interesting observation resulting from the fact that the odd mode is decoupled from terminals of circuit is the independency of the odd mode oscillations from the input and output impedances values. They are dependent only in the internal structure of the circuit. This happens in contrast to the even mode stability of the circuit. These differences between Even and Odd mode results in the end in the ineffectiveness of widely used, common stability tests. At the same time the growing market of the IC power amplifiers faces designers in need for designing amplifiers prone to the odd mode instabilities. Thus, the robust test as well as a designing tool allowing to avoid this particular problem is needed. In the following chapter than, designing reality concerning multi-device power amplifiers will be presented. Then, a few stability tests dedicated to such structures are to be presented along with extensions and example CAD implementation.

2 MULTI-DEVICE POWER AMPLIFIER

Historical start of the electronics could be dated back to 1906 and the invention of the triode lamp. Lee De Forest discovery triggered off interest in electronic that did not weaken till today. In result, new science lead to development of such ubiquitous possessions of nowadays as: radio, radar, TV, or wireless communication, which dramatically changed our life and our perspective of the world. Freedom of the relatively young personal wireless communication was quickly adopted and became a must be in modern world. Increased mobility of the people forces wireless communication systems to a constant development and growing accessibility. This in result leads to hunger for more and more advanced technologies and at the same time costly effective solutions. This tendency has a direct impact on today's microwave electronics as tubes, historically first, are now slowly abandoned holding to the last resort of the high power applications. Moreover, with technology improving each day, more and more circuits built with younger in comparison to tubes solid state discrete devices are integrated into the single chips. Reproducibility obtained in such a way results in a mass production possibility. Combining this fact with the integration capability causes fewer number of the components in the system as well as increased reliability, while integrated circuit approach leads to pricy effective solution. At the same time increasing throughput demands from communication systems forces new standards involving a more complex digital modulations schemes. Speed and complexity of these modulations place designers in a difficult position while linearity and bandwidth requirements are somehow in contradiction to the output power and efficiency of their designs. It is especially evident in the case of the power amplifier which is an essential element of any transmitter and in result, this contradiction will have a direct implication on any mobile device performance. Linearity and bandwidth requirements forced by the system requirements will have negative impact on the efficiency and the output power. These two factors can be observed directly with limited range and battery operation time of the device. Additional requirements to a mobile device like space occupation and thermal performances as well as low cost make the design task very demanding. All these factors have a direct implication on today's power amplifier design reality and it is not only restricted to mobile device power amplifiers. Bandwidth, gain, efficiency, output power, cost and complexity, plus thermal management trade off the existence of any power amplifier designed commercially. Therefore, there are various approaches to the problem of the power amplifier design that allow to find different compromises. Among them a power combining approach serves a very important role. In the following chapter its importance is emphasized along with a specificity of the Integrated Circuit approach to the power combining. A draft of the simple design of the example combining/matching section is presented with a special attention to a widely used cluster matching approach and capacitive loading.

2.1 Way to increase output power of the Power Amplifier

If a question arises: how to design a power amplifier within some specific set of rules? A straightforward answer will be to search for an appropriate active device that can fulfill these requirements. However, what kind of an approach will be possible if the output power requirement is increased? Again, a straightforward idea is to find a bigger device. Unfortunately, this is not always achievable. Moreover, if otherwise, bigger device in comparison to the smaller one will suffer from

bigger parasitics, increased Q-factor and limited maximum frequency of operation. That will have influence on bandwidth performances, poor phase linearity and lower manufacturing tolerance of the final amplifier. The size increase of the multi-finger devices will result in higher phase differences between the fingers what leads to a smaller gain. Moreover, scaling rules at some point are no longer linear restricting device maximum size. And finally, in case of the high power active devices thermal problems become difficult to resolve.

Another approach is a well know possibility of power combining. With an assumption to use the ideal combining structures it is theoretically possible to reach any output power level maintaining performances of the combined amplifiers. Obviously, this is not likely in the real world but in most of the cases combining techniques can greatly extend design possibilities of the power amplifiers. A tendency to use a bigger device is not always better or cheaper solution. Moreover, in the integrated circuit reality it may be not even possible while the biggest size is limited by thermal issues or DC current handling possibilities of the process. Besides all, the previously mentioned limitations will deteriorate performances of the bigger device in comparison to the smaller one. Ultimately, in most of the cases, foundries provide and support device models only in some specific range of the dimensions, making the use of bigger devices inconvenient and risky. Therefore, combining techniques in monolithic approach are very common despite of the low loss combiners design difficulties, limited space and planarity requirement. Further, the combining techniques could be used to introduce additional properties to amplifiers and they may be introduced either onto the device, circuit or system level. Thus, a special attention will be paid to the combining techniques and combining structures in the following paragraph.

Obviously, the simplifications introduced into the idea of the amplifier design and its redesign in case of the increased output power requirement was very serious. Therefore, the initial design was considered as a single ended simplest case. There exists a variety of alternatives that can be used as a starting point or yet as techniques to increase the output power.

2.2 Power combining

As it was already stated before, power combining serves an important role extending design possibilities to the power amplifier designers. Moreover, the power combiner/splitter serves a crucial role as a fundamental building block in mixers, modulators, phase shifters, feed networks of phased-array antennas, linearizers. Thus, there exist various approaches to power combining which reflect special needs of applications where combiners are used. Each type of structures developed for them will possess unique set of advantages and disadvantages that will be additionally strengthen or weakened by technology used for the realization. Importance of the combiners as a building blocks triggered development of counter-measures techniques and a variety of version of original ideas widening subject of power combining even more. While a detailed analysis of power combining structures is outside the scope of this work only brief analysis will be made. (Interested readers can find more deep analysis in Appendix 1).

First of all, a brief division between combining structures is done to allow later to focus on most common combining techniques used in integrated power amplifiers - Figure 23. Spatial and non-spatial combiners can be differentiated by number of the dimensions used to perform the combining action. The difference lies in the use of a full 3D environment for combining power in the spatial combiners. That does not mean that in non-spatial combining the environment is flat but in fact indicates that the third dimension is not used to propagate waves. In multi-layer case the

environment can be described as 2,5D. In contrast, spatial combining uses three dimensional wave interference and diffraction to combine power. Clearly, the main interest in nowadays reality is taken in non-spatial combiners leaving the second case for the very particular and exotic applications. Main division that occurs in case of non spatial power combining circuits is between the resonant circuits and the transmission line circuits. It origins in turn from the interest to use metal conductor in order to propagate wave or to obtain a specific field pattern. In case of resonant circuits we will find application of patches, sector components and rings in various configurations. Their sizes are either bigger or comparable to wavelength. They are mostly narrow band structures but there are examples of structures with fractional bandwidth exceeding 40%.

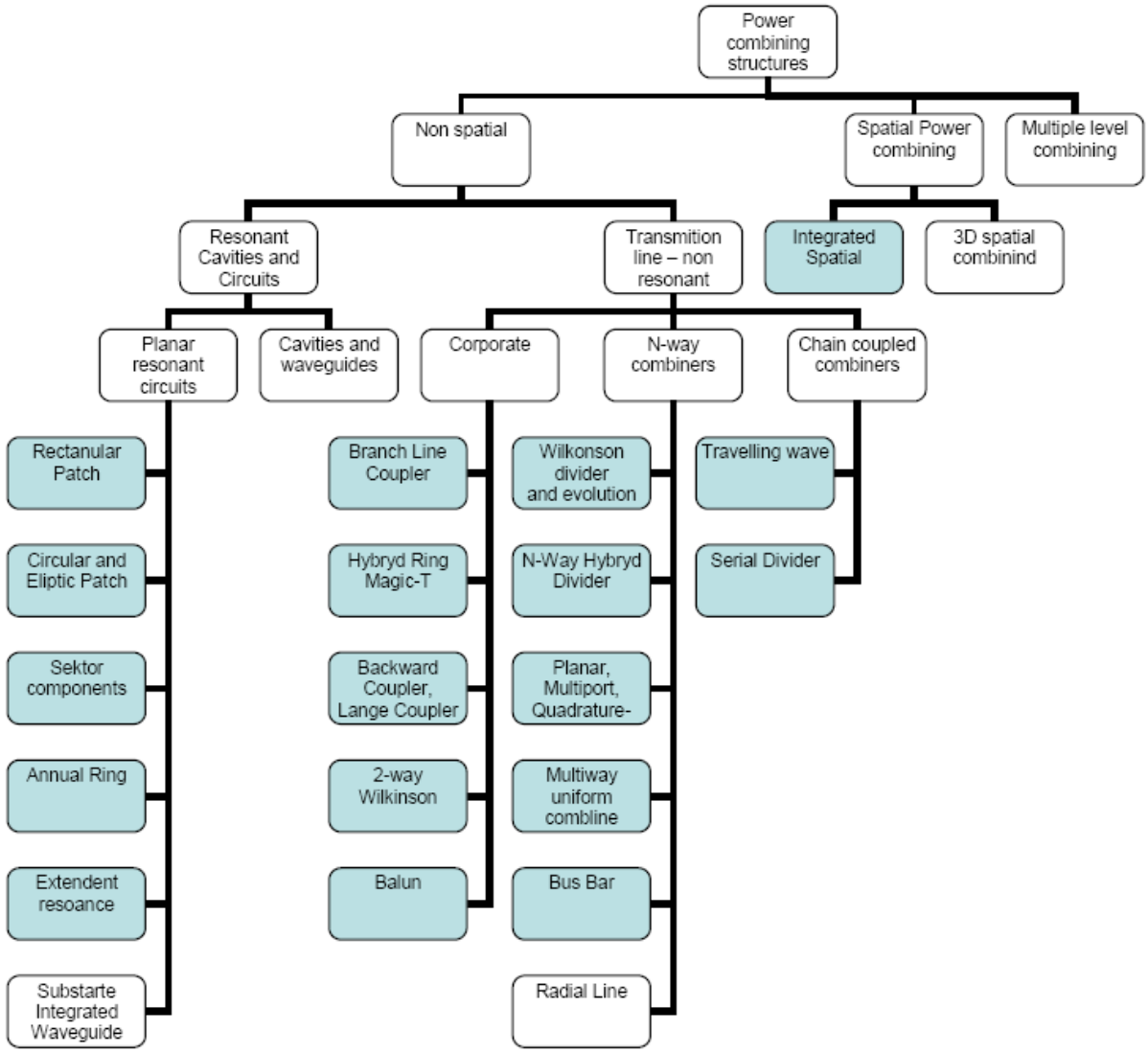

Figure 23 Division of combining structures focused on planar structures.

Transmission line combiners are structures which use the properties of transmission lines to perform power combining. The main division applicable here is differentiating between N-way combiners, corporate (tree) and chain combiners. N-way structures as it may be recognized from their name perform N way combining in one step. They are the most promising structures in obtaining high efficiency because of low loss. Unfortunately, a planarization of the structures when N>2 is often problematic. In many cases N-way combiners for N>2 are fully three dimensional structures and their

planarization leads to the loss or limitation in such important features like isolation or match. In case of corporate and serial combiners the signal needs to travel through n stages of loss network, what lowers the combining efficiency. If combiners will be lossless it is possible to obtain any amount of power at the output. Unfortunately, when they introduce losses, the efficiency of combining network is dependent on the number of stages and the loss of combiner. For corporate combiners it is possible to add a binary number of sources. Number of inputs of the network is than equal to $N=2^n$, where n is the number of combining stages. Network can be built with the use of the same three-port combiner structure, which matches impedance of input ports to the output port and maintains the isolation between inputs. For these purposes hybrid couplers are significantly useful. In case of the chain combining, we need N-1 combiners to combine N inputs. The following combiners have 3 dB to $10*\log_{10}(N)$ dB of unequal power division ratio and they add 1/N power to the main path. Loses are not equal for each combining path. Chain combining scheme is non binary and in ideal case we could combine any number of sources. Limiting factor as in the case of chain network is the loss of combiner but also difficulty to design combiners with high division ratio when N is large.

Problem of decreasing efficiency is more complex than the issue of losses of the combiners used to build the combining network. Other factors related to final quality of design are imbalance of amplitude and phase of combined signals. Problem can occur at the input of network but also inside corporate or chain networks between stages. There occurs another difficulty when large amount of signal sources are to be combined. Combiners are especially sensitive for phase imbalance. For example, to maintain 90% efficiency in case of ideal and symmetric hybrid combiner [8], phase deviation needs to be kept below 30°. Sensitivity on amplitude imbalance is not as big as in the case of phase. These values are dependent on a type of the combining element used and on the combining network topology.

Another very important issue of combining structures is a phenomenon of “graceful degradation” [9]. It is a specially important issue in design of the power amplifier with the use of low N power combiner networks. It refers to the behaviour in the case of failure of the combined amplifiers modules. Output power of m working devices is equal to $N*P*(m/N)^2$ in case of N equal P-power modules in circuit. So, it is not directly proportional to the amount of power which is generated by those working devices (m*P). Term “graceful” is related to the behaviour of the circuit which still generates power, even in the case of a breakdown of some combined modules. This feature could be interpreted as an advantageous possibility of a “soft breakdown” in comparison to the classic single ended amplifiers, but for a small amount of the combined devices the loss of power is high. Furthermore, in case of the monolithic power amplifier, soft breakdown will in the end have exactly the same consequence as a normal one while the whole amplifier needs to be replaced. Moreover, if parameters of the working power amplifier are not monitored in detail, “soft breakdown” could be difficult to detect.

In reality, owing to the fact that resonant structures are narrowband and occupy a large amount of space for the lower frequencies they are rarely considered as a power amplifier building blocks. They became more interesting structures while frequency of operation increases due to the decreasing ration between width and length of transmission lines - Figure 24. The decreasing ratio, increasing mutual coupling and difficulties with the lumped elements rises either difficulties to build transmission line couplers without special techniques. Consequently, except for extremely high microwave frequencies in range of millimeter waves, transmission line couplers are the most popular solution.

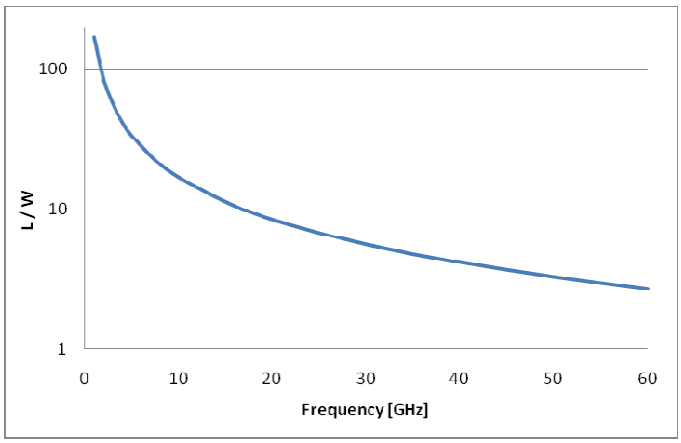

Figure 24 Ratio between length (L) and width (W) of the 35 Ohm quarter-wave transmission line versus frequency. Substrate data: Er=12.9, H=100um, T=1.25um, Cond=5.7e7, TanD=0.006. Source - Agilent LineCalc.

2.2.1 Integrated Circuit reality

If Integrated Circuits reality will be considered as an environment for the power combining, the choice of combining element will be further limited. The most straightforward limitation was already mentioned: planarity, dimension, losses. A limited height of conductor layer increases resistance of transmission lines and restricted current handling capabilities. The first effect is partially reduced by high electric constant of semiconductor substrate which reduces physical dimensions. The second restricts the range of possible transmission line characteristic impedances for the given guided power. In addition, the transmission lines dimensions resulting from a direct application of typical combiners to IC reality are in most of the cases too big. Large in this case means costly, as precious semiconductor substrate is used to create passive component. As a result, the choice of combining scheme is again a compromise, where physical dimension and planar realization is confronted with electrical performance of structures. Unfortunately, the planar restriction affects severely N-way combiner group and even with the additional electrical layer and air bridges planarized versions of N-way combiners lose some of their most appreciated properties. Other complicatedness in combining more than two sources comes from the routing problems and maintaining phase and amplitude balance within the combining network. Space occupation, losses and restricted range of possible transmission line characteristic impedances restrict a chain combining to a low number of the active devices. This results in marginal use of the chain combining idea. For that reason, except some particular ideas, the corporate combining is the most straightforward choice.

A basic version of the corporate combining network could be easily created with the usage of (N-1) hybrid combiner of same type. Loss of the efficiency of combining and routing problems could be minimized due to the symmetry properties of the structures used. Recalling that any signal path travels through $\log_2 N$ combiners, losses could be maintained on an acceptable level for a limited number of combined sources. Taking into account the existence of the general three types of the hybrid combiners designers are able to take advantage of the additional properties in case of combining/spiting network in the power amplifier. Their advantages will be pointed out with the use of uncomplicated two amplifiers cell combined: out of phase, in quadrature, and in-phase [7].

2.2.2 Out of phase combined amplifiers cell

Two amplifier cell was created by feeding two amplifiers from input splitter and recombining the output signals into output combiner network - Figure 25. Combiners provide equal amplitude and out of phase splitting.

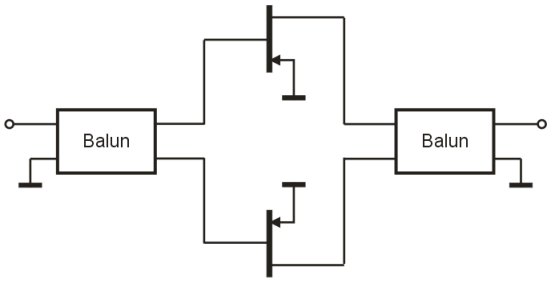

Figure 25 Out of phase combining in case of two active devices.

One of the benefits from this type of the operation is a possibility of the fundamental frequency common lead component cancellation. If the amplifiers' active devices Sources are connected to the ground with the common lead, the opposite phase of the fundamental current components causes cancelation, leading to lack of the voltage feedback from the common lead element. At the same time, such a configuration filters even harmonics, owing to their appearance in the phase at the inputs of the output combiner. However, even more encouraging advantage of this scheme is obtained if balun is used as a combiner element. Balun's characteristic impedance is the same at unbalanced and balanced output. While the balanced port is used to connect pair of amplifiers in series, impedance from the standpoint of the transistor matching section will be two times smaller. This is important feature as the smaller matching ratio sections are less demanding to the design. Alas, in the high frequency implementation benefits of the balun are weakened as wide band version of the element is difficult to design. In the case of the integrated circuits, devices are grounded by direct connection to the via holes or ground plane minimizing source parasitic feedback. Moreover, if an active device is grounded in many points only few of them are shared, which leads to a further dilution of the cancellation effect. In the low frequency region very wide band baluns are easily obtained applying the ferrite cores. Unfortunately, it is not easy at higher frequencies and for the integrated circuits. As a planar versions of the balun can be considered for example: a rat race combiner or Marchand balun. These structures occupy large area in the basic version and not possess a great advantage of decreased impedance at the balanced ports. Existence of other ideas involves creation of lumped element baluns with applying the low pass and high pass filtering structures which are even more narrowband solutions.

2.2.3 Quadrature combined amplifiers cell

Other way to combine two amplifiers is to utilize quadrature hybrids to build splitting and combining network - Figure 26. Theoretically, double amplifier cell created this way posses an incredibly useful property of being perfectly matched at the input and output port. This property is related to the phase shift introduced by the quadrature combiners. If any reflection from the amplifiers occurs, reflected signals will meet in the input/output port out of phase, hence they will not propagate. In contrast, at the isolated port of the coupler the reflected signals will meet in phase, and as a result energy delivered to the dummy load.

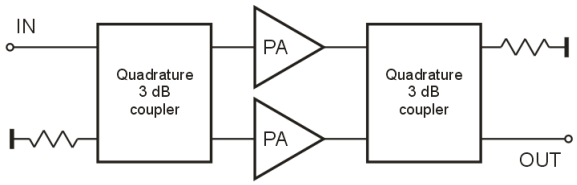

Figure 26 Quadrature combining in case of two active devices.

Such an effect can be compared to bringing into use isolators at the input and the output ports plus two times bigger power amplifier. Additionally, this configuration offers benefit of the easy power stages cascading without any need or risk of interstage matching sections design. What is more, the stability of such amplifier is greatly improved. On the contrast, it occupies a lot of space. To realize it, there exists a variety of different possible combiner structures: branch line coupler, coupled lines, Lange coupler. These structures are well documented and numerous techniques improving their performances have been developed.

2.2.4 In-phase combined amplifiers cell

In-phase combination of the amplifiers is the simplest case and most commonly it is prepared with the employment of Wilkinson combiners - Figure 27.

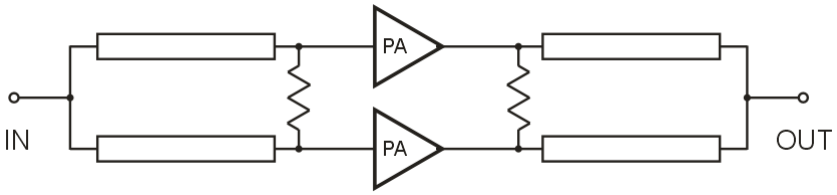

Figure 27 In-phase combined amplifiers cell.

Wilkinson combiner is a three port network created by parallel connection of two quarterwave transmission line impedance transformers and isolating resistors. This is a very particular three port structure which can be matched at all ports and is lossless while operated properly. This is owed to the fact that in reality it is four port network with isolating resistor permanently closing one port. Two amplifiers cell created this way does not have any unique advantages except for the general simplicity in the design. This simplicity comes from a few facts. The used transmission lines impedances are in desirable range for typical Z_0=50Ω application. Full symmetry of structure is highly appreciated in the case of multi level combining schemes. Isolation provided by the structure helps to maintain the odd mode oscillations problems. Regrettably, in-phase combining with the use of Wilkinson combiner suffers from losses in the case of a thin conductor layer and large area occupation. On the other hand, this combining structure is a well known and developed element for which many additional techniques have been applied to improve performances or introduce some additional, particular properties.

By knowing three basic approaches designer is able to trade their complexity for improving some properties of the amplifier. A brief analysis proves that a low frequency nonintegrated design, especially in the case of a dedicated pair of active devices works in favor of the out-phase phase combining. These advantages tend to dilute with higher frequency of the operation along with additional difficulties due to a design of the integrated balun. However, if it is possible, the balun impedance transformation property is a great benefit and should not be discarded. Quadrature

combining offers a benefit of wideband match and improved stability, thus it seems to be very attractive while in-phase combining seems to carry only simplicity, symmetry and the space occupation advantage. In most of the cases these tree factors will be the most important. Taking into account a precious space occupation and simplicity of routing in case of the full symmetry, Wilkinson combiner is compromise winner. Though it happens so only in the theory while it comes to the integrated power amplifiers. Size of the classic structure is unacceptable in most of the cases. Hence, additional several techniques were introduced to a shrink combiner. Among these were: lumped element equivalent, capacitive loading of the transmission lines, shunt and series stub loading of the transmission lines, PBG slow-wave transmission lines structures, meander coupled line with inductive slit, multilayer approaches, active inductors use and stepped impedances. Yet, these techniques if possible to implement into integrated circuits reality, had a price to pay. Certainly, the simplicity benefit disappears. Without a doubt, some reasonable compromise needs to be found again, which may lead to a modification of the initial assumption regarding the combining scheme. To illustrate the problem, a simplified example of the four device amplifier combining and matching the output network design considerations is presented below.

2.3 In-phase combining/matching topology discussion

For the amplifier presented in the Figure 28 design of the output section was considered. Also, an initial assumption was made to use in-phase combining scheme based on Wilkinson combiner to combine four signal sources.

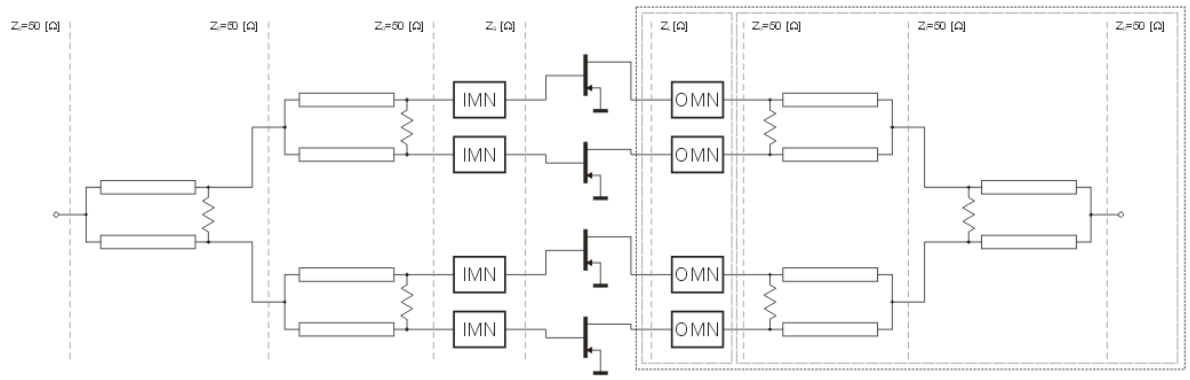

Figure 28 Four device power amplifier.

Then, an optimal impedance of the devices was assumed to achieve straightforwardness as Z_l=5Ω. Consequently 1:10 matching sections (OMN) were needed to connect devices and the combining network. With such a high transformation ratio it is expected that a simple matching circuit will be narrowband. If for simplicity, quarterwave transformer was assumed as an initial solution, it is effortless to observe on the Smith chart that a single matching section needs to have much higher Q than for example three stage one - Figure 29. For the fractional bandwidth defined at Gamma<-20 dB, the following results were obtained: 9% for one section, 34% for two sections, 76% for three sections - Figure 30. While the combining network fractional bandwidth equals 47%, a three stage structure was chosen as not to be a limiting factor of the design. Additionally, one section transformer was also chosen and will serve as a starting reference point as to compare the networks performances.

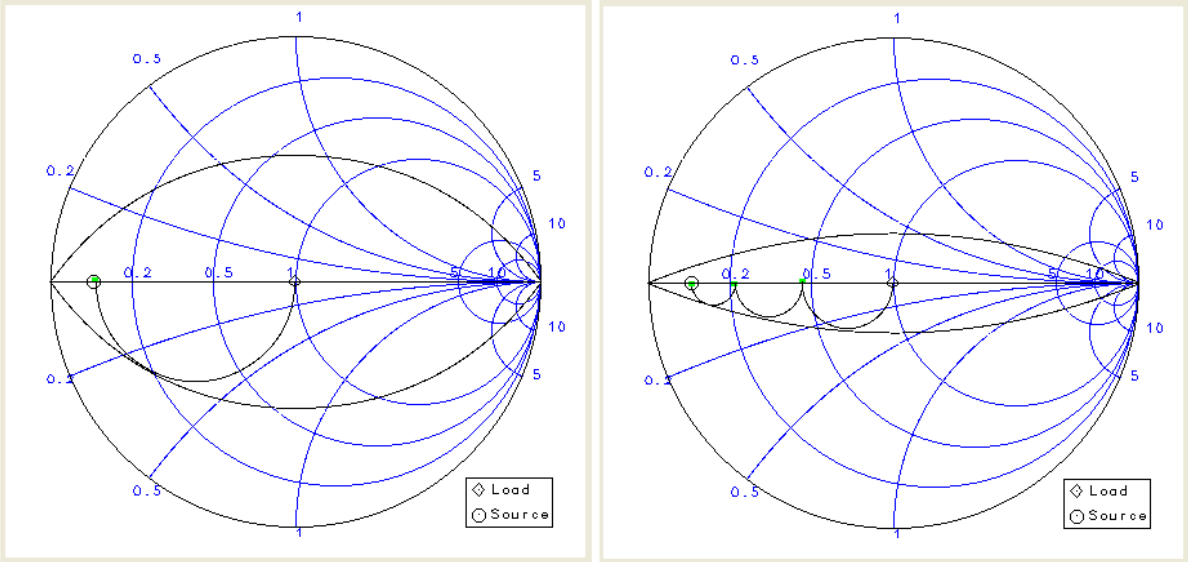

Figure 29 Matching Zs=5 Ohm with one and with three steps.

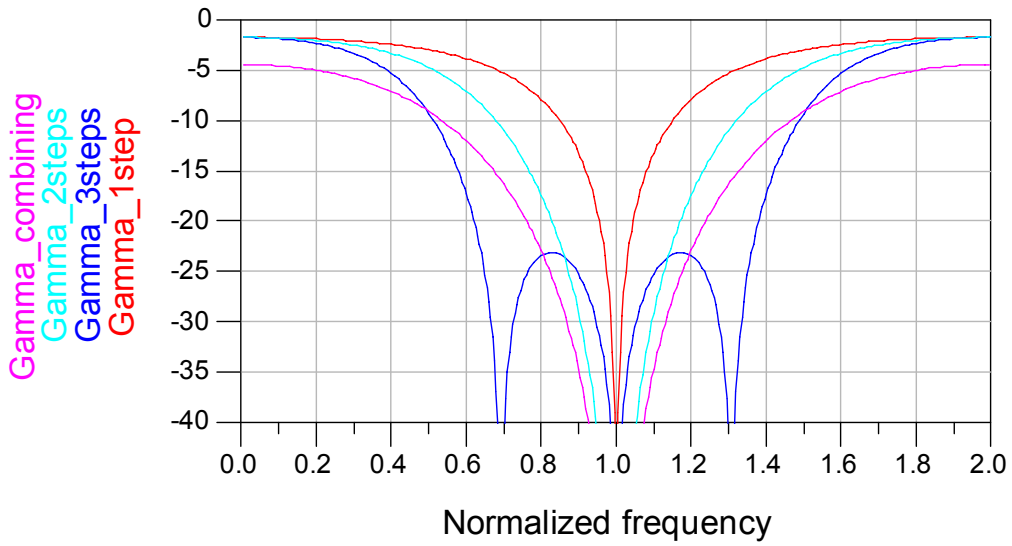

Figure 30 Bandwidth behaviour of: one, two, three sections matching circuits and combining network.

If the chosen initially two variants of the circuit were to be investigated, a few important facts needs to concerned. In general, the size of both structures is in not an acceptable range. If a simple draft is prepared without any precise consideration of the transmission line widths, it is likely to observe that the introduction of the three section quarterwave matching circuit nearly doubled the required substrate area. Furthermore, investigation of the transmission lines impedances of the transformers reveals their realization problems. taking into account a typical range of possible to realize transmission line impedances, both networks fall out of it. One stage transformer uses $Z_{0,q1}\approx15.8\Omega$ quarterwave transmission line. Three section transformer use $Z_{0,q1}\approx7.3\Omega$, $Z_{0,q2}\approx15.8\Omega$ and $Z_{0,q3}\approx34\Omega$ quarterwave transmission lines. Thus, if the range of the possible in order to realize the transmission lines is estimated as: $Z_{0,min} = 40\Omega$ to $Z_{0,max} = 85\Omega$, none of the mentioned transformers could be used.

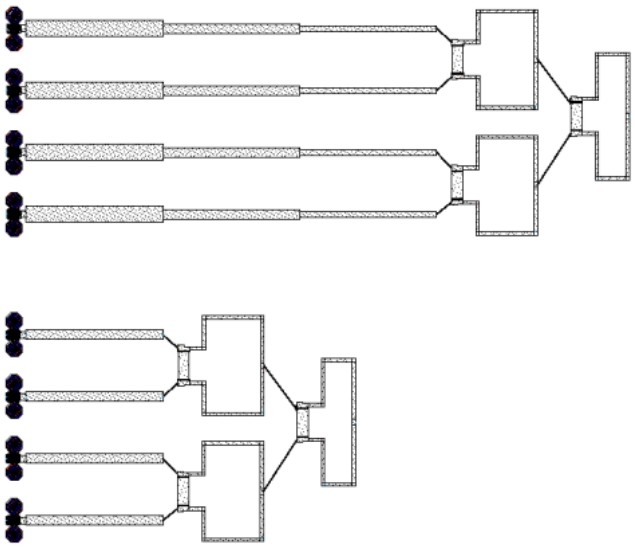

Figure 31 Draft of two basic approaches for output combining/matching section of the example amplifier: three section matching circuit (top) and one section matching circuit (bottom).

If we neglect this difficulty for a moment, it is achievable to notice in the Figure 31 that the combiners in the draft are not connected with the transmission lines. To complete design, 50Ω interconnection lines need to be introduced. This in turn may well be treated as another waste of space. In such an arrangement design is clearly divided into a combining and matching block. A question is raised: what happens if this clear division will be discarded?

2.3.1 Cluster matching

Corporate structures for which matching and combining sections are alternated along the combining line are often described as the ones involving the idea of the cluster matching [14]. It is particularly evident while the symmetry is involved in creation of such a tree. If a simple alternation of sections is introduced to an initial idea of combining/matching circuit, better space arrangement may well be obtained - Figure 32. Further reduction is yet possible if the first quarterwave line transformer will be meandered. Sadly, this circuit is unrealizable whilst in the result of the sections alternation, combiners need to be redesigned for the intermediate values of impedance. In that particular case these values are $Z_{0,I1}$≈10.7Ω and $Z_{0,I2}$≈23.2Ω. Opportunely, Wilkinson's divider designed for impedance Z_0 requires transmission lines of the impedance $Z_{0,TL}=\sqrt{2}\cdot Z_0$, regrettably they are still outside the proper range with the values of the: $Z_{0,TL1}$≈15.2Ω and $Z_{0,TL2}$≈32.8Ω. If realization problems will be neglected another time, a question may raise: is there a possibility to join the combining action and impedance transformation? The response in case of the Wilkinson divider is affirmative - [10]. After this operation, the circuit will resemble the bottom one from the Figure 31 and will be comprised of one quarterwave transformer along with the two Wilkinson combiners that transform impedance with same ratio as transformer. Increased impedance of the transmission lines used for Wilkinson combiners allows a realisation of one of the combiners whereas: $Z_{0,TL1}$≈22.3Ω and $Z_{0,TL2}$≈48.1Ω. Sadly, further problem exists to connect combiners with unrealizable characteristic impedance of $Z_{0,I2}$≈23.2Ω, and once more, first quarterwave transformer is not reachable.

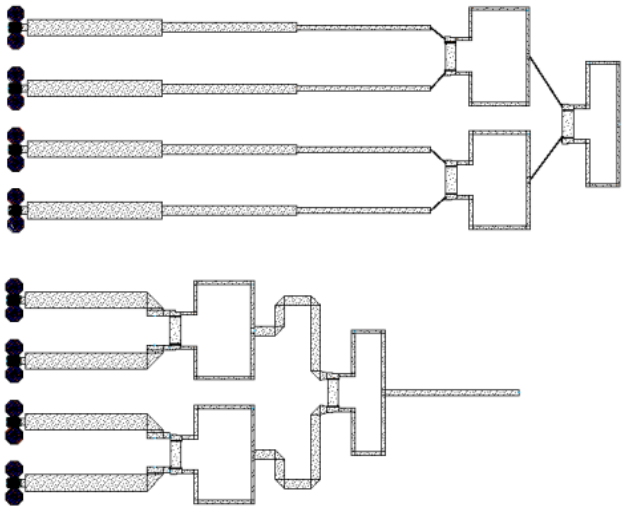

Figure 32 Draft of two approaches for output combining/matching section of the example amplifier: separate blocks for matching and combining (top) and mixed function circuit (bottom).

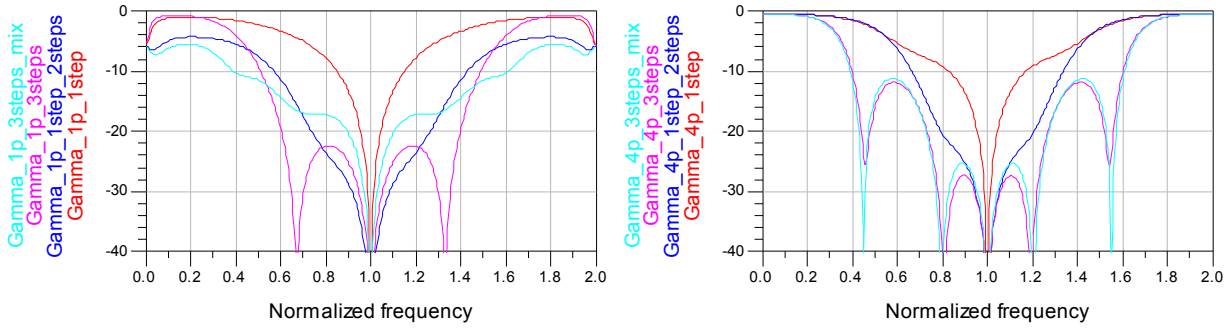

Figure 33 Input reflection coefficient for tested networks: single port excitation (left), in-phase four port excitation (right). 1step – one stage transformer, 3step – three stages transformer, 3step_mix – three stages transformer mixed with combiners, 1step_2steps – one transformer and two impedance transforming power dividers.

If networks performances are to be compared despite the realization doubts, reflection coefficient simulation procedure requests to be clarified. As it is visible in the Figure 33, there exist two ways to measure input reflection coefficient of the combining network. One resembles classical S parameter measurement, when all other ports except the measured one are closed with appropriate terminations. Reflection coefficient measured in this way is evidently valid but describes network excited from one port and in case of this example amplifier such a situation can occur only at the input or output of the whole amplifier circuit. As a result, for this way simulated output matching/combining network, reflection will be valid no more than for the output port. For normal operation of the amplifier all the inputs are excited with the same amplitude and phase. For that reason, to estimate performances of combining network this particular kind of excitation is requested.

As an outcome to this discovery two observations can be made. One is as effortless as an interpretation of the curves which shows that bandwidth computed for Gamma<-20 dB is: B_1=9% for the basic structure with one transformer, B_2=53% for the three stage transformer, B_3=54% for the three stage transformer mixed with combiners, whereas B_4=40% for the one stage transformer and impedance transforming Wilkinson combiners. Thus, the preformed actions resulted in increased bandwidth, according to the intentions. While considering drafts' area occupation, the bandwidth increases from B_1=9% to B_2=53% with a big increase in the circuit size. The second approach resulted

from the components reorganization - attaining more compact structure but still unsatisfactory big. The third approach was to preserve even more space by merging impedance transformation and combing functions into one element. A draft of such circuit is identical to an initial structure with one transformer while the bandwidth was increased to B_4=40%. An idea behind this concept is to introduce intermediate impedance values along the combining path in the same way as it is done in multistage transformer. Smaller impedance changes result in better bandwidth performances, besides their distribution along the combining path allows for the superior space usage. Similar idea as in cluster matching, but here with making use of Wilkinson structure rather than parallel connection of clusters.

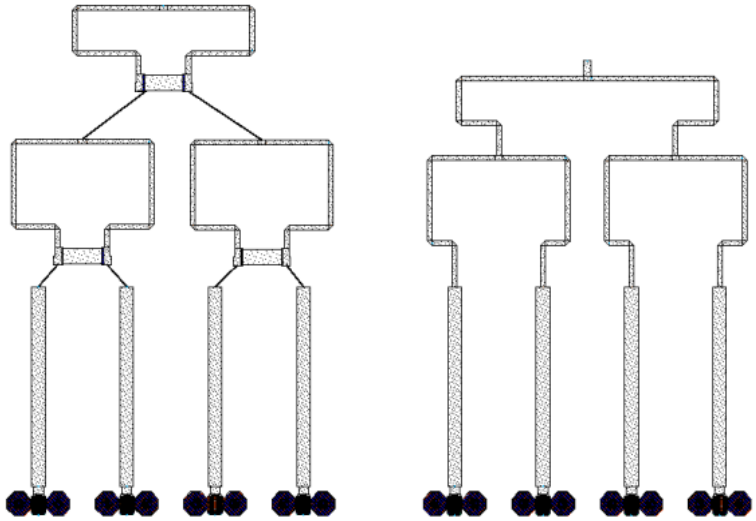

Figure 34 Draft of two approaches for output combining/matching section of the example amplifier: with use of Wilkinson combiners (left) and combiners without isolating resistance (right).

The second observation comes from a problem of reflection coefficient measurement. In-phase excitation of all input ports adopted to test performances of combining/matching network has an interesting impact on the Wilkinson combiners. In this case the voltage at both arms of a combiner at the same distance from common end is equal. Clearly, it also stays the same at the two excited in phase inputs – so there is no voltage difference across an isolation resistor and there is no current. As a result there will not be any change in performances of the combiner excited in-phase if isolating resistor is removed. This is an especially interesting discovery which has potential to solve problem of Wilkinson combiner topology. These problems are related to pure resistance element required between the combiner input ports. The element implies its small size due to an expected lumped nature at microwave frequencies. As an outcome, the problems of coupling, parasitics and difficulties in routing of the interconnection lines for the combining tree structures are inevitable. Without the resistor, the combiner can be “opened” solving most of the problems. Consequently, by removing the resistors it is likely to avoid interconnection lines in not realizable impedance range and increase efficiency of space occupation - Figure 34. Interestingly, the combiner built this way is in fact just a parallel connection of two sources with impedance transformers. If characteristic impedance along combining path is traced, it is possible to observe influence of the transformers and combining on its value at different points - Figure 35. Starting from the one of the input ports, impedance Z_l is transformed to impedance Z_{l1} and then to $Z_{Tee1}=2*Z_{l2}$. At this point, the two signal paths are combined by a parallel connection, thus the impedance is divided by two and decreased to Z_{l2} value.

A parallel connection of these two sources with identical transformers creates the first level cluster (Cluster 1 in the Figure 35). Owing to the symmetry, identical structure is used for the two other sources. Furthermore, to complete the design of the circuit two Clusters 1 subcircuits are required to be combined and matched to characteristic impedance Z_0. Therefore, the quarterwave transformers increase characteristic impedance Z_{I2} of the Cluster 1 subcircuits to $Z_{Tee2}=2*Z_0$ and their parallel connection results in a required value of the final structure output impedance. Combined in this way first level clusters may well be treated as second level cluster in the case of a further combining need. This time approach is an exact reflection of the cluster matching idea. Moreover, it presents a difficulty of the in-phase combining of the N low impedance signal sources, which means a further increase of the transformation ratio between the input and output by N.

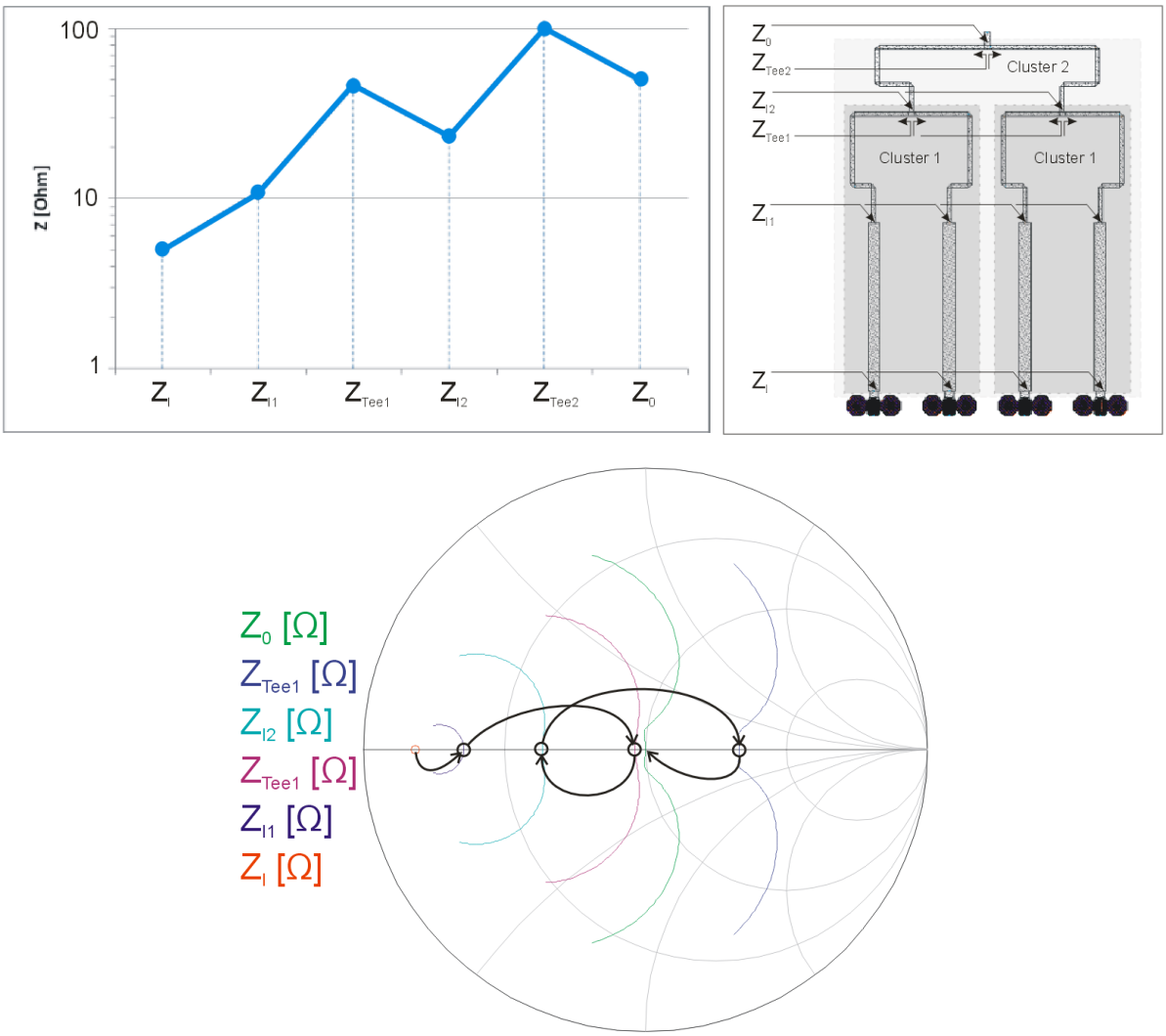

Figure 35 Characteristic impedance change along combining path in circuit comprised of one transformer and two impedance transforming power dividers. Top graph – value at f_0, bottom - characteristic impedance in normalized frequency range of (0.5,1.5).

While this was an evolution of the previous approaches, the impedance transformation steps are not equal and performance of combining matching circuit is not optimal, for that reason could be improved (for Gamma<19dB bandwidth will increase form B=42% to B=64% due to change for equal increment in matching sections). Even if impedance Z_{I2} is below the realizable value, it is probable to

avoid its usage whilst the combiners did not use resistors. Alas, the impedance of the two other transmission lines used is out of the achievable to realize the range.
A removal of the resistor is transparent to performances of the assumed in-phase and equal-amplitude excitation except that it has it cost. The network designed in such a way loses the benefits that the Wilkinson combiner has over a simple Tee structure: an isolation between the inputs.

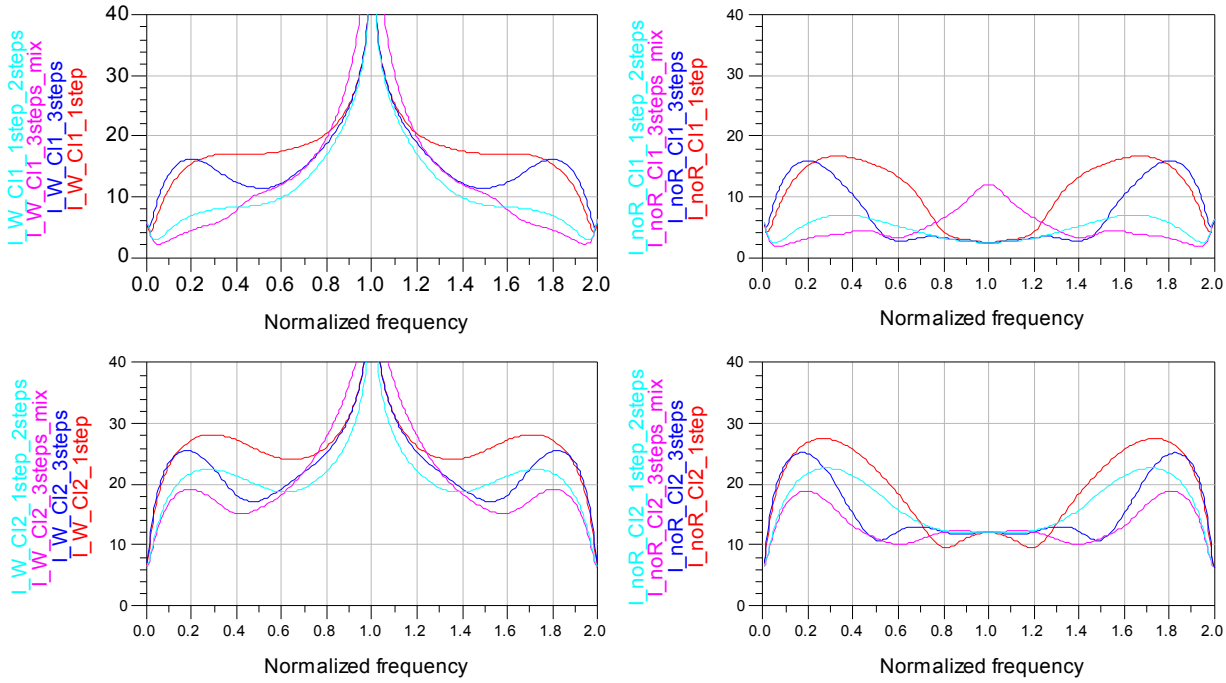

Figure 36 Isolation of input ports of the tested networks based on: Wilkinson combiner (I_W - left), combiner without isolating resistor (I_noR - right). Cl1 – input ports from same first level cluster, Cl2 – input ports from different first level clusters. 1step – one stage transformer, 3step – three stages transformer, 3step_mix – three stages transformer mixed with combiners, 1step_2steps – one transformer and two impedance transforming power dividers.

The Figure 36 portrays the simulated value of isolation for all the tested circuits with the Wilkinson combiners (the graphs on the left) and in the case of the combiners without an isolating resistor (graphs on the right). Moreover, while the combining tree structure is of the second level, two different curves are possible to obtain, depending on the location of the inputs. The first one, for the inputs from the same, first level cluster (the top graphs) and the other while inputs are form different first level clusters. Clearly, the circuit that uses ideal Wilkinson combiner has an infinite isolation at the central frequency, in a distance from the central frequency value drops. In contrast, isolation of the circuits without isolating the resistors has finite and rather small value at central frequency and in band of the combining network. Lack of isolation is responsible for increased problems of the odd mode oscillations. This is the risk that is introduced due to a more efficient space usage.

2.3.2 A capacitive loaded transmission line technique

A solution to the realization problems of low impedance transmission line could be found in many publications, regarding power combiners size reduction [11]. The idea is to exchange quarterwave transmission line Figure 37 (a), with an equivalent circuit. In this case the equivalent circuit will be build from shorter line of different than the original line impedance at which ends shunt capacitors were connected - Figure 37 (b). Smaller size of the substitution could be another benefit of this particular approach.

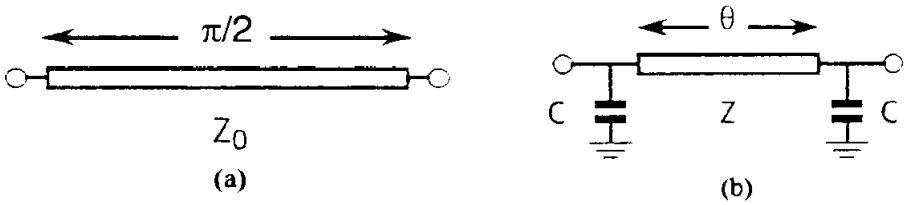

Figure 37 Quarterwave transmission line (a) and capacitive loaded line (b).

If Y parameters computed at central frequency of circuits are compared (90.), Z and C could be calculated as a function of θ and Z_0 – (91.).

$$Y_A = \frac{1}{j \cdot Z_0} \cdot \begin{bmatrix} 0 & 1 \\ 1 & 0 \end{bmatrix}, \quad Y_B = \begin{bmatrix} \frac{\cos\theta}{j \cdot Z \cdot \sin\theta} + j\omega \cdot C & \frac{1}{j \cdot Z \cdot \sin\theta} \\ \frac{1}{j \cdot Z \cdot \sin\theta} & \frac{\cos\theta}{j \cdot Z \cdot \sin\theta} + j\omega \cdot C \end{bmatrix} \tag{90.}$$

$$Z = \frac{Z_0}{\sin\theta}$$
$$C = \frac{\cos\theta}{\omega \cdot Z_0} \tag{91.}$$

Clearly, the reduction of transmission line length in equivalent circuit will artificially increase its impedance. Unfortunately, the equivalent circuit behaves like quarterwave transmission line only at the central frequency. In general this is low pass structure, what is visible if reflection coefficient is plotted on the Smith's chart for a different value of θ - Figure 38.

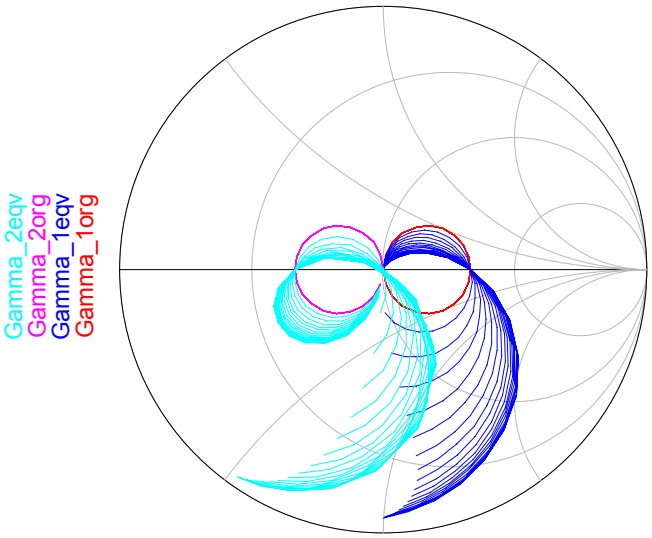

Figure 38 Reflection coefficient of Z_0=35Ω (2) and Z_0=70Ω (1) transmission lines (org) and their equivalent circuits (equ).

How does it influence performance of the designed circuit? A simple experiment has been performed and for the previously designed matching/combining circuits the scale factor was introduced, controlling the length of all quarterwave transmission lines - (92.).

$$\theta = scale \cdot 90° \tag{92.}$$

The performances were simulated for the scale={1,0.6,0.1} and presented in Figure 39. While observing the transmission coefficient, the low pass action of equivalent element circuit is easily visible. With a decrease of the scale factor, characteristics of the circuits became unsymmetrical and deteriorated. Hence, further redesign is needed if the method is to be adopted.

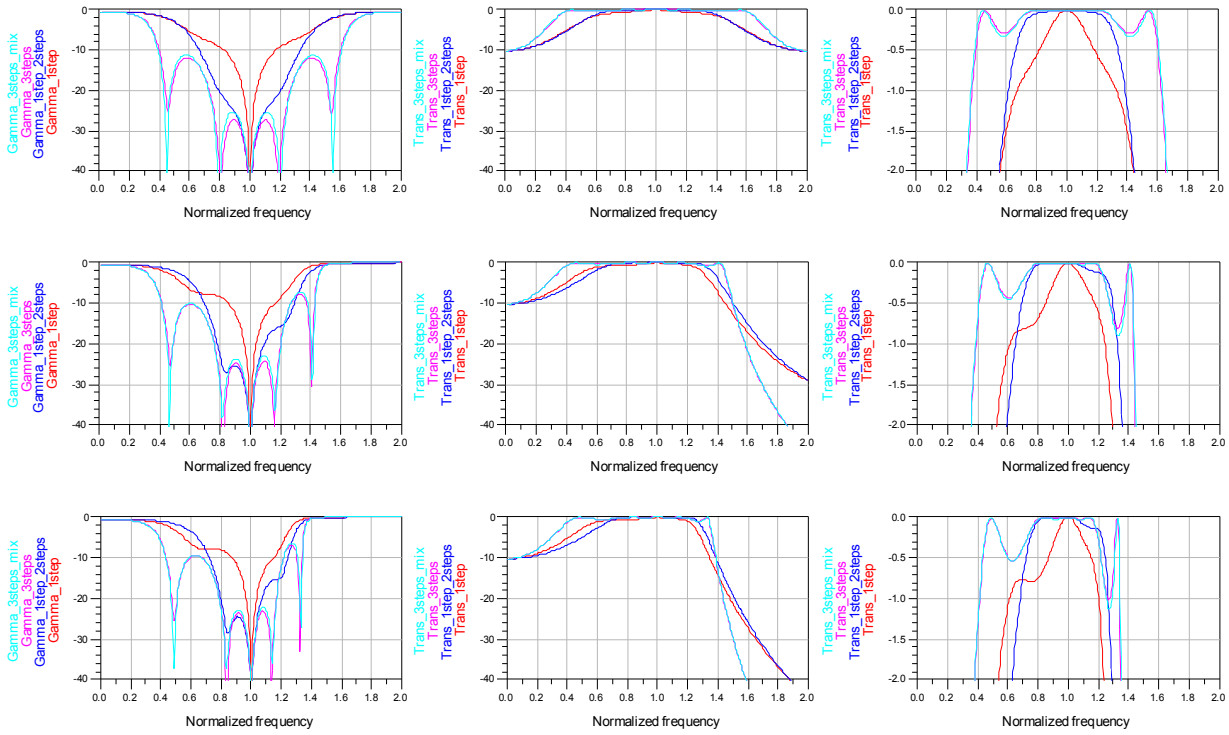

Figure 39 Combining/matching networks performances depending on the scale factor. Top series of graph scale=1, middle sclae=0.6, bottom sclae=0.1. Gamma – reflecion coefficient, Trans- transmision from sources to output port. 1step – one stage transformer, 3step – three stages transformer, 3step_mix – three stages transformer mixed with combiners, 1step_2steps – one transformer and two impedance transforming power dividers.

With a reduced size of the quarterwave transmission lines, their characteristic impedance requests to be increased. If all values used in the four designs are plotted along with the assumed range of a possible realization, any draft should theoretically obtain the green light for the further development, whereas with the decreased scale factor all the curves cross the realizable range of the impedances - Figure 40.

Further development of the circuit includes an introduction of the capacitors at the ends of the transmission lines. This is difficult due to a couple of reasons. One of them is connected with the problems regarding via hole structure in the integrated circuits. Its relative size is much bigger than the one for normal microwave circuits, what in turn decreases significantly freedom of usage. What is more, the proximity of via holes is a subject to strict rules due to the wafer's durability. Relative large dimensions are the issue to an increased coupling to the near elements. Often, dimensions of the via holes force designers to reduce their number by reusing them. As via hole introduces series parasitic to this connection, its reusage introduces the voltage feedback between the commonly grounded subcircuits.

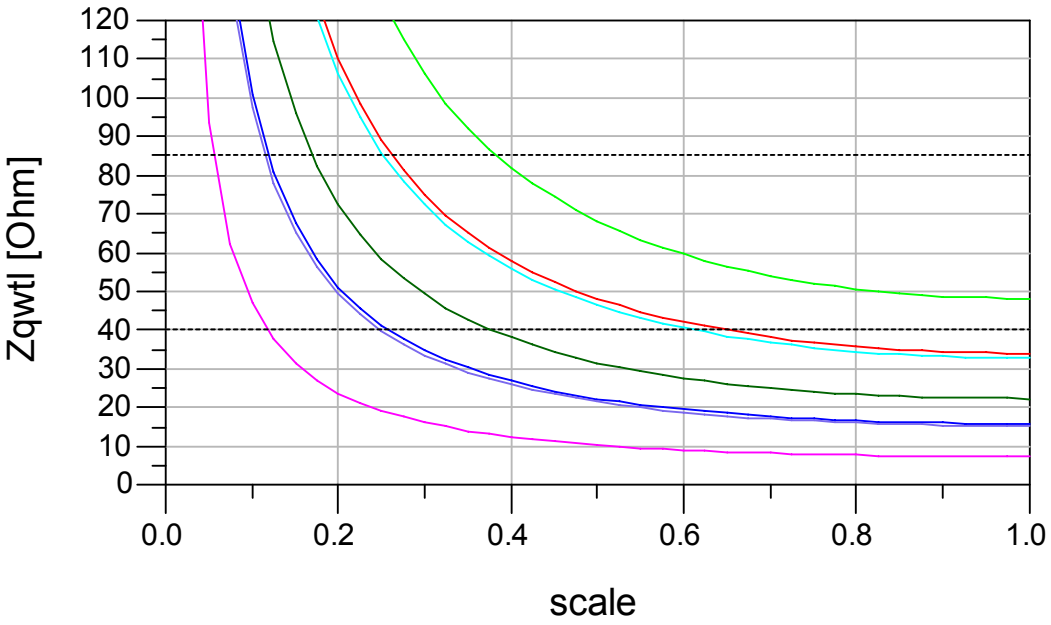

Figure 40 Change of capacitive loaded quarterwave transmission line impedances used in designs depending on the scale factor.

Other problems regard the call for introducing more circuit elements like capacitors, tee junctions as well as interconnection lines. Their parasitic needs to be taken into consideration. A decreased width of the shortened transmission line could be again the matter to limitation from the current handling capability and increased resistive losses. This could be in particular difficult if biasing network is connected to the combining network at high level stage. If we assume that in the presented example each active device conducts in saturation $I_{sat,DC}$=120 mA and the current limit due to electromigration is J=12 mA/um, then the minimum width of transmission line that can bias device will be $W_{min,1}$=10 um. Although, if two devices were to be combined and biased together it would be $W_{min,2}$=20 um, and if the bias circuit was connected at the output, minimum width for the combined current it would be $W_{min,3}$=40 um. This additional restriction in case of a larger number of the combined devices could be burdensome. For that reason, in the next paragraph there was developed another interesting technique, which is to counteract this difficulty.

2.3.3 Bus-bar combiner

A bus-bar approach [12] will be presented on a base combining tree structure introduced in Figure 41 a). Bus bar combiner is introduced into the first combining stage marked with I in the Figure 41 b). To bias all the devices connected to the combining network, a wide strip conductor called “bus-bar” is placed across the network. Combined sources are connected to bus-bar with interconnection lines at the same distance. From the other side of the bus-bar the rest of the combining tree is connected in a middle point between the pairs of the sources - Figure 41 c). While the circuit is excited in phase and with the same amplitude such an arrangement creates virtual openings in the bus-bar at the points marked with the broken line. Evidently it is so only for the combined signals, therefore this wide conductor can be still used for the bias devices. To perform this task, the bias circuit needs to be designed and connected to the one or two ends, providing DC path and the open circuit at the frequencies of the operation. While the whole idea is based on the symmetry of the structure and a combining points connection, the symmetry of double biasing will be highly appreciated. In theory

this can be mixed with any type corporate combining tree, even on the ones not based on two port structure, the only requirement is to maintain the symmetry and the initial even-number of the sources.

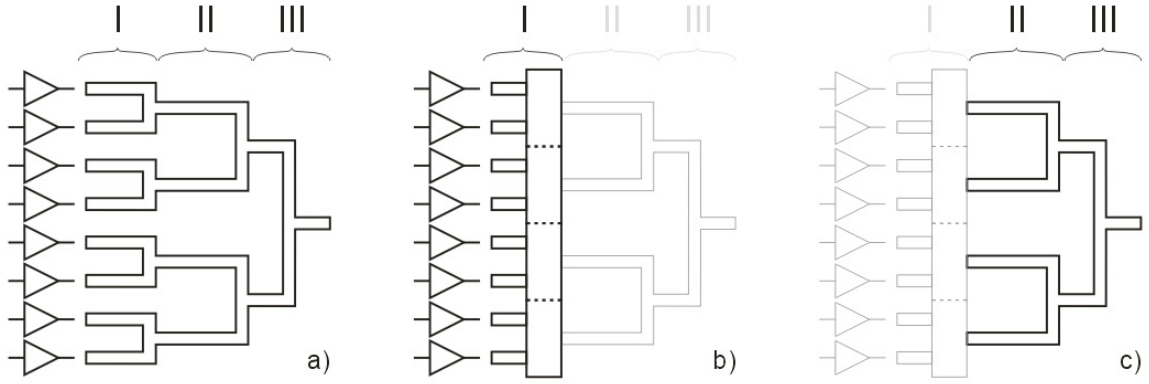

Figure 41 Bus bar combiner idea. a) Corporate network, b) bus bar, c) rest of the network.

A compact structure, high current capability for DC feed, the likelihood of the odd-mode stability problems reduction are the most evident gains. On the contrary, the structure requires electromagnetic simulations to predict the true behaviour. Any matching structures or interconnection lines introduced between the signal sources and bus-bar combiner will influence its odd-mode stability problems reduction ability. While in the base concept impedance seen at the bus bar combiner outputs is half of the source impedances, its usage shifts burden of high ratio matching to the higher order combining stages increasing their design difficulty.

2.3.4 Conclusion

The simple example of matching combining section design draft reflects the compromise strategy: not to lose too much of the electrical performances whilst trying to gain possibly most resourceful space usage. Highly efficient approach to the task is the simplicity as in phase combining is preferred along with the cluster matching. This results in lower complexity, better arrangement of components and their lower parasitic mutual influence. These very features are then related to a much higher accuracy of the circuit simulated by simple circuital models what in turn allows to avoid usage of the demanding electromagnetic simulations. Speed of the circuital simulations is extremely vital at the initial point of the design, especially in the design reality, where the best compromise is often what designers are looking for. Thus, not only specific and demanding approaches like Bus-bar are rejected, but also the highly appreciated ones from the stability point are frequently omitted. Amplifier final tuning and stabilization are often treated as the project final stage problems what may lead to non optimal results or to a profound redesign necessity in case of the stability problems.

2.4 Power combining impact on the stability and a requirement for the tools

Power combining offers a series of advantages when considered in the power amplifier design, moreover it happens that it is inevitable in order to reach the goals of the design. It was existing at the earliest stages of development of the electronic field and it is yet present nowadays. For that reason, there is a variety of approaches to the power combining that are related to the requirements

and the technology of realization. In the event of the Integrated Circuit reality, described more deeply in this chapter, the power combining suffers from highly compromised approach, related mostly to the size reduction imposed by lower cost and the introduced simplicity. This reality puts the designer in the difficult position whereas the amplifier design becomes an art of finding the finest compromise. Among the factors taken into consideration for this compromise there are basic electrical performances or physical properties, so consequently the stability properties often become the last ones to verify. It is above all evident in the case of odd mode stability, which is more difficult to predict. Regrettably, stability is not a subject of any compromise if given not stable circuit. Makes it even harder when the odd mode stability tests are not available in the popular CAD environments and they require additional effort to be conducted. The Integrated Circuit reality is prone to the odd mode stability problems mainly due to the popularity of in-phase combining and compromised approach to the combiners, favouring the use of the simple parallel connection over the bigger structures with isolation. Low cost and efficient space usage force designers to use more risky approach. Thus, counter measured techniques in form of the efficient tools are extremely important in similar way as they are present in the CAD environments for the standard two port stability. It should be possible to address the circuit unconditional stability easily and in case of the conditional stability or the instability, the source of the problem should be located effortlessly. If given the standard two port stability, Rollet k-factor or u-factor fulfill the role of the simple and efficient unconditional stability test. In case of the problems detected by the previously mentioned methods, making use of the Source and Load Stability Circles can provide great help in the understanding and eliminating the stability problems. Comparable approach to the odd mode stability problems is highly desirable while stability of all modes needs to be assured simultaneously. Hence, an effective method cannot merely return final verdict over the circuit stability. It should as well be a tool providing precise information that allows to find source and perform an effective countermeasure action. The same way it should be easy to introduce the method into design at any stage of the project and possibly involve it into the optimization routines. A matter of an existence and usability of such methods will be the content of the very next chapter of this work.

3 SPECIALIZED STABILITY TESTS

It has been already revealed in the paragraph 1.2.4 that the two port representation is not always enough to assure the circuit stability. This happens to be so in case of multi-device power amplifiers which requires new concepts of stability test. Among likely solutions two were chosen for further inspection- Freitag and Ohtomo methods. What is common for them is the first step to divide the circuit under the test into two subcircuits, another shared feature is the final verdict on the circuit stability they gave. However, ideas they are based on are dissimilar and this result in a different weak and strong points of these methods. As a result, more detailed investigation of their usefulness in multi-device power amplifier design will be the scope of the following chapter.

3.1 Freitag method

The author presented the mathematical framework for the stability prediction of all n mode of n-parallel devices amplifier [16]. In favour of clarity, the initial steps of the method will be presented with use of the simple, symmetric in-phase combined parallel amplifier presented in the Figure 42 a). As it was mentioned before, two port representation could be insufficient to assure stability of n-device parallel amplifier, so the method accesses the internal nodes of amplifier to address its stability. The initial step of the procedure is to close the input and output ports used in the two port representation by appropriate terminations - Figure 42 b). Then, the circuit is divided into two parts named accordingly as the input and output. Division will take place at input or output of appropriate amplification stage and will create n-broken connections - Figure 42 c). These broken connections are exchanged to ports for both bisections. Thus, after initial steps of the procedure two n-port subcircuits are created - Figure 42 d).

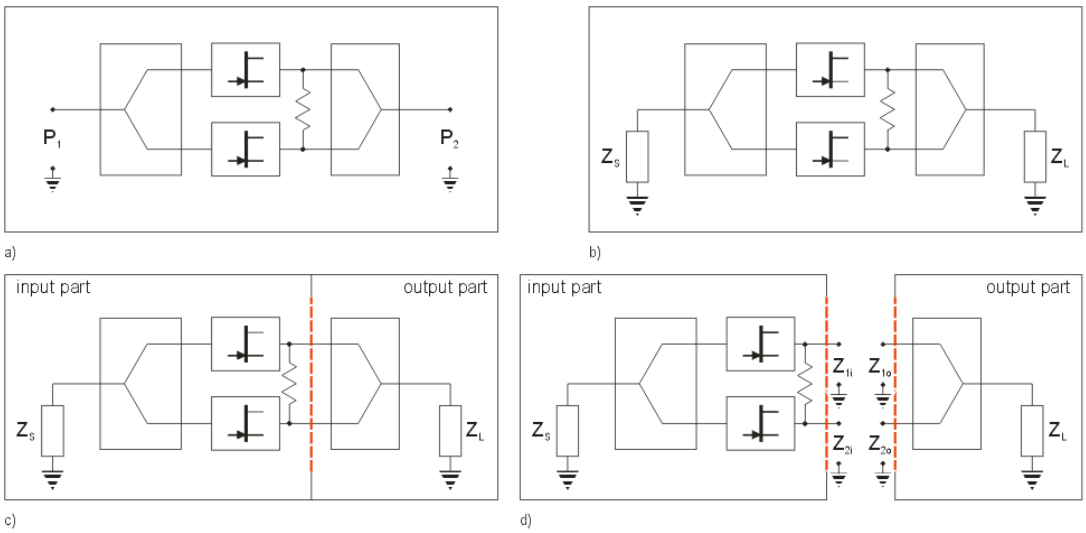

Figure 42 Example parallel amplifier in Freitag method.
a) circuit, b) input oputput port closure, c) division point d)bisection creation.

Each subcircuit created after division can be described by Z matrix equation, in case of the example circuit from Figure 42 d) it will be two port representation as follows:

$$\begin{bmatrix} Z_{11} & Z_{12} \\ Z_{21} & Z_{22} \end{bmatrix} \cdot \begin{bmatrix} I_1 \\ I_2 \end{bmatrix} = \begin{bmatrix} U_1 \\ U_2 \end{bmatrix}$$

(93.)

If eigenvalue and eigenvector relation (13.) will be invoked and rewritten in terms of Z matrix, an interesting discovery is made:

$$[Z] \cdot [I_k] = Z_k \cdot [I_k]$$

(94.)

Such a description reveals that with particular current excitation all ports will present identical value of impedance. These values of impedance will be equal to the eigenvalues of the subnetwork Z matrix and excitations will be equal to eigenvectors associated with them. If given n*n matrixes describing bisections, n linearly independent eigenvectors are expected to be found. They will represent the current/voltage modes that exist in each half of the amplifier. If eigenvectors sets are equal for both bisections it is justified to expect that any current/voltage waveform existing in amplifier can be represented as linear combination of these eigenvectors. As a result eigenvectors correspond to previously mentioned modes of operation- paragraph 1.2.5.

In case of displayed in the Figure 42 d) subcircuits symmetry, not perturbed by the division of the circuit, allows to write $Z_{11}= Z_{22}$ and $Z_{12}= Z_{21}$. For that reason, eigenvectors and eigenvalues are easily found:

$$\begin{bmatrix} Z_{11} & Z_{12} \\ Z_{12} & Z_{11} \end{bmatrix} \cdot [I_k] = Z_k \cdot [I_k]$$

$$I_E = \begin{bmatrix} 1 \\ 1 \end{bmatrix} \qquad \text{eigenvectors} \qquad I_O = \begin{bmatrix} 1 \\ -1 \end{bmatrix}$$

$$Z_E = Z_{11} + Z_{12} \qquad \text{eigenvalues} \qquad Z_O = Z_{11} - Z_{12}$$

(95.)

The results have very intuitive interpretation as the presented example is in the phase symmetric parallel amplifier. The desired way of operation on the circuit assumes in-phase excitation of the active devices and is called even mode. On condition of this analysis vector I_E is responsible for this type of excitation. Impedance Z_E will be sensed at subcircuit ports in this mode. The second mode is called the odd mode and assumes out of phase excitation of active devices. In an ideal parallel amplifier incorporating of in-phase combining odd mode is insensible to the input/output termination, as virtual ground is created in combining points. Vector I_O match odd mode description and eigenvalue Z_O associated to it will describe the impedance noticed in this mode at both ports of the subcircuit.

In this simple case the procedure intuitively resembles Even-Odd analysis [15]. Thus, even mode impedance Z_E could be obtained by application of magnetic wall in the axis of symmetry of the bisections. On the other hand, Z_O could be obtained by application of electric wall in the axis of the symmetry of the bisections. This very process was portrayed in the Figure 43 meant for the lumped element parallel amplifier already divided into bisections. Interestingly, two equivalent circuit were obtained through this way. Linear independence of eigenvectors responsible for different modes of operation allows to divide analysis of the circuit stability to smaller problems of the modes stability.

By observing the results in the Figure 43, a similarity to the oscillator problem is evident. If it happens that eigenvectors sets are exactly the same for both bisections, then all the modes of operation can be addressed by this approach and full stability of the circuit can be assessed.

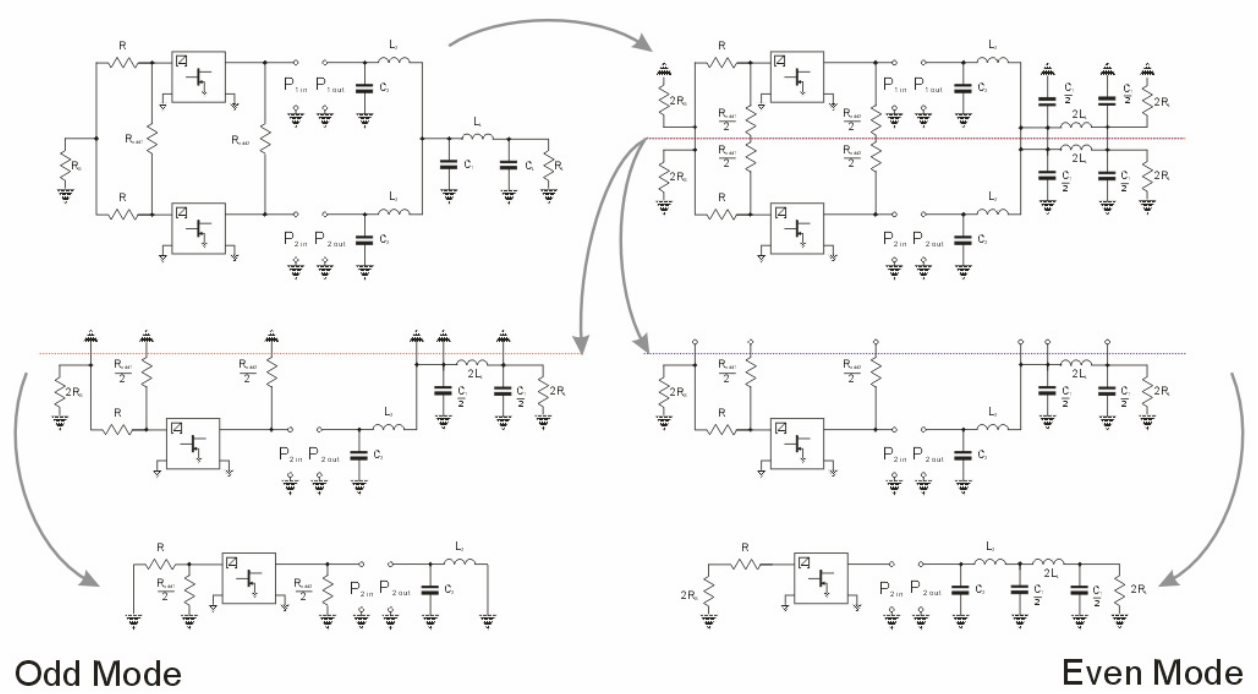

Figure 43 Odd and even mode impedances in case of the symmetric two device lumped element parallel amplifier.

Verdict on the stability of the particular mode is made by application of the onset of the oscillation. While eigenvectors of the bisections are equal, eigenvalues associated to them could be of diverse value for the input and output bisections. Therefore, additional subscript i and o was added in order to distinguish them. With such a description of the bisections equivalent impedances, onset of oscillation based on simplified Kurokawa oscillation condition is formulated [21]:

$$\left.\begin{aligned} \mathrm{Re}\{Z_{ei}(f)+Z_{eo}(f)\}=\mathrm{Re}\{Z_{e}(f)\}<0 \\ \mathrm{Im}\{Z_{ei}(f)+Z_{eo}(f)\}=\mathrm{Im}\{Z_{e}(f)\}=0 \end{aligned}\right\} \text{"even mode"}$$
$$\left.\begin{aligned} \mathrm{Re}\{Z_{oni}(f)+Z_{ono}(f)\}=\mathrm{Re}\{Z_{on}(f)\}<0 \\ \mathrm{Im}\{Z_{oni}(f)+Z_{ono}(f)\}=\mathrm{Im}\{Z_{on}(f)\}=0 \end{aligned}\right\} \text{"n}^{\text{th}}\text{ odd mode"} \qquad (96.)$$

If condition (96.) is met for the particular mode, at any frequency, than the oscillations will occur.

3.1.1 CAD implementation

A method implementation in CAD environment can be divided into three steps: simulation of bisections Z matrixes; eigenvectors and values calculation and application of onset of oscillation. The first step is in general the simplest to perform if manual division of the circuit has been performed. The second step is more complex and depends on the type of the environment the designer uses. Unluckily, most of them are not suitable to compute eigenvalues and eigenvectors through the built functions. So, the best way is to describe eigenvectors and values by means of equations. It is possible for a low number of the devices, regrettably, for more than 4 devices it is difficult task.

Exemption occurs for perfectly symmetrical structures and for $N=2^M$ sources. Finally, an interpretation of the curves is easy subject to manual investigation and in the event of the automation, zero crossing algorithm is required. This additional requirement will decrease efficiency of optimization routines, what is more, either two separate schematics are necessary to compute bisection matrixes or one with double dimension. In the second case the memory and computation time is wasted for coefficients describing non existing connections. Moreover, in basic approaches it is not possible to simultaneously perform Freitag test and simulate two port performance of the circuit.

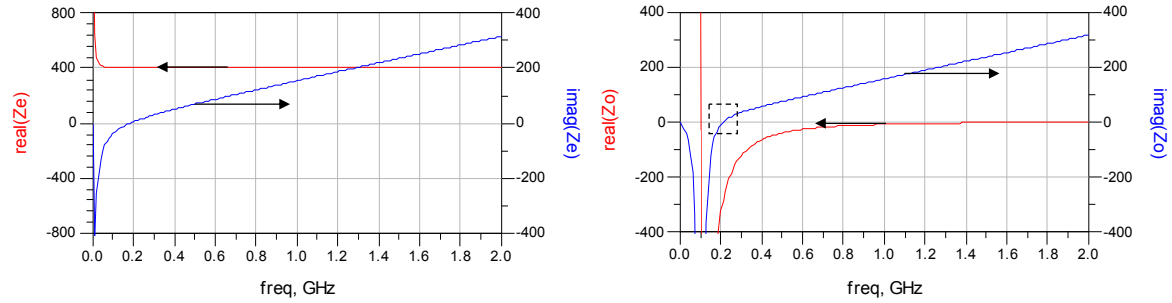

Figure 44 Odd and Even impedance analysis for the example amplifier from paragraph 1.2.4 (Figure 16).

If example amplifier presented in paragraph 1.2.4 (Figure 16) is tested with Freitag method, results in the Figure 44 are in agreement with the previous discoveries. Circuit was unconditional stable from the two port stability tests point of view and unstable in Time domain simulations. Results of the analysis shows even mode stability for $Z_s=Z_l=Z_0=50\Omega$ while real part of Z_e is higher than zero for all analysed frequencies. Same time imaginary part of Z_o impedance plot is crossing zero value while real part is negative at that frequency point. This clearly indicate that circuit is odd mode instable and method predict correctly instability and its type. While onset of oscillation can assure even mode stability only for initially chosen input/output terminations. Therefore it is necessary to use additional test if unconditional even mode stability is to be guaranteed.

3.2 Ohtomo method

Nyquist criteria [18] is an important and useful stability tool. Sadly, its powerful idea in case of multi-loop circuits became its weakness. The idea is to test the presence in the right half complex plane poles instead of finding their precise positions on the complex plain. Nyquist addresses this necessity providing the value of the difference between the number of poles and zeros in the right half complex plane. Such quantity is achieved from the analysis of the open loop transfer function- a more detailed description of the criteria is presented in Appendix 2.

Unfortunately, the result in multi-device/multi-loop circuits of the Nyquist analysis could be misleading. Therefore, the method presented by Ohtomo in [17] can be perceived as an extension of Nyquist criteria for multi loop circuits. The method of the analysis assumes the division of the circuit to the two subcircuits described by s-parameters. One is created from all the active devices and is represented by the scattering matrix S. The remaining passive circuit components are represented by the matrix S'. It is assumed that there is no coupling existing between the active devices within the subcircuit. Graphical representation of that action is showed in Figure 45 a), the circuit representation with matrixes S and S' and the interconnection ports interpreted as the signal nodes

are showed in Figure 45 b). In the Figure 45 c) for, clarity nodes were separated with paths t_i and t'_i. Clearly, for any interconnecting ports $a_{Pi}= b'_{Pi}$ and $b_{Pi}= a'_{Pi}$, where n is the port number.

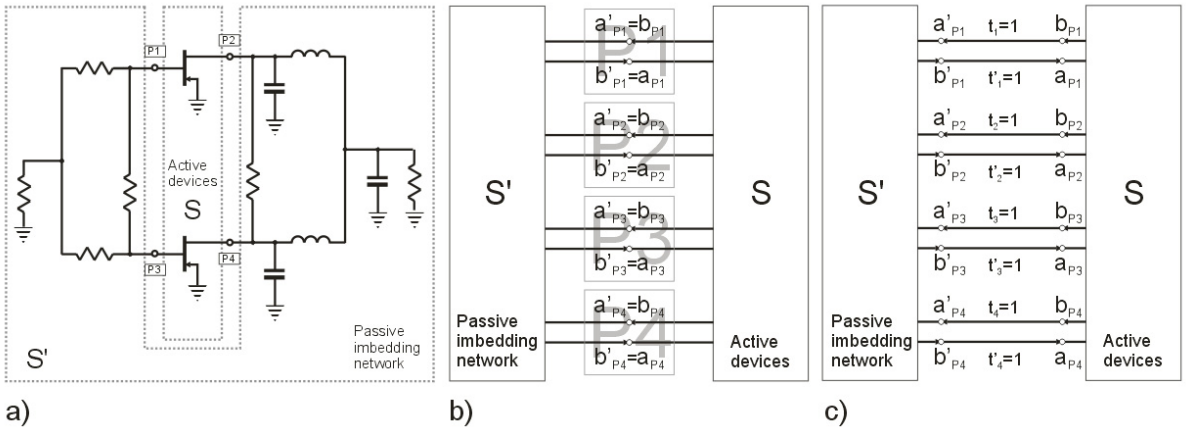

Figure 45 Circuit prepared for analyze with multi-loop Nyquist approach.

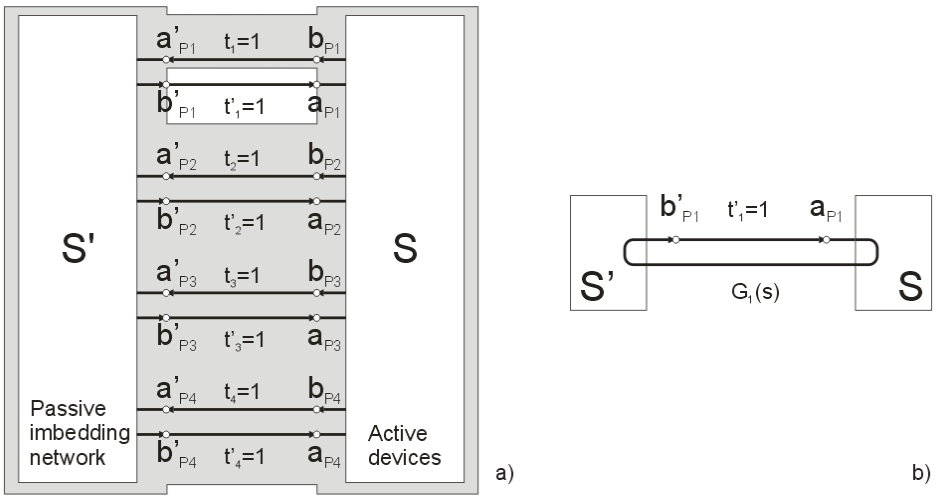

Figure 46 Relation between a_{P1} and b'_{P1} at port 1.

If relation between $a_{Pi}= b'_{Pi}$ at port i is considered, the signal flow graph of a feedback loop is obtained. Example for port 1 was presented in the Figure 46 where the graph a) was reduced to b) that contains only nodes a_{P1} and b'_{P1}. The graph forward the path is named $G_1(s)$ and the feedback path is named t'_1. Clearly, the graph in the Figure 46 b) can be analyzed with the usage of Nyquist criteria - paragraph A2.2. While a_{P1} is treated as a source, the closed loop transfer function $H_1(s)$ is described as:

$$H_1(s)=\frac{b'_{P1}(s)}{a_{P1}(s)}=\frac{G_1(s)}{1-G_1(s)\cdot t'_1}=\frac{G_1(s)}{1-G_1(s)} \tag{97.}$$

The open loop transfer function in this example is simply $G_1(s)$. Nyquist criteria can be applied in the same way at any of the circuit interconnecting port i and the stability of feedback loops can be tested with the usage of the open loop functions $G_i(s)$. The author defines open and close transfer functions in terms of the s-parameters of two subcircuits: S and S' - (98.).

$$G_i(s)=1+\frac{\Delta}{\Delta_{ii}(M_n)} \qquad H_i(s)=-\left[1+\frac{\Delta_{ii}(M_n)}{\Delta}\right]$$

where:

$$M_n = S'\cdot S - I_n$$
$$\Delta = \det(M_n)$$
$$\Delta_{ii}(M_n) = \text{cofactor of } (i,i) \text{ component of } M_n$$
$$I_n \text{ - is the } n\times n \text{ identity matrix}$$

(98.)

Sadly, as it was mentioned previously, the analysis of Nyquist locus gives an answer to the question about difference between the pole numbers p_i and zero numbers z_i in the right complex plane of the 1-G_i(s). Thus, the number of the locus encirclement $N_{ri}= z_i - p_i$ will not provide answer about z_i until p_i is unknown. For a single loop amplifiers p=0 is treated as a proviso to the Nyquist criteria and it guarantees $N_{ri}= z_i$ for the open loop transfer function. This very approach fails in case of the multi-loop. The simplified example circuit presented in Figure 47 a) illustrates this problem. While the open loop transfer function G_2 is inspected in the Figure 47 b),the red broken line indicates internal loops that exist in the circuit. Therefore, even if subcircuits S and S' did not possess any poles, p=0 and p'=0, these loops are potential sources of the right complex poles of the open loop transfer function G_2. Consequently, p_2=0 cannot be guaranteed by p=0 and p'=0 and final stability analysis result is not certain with a simple application of the Nyquist criteria.

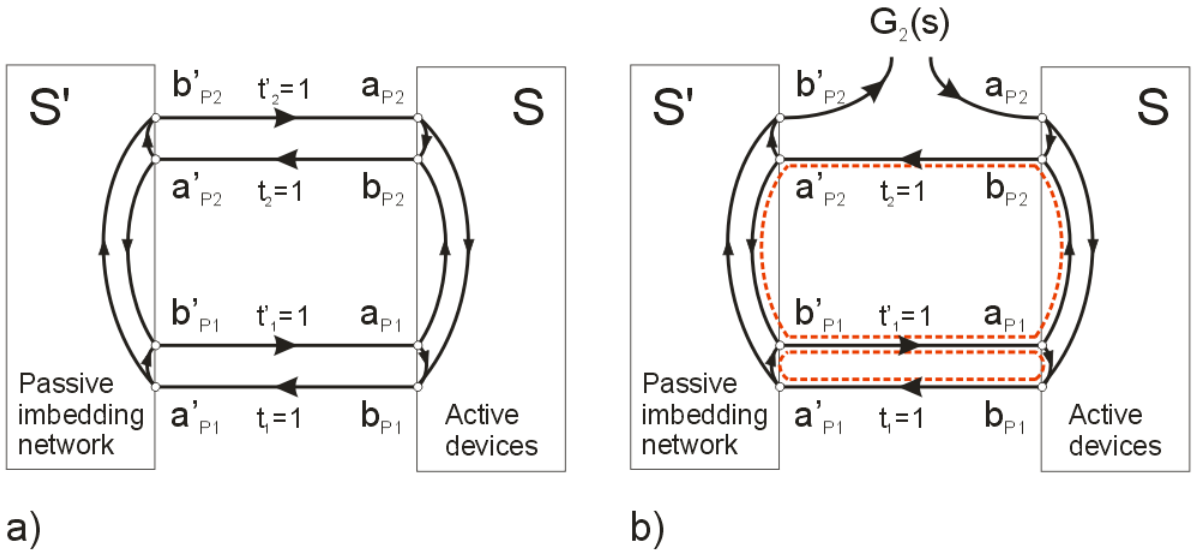

Figure 47 Open loop transfer function in simplified multi loop circuit example.

Ohtomo responds to this drawback by defining subgraphs of the original circuit graph. In order to create k^{th} subgraph, k-1 t branches were broken, $t'_1=t'_2=\ldots=t'_{k-1}=0$ (according to the Figure 45 c)). The k^{th} subgraph may still retain some information of the feedback loops from the original circuit. With $a_1=a_2=\ldots=a_{k-1}=0$, Open Loop Transfer Functions denoted as $\underline{G}_k(s)$ for the path $a_k \rightarrow b'_k$ in the k-th subgraph. $\underline{G}_k(s)$ is given by:

$$\underline{G}_k(s)=1+\frac{\det(M_{n-k+1})}{\det(M_{n-k})} \quad \text{where:} \quad 1\le k\le n$$

$$M_{n-k+1}=\begin{bmatrix} M_{k,k} & M_{k,k+1} & \cdots & M_{k,n} \\ M_{k+1,k} & M_{k+1,k+1} & \cdots & M_{k+1,n} \\ \vdots & \vdots & \ddots & \vdots \\ M_{n,k} & M_{n,k+1} & \cdots & M_{n,n} \end{bmatrix}$$

$$M_0=1$$

$$M_{i,m}=(i,m)\,\text{component of}\,M_n \quad 1\le i,m\le n$$

(99.)

Since $\det(M_{n-1})=\Delta_{ii}(M_n)$ for k=1, the subgraph is an original graph itself and $\underline{G}_1(s)=G_1(s)$. The differences between functions $\underline{G}_i(s)$ and $G_i(s)$ were presented in the Figure 48 basing on the same simplified example from the Figure 47 a) and the functions $\underline{G}_2(s)$ and $G_2(s)$. Obviously, after breaking branch t'_1 subgraph became free of internal loops, this happens when k=n due fact that n^{th} subgraph is cascade graph. It could be expected that in this particular case the results of Nyquist locus analysis of the open loop transfer function of n^{th} subgraph will respond to: $N_{rn}= z_n$ while $p_n=0$. Author uses this fact as a base for the calculation of the total number of zeros and poles of open loop transfer function $1-G_1(s)$.

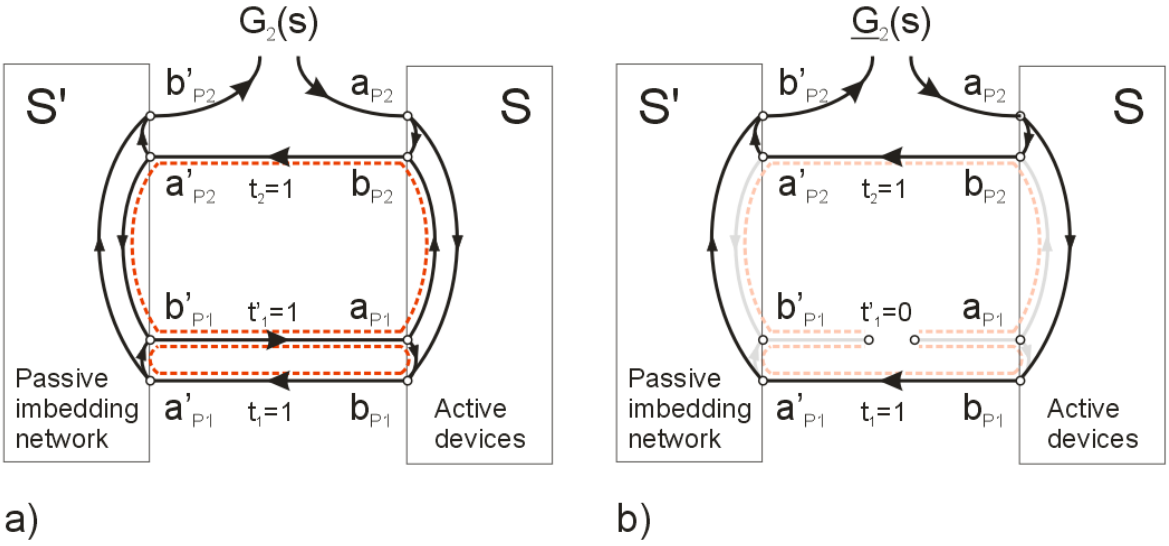

Figure 48 Open loop transfer function $G_2(s)$ a) and open loop transfer function of the subgraph $\underline{G}_2(s)$ b) in simplified multi loop circuit example.

When all the matrix elements of the S and S' matrixes do not possess poles in Right Half of the Complex Plane, it means that the elements of M_n matrix do not have any Right Half Complex Plane poles. Based on that assumption the number of zeros - z_k and poles - p_k of $1-\underline{G}_k(s)$ are defined as:

$$z_k=z\{\det(M_{n-k+1})\}$$
$$p_k=z\{\det(M_{n-k})\}$$

(100.)

Where function z{ f(s) } in the (100.) denotes number of the Right Half Complex Plane zeros of function f(s). Hence, from Nyquist criterion number $N_{r\,k}$ of clockwise revolutions of Nyquist plot $\underline{G}_k(s)$ around the critical point (1+j*0) is defined as:

$$N_{r\,k} = z_k - p_k = z\{\det(M_{n-k+1})\} - z\{\det(M_{n-k})\} \quad 1 \le k \le n$$

(101.)

Evaluation of the sum of the $N_{r\,k}$ for k from 1 to n lead to following equation:

$$\sum_{k=1}^{n} N_{r\,k} = z\{\det(M_n)\} - z\{\det(M_0)\} = z\{\det(M_n)\} = z\{\Delta\}$$

(102.)

So, the total number of the right half complex plane zeros of the function 1-G_1(s) is equal to:

$$N_z = z\{\Delta\} = \sum_{k=1}^{n} N_{r\,k}$$

(103.)

In this way investigation of all locuses: G_1(s) and G_k(s) for k=2..n is sufficient to determine the number of right half complex plane zeros of the circuit determinant z{Δ} and forms necessary and sufficient condition for the circuit stability - (104.).

$$N_z = \sum_{k=1}^{n} N_{r\,k} = 0$$

(104.)

3.2.1 CAD implementation

Implementation of the method in a CAD environment forces the computation and interpretation of the n Nyquist locuses in terms of their encirclement over the critical point (103.). In case of typical N-device power amplifier, if the active devices can be treated as two port networks this means that n=2*N. In a classical approach this results in 2*N simulation setups. Fortunately, the method gives an opportunity for the relatively simple application exploited by Ramberger et al. in [19]. If the open loop function of k^{th} subgraph $\underline{G}_k(s)$ is to be simulated, the original circuit needs to be modified. Creation of the k^{th} subgraph requires modifications of interconnecting paths t'_i. A simple observation can be made basing on the Figure 45 c): all interconnecting paths at ports i are intact for i>k. Same time for i<k paths t'_i are broken. This rule is summarized with (105.). Evidently, at port k the open loop function $\underline{G}_k(s)$ is measured.

$$\begin{cases} t'_i = 0 \\ t_i = 1 \end{cases} \quad k > i$$
$$\begin{cases} t'_i = 1 \\ t_i = 1 \end{cases} \quad i > k$$

(105.)

Basing on this observation, three cases can be easily distinguished and transformed into elements that can be placed between passive embedding network and active devices at interconnecting ports. While $t'_i = t_i = 1$, element is simply through connection. For $t'_i = 0$ and $t_i = 1$ it is an ideal isolator and finally to measure $\underline{G}_k(s)$ a three port circulator is required. While there exists a strict rule defining which element should be placed at port i while k^{th} locus $\underline{G}_k(s)$ is searched, this is a chance for the automation of the method. A universal component can be defined to be placed at each interconnection port with an individual number corresponding to the internal port number and control variable k- Figure 49.

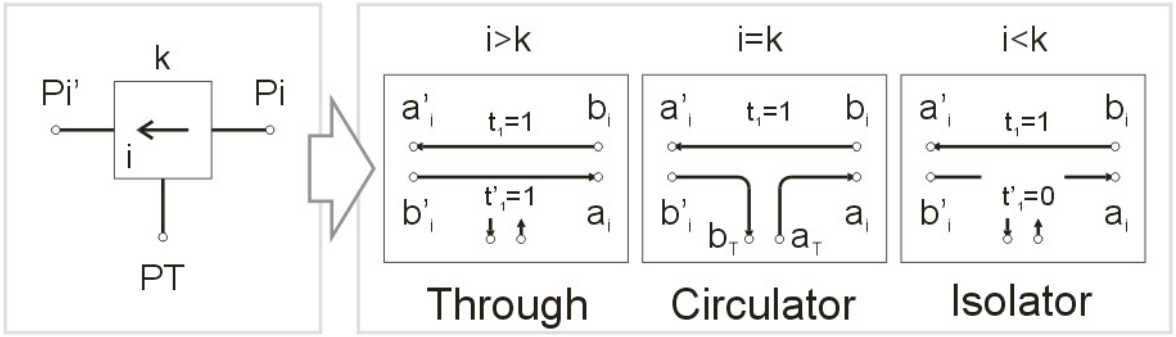

Figure 49 Component used for automation of Ohtomo stability test.

If presented above elements would be placed at all interconnecting ports and differentiated with individual port numbers, such prepared circuit will be prepared to simulate $\underline{G}_k(s)$ at port PTk. In the Figure 50 a) 3rd subgraph was prepared for simulation of the $\underline{G}_3(s)$ at port T, the same functionality possesses the circuit in the Figure 50 b) while variable k=3. An open loop transfer function of 3rd subgraph can be simulated at port PT3. A key drawback of this approach is a necessity for n simulation ports for each simulation, whereas in reality only one port is connected to the circuit under the test. If an element is not working as circulator, its third port is left open, as a result all PT ports can be connected and treated as single test port PTk - Figure 50 c). Simulation of the open loop transfer functions of subgraphs $\underline{G}_k(s)$ prepared in this way can be performed with the use of one simulation setup, for which k parameter is swept from 1 to n. Besides, if the sweep is done from 0 value and original input/output ports are retained, the standard two port simulation can be performed to check the circuit performance and two port stability in a single simulation setup.

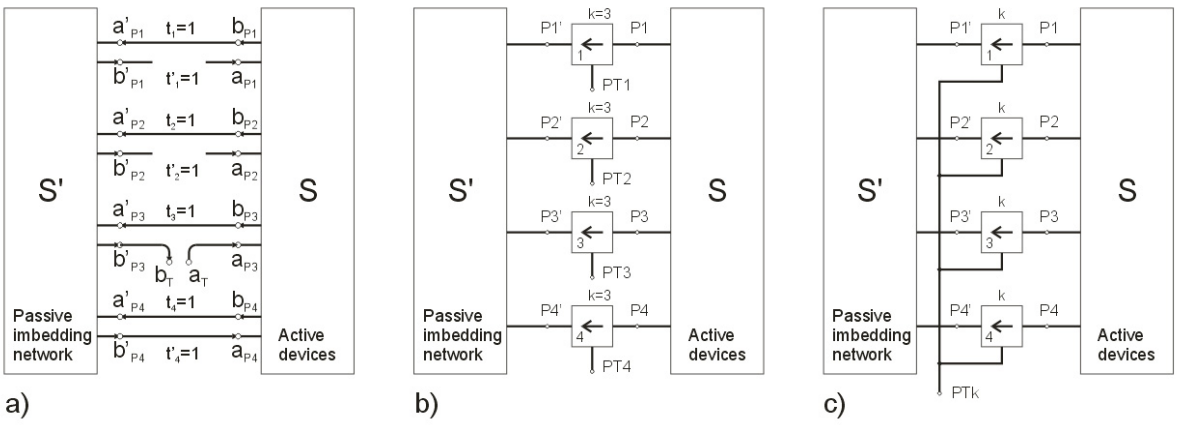

Figure 50 Implementation of automated Ohtomo stability test.

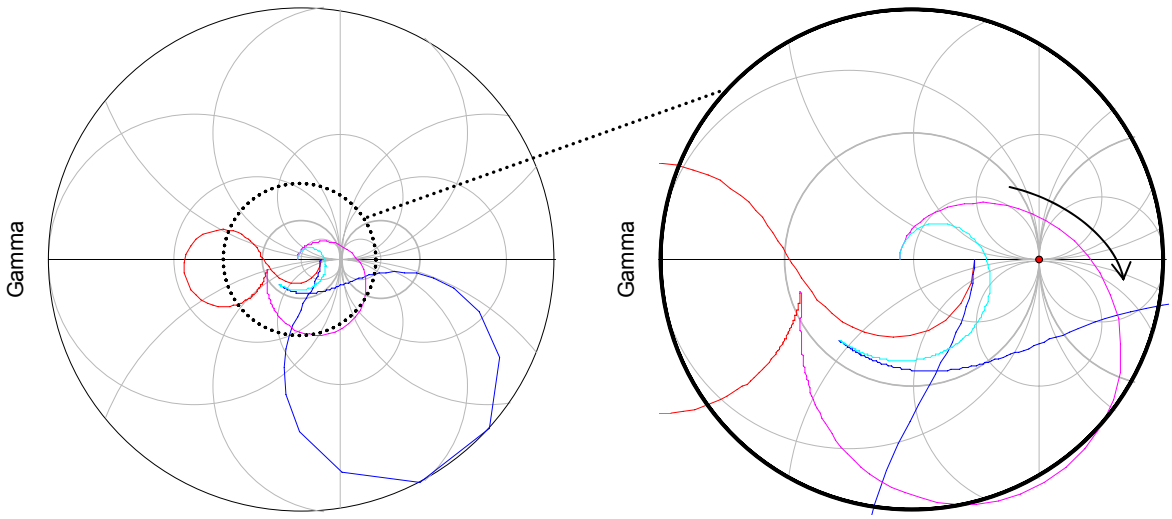

Figure 51 Ohtomo test results for the example amplifier from paragraph 1.2.4 (Figure 16).

Next step in the procedure is to interpret locuses and give verdict on the stability. In general it is not difficult to carry it out manually, but becomes quite problematic while the automation is required. In most cases, an additional algorithm that processes the result is needed. This is not always possible when the designer is restricted by the abilities of the CAD environment, also any algorithm introduces computational cost and decreases efficiency of optimization routines.

If presented CAD implementation of the Ohtomo method would be applied to the presented in the paragraph 1.2.4 (Figure 16) example amplifier, in result we obtain the four Nyquist locuses - Figure 51. The four interconnecting port requires an analysis of the four Nyquist locuses. In the Figure 51 it is apparent, that the violet curve encircles the critical point, and so N_z=1 and the circuit is instable. Again, result is in agreement with the time domain simulation results of the amplifier.

Unfortunately, the method does not indicate a type of instability nor the potential source. At the same time there is no restriction on the number of devices or topological properties of circuits that can be tested. In case of the stable circuit, the even mode is guaranteed only for the initially chosen input/output terminations. Thus, the unconditional even mode stability can be guaranteed with the appliance of an additional test if required.

3.3 Conclusion

Freitag and Ohtomo methods have potentials beyond standard two port stability tests and their basic advantage is to address stability of all the modes of operation of the tested circuit. Freitag method uses in this case a modal analysis of the bisected circuit under the test. For that reason, the analysis based on eigenvalue computation is restricted to situations when both bisections possess identical set of eigenvectors. If an application of the method is achievable, the original stability problem of the n-device power amplifier is in result transformed into n stability problems of each mode of the operation. Even if bisection eigenvectors are diverse, it is still possible to estimate the value of the impedance on each side, what may constitute important information. The method is extremely easy and efficient to apply in case of ideal in-phase corporate parallel amplifiers as eigenvectors of such structures are easy to predict. This is also true in case of low number of the devices as it is relatively easy to find closed formulas for eigenvectors and eigenvalues. The biggest advantage of the method is not only information about the stability that it provides but the source of eventual problems in sense of an unstable mode. Knowledge about instability source is invaluable information in terms of

speed and an optimal choice of the countermeasure action. Thus, Freitag method could be treated as a stability tool. Also, the list of pros and cons for the Freitag method may be completed with a low computation cost and easy results interpretation for the mentioned cases as well as with an inconvenience to reconcile the stability test and circuit performance check.

On the other hand, the Ohtomo method can be perceived more like a complete approach based on the powerful Nyquist criteria, even with a detailed CAD implementation description. Its power comes from almost no restriction to topology, number of devices and their character. With very few assumptions the method is robust, but functions more like a test and except for the binary result in terms of: stable / not stable, the Nyquist locuses of the subgraphs are quite tricky to interpret. As a result, these two methods do not compete to be an extension to the standard two port stability tests, since they are likely to complete themselves. Regarding this, a more detailed investigation of the Freitag method will be conducted.

4 FREITAG METHOD AS A CAD ORIENTED APPROACH

Freitag method presented in the previous paragraph is a very promising method to verify the stability of the parallel amplifier circuits. Whereas it bases on the knowledge of the eigenvectors and eigenvalues their recognition becomes crucial. The most efficient way to check their values in terms of CAD implementation is a possibility to express all eigenvalues with the predefined equations. If it is not possible, numerical iterative methods need to be involved. An introduction of the iterative methods complicate analysis, increase computation cost and introduce error to the results. For that reason, it is highly desirable to be able to use the predefined equations. Regrettably, it is very difficult to provide closed formulas for eigenvalues and eigenvectors for the circuits with higher number of the active devices. Nevertheless, analysis is much simpler while symmetry is introduced to the circuit and becomes trivial while ideal corporate in phase combining scheme is investigated. As it was emphasized in chapter 3, such scheme is very popular due to its simplicity and efficient space occupation. Hence, if Freitag method is restricted to the corporate structures it does not narrow down usefulness of the approach severely, instead it gains intuitive and easy application scheme.
While the combining tree is based on the hybrid combiners, it restricts number of the signal sources to $N=2^n$. While N=2, two different situations are possible, a non symmetric reciprocal bisection and a symmetric reciprocal bisection. Equations (106.) and (107.) describe eigenvalues and eigenvectors of the first case. While bisections are symmetrical and reciprocal description of the eigenvalues and eigenvectors simplifies to (108.) and (109.).

$$Z_A = \begin{bmatrix} Z_{11} & Z_{12} \\ Z_{12} & Z_{22} \end{bmatrix} \rightarrow \begin{cases} Z_{A1} = \dfrac{Z_{11}}{2} + \dfrac{Z_{22}}{2} + \dfrac{\sqrt{Z_{11}^{\,2} - 2 \cdot Z_{11} \cdot Z_{22} + \cdot Z_{22}^{\,2} + 4 \cdot Z_{12}^{\,2}}}{2} \\ Z_{A2} = \dfrac{Z_{11}}{2} + \dfrac{Z_{22}}{2} - \dfrac{\sqrt{Z_{11}^{\,2} - 2 \cdot Z_{11} \cdot Z_{22} + \cdot Z_{22}^{\,2} + 4 \cdot Z_{12}^{\,2}}}{2} \end{cases} \tag{106.}$$

$$Z_A = \begin{bmatrix} Z_{11} & Z_{12} \\ Z_{12} & Z_{22} \end{bmatrix} \rightarrow \begin{cases} I_{A1} = \begin{bmatrix} -\dfrac{Z_{12}}{\dfrac{Z_{11}}{2} - \dfrac{Z_{22}}{2} - \dfrac{\sqrt{Z_{11}^{\,2} - 2 \cdot Z_{11} \cdot Z_{22} + \cdot Z_{22}^{\,2} + 4 \cdot Z_{12}^{\,2}}}{2}} \\ 1 \end{bmatrix} \\ I_{A2} = \begin{bmatrix} -\dfrac{Z_{12}}{\dfrac{Z_{11}}{2} - \dfrac{Z_{22}}{2} + \dfrac{\sqrt{Z_{11}^{\,2} - 2 \cdot Z_{11} \cdot Z_{22} + \cdot Z_{22}^{\,2} + 4 \cdot Z_{12}^{\,2}}}{2}} \\ 1 \end{bmatrix} \end{cases} \tag{107.}$$

$$Z_A = \begin{bmatrix} Z_{11} & Z_{12} \\ Z_{12} & Z_{11} \end{bmatrix} \rightarrow \begin{cases} Z_{A1} = Z_{11} + Z_{12} \\ Z_{A2} = Z_{11} - Z_{12} \end{cases} \tag{108.}$$

$$Z_A = \begin{bmatrix} Z_{11} & Z_{12} \\ Z_{12} & Z_{11} \end{bmatrix} \rightarrow \begin{cases} I_{A1} = \begin{bmatrix} 1 \\ 1 \end{bmatrix} \\ I_{A2} = \begin{bmatrix} -1 \\ 1 \end{bmatrix} \end{cases}$$

(109.)

If similar comparison will be repeated for N=4 with additional simplified assumption of mirror symmetry eigenvalues, description (110.) becomes cumbersome but still useful in terms of CAD implementation. Same time description of the eigenvalues of the bisections involving corporate power combining remain extremely simple - (111.). In that case it is also very easy task to find possible eigenvector set - (112.).

$$Z_A = \begin{bmatrix} Z_{11} & Z_{12} & Z_{13} & Z_{14} \\ Z_{12} & Z_{22} & Z_{23} & Z_{13} \\ Z_{13} & Z_{23} & Z_{22} & Z_{12} \\ Z_{14} & Z_{13} & Z_{12} & Z_{11} \end{bmatrix} \rightarrow \begin{cases} Z_{A1} \\ Z_{A2} \\ Z_{A3} \\ Z_{A4} \end{cases} \rightarrow$$

$$\begin{cases} Z_{A1} = \frac{Z_{11}}{2} + \frac{Z_{22}}{2} + \frac{Z_{14}}{2} + \frac{Z_{23}}{2} + \frac{1}{2} \cdot \left({Z_{22}}^2 - 2 \cdot Z_{14} \cdot Z_{22} - 2 \cdot Z_{22} \cdot Z_{11} + 2 \cdot Z_{22} \cdot Z_{23} + \cdot {Z_{14}}^2 \right. \\ \left. + 2 \cdot Z_{11} \cdot Z_{14} - 2 \cdot Z_{14} \cdot Z_{23} + {Z_{11}}^2 - 2 \cdot Z_{23} \cdot Z_{11} + {Z_{23}}^2 + 4 \cdot {Z_{12}}^2 + 8 \cdot Z_{12} \cdot Z_{13} + 4 \cdot {Z_{13}}^2 \right)^{\frac{1}{2}} \\ Z_{A2} = \frac{Z_{11}}{2} + \frac{Z_{22}}{2} - \frac{Z_{14}}{2} - \frac{Z_{23}}{2} - \frac{1}{2} \cdot \left({Z_{22}}^2 + 2 \cdot Z_{14} \cdot Z_{22} - 2 \cdot Z_{22} \cdot Z_{11} - 2 \cdot Z_{22} \cdot Z_{23} + \cdot {Z_{14}}^2 \right. \\ \left. - 2 \cdot Z_{11} \cdot Z_{14} - 2 \cdot Z_{14} \cdot Z_{23} + {Z_{11}}^2 + 2 \cdot Z_{23} \cdot Z_{11} + {Z_{23}}^2 + 4 \cdot {Z_{12}}^2 - 8 \cdot Z_{12} \cdot Z_{13} + 4 \cdot {Z_{13}}^2 \right)^{\frac{1}{2}} \\ Z_{A3} = \frac{Z_{11}}{2} + \frac{Z_{22}}{2} - \frac{Z_{14}}{2} - \frac{Z_{23}}{2} + \frac{1}{2} \cdot \left({Z_{22}}^2 + 2 \cdot Z_{14} \cdot Z_{22} - 2 \cdot Z_{22} \cdot Z_{11} - 2 \cdot Z_{22} \cdot Z_{23} + \cdot {Z_{14}}^2 \right. \\ \left. - 2 \cdot Z_{11} \cdot Z_{14} - 2 \cdot Z_{14} \cdot Z_{23} + {Z_{11}}^2 + 2 \cdot Z_{23} \cdot Z_{11} + {Z_{23}}^2 + 4 \cdot {Z_{12}}^2 - 8 \cdot Z_{12} \cdot Z_{13} + 4 \cdot {Z_{13}}^2 \right)^{\frac{1}{2}} \\ Z_{A4} = \frac{Z_{11}}{2} + \frac{Z_{22}}{2} + \frac{Z_{14}}{2} + \frac{Z_{23}}{2} - \frac{1}{2} \cdot \left({Z_{22}}^2 - 2 \cdot Z_{14} \cdot Z_{22} - 2 \cdot Z_{22} \cdot Z_{11} + 2 \cdot Z_{22} \cdot Z_{23} + \cdot {Z_{14}}^2 \right. \\ \left. + 2 \cdot Z_{11} \cdot Z_{14} - 2 \cdot Z_{14} \cdot Z_{23} + {Z_{11}}^2 - 2 \cdot Z_{23} \cdot Z_{11} + {Z_{23}}^2 + 4 \cdot {Z_{12}}^2 + 8 \cdot Z_{12} \cdot Z_{13} + 4 \cdot {Z_{13}}^2 \right)^{\frac{1}{2}} \end{cases}$$

(110.)

$$Z_A = \begin{bmatrix} Z_{11} & Z_{12} & Z_{13} & Z_{13} \\ Z_{12} & Z_{11} & Z_{13} & Z_{13} \\ Z_{13} & Z_{13} & Z_{11} & Z_{12} \\ Z_{13} & Z_{13} & Z_{12} & Z_{11} \end{bmatrix} \rightarrow \begin{cases} Z_{A1} = Z_{11} + Z_{12} + 2 \cdot Z_{13} \\ Z_{A2} = Z_{11} + Z_{12} - 2 \cdot Z_{13} \\ Z_{A3} = Z_{11} - Z_{12} \\ Z_{A4} = Z_{11} - Z_{12} \end{cases}$$

(111.)

$$Z_A = \begin{bmatrix} Z_{11} & Z_{12} & Z_{13} & Z_{13} \\ Z_{12} & Z_{11} & Z_{13} & Z_{13} \\ Z_{13} & Z_{13} & Z_{11} & Z_{12} \\ Z_{13} & Z_{13} & Z_{12} & Z_{11} \end{bmatrix} \rightarrow I_{A1} = \begin{bmatrix} 1 \\ 1 \\ 1 \\ 1 \end{bmatrix}, I_{A2} = \begin{bmatrix} 1 \\ 1 \\ -1 \\ -1 \end{bmatrix}, I_{A3} = \begin{bmatrix} 1 \\ -1 \\ 1 \\ -1 \end{bmatrix}, I_{A4} = \begin{bmatrix} 1 \\ -1 \\ -1 \\ 1 \end{bmatrix}$$

(112.)

This simplicity is encouraging from the CAD implementation frame of reference as simple rules could be created for eigenvalues computation. Moreover, it is clear that existing eigenvalues are not distinct. Number of the independent modes in parallel amplifiers incorporating ideal corporate structures is not equal to the number of the combined amplifiers $N=2^{(n-1)}$ however it is equal to the order of the combining network n. This way it is also easy to identify and intuitively ascribe different odd modes and corresponding eigenvalues to the different level loops existing in amplifier.

$$I_{Ax,m} = (-1)^{\left\lfloor \frac{m-1}{2^{(n+1-x)}} \right\rfloor} \text{ where } \lfloor x \rfloor = \max \{ n \in Z \mid n \leq x \}$$

(113.)

$$Z_{Ax} = \sum_{m=1}^{2^n} (-1)^{\left\lfloor \frac{m-1}{2^{(n+1-x)}} \right\rfloor} \cdot Z_{1m} \text{ where } \lfloor x \rfloor = \max \{ n \in Z \mid n \leq x \}$$

(114.)

The rules describing eigenvectors (113.) and eigenvalues (114.) were created easily by means of the floor function and they were used to create a description of the distinct eigenvalues and eigenvectors in case of N=8.

Equations (115.) and (116.) allow to test for the N=8 amplifier stability with the Freitag method. Furthermore, equation (114.) along with the measurement procedure of the bisections Z matrixes create a complete approach in order to obtain equivalent modes impedances values for the parallel amplifiers incorporating ideal corporate structures.

$$Z_A = \begin{bmatrix} Z_{11} & Z_{12} & Z_{13} & Z_{13} & Z_{14} & Z_{14} & Z_{14} & Z_{14} \\ Z_{12} & Z_{11} & Z_{13} & Z_{13} & Z_{14} & Z_{14} & Z_{14} & Z_{14} \\ Z_{13} & Z_{13} & Z_{11} & Z_{12} & Z_{14} & Z_{14} & Z_{14} & Z_{14} \\ Z_{13} & Z_{13} & Z_{12} & Z_{11} & Z_{14} & Z_{14} & Z_{14} & Z_{14} \\ Z_{14} & Z_{14} & Z_{14} & Z_{14} & Z_{11} & Z_{12} & Z_{13} & Z_{13} \\ Z_{14} & Z_{14} & Z_{14} & Z_{14} & Z_{12} & Z_{11} & Z_{13} & Z_{13} \\ Z_{14} & Z_{14} & Z_{14} & Z_{14} & Z_{13} & Z_{13} & Z_{11} & Z_{12} \\ Z_{14} & Z_{14} & Z_{14} & Z_{14} & Z_{13} & Z_{13} & Z_{12} & Z_{11} \end{bmatrix} \rightarrow \begin{cases} Z_{A1} = Z_{11} + Z_{12} + 2 \cdot Z_{13} + 4 \cdot Z_{14} \\ Z_{A2} = Z_{11} + Z_{12} + 2 \cdot Z_{13} - 4 \cdot Z_{14} \\ Z_{A3} = Z_{11} + Z_{12} - 2 \cdot Z_{13} \\ Z_{A4} = Z_{11} - Z_{12} \end{cases}$$

(115.)

$$Z_A = \begin{bmatrix} Z_{11} & Z_{12} & Z_{13} & Z_{13} & Z_{14} & Z_{14} & Z_{14} & Z_{14} \\ Z_{12} & Z_{11} & Z_{13} & Z_{13} & Z_{14} & Z_{14} & Z_{14} & Z_{14} \\ Z_{13} & Z_{13} & Z_{11} & Z_{12} & Z_{14} & Z_{14} & Z_{14} & Z_{14} \\ Z_{13} & Z_{13} & Z_{12} & Z_{11} & Z_{14} & Z_{14} & Z_{14} & Z_{14} \\ Z_{14} & Z_{14} & Z_{14} & Z_{14} & Z_{11} & Z_{12} & Z_{13} & Z_{13} \\ Z_{14} & Z_{14} & Z_{14} & Z_{14} & Z_{12} & Z_{11} & Z_{13} & Z_{13} \\ Z_{14} & Z_{14} & Z_{14} & Z_{14} & Z_{13} & Z_{13} & Z_{11} & Z_{12} \\ Z_{14} & Z_{14} & Z_{14} & Z_{14} & Z_{13} & Z_{13} & Z_{12} & Z_{11} \end{bmatrix} \rightarrow I_{A1} = \begin{bmatrix} 1 \\ 1 \\ 1 \\ 1 \\ 1 \\ 1 \\ 1 \\ 1 \end{bmatrix}, I_{A2} = \begin{bmatrix} 1 \\ 1 \\ 1 \\ 1 \\ -1 \\ -1 \\ -1 \\ -1 \end{bmatrix}, I_{A3} = \begin{bmatrix} 1 \\ 1 \\ -1 \\ -1 \\ 1 \\ 1 \\ -1 \\ -1 \end{bmatrix}, I_{A4} = \begin{bmatrix} 1 \\ -1 \\ 1 \\ -1 \\ 1 \\ -1 \\ 1 \\ -1 \end{bmatrix}$$

(116.)

4.1 Example PA.1

To verify the correctness of the obtained equations, the simplified Freitag method was used in the design process of the example power amplifier designed with commercial D01PH Ommic. Test examples were designed to operate at F_0=20 GHz, with the output power P_{out}>32 dBm. Three stage structure was assumed what resulted with topology of the 1,2,8 devices at appropriate stages.
The layout of the amplifier is displayed in the Figure 52. A small signal gain and Rollet k-factor was laid out in the Figure 53. The circuit is unconditionally stable from the two port representation perspective. Large signal simulation at F_0 is presented in the Figure 54.

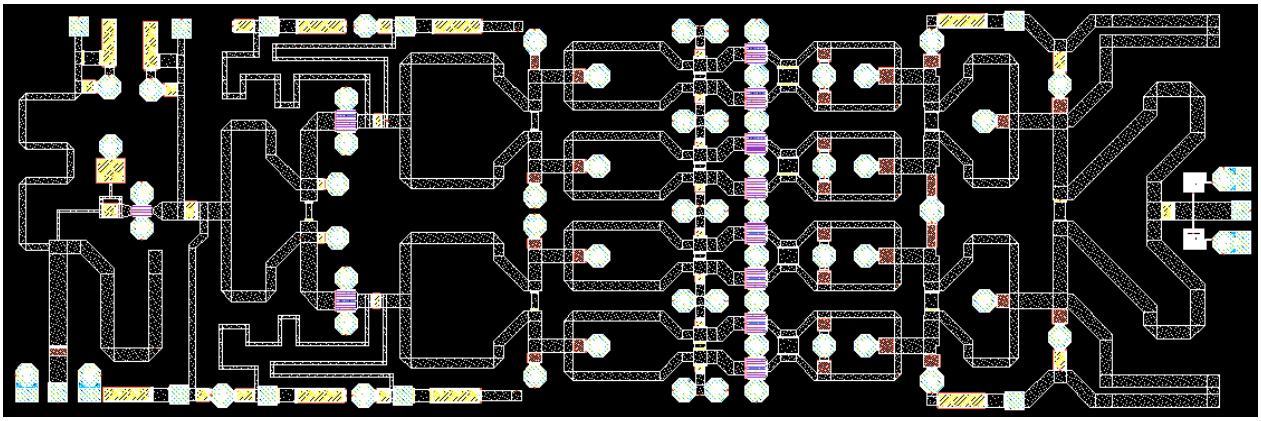

Figure 52 Example power amplifier PA.1 layout.

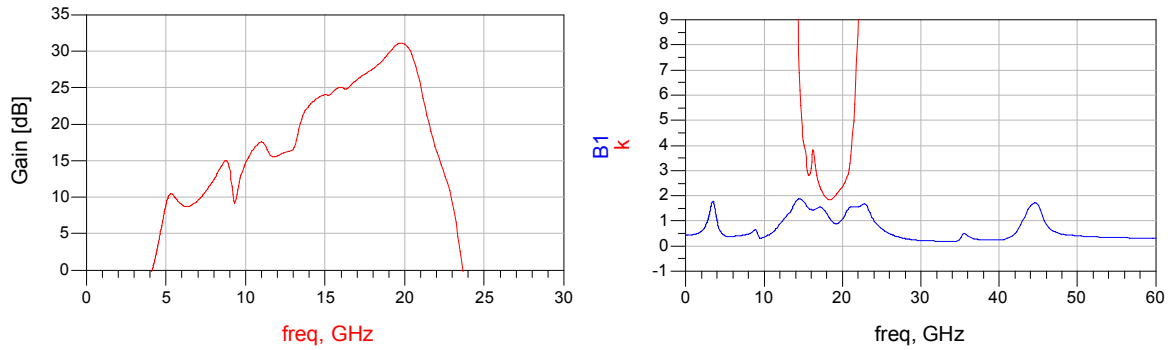

Figure 53 Gain and Rollet stability factor of the example power amplifier PA.1.

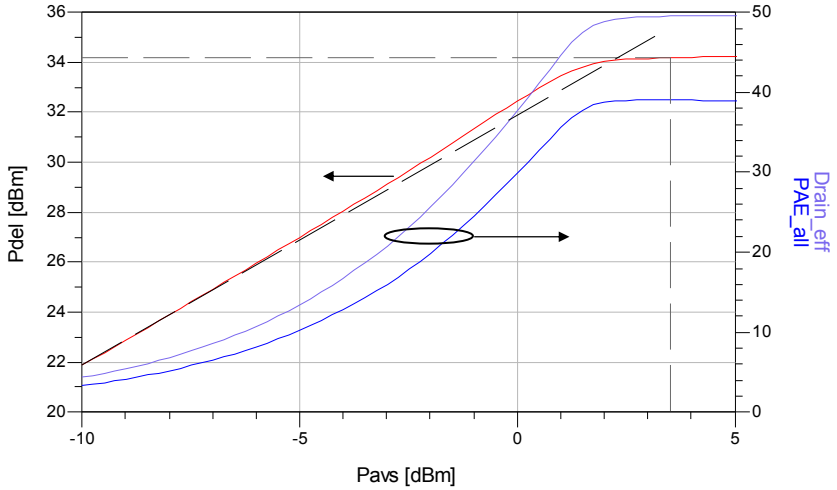

Figure 54 Power performance of the example power amplifier PA.1.

While Freitag method was applied, amplifier Even mode - Figure 55, Odd mode 1 - Figure 56 and Odd mode 2 - Figure 57 were discovered to be unstable at the output of the last stage. For the output of the second stage Even mode was revealed as unstable. Finally, at the output of the first stage the amplifier was stable with the Even mode.

A verification with the Ohtomo method assured the correctness of the predicted stability problems - Figure 59. Basing on the obtained information, the sources of the problems were identified and PA circuit has been corrected. In consequence, the onset of the oscillation was not fulfilled any longer for any of the modes. The Ohtomo method confirmed these assumptions, while the curves which previously encircled the critical point remained inside of the circle of the radius equal to one.

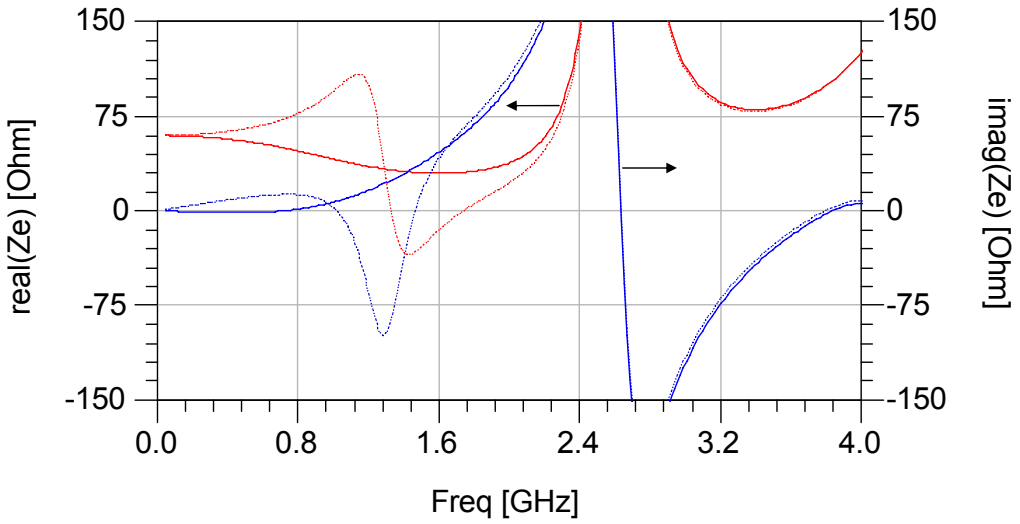

Figure 55 PA.1 Even mode impedance before (broken line) and after the corrective actions (solid line).

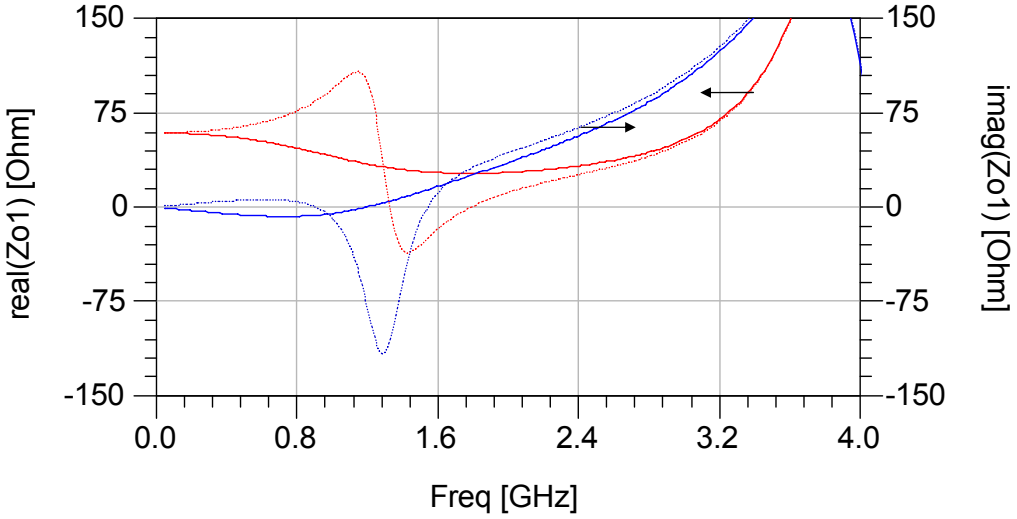

Figure 56 PA.1 Odd mode 1 impedance before (broken line) and after the corrective actions (solid line).

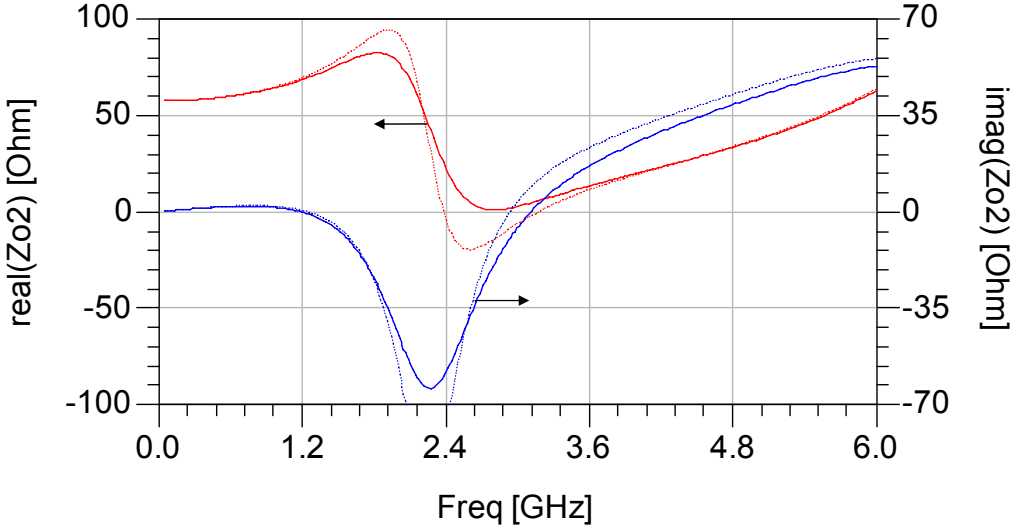

Figure 57 PA.1 Odd mode 2 impedance before (broken line) and after the corrective actions (solid line).

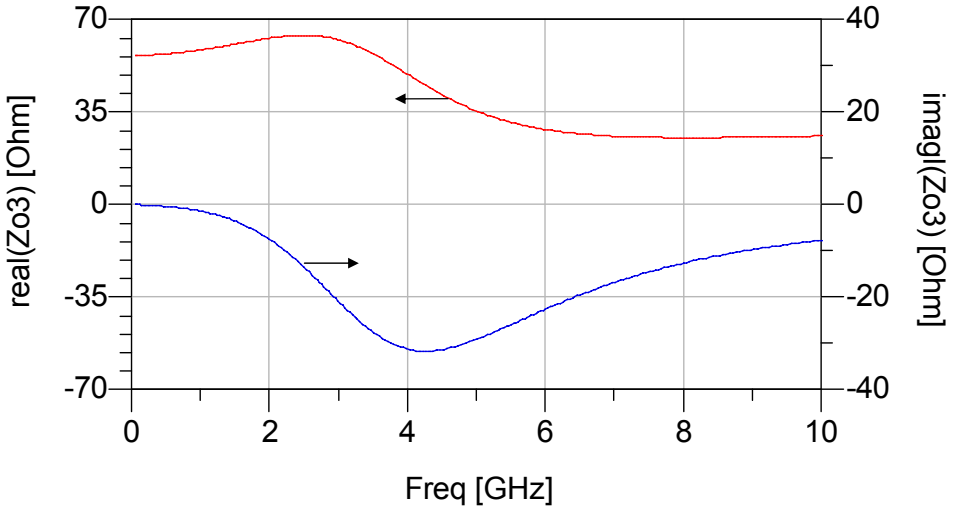

Figure 58 PA.1 Odd mode 3 impedance before (broken line) and after corrective the actions (solid line)- curves are superimposed.

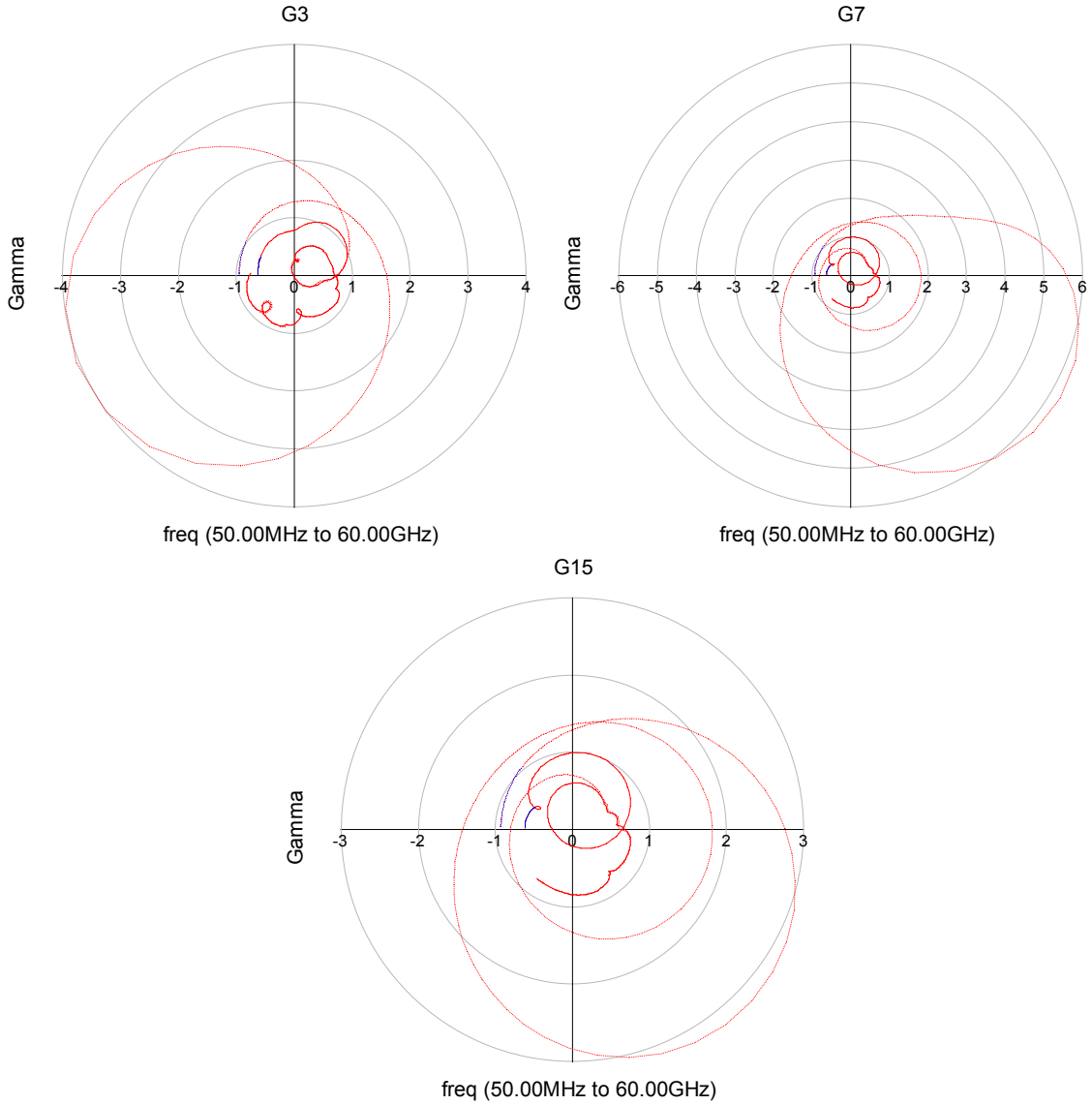

Figure 59 PA.1 Ohtomo curves nr: 3, 7, 15 before (broken line) and after the corrective actions (solid line).

4.2 Example PA.2

To test the simplified Freitag method more intensively a second example power amplifier was designed by utilizing the cluster matching approach. The second test example was planned with identical assumptions as the previous one, but this time more stress was put on the small dimensions of the amplifier. The three stage structure with a topology of the 1,2,8 devices at the appropriate stages was used as it was also done earlier. The layout of the amplifier is shown in the Figure 60. A small signal gain and Rollet k-factor were portrayed in the Figure 61. The circuit is unconditionally stable due to the two port representation frame of reference. A large signal simulation at F_0 is presented in the Figure 62.

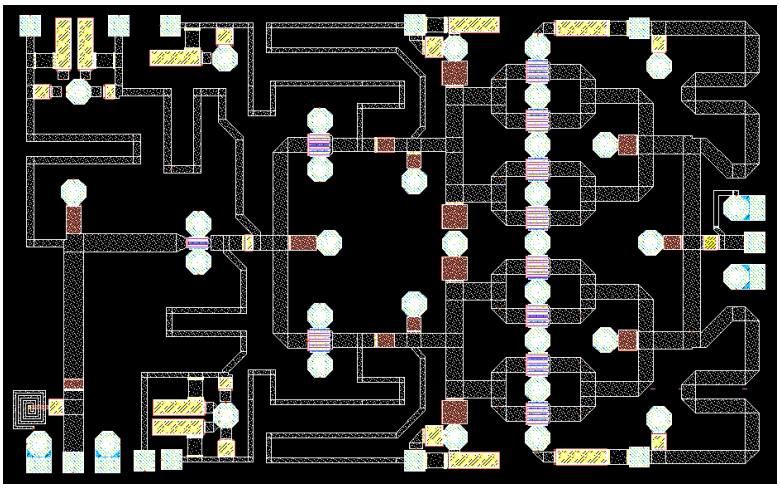

Figure 60 Example power amplifier PA.2 layout.

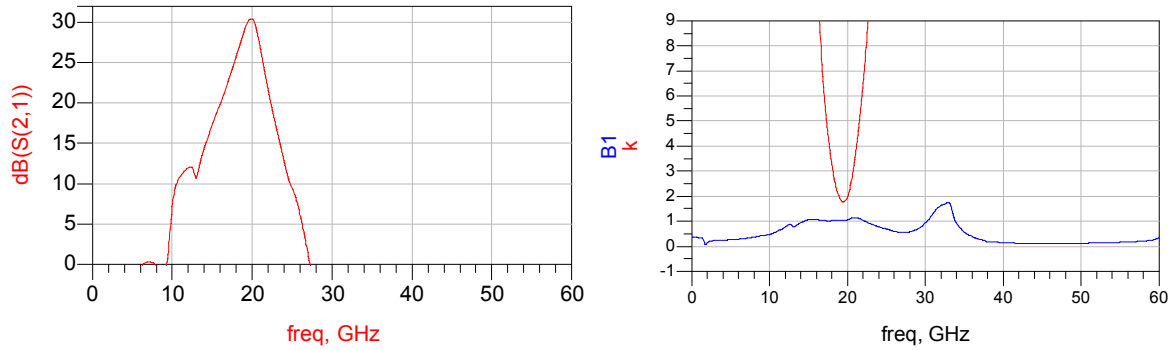

Figure 61 Gain and Rollet stability factor of the example power amplifier PA.2.

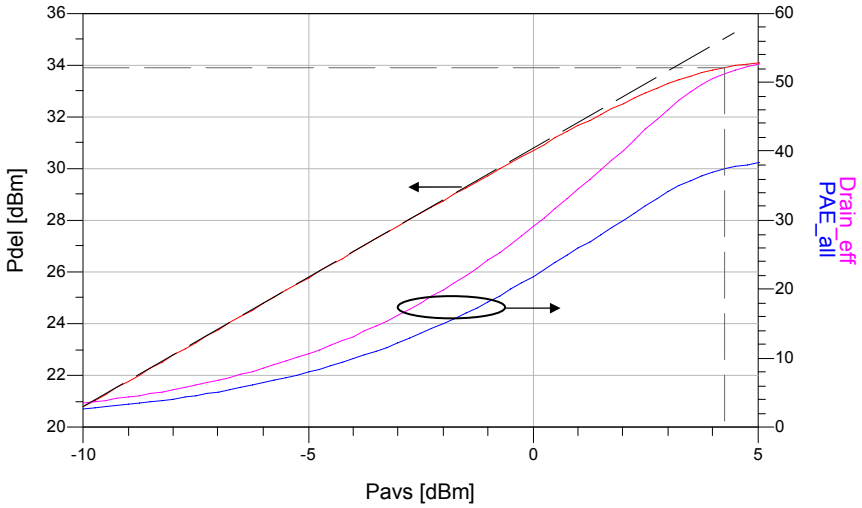

Figure 62 Power performance of the example power amplifier PA.2.

While the Freitag method was applied, the amplifier Even mode - Figure 63, Odd mode 1 - Figure 64 and Odd mode 2 - Figure 65 were exposed as unstable at the output of the last stage. For the output of the second stage the Even mode was discovered to be unstable the output of the first stage. A verification with the Ohtomo method assured correctness of the predicted stability problems - Figure 67. Basing on the obtained information, sources of the problems were identified and PA circuit was corrected. In an outcome, the onset of oscillation was no longer fulfilled for any of the modes.

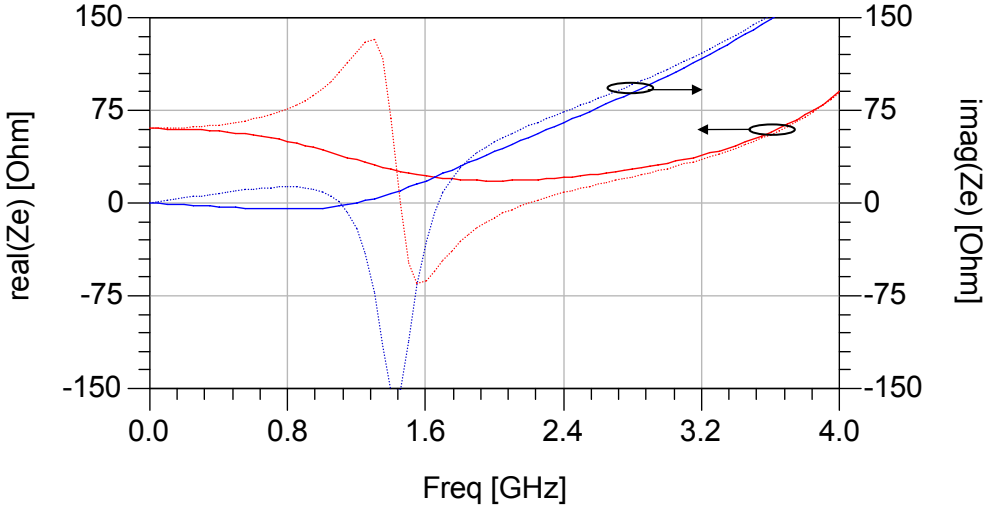

Figure 63 PA.2 Even mode impedance before (broken line) and after the corrective actions (solid line).

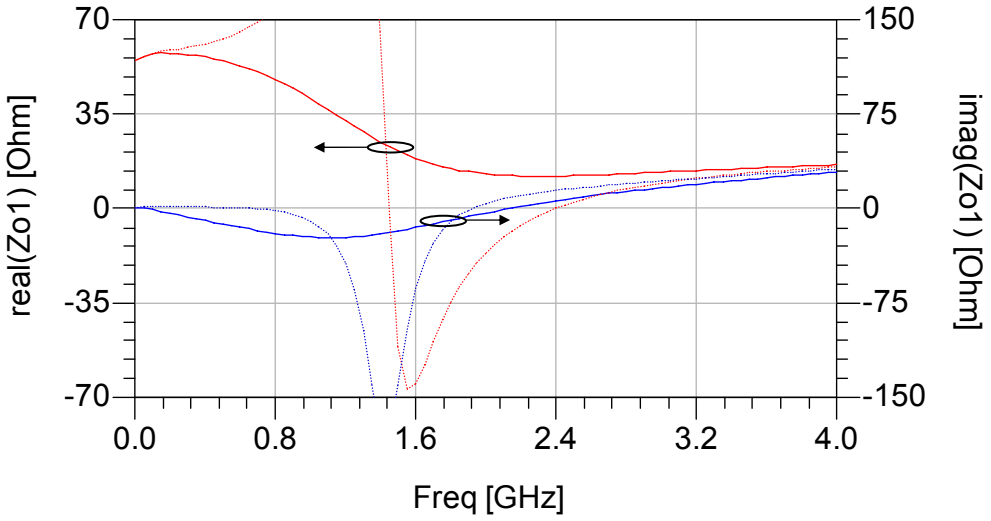

Figure 64 PA2. Odd mode 1 impedance before (broken line) and after the corrective actions (solid line).

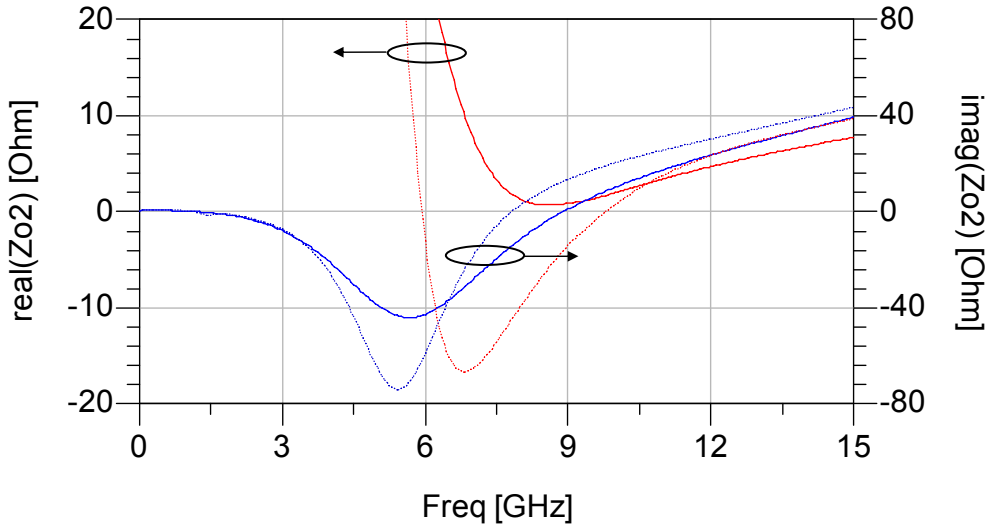

Figure 65 PA2. Odd mode 2 impedance before (broken line) and after the corrective actions (solid line).

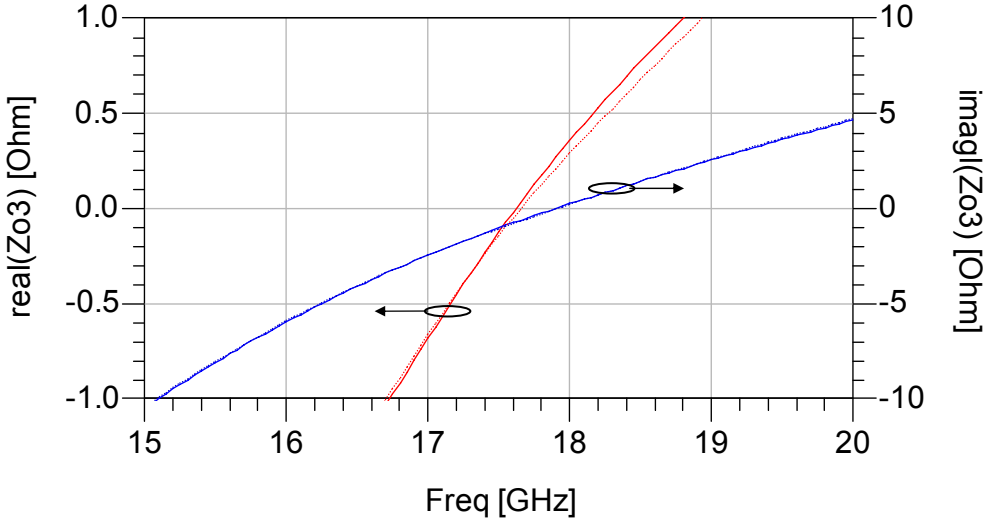

Figure 66 PA2. Odd mode 3 impedance before (broken line) and after the corrective actions (solid line).

This time Ohtomo method did not confirm Freitag method results while curves no: 7 and 15 after the corrective actions were still encircling the critical point - Figure 67 (page 75). In this situation the two methods have given different outcome. Than, without an additional study the judgement about stability is not possible. Moreover, uncertainty questions credibility of the methods while one of them clearly gave wrong answer to the question of the tested circuit stability. Unfortunately, to be certain which one and why it failed**,** another method needs to be involved. For the outcome to be confident, verification with Time Domain simulations is performed. This is equivalent of the virtual experiment allowing to determine the circuit behaviour and leads to a discovery source of the incorrect judgement in case of one of the methods.

4.3 Example PA.3

While the motivation to develop the frequency domain stability methods was underlined in Chapter 1, it will be just reminded that the distributed components ubiquitous in the microwave circuits are very inconvenient in the time domain. This has a direct implication in modelling and simulating such circuits in the Time Domain simulators. The difficulty in question was observed directly upon simulation trials of the problematic PA.2 example. Lack of the trustworthy results with the realistic power amplifier lead to design of the simplified example using combination of the real and ideal elements - PA.3. The amplifier fulfils the same requirements as the example circuits PA.1 and PA.2, therefore it operates at F_0=20 GHz, with output power P_{out}>32 dBm. A three stage structure with topology of the 1,2,8 devices in appropriate stages was maintained - Figure 68. Complete and actual nonlinear device models form D01PH Ommic commercial process have been used for the design of the independently pre-matched amplifiers: AMP1, AMP2 and AMP3. Amplifiers use ideal lumped elements for the matching and stabilization of the even mode. Corporate combining network is designed with applying capacitive loaded microstrip transmission lines which reflects the commonly used approach. Small signal gain and Rollet k-factor were presented in the Figure 69. The circuit is unconditionally stable form the two port representation frame of reference. Large signal simulation at F_0 is presented in the Figure 70.

While Freitag method was applied, amplifier Even mode - Figure 71, Odd mode 1 - Figure 72 and Odd mode 3 - Figure 74 were discovered to be stable, Odd mode 2 - Figure 73 was determined to be unstable at the output of the last stage.

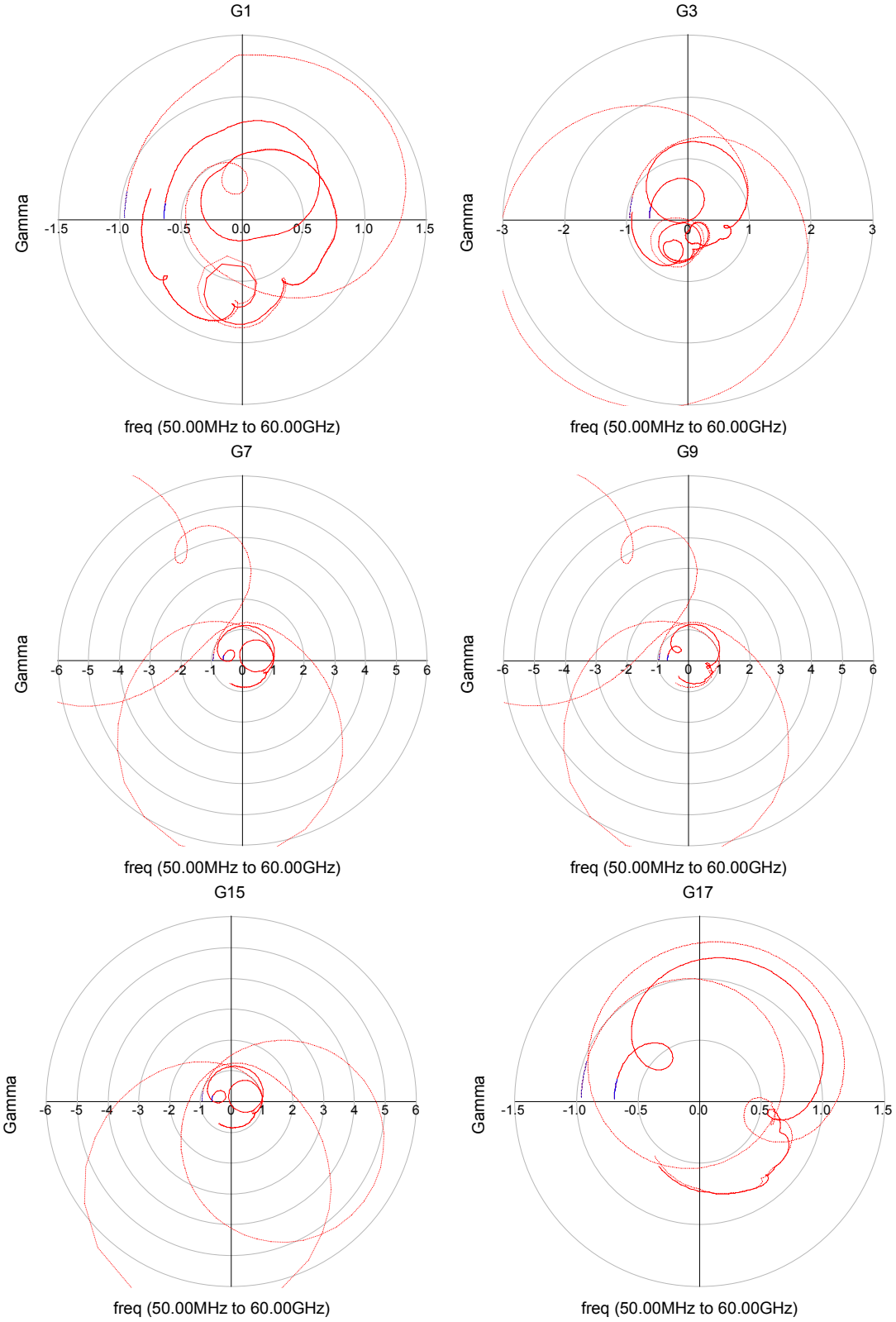

Figure 67 Ohtomo curves nr: 1, 3, 7, 9, 15, 17 before (broken line) and after corrective actions (solid line).

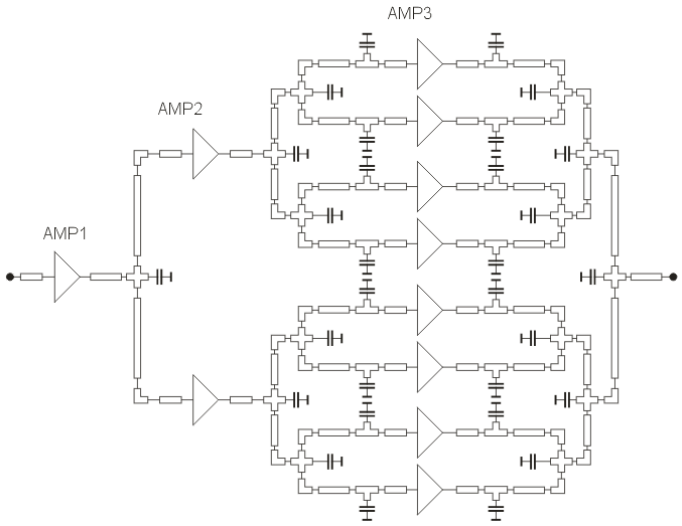

Figure 68 Example power amplifier PA.3 structure.

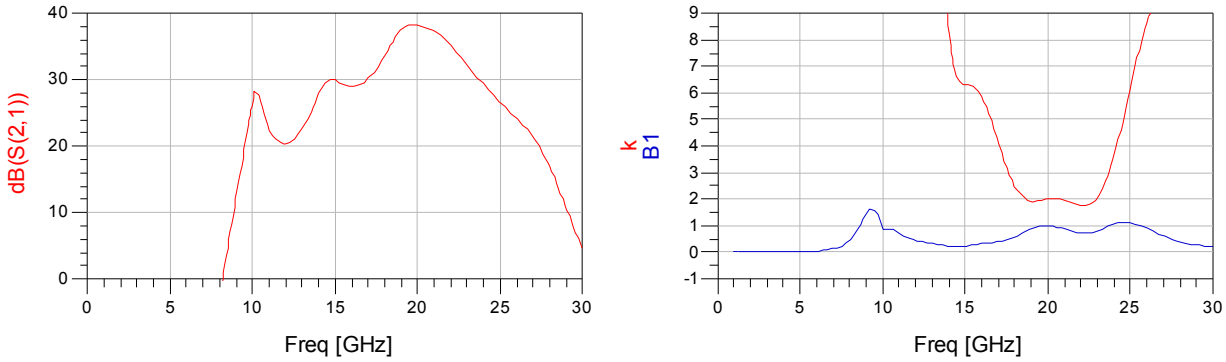

Figure 69 Gain and Rollet stability factor of the example power amplifier PA.3.

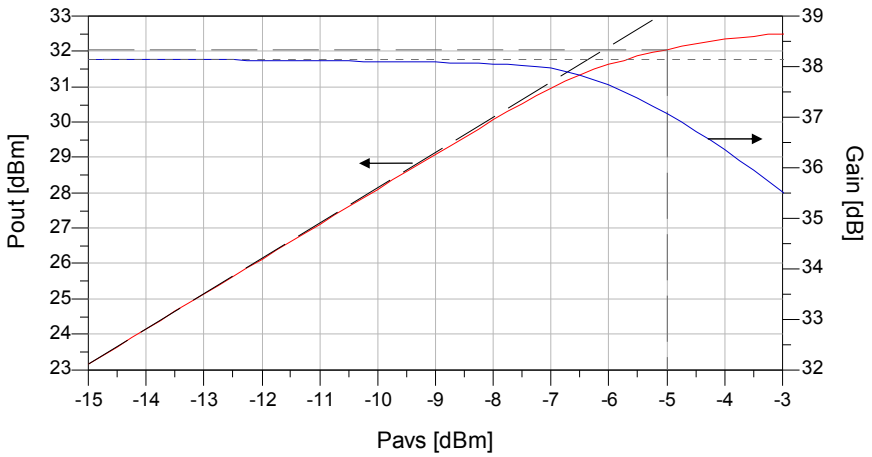

Figure 70 Power performance of the example power amplifier PA.3.

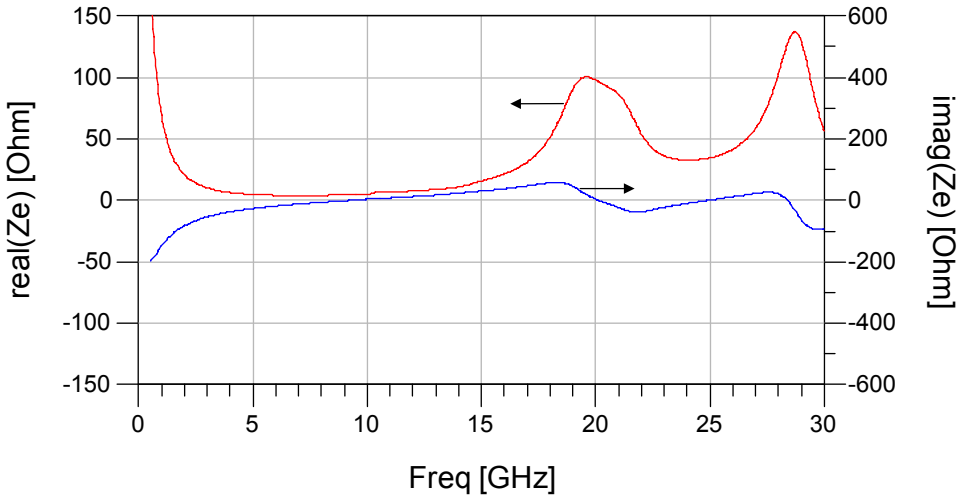

Figure 71 Even mode impedance of the example power amplifier PA.3.

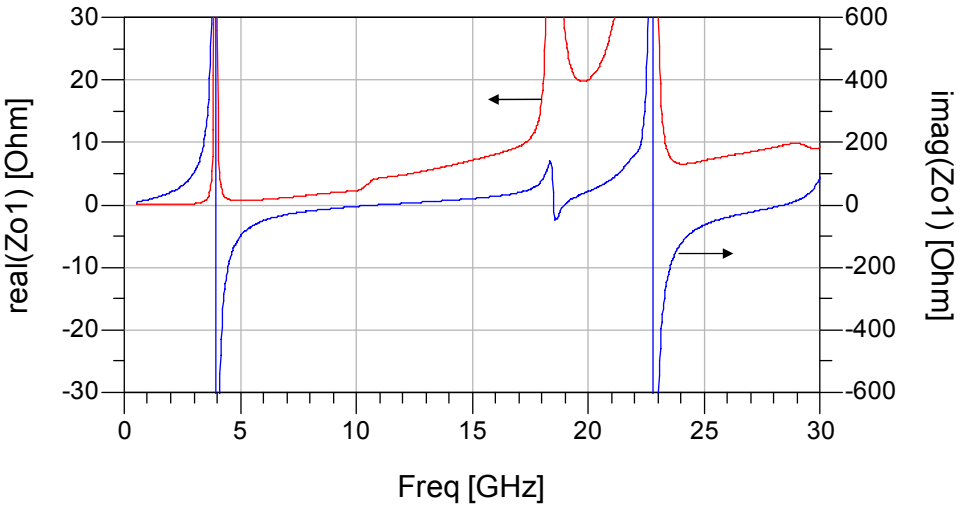

Figure 72 Odd mode 1 impedance of the example power amplifier PA.3.

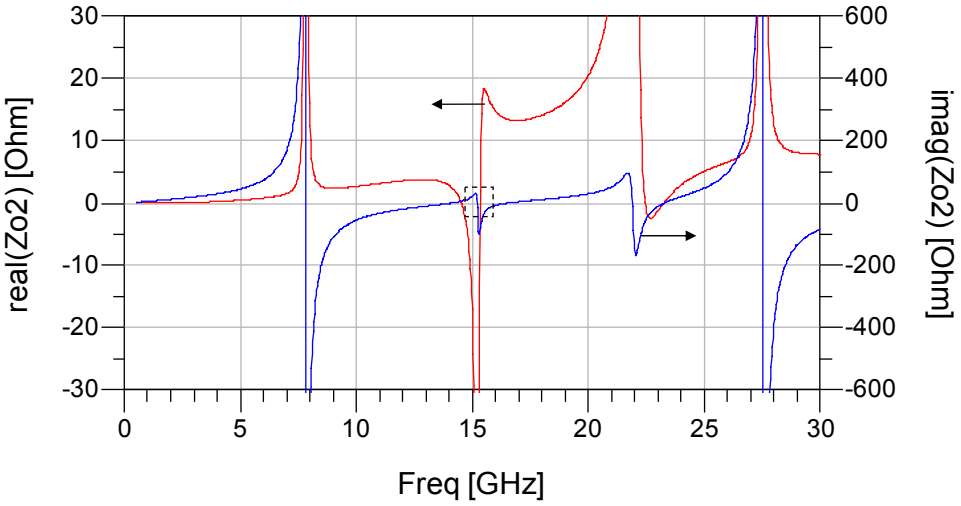

Figure 73 Odd mode 2 impedance of the example power amplifier PA.3.

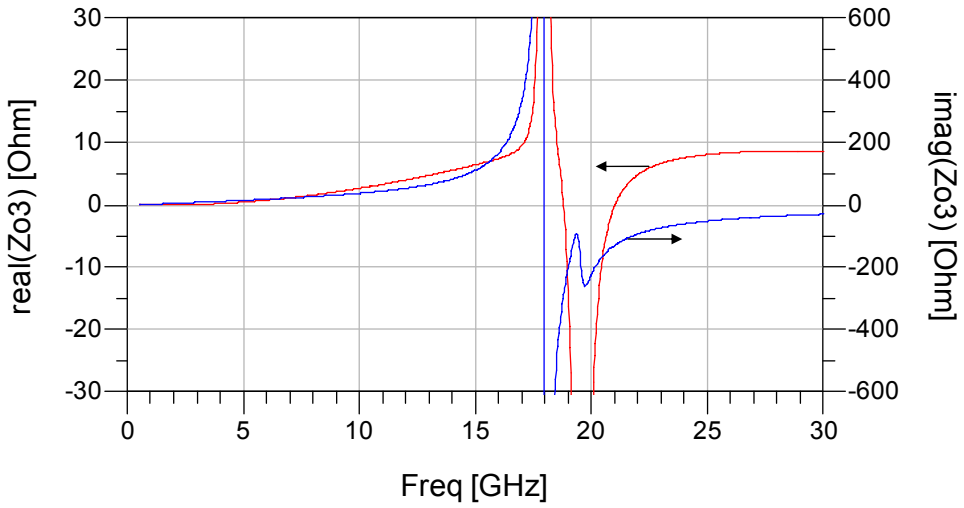

Figure 74 Odd mode 3 impedance of the example power amplifier PA.3.

Also Ohtomo method predicts stability problems while the curves no: 7 and 15 encircled the critical point - Figure 75. But again, the result does not enlighten in detail the circuit behaviour- the source of instability is still unknown, so it is not validating the Freitag method. Thus, Time Domain simulations will be performed to discover the sources of the previous inconsistencies.

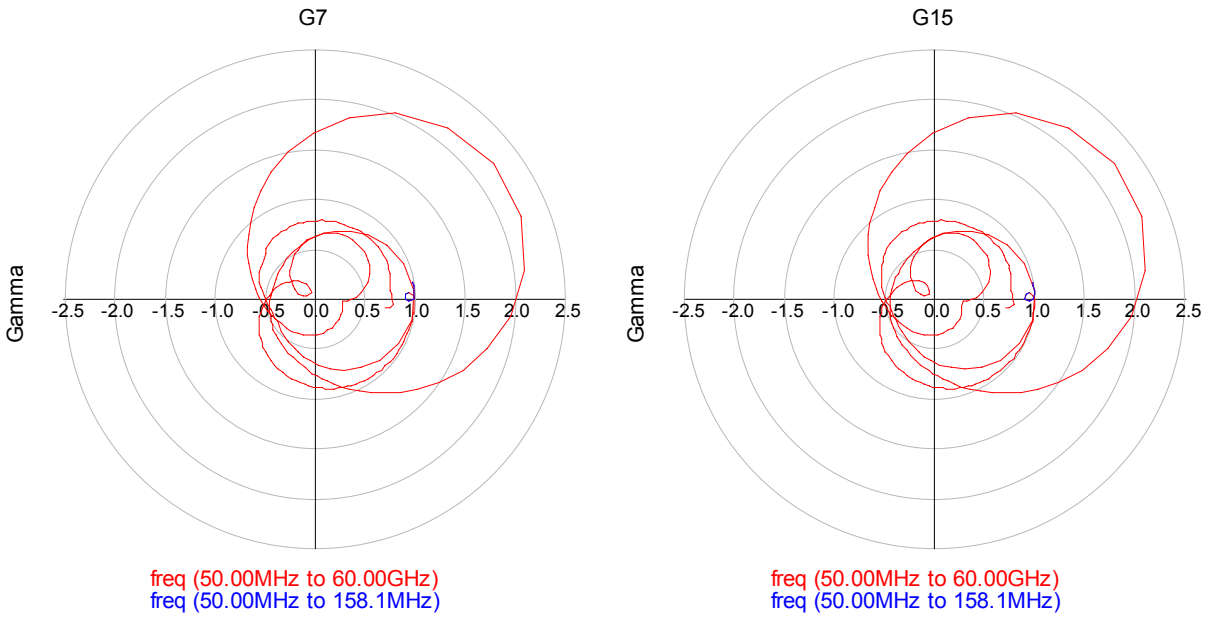

Figure 75 Ohtomo curves no: 7, 15 of the example power amplifier PA.3.

4.4 Time domain simulations of PA.3

Simulations were performed by means of Agilent ADS Transient simulator. Each mode was addressed with separate simulation setup. In each case the current pulse source was used to excite an appropriate mode. To maintain single mode excitation in case of the Odd modes 2 and 3: 2 and 4 the current sources were used to simultaneously excite all the loops and maintain the required balance. Odd modes were represented with differential voltages at the input of the appropriate level

output combiner and even mode was represented with voltage at the output of the amplifier - Figure 76. Excitation pulse was initiated at t=1ns to confirm steady state conditions of the circuit.

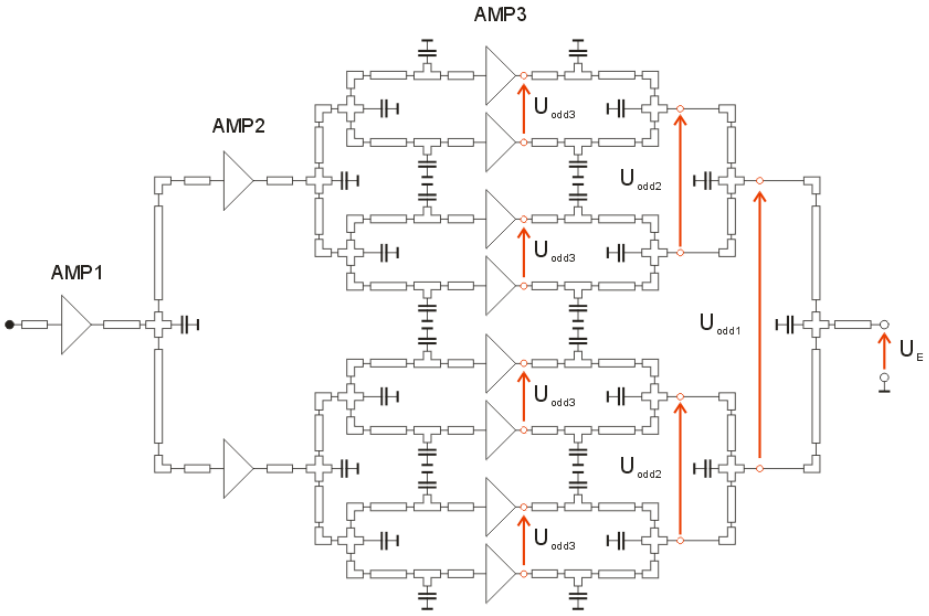

Figure 76 Voltages used to represent different modes of the example power amplifier PA.3.

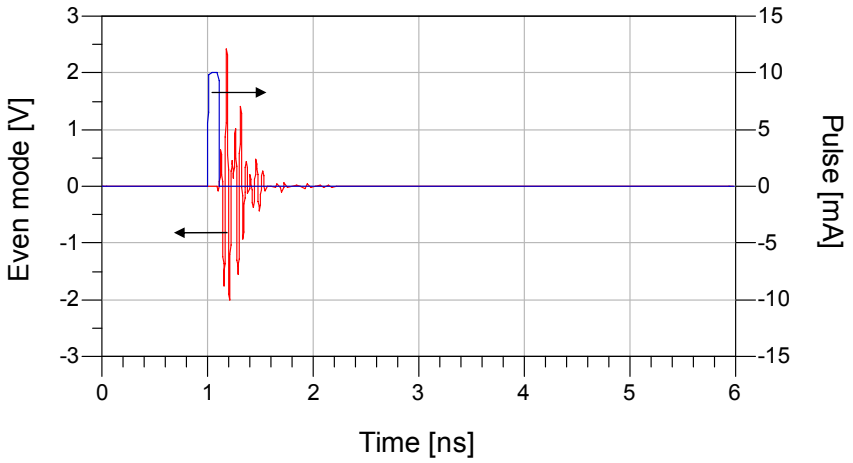

Figure 77 Response of the PA.3 example for the Even mode excitation together with the stimulus (pulse).

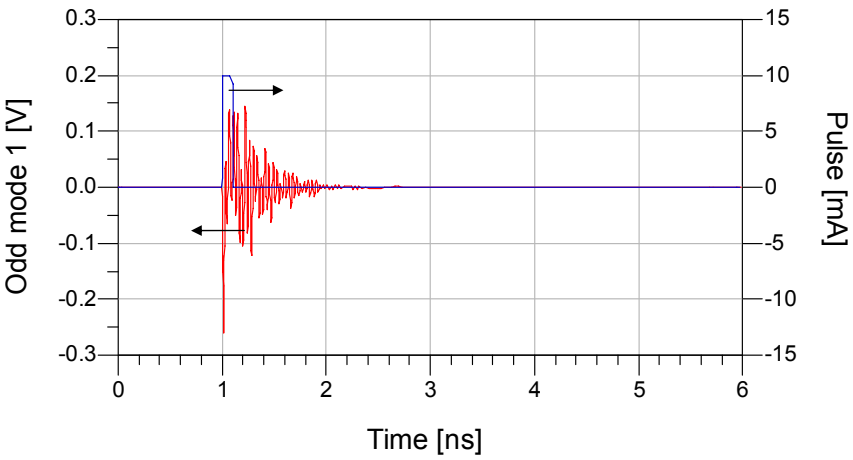

Figure 78 Response of the PA.3 example for the Odd mode 1 excitation together with the stimulus (pulse).

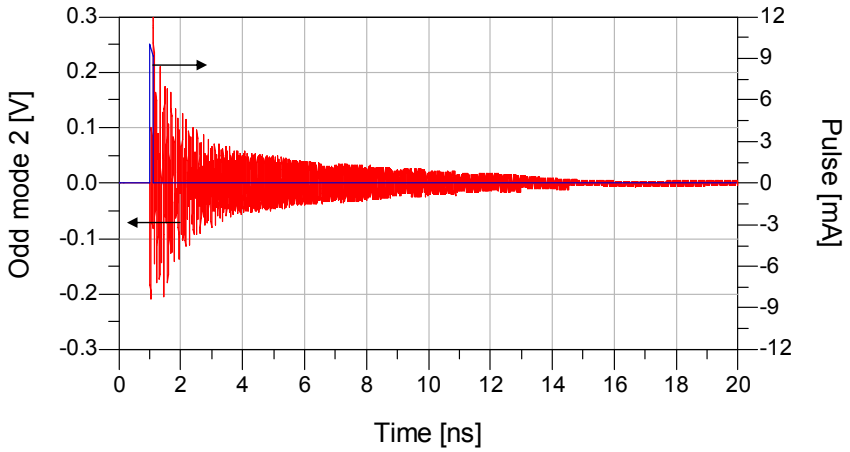

Figure 79 Response of the PA.3 example for the Odd mode 2 excitation together with the stimulus (pulse).

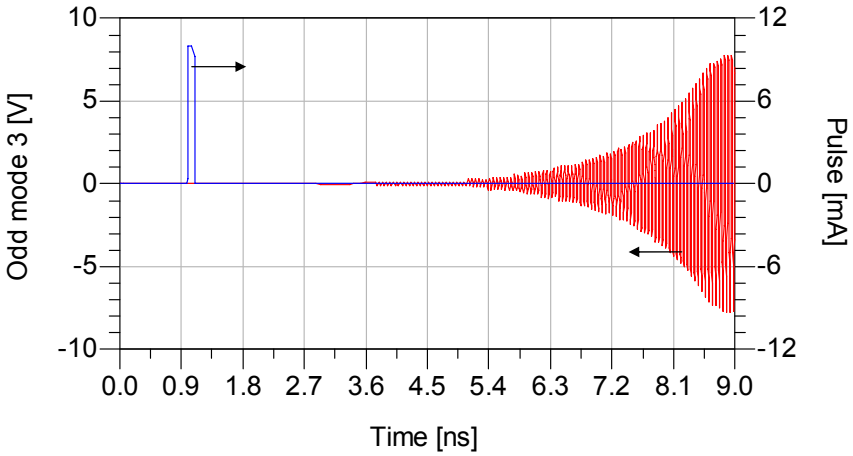

Figure 80 Response of the PA.3 example for the Odd mode 3 excitation together with the stimulus (pulse).

Time domain analysis results confirm the existence of the instability in the PA.3 example as it was predicted by both Freitag and Ohtomo methods. However, the source of the problems was recognized incorrectly by the Freitag method. It predicted correctly the stability of the Even mode - Figure 71 and Odd mode 1 - Figure 72. At the same time the method declares Odd mode 2 to be unstable - Figure 73. The time domain response for Odd mode 2 excitation is the dumped one and the circuit returns to zero the state, proving mode stability - Figure 79. Moreover, Odd mode 3 impedance does not fulfil onset of the oscillation and is declared to be stable - Figure 74, while time domain analysis shows a successful excitation of the Odd mode 3 - Figure 80. This inconsistency proves that Freitag method is not completely applicable to all cases and there is still space for improvement.

4.5 The Freitag method improvement

An example power amplifier PA.3 serving as a test vehicle to the Freitag method has potential to reveal two types of situation leading to incorrect result. The first one, where stable Mode was declared unstable and the latter, even more serious, where instability was not detected. Both of the mistakes came from an initial assumption that Z matrix description is enough to address the tested circuit stability. While the stability problem was treated as the oscillator problem, it is not a correct assumption. This is due to two types of resonance that could exist in resonant structures. Impedance

description addresses correctly only one of them – the series resonance. It is exact source of error in case of the Odd mode 2.

4.5.1 Fake resonance error

To address the error in question, the analysis of the Odd mode 2 impedance was repeated and the area where the onset of oscillation was fulfilled was scaled up and presented in the Figure 81. It is clearly visible in the scaled up graph that imaginary part of the impedance is crossing axis with the negative slope. If at the same time series LC and RLC circuit are analyzed at the resonant frequency, it can be discovered that the imaginary part of both circuits is positively crossing zero value at resonance - Figure 82. On the other hand, imaginary part of the impedance of the parallel RLC circuit is crossing zero with negative slope at the resonant frequency while ideal parallel LC circuit is not crossing zero at all - Figure 83.

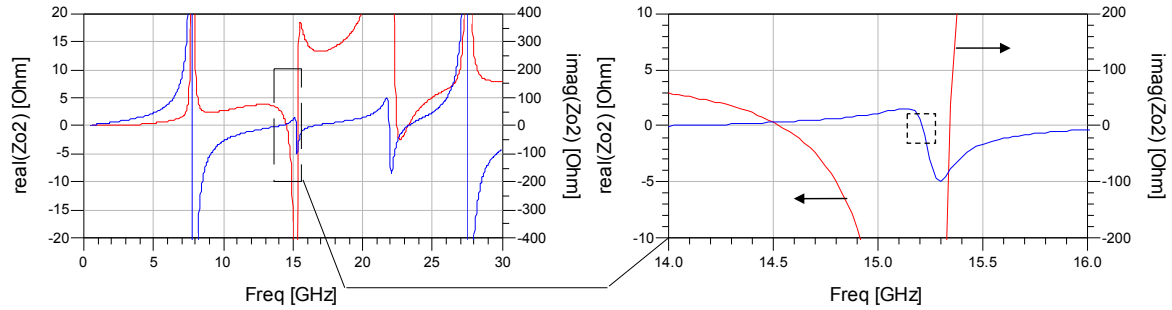

Figure 81 Odd mode 2 impedance of the example power amplifier PA.3 and scaled up area around the resonance.

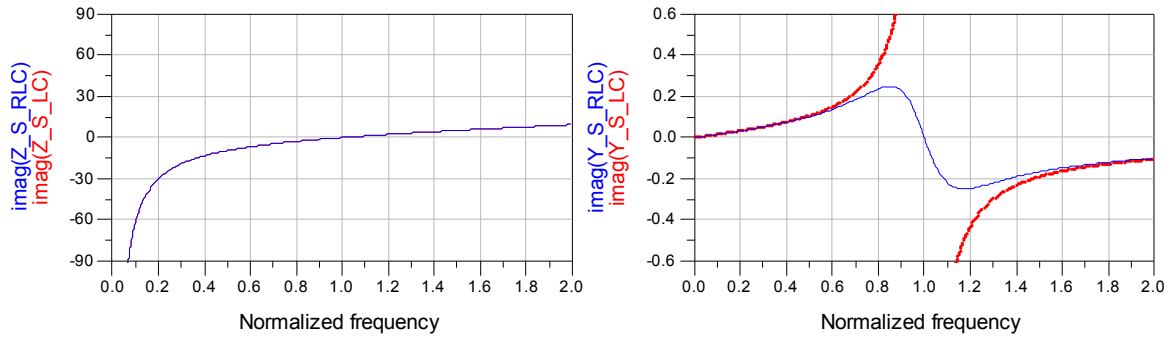

Figure 82 Imaginary part of the impedance (on the left) and admittance (on the right) of the series LC (blue) and RLC (red) circuits.

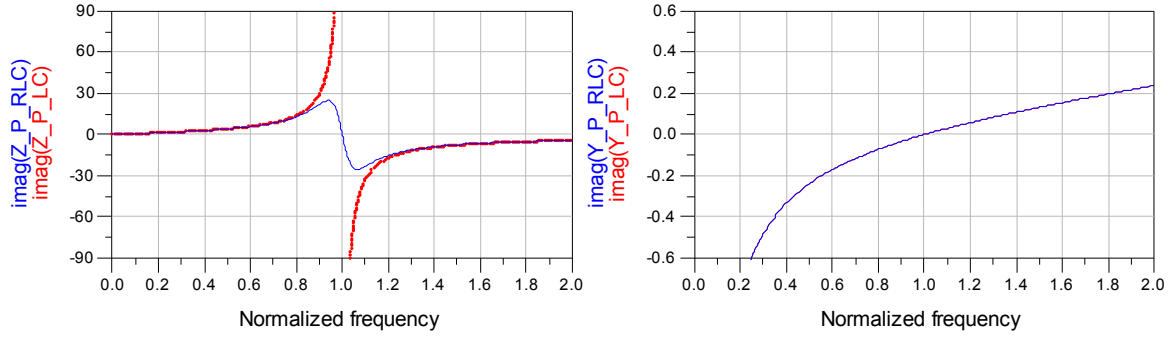

Figure 83 Imaginary part of the impedance (on the left) and admittance (on the right) of the parallel LC (blue) and RLC (red) circuits.

This mechanism is responsible for confusion of the resonance type and is related to the simple mathematics. If parallel LC and RLC circuits admittance will be described with equations (117.) and (118.) accordingly, it is easy to calculate value of the admittance at resonant frequency.

$$\mathrm{Y_{LC}} = j\omega\mathrm{C} + \frac{1}{j\omega\mathrm{L}} = j\left(\omega\mathrm{C} - \frac{1}{\omega\mathrm{L}}\right) = j0\Big|_{f=f_r} \tag{117.}$$

$$\mathrm{Y_{RLC}} = \frac{1}{\mathrm{R}} + j\omega\mathrm{C} + \frac{1}{j\omega\mathrm{L}} = \frac{1}{\mathrm{R}} + j\left(\omega\mathrm{C} - \frac{1}{\omega\mathrm{L}}\right) = \frac{1}{\mathrm{R}}\Big|_{f=f_r} \tag{118.}$$

If impedance is calculated now as inverse of the admittance in case of LC, its real part remains zero while the admittance was purely imaginary value. Meanwhile, imaginary part will be described with rectangular hyperbola and will poses asymptote at resonant frequency. That is not the case for the RLC circuit for which there exists constant value of the real part, due to which at the resonant frequency the circuit is purely resistive and the imaginary part crosses zero with the negative slope. Therefore, the negative slope at zero crossing for the imaginary part of the impedance cannot be interpreted as series resonance. An identical rule applies to admittance and parallel resonance. Therefore, the onset of oscillations needs to be complemented with additional term accepting positive zero crossing of the imaginary part only as a sign of the resonance. Equation (119.) represents this condition in case of the impedance and series resonance.

$$\frac{d}{df}\mathrm{Im}\{\mathrm{Z}(f)\}\Big|_{f=f_r} > 0 \tag{119.}$$

4.5.2 Not recognized instability

Second error is related to the Odd mode 3 instability, not discovered by the original Freitag method. The wrong judgment in that case is again due to pure impedance description being adopted as a base for stability test. In that case, the method produces reliable results only in case of the series resonance at the division plane. Therefore, to complete the method, the area of its functionality requires to be extended for the parallel resonance, what results in adding up the admittance description of the circuit bisections. Then, the same analysis as in case of the impedance description requests to be performed. A major difference is that this time eigenvectors will describe voltage excitation and eigenvalues will be associated with the admittance observed at all ports. In general case, separate analysis of admittance matrix will be done to find eigenvectors and eigenvalues. However, for the ideal corporate amplifiers eigenvectors of the Z and Y matrix are equal. Thus, a similar simplified scheme used to compute eigenvalues of the impedance description can be reused with the admittance matrix - (120.). This feature greatly reduces the effort required to correct the method subject to the ideal corporate structure.

$$\mathrm{Y_{Ax}} = \sum_{m=1}^{2^n} (-1)^{\left\lfloor \frac{m-1}{2^{(n+1-x)}} \right\rfloor} \cdot \mathrm{Y}_{1m} \text{ where } \lfloor x \rfloor = \max\{n \in \mathrm{Z} \mid n \le x\}$$

(120.)

4.5.3 An improved method and its verification

Two proposed improvements were applied to the Freitag method in order to overcome limitations related to the parallel resonance detection. For that reason, after an initial step of closing and dividing the circuit, bisections are to be described with the impedance and admittance matrixes. Then, the analysis of the eigenvalues is performed for both representations. In result, equivalent impedances and admittances of each mode are computed. In the end they have to be analyzed with a modified onset of the oscillation - (121.). A dissimilarity from original onset of oscillation lies in additional conditions introduced to describe the possibility of the parallel resonance. Besides, new onset of oscillation comprises an additional term preventing from resonance confusion and fake instability detection.

$$
\begin{array}{cc}
Z-conditions & Y-conditions \\
\begin{cases} \mathrm{Re}\{Z_e(f)\}<0 \\ \mathrm{Im}\{Z_e(f)\}=0 \\ \dfrac{d}{df}\mathrm{Im}\{Z_e(f)\}\Big|_{f=f_r}>0 \end{cases} & \begin{cases} \mathrm{Re}\{Y_e(f)\}<0 \\ \mathrm{Im}\{Y_e(f)\}=0 \\ \dfrac{d}{df}\mathrm{Im}\{Y_e(f)\}\Big|_{f=f_r}>0 \end{cases} \quad \text{"even mode"} \\
\begin{cases} \mathrm{Re}\{Z_{on}(f)\}<0 \\ \mathrm{Im}\{Z_{on}(f)\}=0 \\ \dfrac{d}{df}\mathrm{Im}\{Z_{on}(f)\}\Big|_{f=f_r}>0 \end{cases} & \begin{cases} \mathrm{Re}\{Y_{on}(f)\}<0 \\ \mathrm{Im}\{Y_{on}(f)\}=0 \\ \dfrac{d}{df}\mathrm{Im}\{Y_{on}(f)\}\Big|_{f=f_r}>0 \end{cases} \quad \text{"n}^{\text{th}}\text{ odd mode"}
\end{array}
$$

$$
\text{where: } \begin{cases} Z_e(f)=Z_{ei}(f)+Z_{eo}(f) \\ Z_{on}(f)=Z_{oni}(f)+Z_{ono}(f) \\ Y_e(f)=Y_{ei}(f)+Y_{eo}(f) \\ Y_{on}(f)=Y_{oni}(f)+Y_{ono}(f) \end{cases}
$$

(121.)

Example circuits PA.2 and PA.3 used previously to discover the Freitag method limitations will be reexamined to validate new approach.

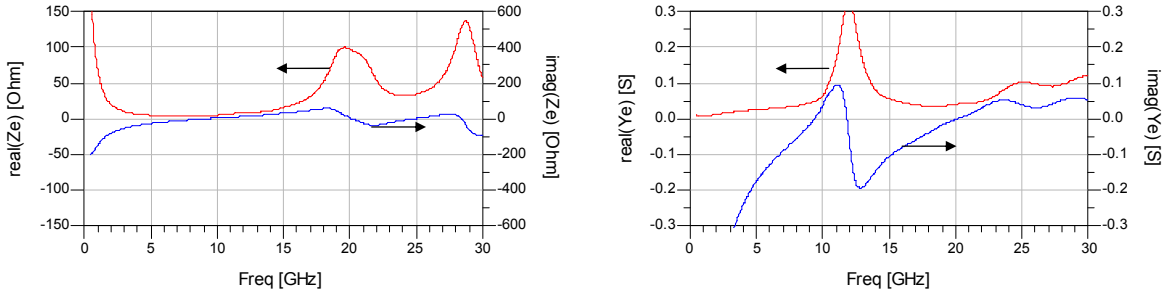

Figure 84 Even mode impedance (Ze) and admittance (Ye) of the example power amplifier PA.3.

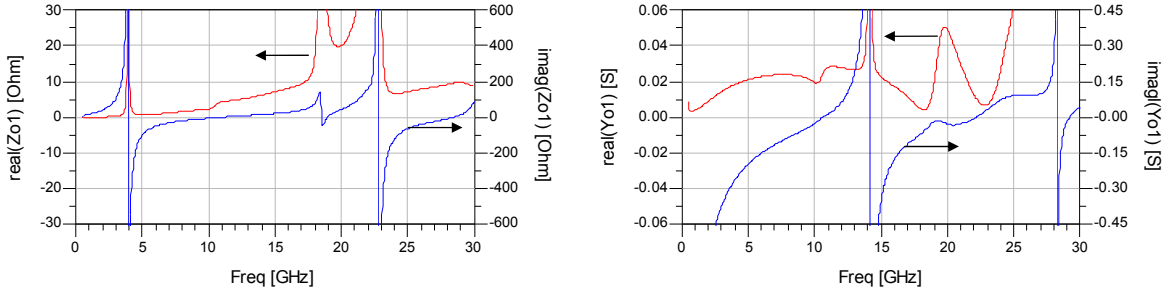

Figure 85 Odd mode 1 impedance (Zo1) and admittance (Yo1) of the example power amplifier PA.3.

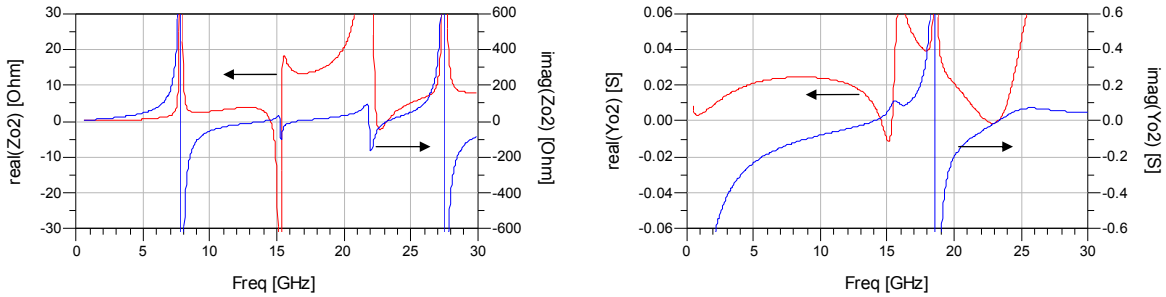

Figure 86 Odd mode 2 impedance (Zo2) and admittance (Yo2) of the example power amplifier PA.3.

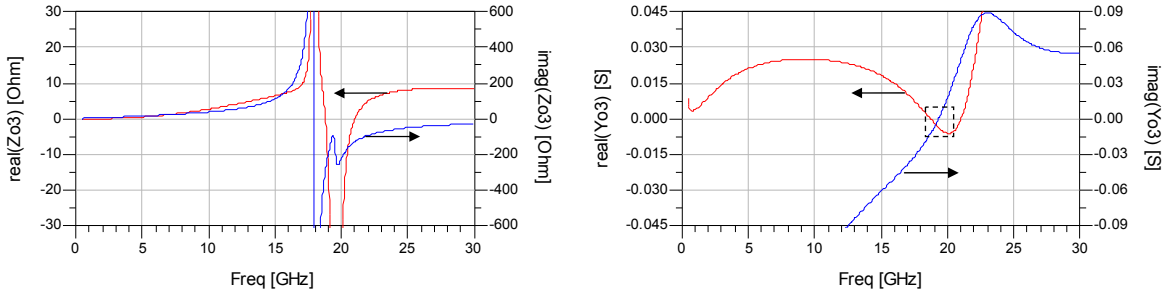

Figure 87 Odd mode 3 impedance (Zo3) and admittance (Yo3) of the example power amplifier PA.3.

Analysis of the equivalent impedance and admittance lead to confirmation of the Time domain simulation results. This time Odd mode 2 is not considered as unstable due to additional term disqualifying the negative zero crossing of the imaginary part , while the real part is negative. Moreover, Odd mode 3 instability discovered with Time domain simulation is clearly visible for equivalent admittance - Figure 87. A positive zero crossing with simultaneous negative real part is noticed at F≈19.33 GHz.

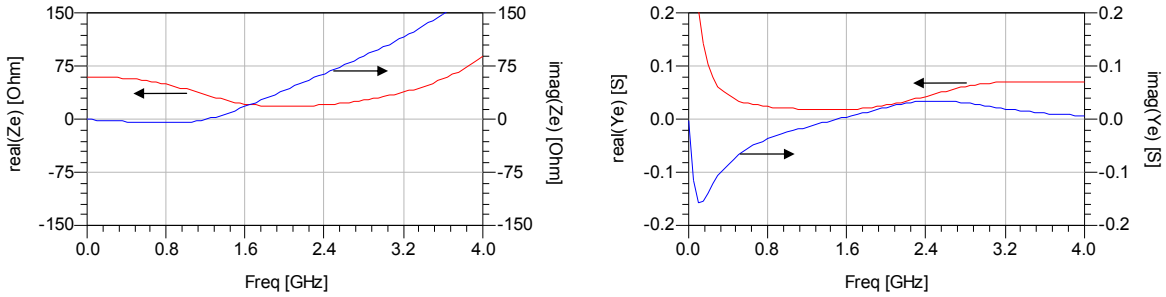

Figure 88 Even mode impedance (Ze) and admittance (Ye) of the example power amplifier PA.2.

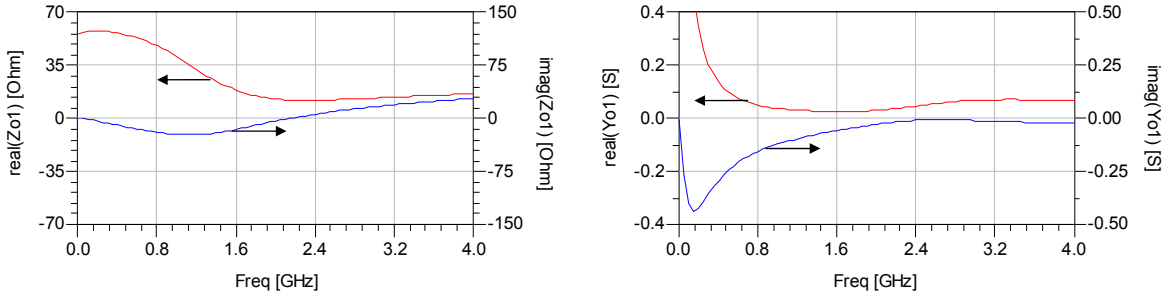

Figure 89 Odd mode 1 impedance (Zo1) and admittance (Yo1) of the example power amplifier PA.2.

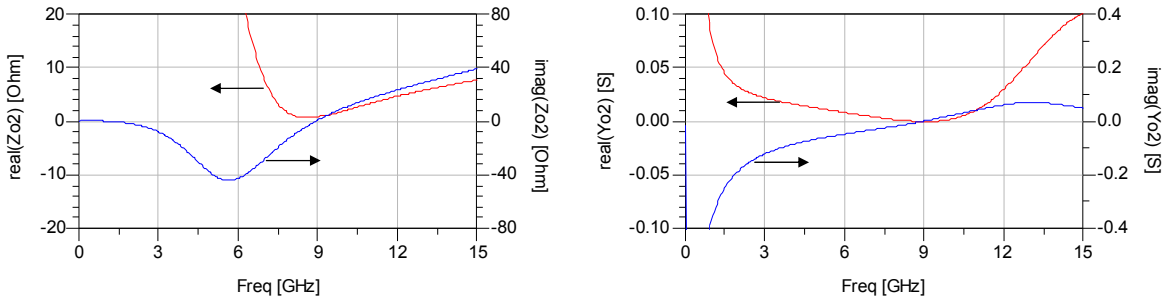

Figure 90 Odd mode 2 impedance (Zo2) and admittance (Yo2) of the example power amplifier PA.2.

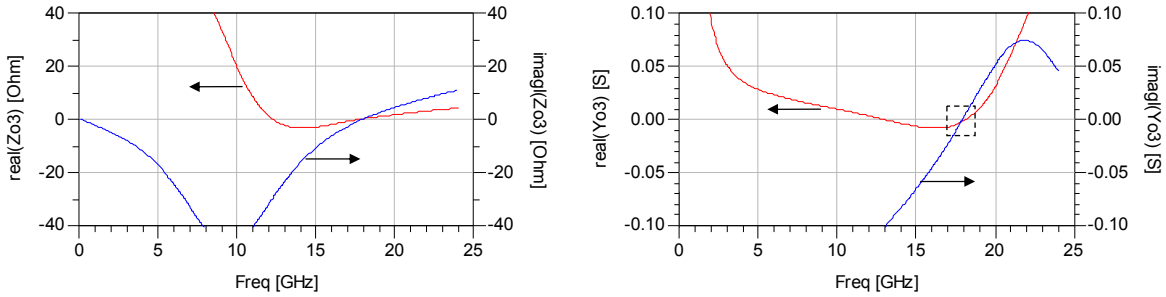

Figure 91 Odd mode 3 impedance (Zo3) and admittance (Yo3) of the example power amplifier PA.2.

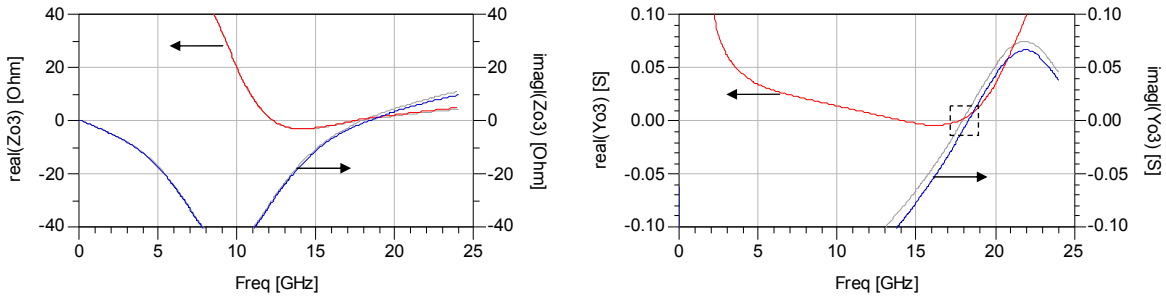

Figure 92 Odd mode 3 impedance (Zo3) and admittance (Yo3) before (grey line) and after the corrective action (solid line).

While example PA.2 is reexamined, Odd mode 3 instability, not discovered before, became obvious confirming Ohtomo method results- Figure 91. Results of the improved Freitag method allowed to identify the source of instability and perform the corrective action. A final amplifier was declared stable by both: improved Freitag – Figure 92 and Ohtomo - Figure 93 methods.

Ultimately, there were no inconsistencies in the results of the improved Freitag method and Ohtomo method for all of the examples. Moreover, Time Domain simulations were in agreement for the PA.3 example. This situation allows to confirm the validity and usefulness of the improved method as a

stability test. In addition, the information which method provides on the source of the instability is invaluable in speeding up the design and stabilization process. This fact combined with the method's easy and effective implementation, especially for the corporate amplifier structures, makes it a very attractive tool in the design process.

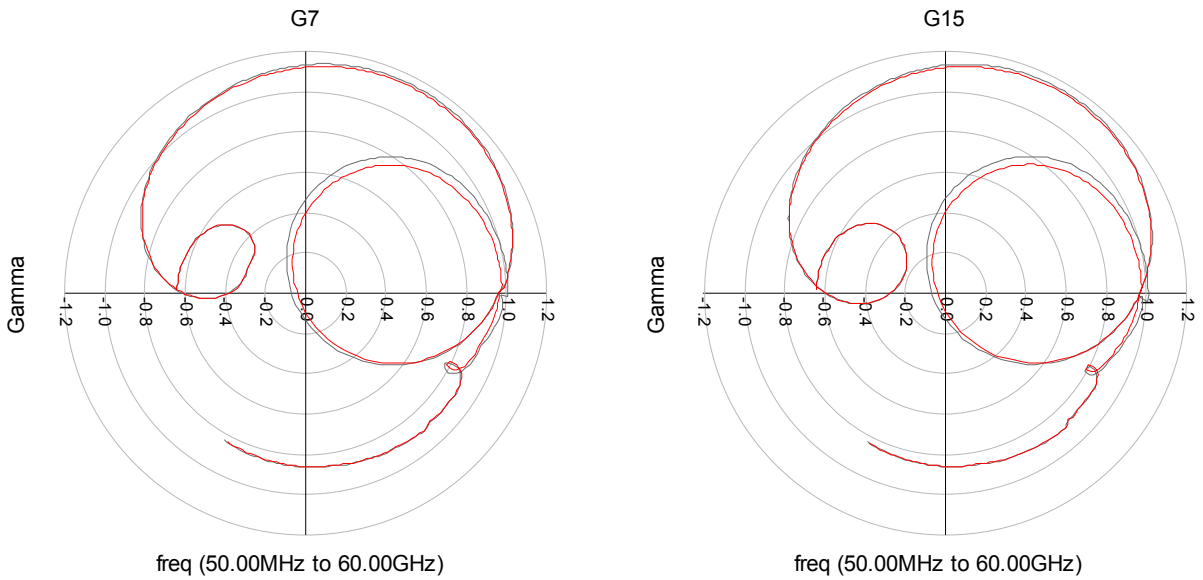

Figure 93 Ohtomo curves nr: 7, 15 before (grey line) and after corrective action (red line).

4.6 Automation of the method

To apply the Freitag method, the circuit needs to be divided into two bisections which forces the designer to create the copy of the amplifier dedicated only to test the stability. This is quite an inconvenient situation while any corrective action can influence two port performances and cannot be tested simultaneously without additional effort to synchronize two tests. Minimal effort to optimize performances of simple PA structure requires at last two simultaneous simulations - Figure 94.

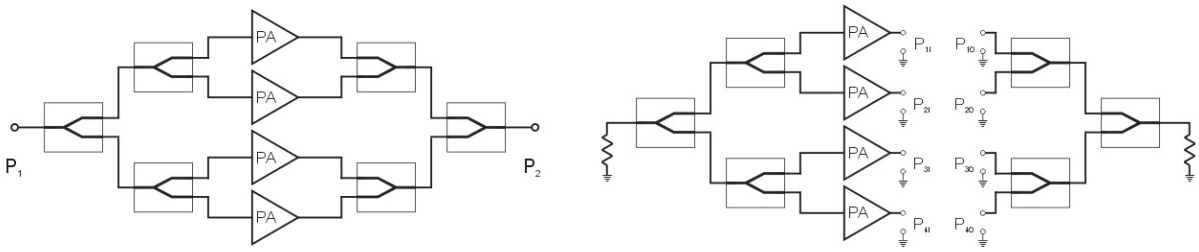

Figure 94 Power amplifier ready for two port simulation (left) and Freitag stability test (right).

If Freitag test is to be implemented in different stages even more copies of the original circuit have to be made and synchronized in the design process. Hence, it is very convenient to overcome this shortcoming, especially if the method is to be included into optimisation routines.

To perform this operation there needs to be found the measurement procedure which provides valid two port S parameters and describes both bisection with Z and Y parameters, which then are used to

compute the equivalent mode's impedances and admittances. This is achievable with a simulation setup containing special components and increased number of ports.
In general, the method bases on the possibility of the Z and Y matrix reduction to a lower dimension. In practice this means that the circuit will be measured with additional ports and the required simulation results will be obtained in the post-processing phase. The technique grounds on the single measurement setup and performs two simulations providing Y and Z matrix for further computations. The special added components interconnect simulation ports with the tested circuit. Their task is to provide an appropriate connection that depends on the searched description: series connection for the impedance matrix calculation and a parallel one for the admittance matrix calculation. An additional element separates input and output ports in Z measurement mode to improve the robustness of the method.
To explain the method fully, a simple example of the four stage power amplifier is applied and simulated. To validate the approach, simulation results will be compared with the results of the separate simulation setups results.

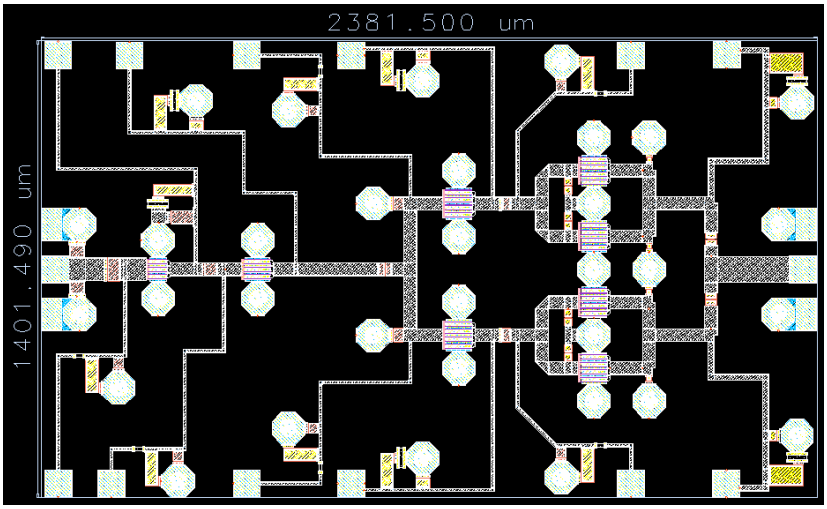

Figure 95 Example power amplifier PA.4 layout.

Example power amplifier was designed by the means of the comercially available, Ommic D01MH commercial process. It operates at F_0=60 GHz with P_{out}≈ 31 dBm output power at 1dB compression point. Four stage structure was assumed with the topology of the 1,1,2,4 devices at appropriate stages. Layout of the amplifier is presented in the Figure 95. Small signal gain and Rollet k-factor were presented in the Figure 96. The circuit is unconditionally stable form the two port representation standpoint. Large signal simulation result at F_0 is presented in the Figure 97.

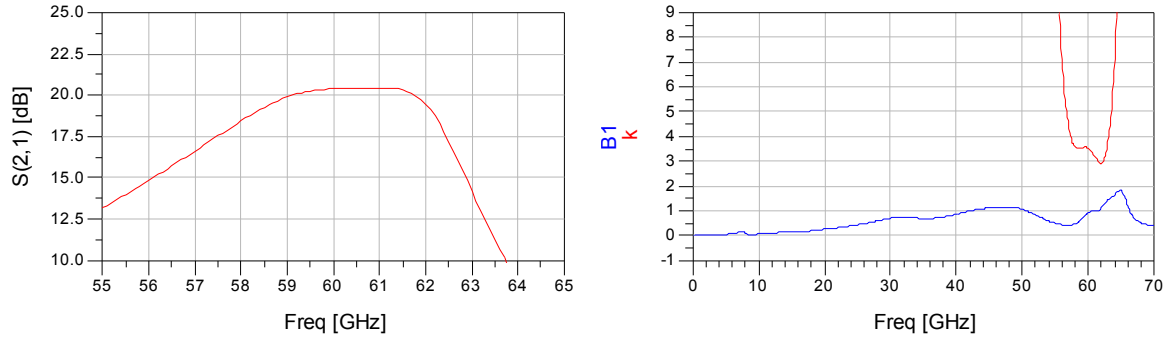

Figure 96 Gain and Rollet stability factor of the example power amplifier PA.4.

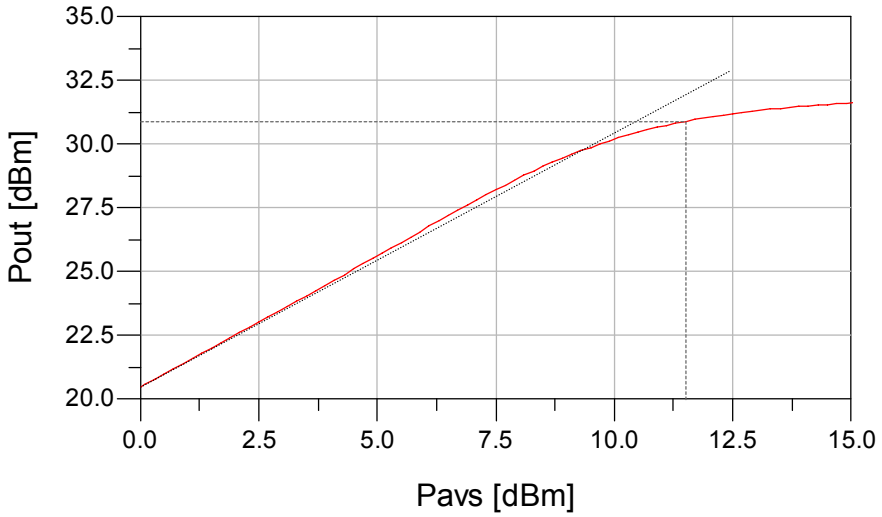

Figure 97 Power performance of the example power amplifier PA.4.

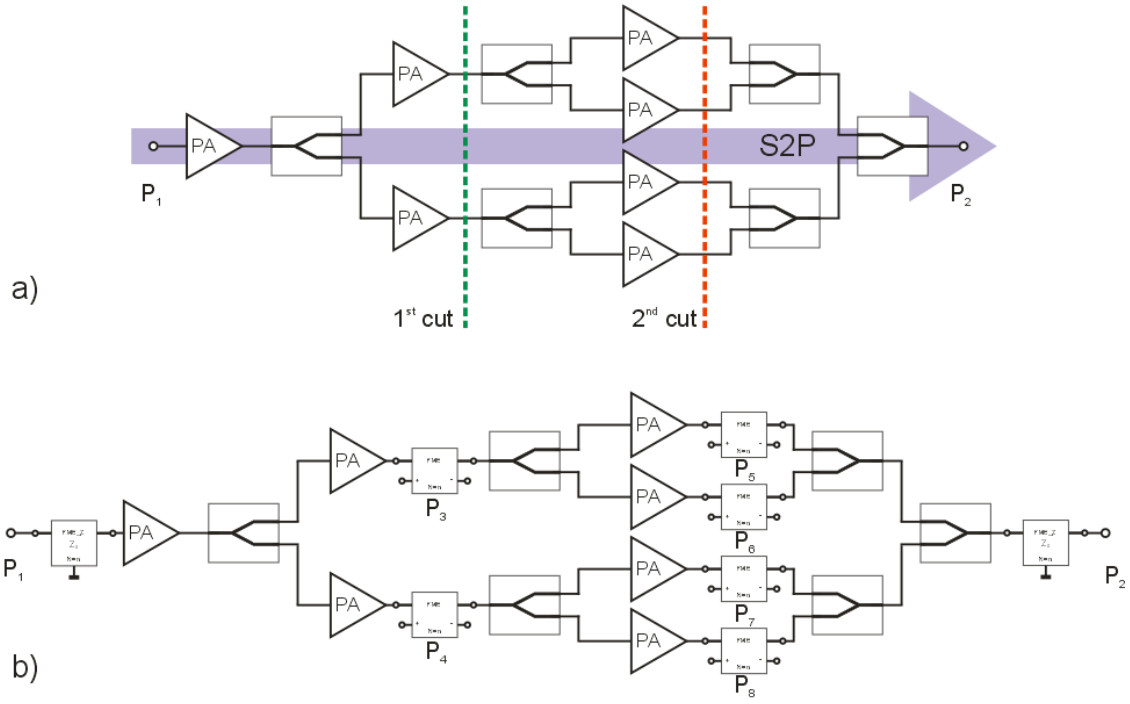

Figure 98 Example PA.4 - graphical representation of simultaneous simulations a); measurement setup realizing them b).

The automated Freitag method is presented with an example of the simultaneous measurement of the two port performances and the Freitag analysis is shown in two different cut planes. Two port performances will be measured as a S parameters and the Freitag tests will be applied at the drains of fourth and third stage transistors (output of the amplifiers on the diagrams). This task was graphically explained in the Figure 98 a). In the Figure 98 b) simulation setup addressing the assignment in question is presented. In result, two special components can be noticed: FEM and FEM_Z. They are controlled with variable N, which in turn controls their functionality. While N=0 FEM component connects the element between the ports 3 and 4 into parallel connection to ports 1 and 2 - Figure 99 b). While N=1 FEM elements introduce the direct connection between the pairs of ports 1-3 and 2-4. Therefore, any element connected between ports 3 and 4 became introduced in series between ports 1 and 2 - Figure 99 c). In case FEM_Z element N=0 state change it to simple ideal zero

delay through the connection. While N=1 element connects internally matched load and separates ports 1 and 2.

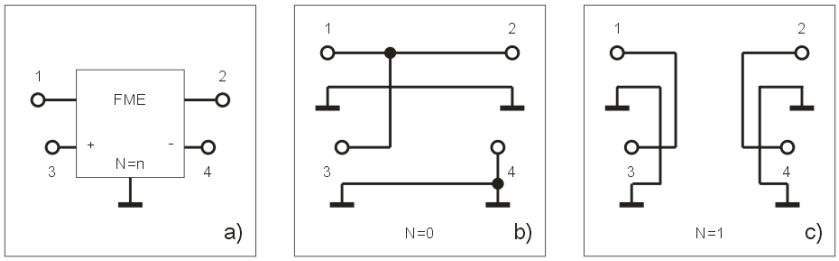

Figure 99 FEM component: a) symbol b) circuit representation in Y measurement C) circuit representation in Z measurement.

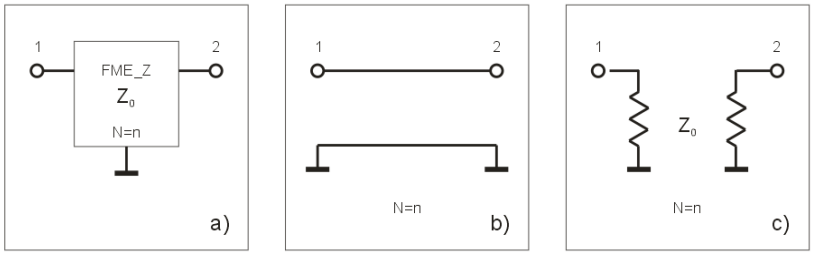

Figure 100 FEM_Z component: a) symbol b) circuit representation in Y measurement C) circuit representation in Z measurement

FEM_Z elements are used between the circuit and simulator input, and output ports. FEM elements are used at cut planes related to the Freitag test. Thus, they can be observed at the output of the third and fourth stage amplifiers at the schematic diagram - Figure 98 b). To circuit prepared in such a way, the simulator ports are connected according to particular rules. That is, ports one and two are linked to the input and output at FEM_Z component port. The following ports are connected sequentially to FEM components at each cut plane. Ports are attached to FEM elements between pins 3 and 4 as to maintain the polarity. In the end, the groups of sequential numbers can be distinguished for the input as well as for the output ports and for any of the cut planes. In the example displayed in the Figure 98 b) input output ports create group {1,2}. The first cut creates group {3,4}, and the second cut creates group {5,6,7,8}. This ordering is important for further compatibility of the simulation results with the algorithm processing data into the final results.
Variable N introduced previously represents the simulation mode. Measurement procedure requires double pass of the simulator and changes value of the N parameters. That in the end produces two different simulation setups. In case of this example it results with the subsequent measurement setups - Figure 101. They are used to find Y and Z circuit descriptions accordingly.

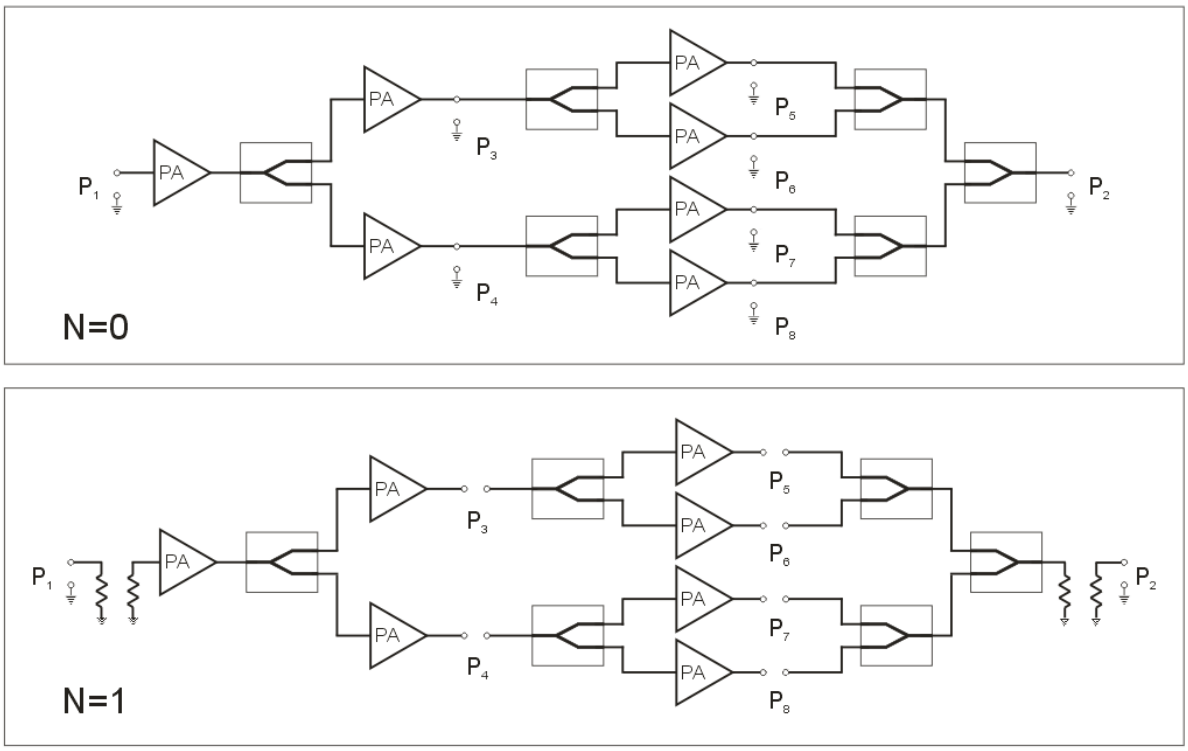

Figure 101 Example PA.4 simulation setup resulting from different value of N parameter: 0 – top one, 1 – bottom one.

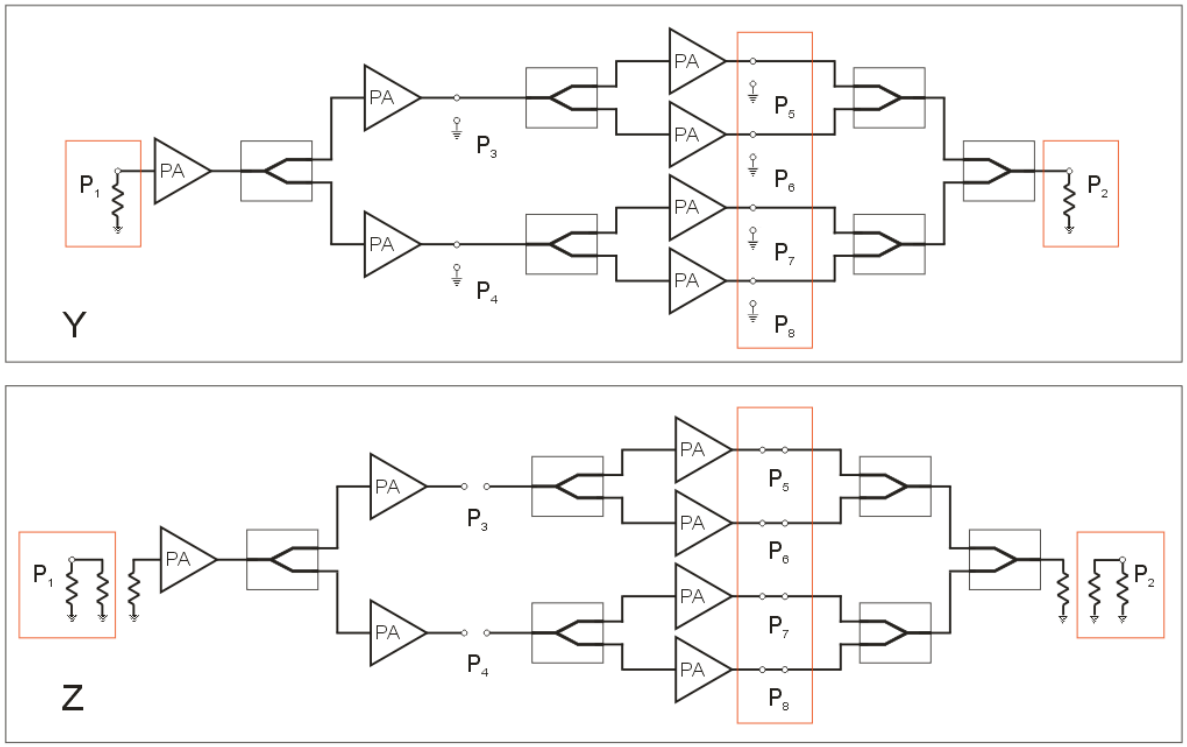

Figure 102 Reduction of the unnecessary ports in order to perform Freitag test in 1st cut plane.

As a result of these simulations Z and Y description of the circuit are obtained. If Freitag method is to be applied at the chosen cut plane, unnecessary ports need to be reduced. What is more, the input and output ports require to be closed with appropriate terminations. This very process was visualized for the 1st cut plane in the Figure 102. In case of Y matrix the unnecessary ports are left open, in case

of Z matrix they became shortened out. The input and output ports are closed with appropriate impedance. As a result of this operation, the simplified circuit with only two ports left is represented by new Y and Z matrix at the cut plane - Figure 103. This task is performed by algorithm implemented in AEL language of Agilent ADS simulator in the post processing phase.

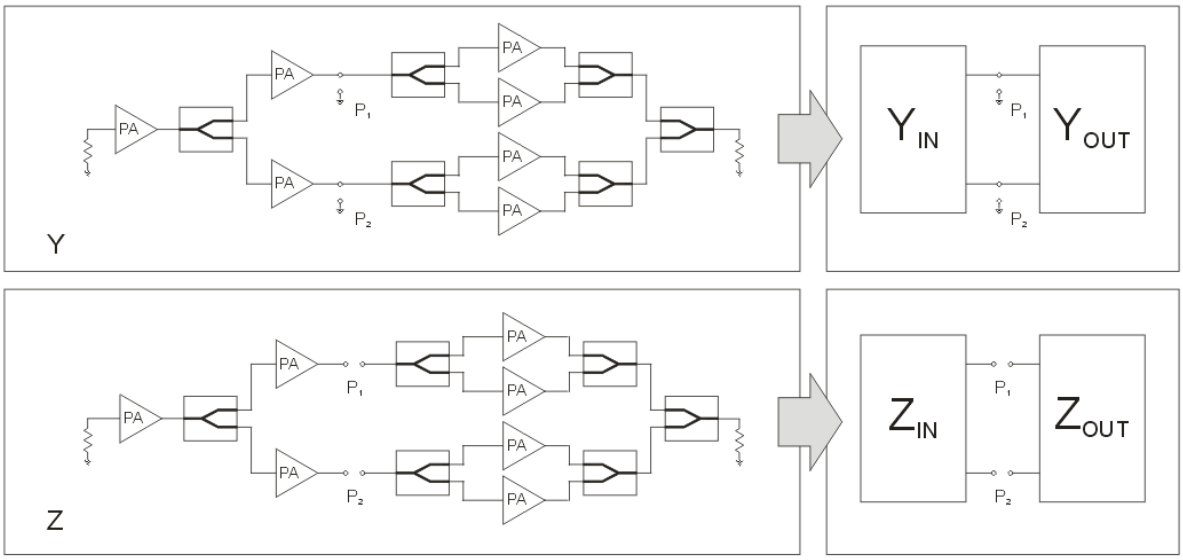

Figure 103 Result of the reduction of the unnecessary ports algorithm for the 1st cut plane.

In consequence, Y matrix obtained from the procedure describes the parallel connection of the Input and Output bisections at the cut plane. In case of Z matrix, it defines serial connections of the Input and Output bisections. The original Freitag method assumed that the bisections modes impedance and admittance computation will be performed separately before they will be added into the onset equation. However, in case of bisections possessing the same set of eigenvectors, the matrix representing the sum of the Z and Y parameters of the bisections may be applied with the same result. This may be easily laid out with the equations applied to the Odd mode 1 impedance. Bisections Z matrix elements are differentiated with subscript *in* and *out*. Matrix Z describes their series connection, that is- it is simply their sum. If Z_{o1} is computed with the assumption of identical eigenvector set {1,-1} the result will be the same in both cases: separate computation of Z_{o1in} and Z_{o1out} of the bisections and addition - (123.) or computation of the Z_{o1} directly from the Z matrix - (122.).

$$\begin{bmatrix} Z_{11} & Z_{12} \\ Z_{21} & Z_{22} \end{bmatrix} = \begin{bmatrix} Z_{11in} & Z_{12in} \\ Z_{21in} & Z_{22in} \end{bmatrix} + \begin{bmatrix} Z_{11out} & Z_{12out} \\ Z_{21out} & Z_{22out} \end{bmatrix}$$
$$Z_{o1} = Z_{11} - Z_{12}$$

(122.)

$$Z_{o1in} = Z_{11in} - Z_{12in}$$
$$Z_{o1out} = Z_{11out} - Z_{12out}$$
$$Z_{o1} = Z_{o1in} + Z_{o1out}$$
$$Z_{o1} = (Z_{11in} - Z_{12in}) + (Z_{11out} - Z_{12out}) = (Z_{11in} + Z_{11out}) - (Z_{12in} + Z_{12out}) = Z_{11} - Z_{12}$$

(123.)

Using this particular property it is doable to compute modes impedance and admittance, which provides data to be analysed with the Freitag method onset of oscillation.
Given two port parameters, the situation is similar and the results are obtained by reducing all the ports except 1 and 2 of the circuit Y description - Figure 104. The last step of the procedure is an undemanding conversion of the two port Y to S matrix.

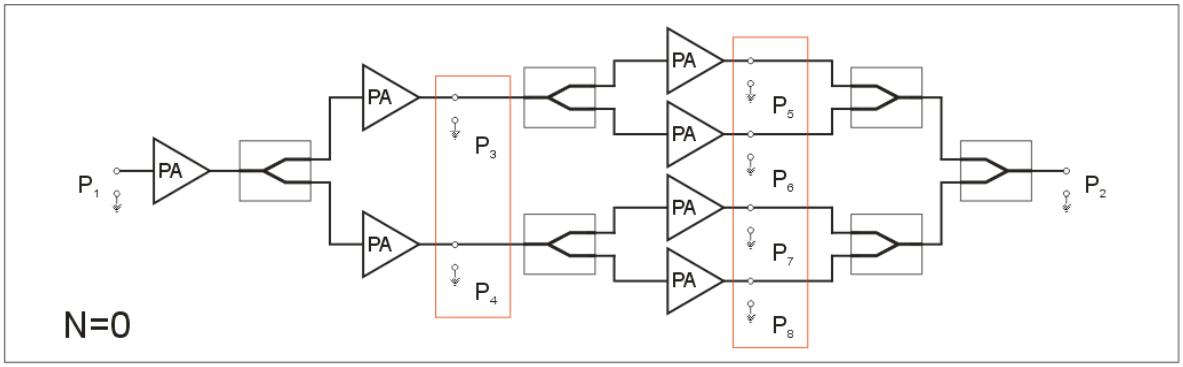

Figure 104 Reduction of the unnecessary ports in order to find two port description of the circuit.

Next, in order to verify the method an example circuit PA.4 was tested and results were compared to the results of the separate simulations implemented in the classic way. There were no differences, for that reason curves in the Figure 105 - Figure 111 are superimposed. This fact proves the correctness of the manner. Also, the circumstance that only one measurement setup was used to obtain this results increases the comfort of the design process and eliminates schematic synchronization errors. While this was purely demonstrative application of the method, the algorithms used leave room for optimization. Moreover, the useful and convenient for a demonstrative purpose AEL language is not efficient enough to be considered an environment for the professional application of the technique.

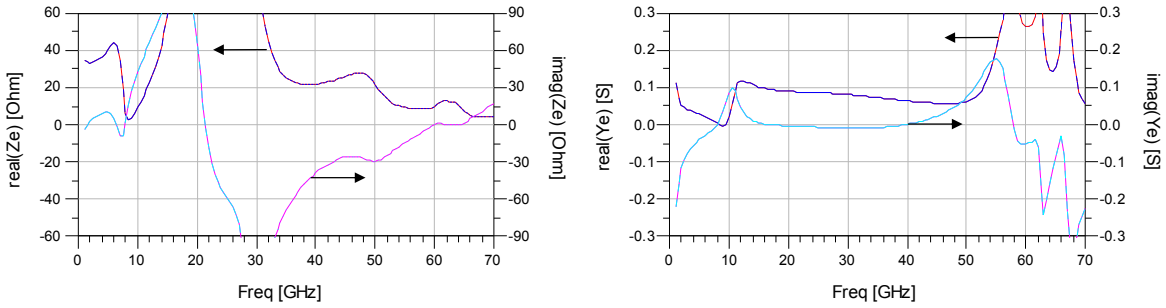

Figure 105 Even mode impedance (Ze) and admittance (Ye) of the example power amplifier PA.4 at 1st cut. Simulation results from automated Freitag method (broken lines) and separate test (solid lines).

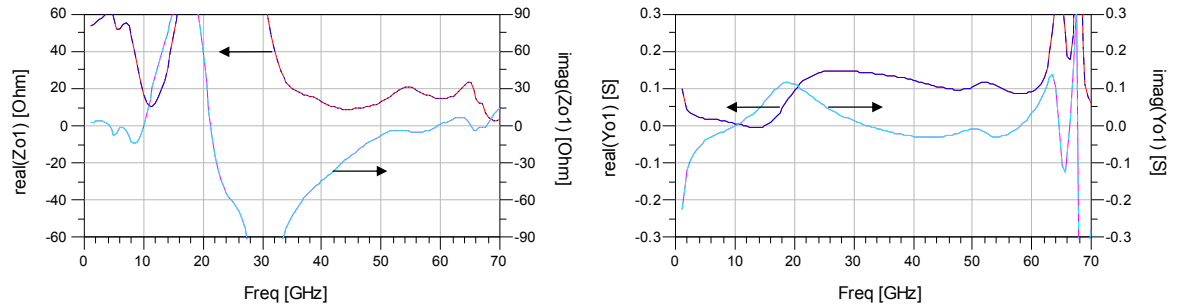

Figure 106 Odd mode 1 impedance (Zo1) and admittance (Yo1) of the example power amplifier PA.4 at 1st cut. Simulation results from automated Freitag method (broken lines) and separate test (solid lines).

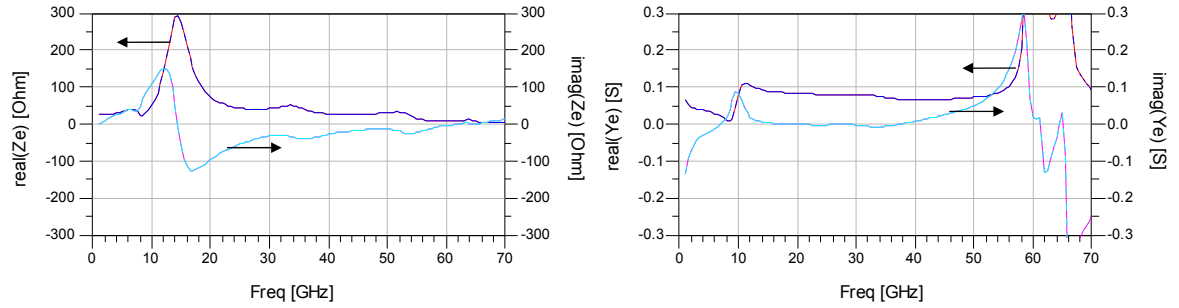

Figure 107 Even mode impedance (Ze) and admittance (Ye) of the example power amplifier PA.4 at 2nd cut. Simulation results from automated Freitag method (broken lines) and separate test (solid lines).

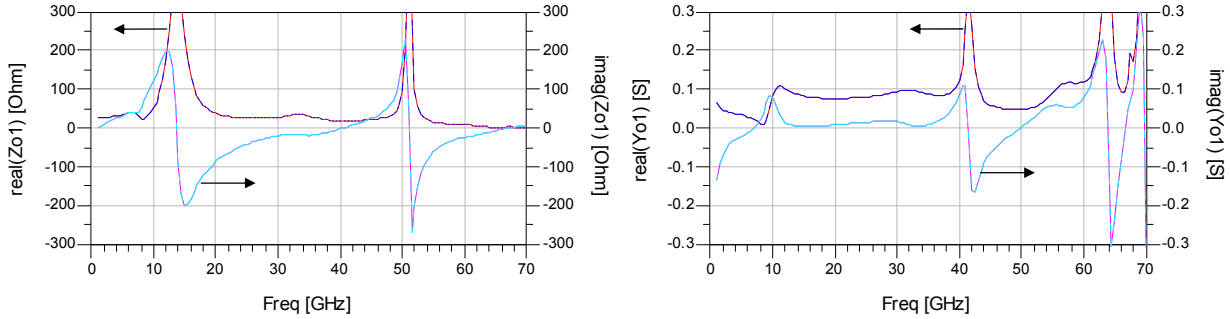

Figure 108 Odd mode 1 impedance (Zo1) and admittance (Yo1) of the example power amplifier PA.4 at 2nd cut. Simulation results from automated Freitag method (broken lines) and separate test (solid lines).

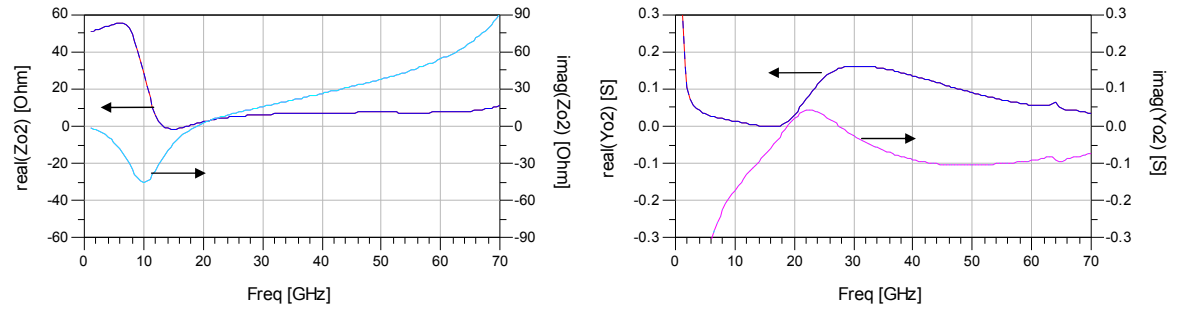

Figure 109 Odd mode 2 impedance (Zo2) and admittance (Yo2) of the example power amplifier PA.4 at 2nd cut. Simulation results from automated Freitag method (broken lines) and separate test (solid lines).

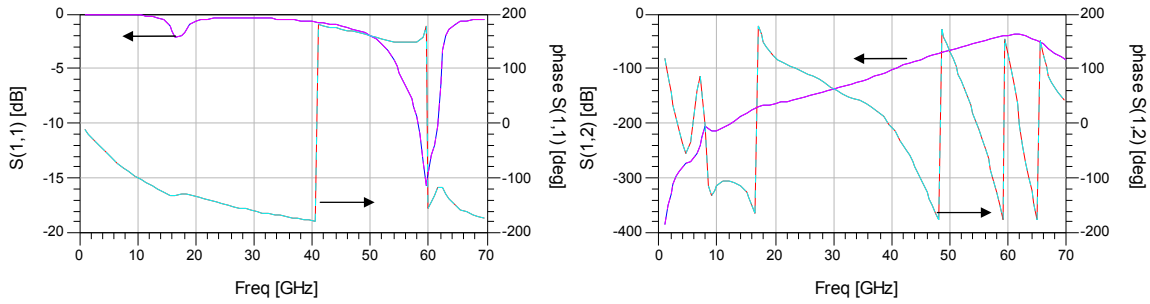

Figure 110 S parameters S(1,1) and S(1,2) of the example power amplifier PA.4. Simulation results from the automated Freitag method (broken lines) and separate test (solid lines).

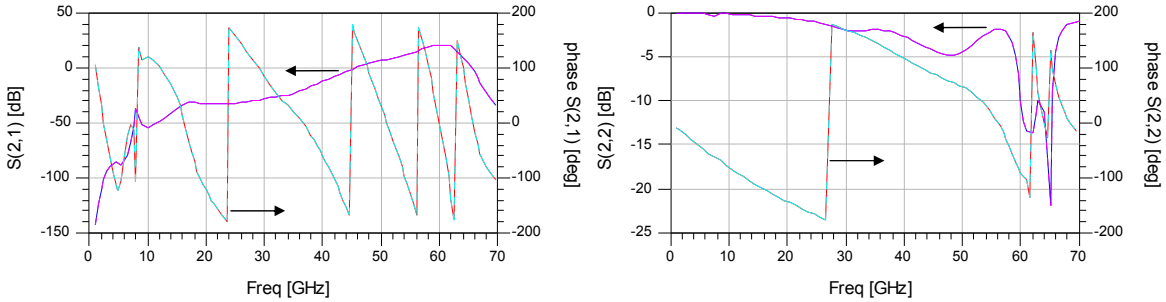

Figure 111 S parameters S(2,1) and S(2,2) of the example power amplifier PA.4. Simulation results from automated Freitag method (broken lines) and separate test (solid lines).

5 LARGE-SIGNAL/SMALL-SIGNAL FREITAG METHOD EXTENSION

In real life, the term linear circuit is no more than an idea due to ubiquitous presence of the nonlinearities in all real elements, not excluding the passive ones. Thus, the treatment of the elements and circuits as linear ones means to apply approximation which is valid under particular conditions. In this case nonlinearities are treated as harmful phenomena and a lot of effort is made to minimize them. On the opposite side, nonlinear circuits, like frequency multipliers, exploit the nonlinear properties of the devices as a base for their operation. That is why, maximization of the nonlinear effect is crucial for such circuits in order to maximize their performances. Power amplifiers exist somewhere between these extremes as the high linearity power amplifiers are crucial elements of the modern communication systems. At the same time high efficiency power amplifiers are important when linearity is not as crucial as efficiency. Although the assumption, that the power amplifier is working in the small signal condition is hard to be justified even with the high linearity ones. In consequence, the power amplifier's stability analysis done under this assumption cannot be considered as a complete one.

5.1.1 Small signal regime linearization

As it was underlined before, the methods introduced previously address the linear stability, that is why, to apply them to a power amplifier, its nonlinear elements have to be represented as the linear ones. In order to do this, an appropriate nonlinear characteristic of each element needs to be expressed as a Taylor expansion around the point of interest [20]. This process can be presented with the example diode element which I/V characteristic is presented in the Figure 112.

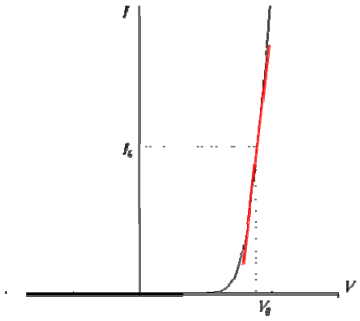

Figure 112 I/V characteristic diode.

While diode is biased with voltage $V_{0,}$ the current $I_0=f(V_0)$ is flowing through the element. If small voltage perturbation is applied to the element in form of ac voltage v(t), the diode current will be than described as $I(t) = f(V_0+v(t))$. Now, expanding it in a Taylor series around V_0 will result in a following equation - (124.).

$$I(t)=f(V_0+v(t))=f(V_0)+\frac{d}{dV}f(V)\Big|_{V=V_0}v(t)+\frac{1}{2}\frac{d^2}{dV^2}f(V)\Big|_{V=V_0}v^2(t)+\frac{1}{6}\frac{d^3}{dV^3}f(V)\Big|_{V=V_0}v^3(t)+\cdots \quad (124.)$$

The small signal response i(t) will be described as:

$$i(t) = f(V_0 + v(t)) - f(V_0) = \frac{d}{dV} f(V)\Big|_{V=V_0} v(t) + \frac{1}{2}\frac{d^2}{dV^2} f(V)\Big|_{V=V_0} v^2(t) + \frac{1}{6}\frac{d^3}{dV^3} f(V)\Big|_{V=V_0} v^3(t) + \cdots$$

(125.)

Two assumptions are essential to obtain the final result. The first assumption is that small signal voltage v(t) is negligibly small in comparison to V_0. The second one is, that DC component introduced due to the existence of the even-degree terms is also negligible, thus is not changing the operating point of the device. Due to those assumptions, the linear description of the diode at bias point V_0 can be created:

$$i(t) = \frac{d}{dV} f(V)\Big|_{V=V_0} v(t) = g(V_0) \cdot v(t)$$

(126.)

These results can be obtained experimentally by applicating a small perturbation. The ratio between the perturbation and its response will be an equivalent of the (126.). Expressed graphically, this ratio will be the tangent line of the I/V characteristics at the bias point V_0.

5.1.2 Large signal regime linearization

Small signal regime guarantees the validity of linearization process but leads to severe restriction in case of the power amplifier- lack of input signal or its negligible value. That in the end restricts the validity of the test to idle or low power operation of the power amplifier. By no means results of such analysis are meaningless, but as it was stated before, low power operation is not a state for which the power amplifier was anticipated. Thus, in normal operating conditions, large signal excitation will be present in the amplifier and needs to be accounted in the stability analysis. If this problem is applied to the Freitag stability test, it arises certain questions. What will happen with the obtained for the small signal operation Freitag test results, while the desired signal power at the input is increased? Then: how to perform a test beyond small signal regime for which linearization of the nonlinear devices at the bias point will not be longer valid?

Fortunately, the above questions do not force method to move towards the nonlinear stability analysis of the circuit. This is still an issue of linear, small signal stability of the circuit working in large signal regime. Therefore, prior to any test implementation, the circuit requires to be linearized. In case of small signal regime, the linear description was relatively easy found from the Taylor expansion or from the experimental response to the small perturbation. Regrettably, if the device's response for the small signal perturbation is searched for, a simultaneous existence of the large signal component makes the previous approach invalid. Dilemma still can be solved though, what will be presented with the previously utilized example of the diode circuit.

In this case, the diode will be driven simultaneously by the large signal voltage $V_0(t)$ and small voltage perturbation in form of ac voltage v(t). In result, the element responds with current $I(t) = f(V_0(t)+v(t))$. Expanding this response in a Taylor series around V_0 the outcome will be the following equation:

$$I(t) = f(V_0(t) + v(t)) = f(V_0(t)) + \frac{d}{dV} f(V)\Big|_{V=V_0(t)} v(t) + \frac{1}{2}\frac{d^2}{dV^2} f(V)\Big|_{V=V_0(t)} v^2(t) + \frac{1}{6}\frac{d^3}{dV^3} f(V)\Big|_{V=V_0(t)} v^3(t) + \cdots$$

(127.)

Then, the small signal response i(t)is described as:

$$i(t)=f(V_0(t)+v(t))-f(V_0(t))=\frac{d}{dV}f(V)\Big|_{V=V_0(t)}v(t)+\frac{1}{2}\frac{d^2}{dV^2}f(V)\Big|_{V=V_0(t)}v^2(t)+\frac{1}{6}\frac{d^3}{dV^3}f(V)\Big|_{V=V_0(t)}v^3(t)+\cdots \quad (128.)$$

Again, there will be made an assumption that small voltage perturbation is much smaller than a large signal voltage as well as higher order terms are negligible, than it is justified to define small signal response as:

$$i(t)=\frac{d}{dV}f(V)\Big|_{V=V_0(t)}v(t)=g(t)\cdot v(t) \quad (129.)$$

So, diode will be described as a time varying conductance. This conductance is derivative of the diode I/V characteristic at the large signal voltage. In other words, it represents the tangential line of the I/V characteristic at dynamically changed bias point - Figure 113.

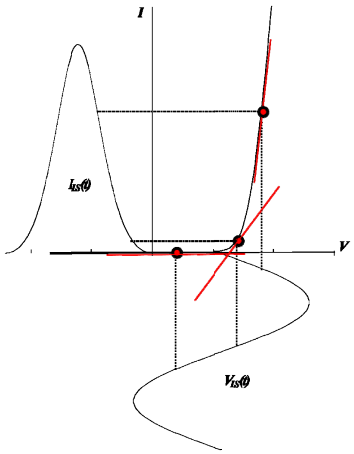

Figure 113 Dynamic point linearization.

5.1.3 Conversion matrix and an equivalent two tone analysis

When two tones are present in the circuit containing nonlinear elements it is natural to expect responses at the original and their harmonics $n\omega_1$, $m\omega_2$ as well as at the mixing frequencies $n\omega_1+m\omega_2$ (where n and m are integers). We assume than that tones are not related harmonically and the mixing products do not fall into same frequency. Also, considering the prior hypothesis that only one of the tones is large allows us to that only one of them produce harmonics. Hence, the resulting mixing product content should be described as follows: $\omega=\pm\omega_{SS}+n\omega_{LS}$ where ω_{SS} represents a small signal component and ω_{SS} represents a large signal component. If only half of the frequencies is considered due to the linear properties of the linearized circuit, the simplified description can be assumed as: $\omega_n=\omega_{SS}+n\omega_{LS}$. Than, small signal currents and voltages in the circuit are described as sum of the frequency phasor components (not Fourier series) - (130.). In the case of the simple diode the circuit linearized in large signal regime voltage and current is related to the time varying conductance - (129.).

$$v'(t) = \sum_{n=-\infty}^{\infty} V_n e^{j\omega_n t}$$
$$i'(t) = \sum_{n=-\infty}^{\infty} I_n e^{j\omega_n t}$$

(130.)

$$g(t) = \sum_{n=-\infty}^{\infty} G_n e^{jn\omega_{LS} t}$$

(131.)

If conductance is expressed as a Fourier series - (131.), than a new form of the equation can be obtained (129.):

$$\sum_{k=-\infty}^{\infty} I_k e^{j\omega_k t} = \sum_{n=-\infty}^{\infty} \sum_{m=-\infty}^{\infty} G_n V_m e^{j\omega_{m+n} t}$$

(132.)

If now k and m will be limited to N and n will be limited to 2N due to negligible values of: $I_{k=N+1}$, $V_{m=N+1}$ and $G_{n=2N+1}$ terms, the conversion matrix for the time varying conductance of the diode can be delivered from (132.):

$$\begin{bmatrix} I^*_{-N} \\ I^*_{-N+1} \\ \vdots \\ I^*_{-1} \\ I_0 \\ I_1 \\ \vdots \\ I_N \end{bmatrix} = \begin{bmatrix} G_0 & G_{-1} & G_{-2} & \cdots & G_{-2N} \\ G_1 & G_0 & G_{-1} & \cdots & G_{-2N+1} \\ \vdots & \vdots & \vdots & \ddots & \vdots \\ G_{N-1} & G_{N-2} & G_{N-3} & \cdots & G_{-N-1} \\ G_N & G_{N-1} & G_{N-2} & \cdots & G_{-N} \\ G_{N+1} & G_N & G_{N-1} & \cdots & G_{-N+1} \\ \vdots & \vdots & \vdots & \ddots & \vdots \\ G_{2N} & G_{2N-1} & G_{2N-2} & \cdots & G_0 \end{bmatrix} \cdot \begin{bmatrix} V^*_{-N} \\ V^*_{-N+1} \\ \vdots \\ V^*_{-1} \\ V_0 \\ V_1 \\ \vdots \\ V_N \end{bmatrix}$$

(133.)

Negative frequencies components are shown as conjugate due to the way the mixing frequencies were defined. In conclusion, the conversion matrix relates the ordinary phasor voltages to the currents at each mixing frequency and is completely compatible with conventional linear and sinusoidal steady-state analysis. In case of time varying capacitance additional derivative that is present in the relation between the current and the voltage results in following description:

$$\mathrm{I} = j\Omega \mathrm{CV}$$
$$\Omega = \begin{bmatrix} j\omega_{-N} & 0 & \cdots & 0 \\ 0 & j\omega_{-N+1} & \cdots & 0 \\ \vdots & \vdots & \ddots & \vdots \\ 0 & 0 & \cdots & j\omega_N \end{bmatrix}$$

(134.)

What is more, ordinary time invariant linear elements are easily introduced to this description. In example impedance Z(ω) is described with a diagonal matrix containing impedances at the frequency corresponding to the location in matrix:

$$Z(\omega)=\begin{bmatrix} Z^*(-\omega_{-N}) & 0 & \cdots & 0 \\ 0 & Z^*(-\omega_{-N+1}) & \cdots & 0 \\ \vdots & \vdots & \ddots & \vdots \\ 0 & 0 & \cdots & Z(\omega_N) \end{bmatrix}$$

(135.)

This way linear description of the time varying circuit is possible and can be used to answer the previously inquired issues. At the same time the conversion matrix is a particular type of the two tone harmonic balance simulation. So, identical results can be obtained by applying the standard two tone harmonic balance under the assumptions used while deriving the conversion matrix approach. The biggest advantage of the method is its efficiency when only small signal response is searched. In contrast, the full two tone harmonic balance is able to provide knowledge regarding both types of behaviours – the small-signal and the large-signal.

5.2 Extension of the Freitag method

When extension of the Freitag method application is considered, both approaches: conversion matrix and two tone harmonic balance simulation may be used. Moreover, full knowledge about the frequency conversion phenomena of the circuit is not necessary. The circuit must be described only at the first harmonic of the small signal frequency. It is important to include the effect of the large signal operation of the power amplifier caused by the existence of the desired input signal on that description.

This signal in the analysis will be purely sinusoidal of the frequency F_0 and available power P_{avs}. As an outcome, the description of the PA bisection containing nonlinear devices and the final result of the method will be parameterized with these two variables - Figure 114.

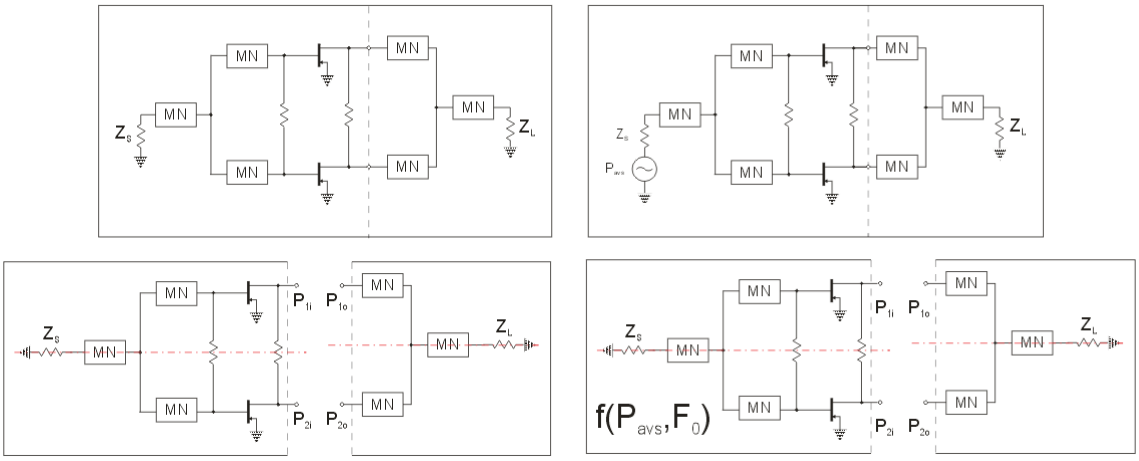

Figure 114 Bisection description in small signal Freitag method (left) and extended Freitag method (right).

Due to this change, the mode impedances and admittances also became parametric. Ergo, additional subscripts were added to the their description and consequently, to the formulation of the onset of oscillation. - (136.).

By investigating the Figure 114 we notice a practical problem of the method application in the power amplifier circuit. That is, to perform linearization the circuit needs to be excited by large signal source as well as an amplifier must work in a normal anticipated state. In contrast, Freitag method requires division of the circuit into bisections for which Z and Y matrix linear descriptions will be found. This requires to simultaneously maintain an integrity of the amplifier for large signal component and a division at the chosen cut plane for the small signal. Fortunately, due to non harmonical relation between the two tones exciting circuit, the requirements can be fulfilled by an arrangement of two diplexers for each connection between the bisections - Figure 115.

$$
\begin{array}{ll}
Z-conditions & Y-conditions \\
\begin{cases} \mathrm{Re}\{Z_e(P_{avs},F_0,f)\}<0 \\ \mathrm{Im}\{Z_e(P_{avs},F_0,f)\}=0 \\ \left.\frac{d}{df}\mathrm{Im}\{Z_e(P_{avs},F_0,f)\}\right|_{f=f_r}>0 \end{cases} & \begin{cases} \mathrm{Re}\{Y_e(P_{avs},F_0,f)\}<0 \\ \mathrm{Im}\{Y_e(P_{avs},F_0,f)\}=0 \\ \left.\frac{d}{df}\mathrm{Im}\{Y_e(P_{avs},F_0,f)\}\right|_{f=f_r}>0 \end{cases} \quad \text{"even mode"} \\
\begin{cases} \mathrm{Re}\{Z_{on}(P_{avs},F_0,f)\}<0 \\ \mathrm{Im}\{Z_{on}(P_{avs},F_0,f)\}=0 \\ \left.\frac{d}{df}\mathrm{Im}\{Z_{on}(P_{avs},F_0,f)\}\right|_{f=f_r}>0 \end{cases} & \begin{cases} \mathrm{Re}\{Y_{on}(P_{avs},F_0,f)\}<0 \\ \mathrm{Im}\{Y_{on}(P_{avs},F_0,f)\}=0 \\ \left.\frac{d}{df}\mathrm{Im}\{Y_{on}(P_{avs},F_0,f)\}\right|_{f=f_r}>0 \end{cases} \quad \text{"n}^{\text{th}}\text{ odd mode"}
\end{array}
$$

$$
\text{where: } \begin{cases} Z_e(P_{avs},F_0,f)=Z_{ei}(P_{avs},F_0,f)+Z_{eo}(f) \\ Z_{on}(P_{avs},F_0,f)=Z_{oni}(P_{avs},F_0,f)+Z_{ono}(f) \\ Y_e(P_{avs},F_0,f)=Y_{ei}(P_{avs},F_0,f)+Y_{eo}(f) \\ Y_{on}(P_{avs},F_0,f)=Y_{oni}(P_{avs},F_0,f)+Y_{ono}(f) \end{cases} \qquad (136.)
$$

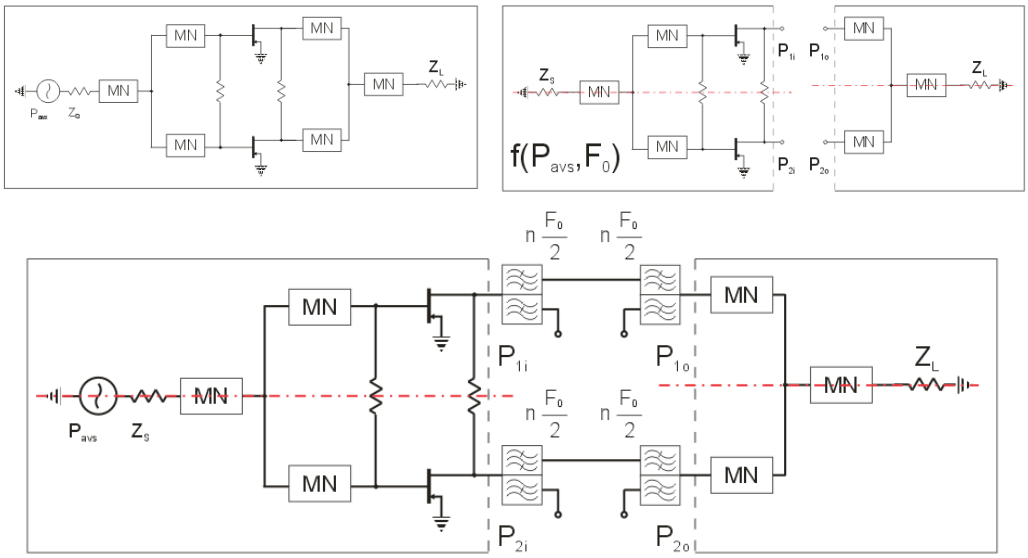

Figure 115 Simulation setup idea for the extended Freitag method.

As it was expected, to perform the simulation two sinusoidal signal sources are used. The large signal source is connected to the input of the amplifier - Figure 115. The small signal source is attached to one of the bisection's ports. One pass of the simulator is than able to describe the interactions related to the port of the small signal source placement only. Accordingly, only one row of the impedance/admittance matrix can be created. Luckily, due to the symmetry of the ideal corporate amplifier, the results are sufficient to calculate the equivalent impedances and admittances of diverse amplifier modes.

In outcome of the analysis it is expected to observe a similar result for a very small power of the input excitation resembling the small signal operation of the amplifier. At the same time the differences should appear while amplifier nonlinearities will modify the circuit's behaviour owing to the input power increase. To confront these expectations the extended Freitag method will be applied to the power amplifier example – PA.5. This lumped element power amplifier uses a full nonlinear model of the active element from the commercial D01PH Ommic process. It is a single stage parallel amplifier consisting of eight pre-matched amplifiers cells PA1. Structure of the amplifier along with the internal structure of the PA1 cell is presented in the Figure 116. Gain, input and output reflection coefficients, and even mode stability are presented in the Figure 117. Power performances are presented in the Figure 118.

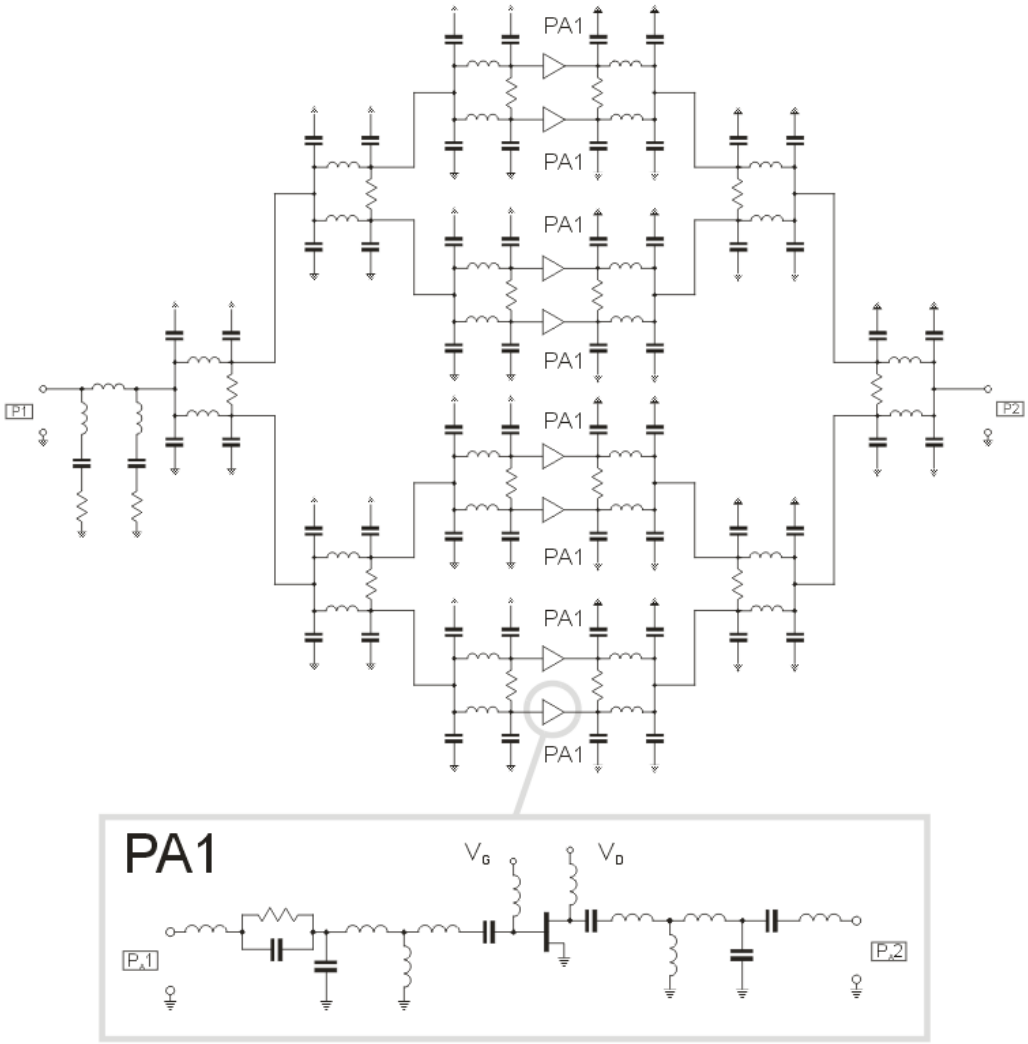

Figure 116 Example lumped power amplifier PA.5 and its PA1 amplifier cell.

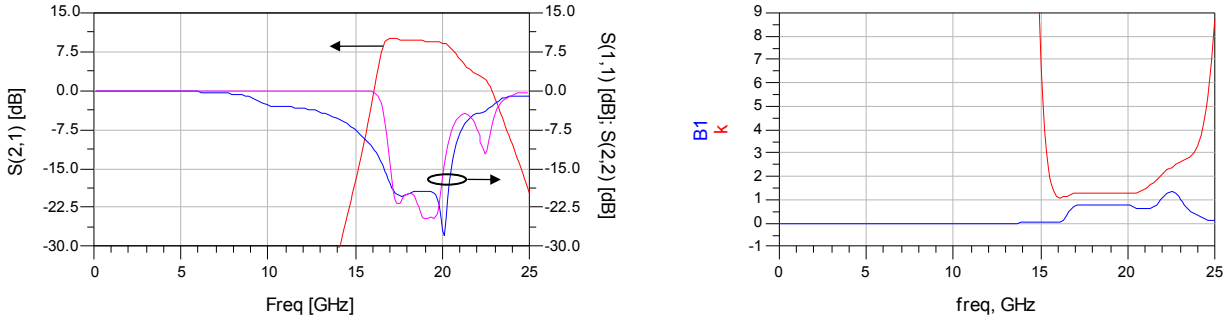

Figure 117 Gain input and output reflection coefficients and Rollet's stability factor of the example power amplifier PA.5.

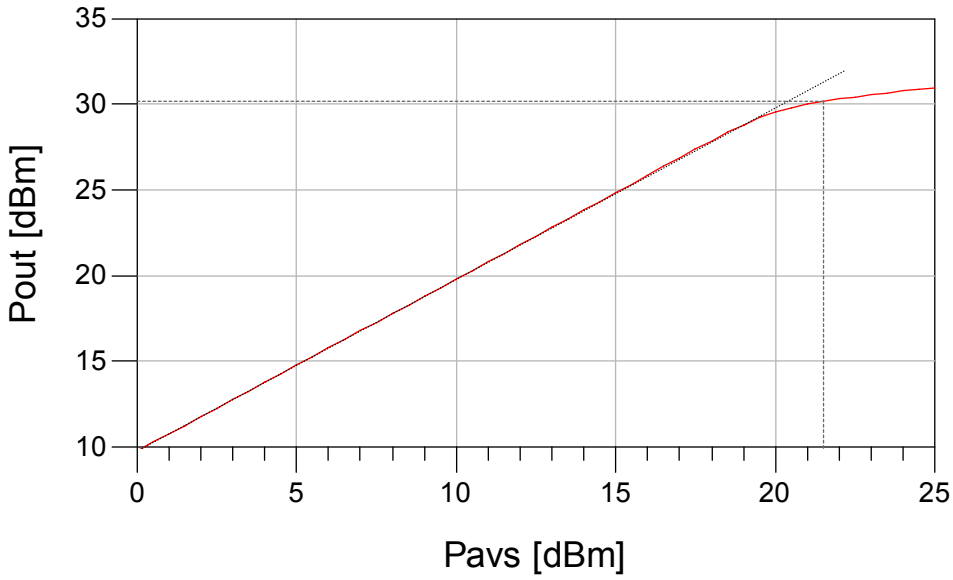

Figure 118 Power performance of the example power amplifier PA.5.

Extended Freitag method was applied in the Agilent ADS environment to benefit from the possibility of AEL programming. AEL language was used to create the implementation scheme and measuring functions that ease the effort needed to apply the method to the amplifier in ADS. However, the method is not only restricted to Agilent ADS as it was also successfully implemented in AWR Microwave Office.

5.2.1 Results of the extended Freitag method applied to PA.5 example

An example power amplifier was tested with the extended Freitag method for the fixed input signal frequency F_0=18 GHz and different input power values P_{avs}. Further, the analysis with a small signal Freitag method have been conducted as a point of reference. The results of the simulations support previously expressed expectations. Figure 119 presents comparison between Odd mode 3 equivalent impedance obtained from small signal Freitag method and extended Freitag method for the input power P_{avs}=-40 dBm. By looking at the power performance of the amplifier we may state that for the the P_{avs}=-40 dBm, the amplifier works in the small signal state. The results are in agreement in this case while the curves are almost completely overlapped. While the power has been increased to P=17.5 dBm, the differences are visible at some frequency points in the Figure 120. Mostly, an increase in the input power causes departure of the impedance curves at some frequencies. It proves an assumption that a large signal operation of the amplifier can affect its small signal stability. This

may be an unsafe situation if the amplifier is not stabilized with enough margin. Such a situation appears in the PA.5 example for Odd mode 2.

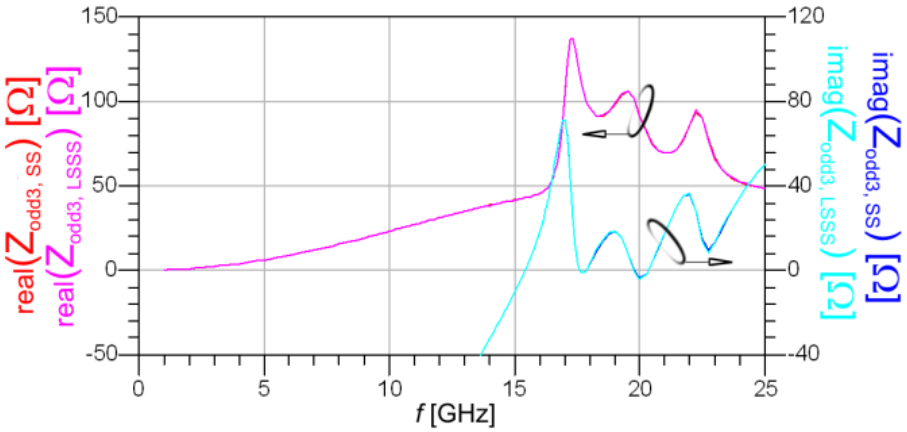

Figure 119 PA.5 example odd mode 3 equivalent impedance simulation results of the small signal Freitag method (SS) and the extended Freitag method for P_{avs}=-40 dBm (LSSS).

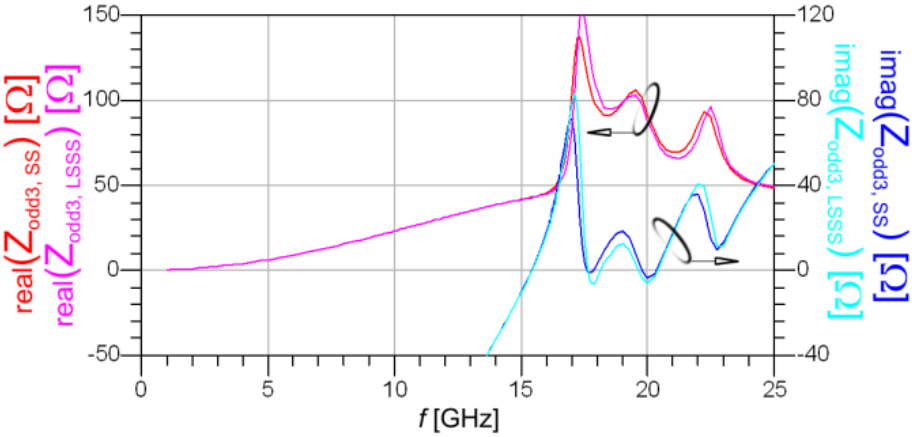

Figure 120 PA.5 example odd mode 3 equivalent impedance simulation results of the small signal Freitag method (SS) and the extended Freitag method for P_{avs}=17.5 dBm (LSSS).

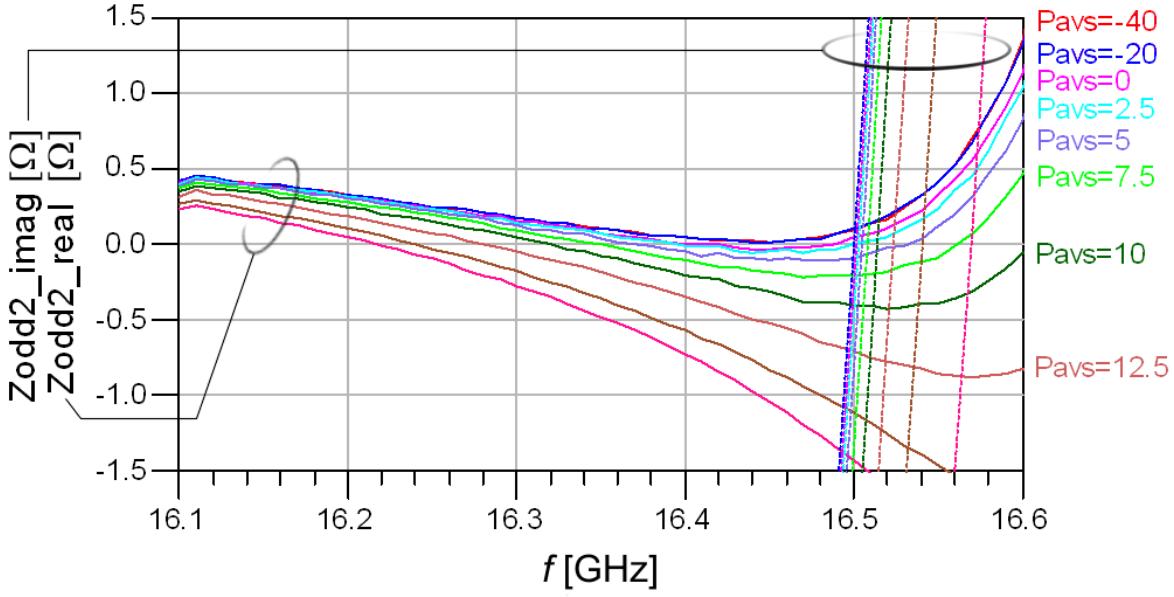

Figure 121 Odd mode 2 equivalent impedance simulated for a different input power of the example power amplifier PA.5.

While analyzing the results of the Odd mode 2 equivalent impedance simulation we observe a situation, when increase of the input power turns small signal stable circuit into an unstable one - Figure 121. While the circuit works with the input signal up to P_{avs}=2.5 dBm, the real part of the impedance value is positive at the positive zero crossing point of the imaginary part, ergo the circuit is stable. If input power will be increased even further, the onset of oscillation will be fulfilled for the Odd mode 2. This outcome reveals possibility of the parametric Odd mode 2 oscillation creation and at the same time an ability of the extended Freitag method to detect it. In order to verify the result, the Time Domain simulations there will be performed .

5.2.2 Verification of the results of the extended method

On this occasion, the Time Domain simulations have been even more demanding to perform due to the presence of the input signal at F_0=18 GHz. Each mode was addressed with a separate simulation setup. The Even mode was tested by applying only the desired input signal. In case of the Odd Modes, in presence of the input signal additional the current pulse source was used as to excite the appropriate mode. As to maintain the single mode excitation in case of the Odd modes, 2 and 3: 2 and 4 current sources were used to simultaneously excite all the loops and maintain the required balance. Odd modes were represented with differential voltages at the input of the appropriate level output combiner and the even mode was represented with the voltage at the output of the amplifier - Figure 122. Excitation pulse was initiated at t=100 ns to confirm the steady state conditions of the circuit. Input source was fixed at F_0=18 GHz and each mode was tested with the two input power values, with P_{avs}=-40 dBm representing small signal regime and P_{avs}=10 dBm representing a weakly nonlinear operation.

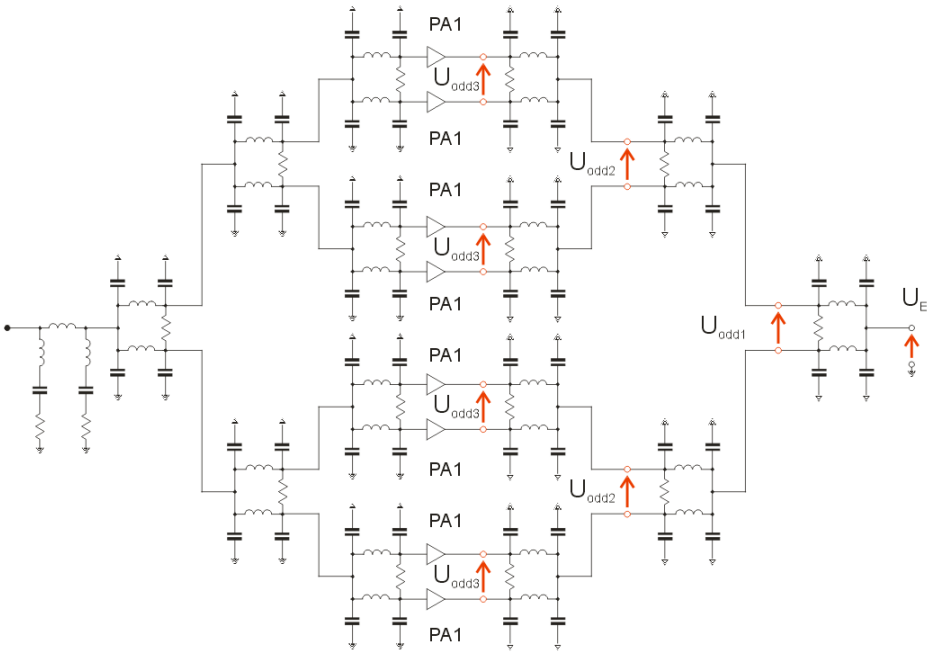

Figure 122 Voltages used to represent different modes of the example power amplifier PA.5.

Outcome of the simulations confirm previously obtained simulation results. The circuit is stable for all the modes of operation in the small signal conditions: Even mode - Figure 123, Odd mode 1 - Figure 125, Odd mode 2 - Figure 127 and Odd mode 3 - Figure 129. When the input power has been

increased, the Odd mode 2 was successfully excited - Figure 128. At the same time the Even mode - Figure 124, Odd mode 1 -Figure 126 and Odd mode 3 - Figure 130 were stable.

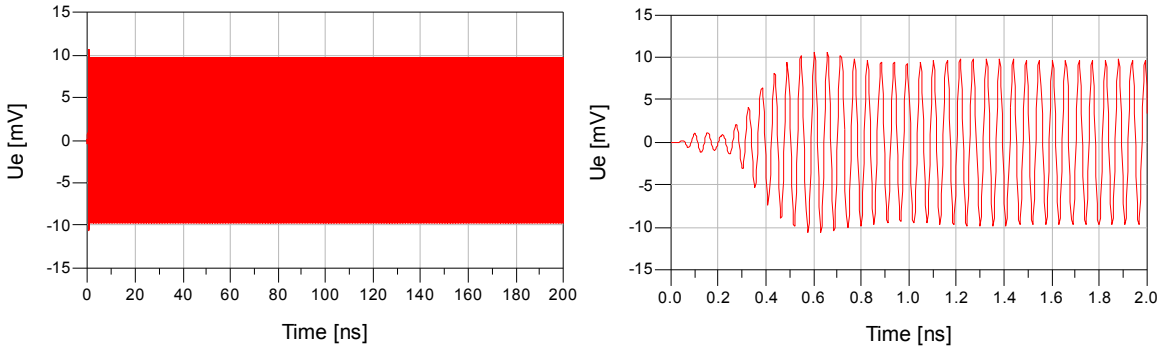

Figure 123 Even mode response U_E for the input power P_{avs}=-40 dBm and F_0=18 GHz.

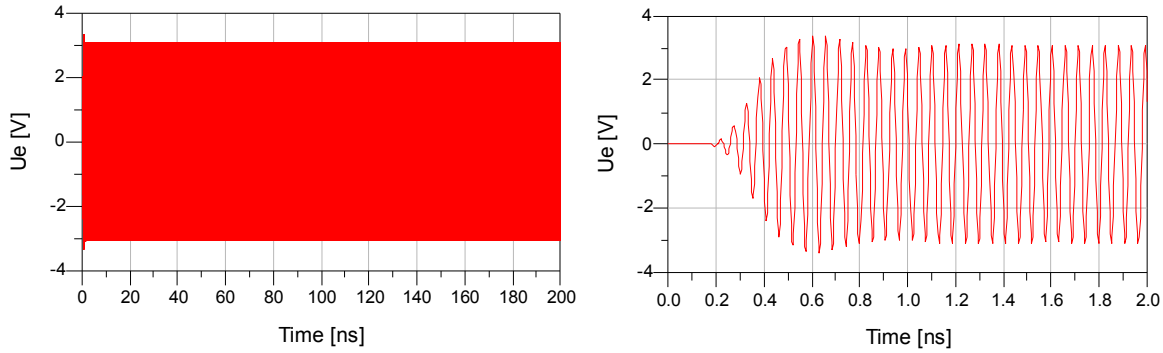

Figure 124 Even mode response U_E for the input power P_{avs}=10 dBm and F_0=18 GHz.

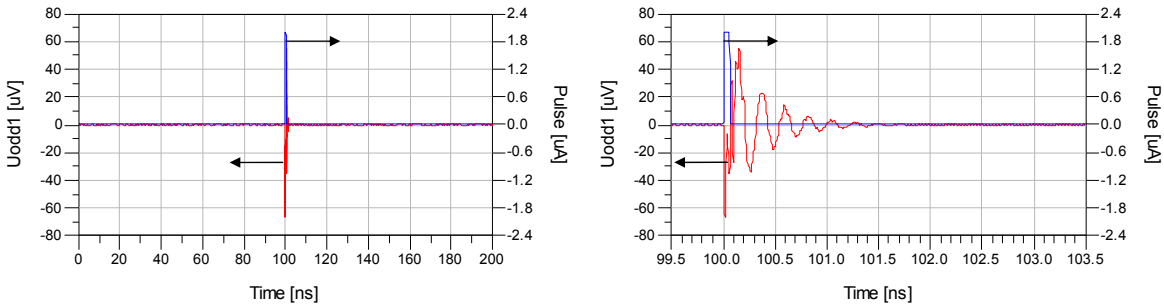

Figure 125 Response of the PA.5 example for the Odd mode 1 excitation together with the stimulus (pulse) for the input power P_{avs}=-40 dBm and F_0=18 GHz.

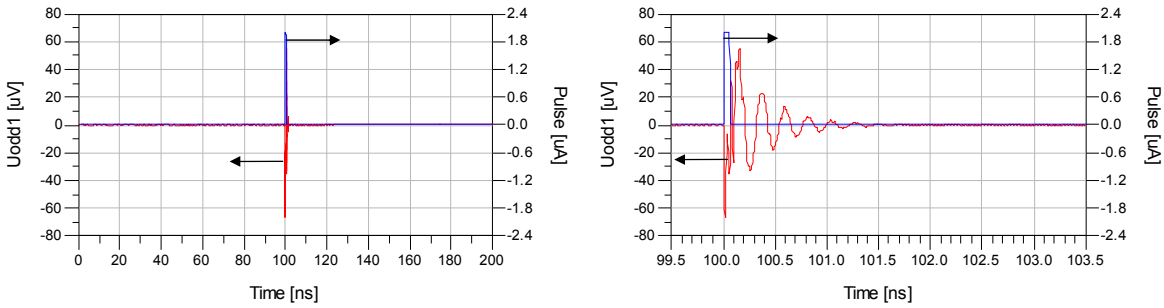

Figure 126 Response of the PA.5 example for the Odd mode 1 excitation together with the stimulus (pulse) for the input power P_{avs}=10 dBm and F_0=18 GHz.

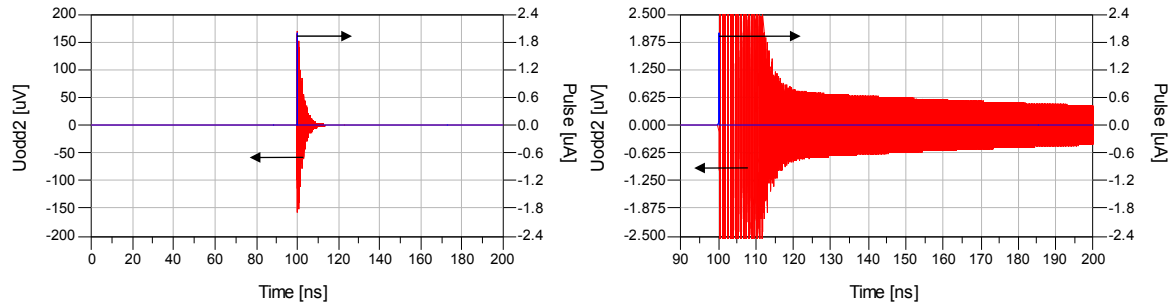

Figure 127 Response of the PA.5 example for the Odd mode 2 excitation together with the stimulus (pulse) for the input power P_{avs}=-40 dBm and F_0=18 GHz.

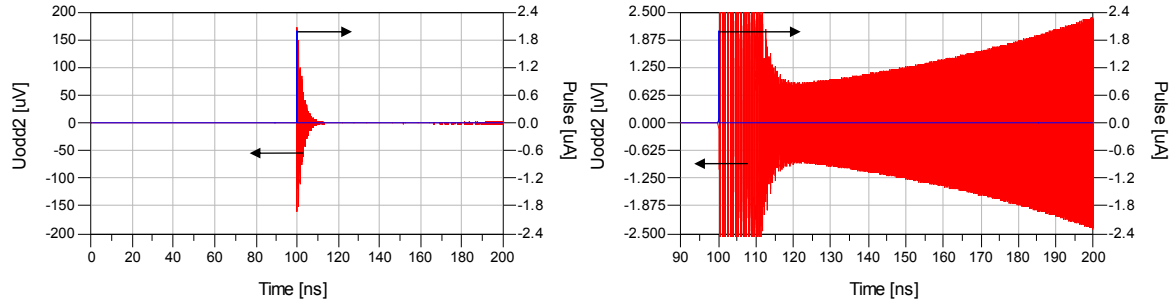

Figure 128 Response of the PA.5 example for the Odd mode 2 excitation together with the stimulus (pulse) for the input power P_{avs}=10 dBm and F_0=18 GHz.

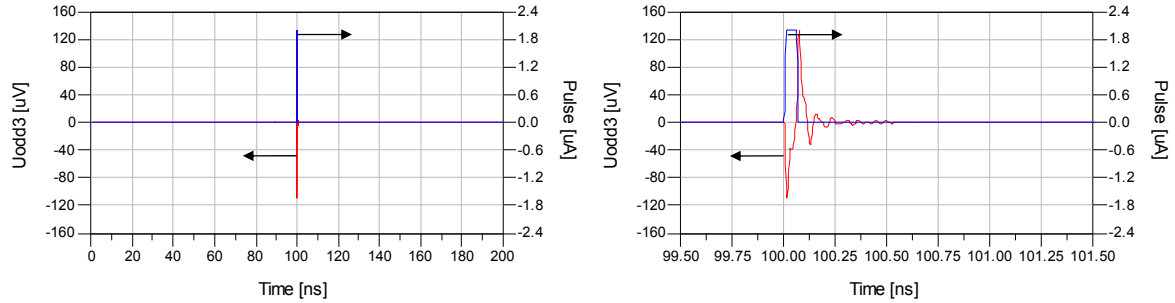

Figure 129 Response of the PA.5 example for the Odd mode 3 excitation together with the stimulus (pulse) for the input power P_{avs}=-40 dBm and F_0=18 GHz.

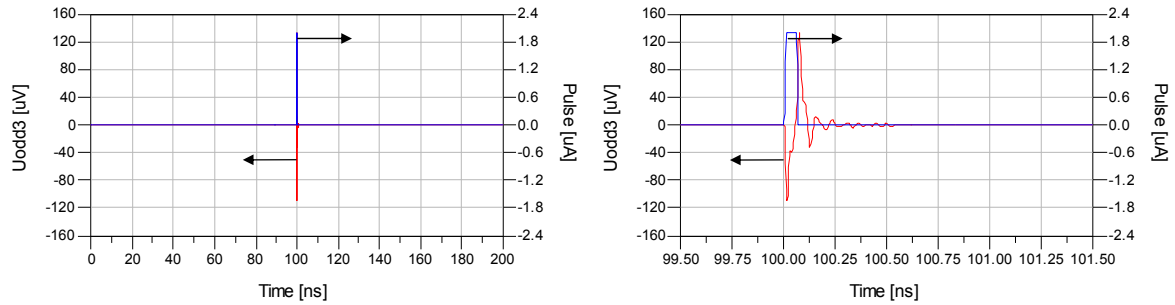

Figure 130 Response of the PA.5 example for the Odd mode 3 excitation together with the stimulus (pulse) for the input power P_{avs}=10 dBm and F_0=18 GHz.

Additional simulations have been performed to get more accuracy with the value of the input power that turns the circuit instable. Odd mode 2 was excited for the input power of P_{avs}=2.5 dBm, P_{avs}=5 dBm and P_{avs}=7.5 dBm. As the simulations results were superimposed in the same graph we may come to a conclusion that the oscillations are not dumped nor amplified for P_{avs}=5 dBm - Figure 131. This roughly estimated value seems to be the one at which the circuit changes its behavior. Same

change of behaviour was predicted by the extended Freitag method. Value of the input power at which it occurs owing to the extended Freitag method can be estimated from the Figure 121, as P_{avs}=2.5 dBm. Clearly, the values obtained from the results of the experiments in two different domains are slightly different.

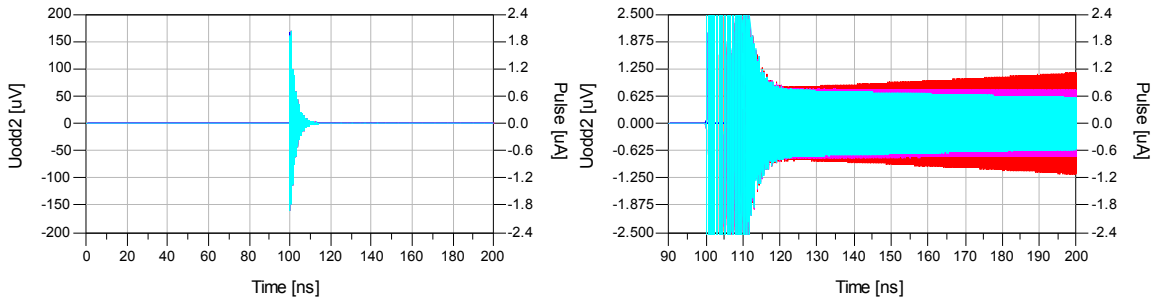

Figure 131 The superimposed responses of the PA.5 example for the Odd mode 2 excitation together with the stimulus (pulse) for the input powers: P_{avs}=2.5 dBm (cyan), P_{avs}=5 dBm (magenta) , P_{avs}=7.5 dBm (red) and fixed frequency F_0=18 GHz.

The difference may be justified by the dissimilarity between the Frequency Domain and the Time Domain active device model. To validate this thesis, the Time Domain simulations were used to characterize the amplifier bisections. Then, the Freitag method was applied to the description, allowing to calculate equivalent modes impedances and admittances. Eventually, a comparison between the Frequency Domain and Time Domain Freitag method results has been made and differences were revealed. An outcome of the final analysis for Odd mode 2 is portrayed in the Figure 132.

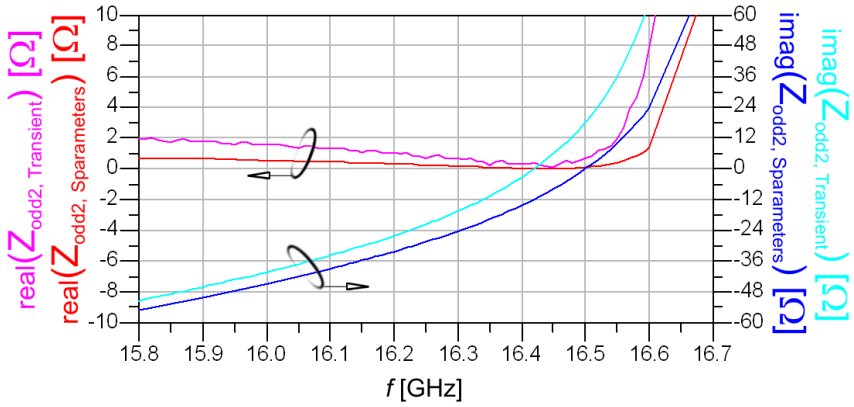

Figure 132 The comparison between the Odd mode 2 equivalent impedance simulation results obtained with the frequency domain models (S-parameters) and time domain models (Transient).

All in all, the contrararies among the Freitag method results obtained from the Frequency Domain and the Time Domain models can be justified by the difference in value of the input power. That change leads then to a change in the behaviour of the circuit. Meanwhile, a general agreement between the behaviour of the circuit in Time Domain and the predictions from the extended Freitag method validates the idea and its practical implementation. Such a simple and effective extension to the Freitag method allows the prediction of unwanted even/odd mode oscillations, when the power amplifier operates outside the small-signal regime, that is it extends the usefulness of the Freitag stability test. Also, the method prevents the designers from mistakes, when the stability of the Odd modes are guaranteed with a small margin due to the typical amplifier's layout design complications.

6 NON IDEAL SYMMETRY PROBLEMS IN THE FREITAG METHOD

When considering Freitag method application into CAD environments in the chapter 4, a simplifying assumption of the ideal symmetry of the corporate amplifiers were made. Benefits of this simplification were so great that nonidealities were neglected and other approaches were treated as the ones having marginal significance. This is true in a sense , when in most cases symmetrical, in-phase and equi-amplitude ideal combiner is a goal of the design. Unfortunately, even with a careful design some degree of asymmetry is always present in the designed structures. So, to avoid errors, eigenvectors and eigenvalues cannot be computed with a simplified approach forcing the standard method application. Nevertheless, even then it is highly probable that the bisection's eigenvectors sets will be slightly different, thus ruling out a possibility of the Freitag method application completely. Moreover, it could happen that the amplifier input and output combining networks are intentionally designed with different symmetry properties, ergo leading to different eigenvector sets. Consequently, there are going to be conducted experiments that prove it is still possible to apply the Freitag method to test the stability of such circuits.

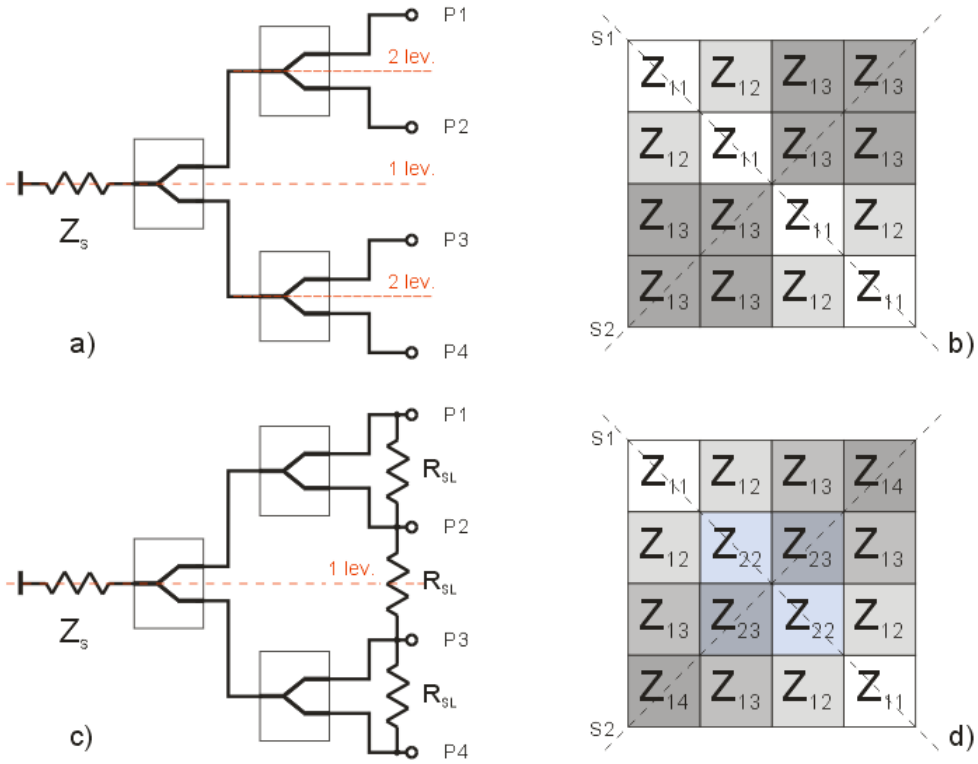

Figure 133 Second level combiner closed with impedance at common port Zs. Ideal corporate structure (a) and its Z matrix description (b). Mirror symmetry combiner (c) and its Z matrix description (d).

To simplify the design process of the parallel power amplifier, the symmetry is often involved, what results in popularity of the corporate structure. If given ideal corporate combiner, symmetry appears in multiple points in the circuit and owing to this fact, the matrix describing combiner possesses unique features and less independent terms. Example of such structure is laid out in the Figure 133 a) as the second level combiner closed at the common port with impedance Z_L. It is noticeable that this

circuit possesses diverse symmetry planes. The 1st level symmetry affects two groups of the ports and the 2nd level symmetry influences the planes that exist at these groups of the ports: 1,2 and 3,4. In the end, the existence of this multiple symmetry planes causes the matrix to possess only three independent terms - Figure 133 b). In reality, the parasitic effects, layout restrictions or intentional actions of the designer often perturb an ideal corporate symmetry scheme and in the end they often only mirror symmetry stands. Such a situation occurs if ladder of the resistors R_{SL} is connected between the ports - Figure 133 c), as a consequence, the description of the combiner is richer and consists of the six independent terms - Figure 133 d). If these structures were used to build a parallel amplifier, even with reciprocity and symmetry as allies decreasing number of the independent terms, a simplified Freitag approach derived in chapter 4 would lead to inaccurate results. This is due to the fact that amplifiers based on these two combining structures possess similar but not identical modes of the operation. From a more customary point of view, a corporate amplifier based on the ideal corporate symmetry combiners is a particular case of general N device parallel amplifier and possesses $\log_2(N)+1$ independent modes of operation from which: one is the Even mode and $\log_2(N)$ are the Odd modes. The general corporate N device power amplifier circuit can work in N different modes from which one is defined as the Even mode. This particular difference is presented in the Figure 134 where the modes present in ideal corporate amplifier are compared to the general case for N={2,4,8}. Than, red and blue fields represent eigenvectors an signs of their elements allowing to comprehend interactions between the devices and creation of the loops in the amplifier.

Dev.	Eigen val.	Modes								Eigen val.	Modes								
2	2	Even	+	+						2	Even	+	+						
		Odd1	+	-							Odd1	+	-						
4	3	Even	+	+	+	+				4	Even	+	+	+	+				
		Odd1	+	+	-	-					Odd1	+	+	-	-				
		Odd2	+	-	+	-					Odd2 a	+	-	+	-				
											Odd2 b	+	-	-	+				
8	4	Even	+	+	+	+	+	+	+	+	8	Even	+	+	+	+	+	+	+	+
		Odd1	+	+	+	+	-	-	-	-		Odd1	+	+	+	+	-	-	-	-
		Odd2	+	+	-	-	+	+	-	-		Odd2 a	+	+	-	-	+	+	-	-
												Odd2 b	+	+	-	-	-	-	+	+
		Odd3	+	-	+	-	+	-	+	-		Odd3 a	+	-	+	-	+		+	-
												Odd3 b	+	-	+	-	-	+	-	+
												Odd3 c	-	+	+	-	-	+	+	-
												Odd3 d	-	+	+	-	+	-	-	+

Figure 134 Different modes of the operation for the corporate amplifiers: ideal symmetry (left) and general case (right).

As a consequence of analysis of the modes for the example amplifiers with 4 or 8 devices we detect that when compared to the general case some combinations are missing from the ideal combiner mode description. In an example of the ideal symmetry the corporate structure modes Odd 3 a,b,c,d are equivalent and described simply as Odd mode 3. This is due to lack of interaction between the most inner loops depicted by the mode in ideal structure. While the loops' relative direction does not influence the mode, its behaviour variations do not exist. In a more empirical way Freitag method's

results for the modes' variations are equal while the eigenvalues which describe them are not distinct. Such an outcome is very useful and was exploited as to create a simplified approach to calculate the eigenvalues. On the other hand, in case of the amplifier for which bisections do not possess these features all the eigenvalues have to be computed with the help of other common methods. For a circuit with a number of the devices higher than four it is not a trivial task, but until the eigenvectors describing appropriate modes are equal, application of the Freitag method is still achievable. The mode impedance/admittance value cannot be computed since they are not equivalent, neither mode stability can be judged by the method presented originally. Such circumstances exist in already divided and prepared for the Freitag analysis simplified circuit shown in the Figure 135. It uses only resistive components and voltage controlled current source and imitates parallel corporate amplifier to become a test vehicle for another Freitag method modification. The circuit's resistive combining structures are characterized with symmetry identical to the ideal corporate combiners. Next, in order to differentiate the eigenvectors sets of the input and output bisections the resistor ladder that connects adjacent branches with each other has been added. Such a resistor structure can be easily justified as in the example odd mode stabilizing network. Sadly, existence of the resistor ladder structure has denied the full stability check through the Freitag method.

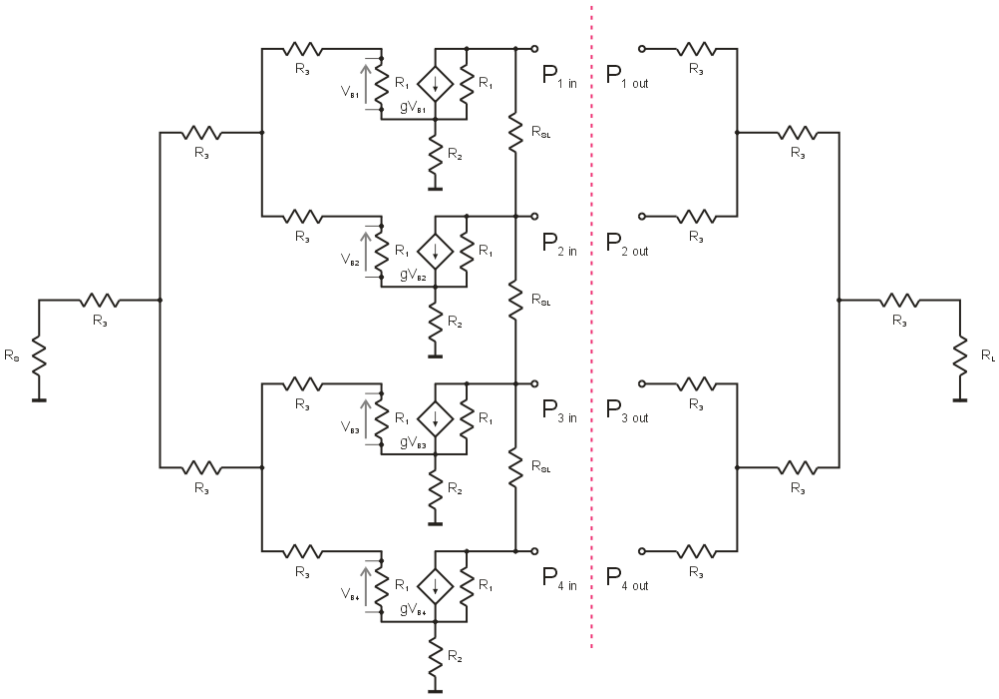

Figure 135 Simplified parallel amplifier circuit with bisections possessing not equal eigenvectors sets.

$$Z_{in} = \begin{bmatrix} 80.925 & 21.749 & 4.656 & -0.004 \\ 21.749 & 63.633 & 17.288 & 4.656 \\ 4.656 & 17.288 & 63.633 & 21.749 \\ -0.004 & 4.656 & 21.749 & 80.925 \end{bmatrix} \qquad Z_{out} = \begin{bmatrix} 60 & 55 & 50 & 50 \\ 55 & 60 & 50 & 50 \\ 50 & 50 & 60 & 55 \\ 50 & 50 & 55 & 60 \end{bmatrix} \tag{137.}$$

$$\mathrm{I}_{1\mathrm{in}}=\begin{bmatrix}1\\1\\1\\1\end{bmatrix},\mathrm{I}_{2\mathrm{in}}=\begin{bmatrix}1.418\\0.582\\-0.582\\-1.418\end{bmatrix},\mathrm{I}_{3\mathrm{in}}=\begin{bmatrix}-1\\1\\1\\-1\end{bmatrix},\mathrm{I}_{4\mathrm{in}}=\begin{bmatrix}0.582\\-1.418\\1.418\\-0.582\end{bmatrix},\mathrm{Z}_{\mathrm{EV\,in}}=\begin{bmatrix}107.326\\87.951\\54.516\\39.323\end{bmatrix} \tag{138.}$$

$$\mathrm{I}_{1\mathrm{out}}=\begin{bmatrix}1\\1\\1\\1\end{bmatrix},\mathrm{I}_{2\mathrm{out}}=\begin{bmatrix}1\\1\\-1\\-1\end{bmatrix},\mathrm{I}_{3\mathrm{out}}=\begin{bmatrix}-1\\1\\1\\-1\end{bmatrix},\mathrm{I}_{4\mathrm{out}}=\begin{bmatrix}1\\-1\\1\\-1\end{bmatrix},\mathrm{Z}_{\mathrm{EV\,out}}=\begin{bmatrix}215\\15\\5\\5\end{bmatrix} \tag{139.}$$

Afterward, for the fixed values of the components input (138.) and output (139.) bisection eigenvectors and eigenvalues were computed numerically for the Z matrix description - (137.). Their analysis clearly indicates that the standard Freitag method can be successfully conducted only for the Even mode and Odd mode 2b - according to the Figure 134. Moreover, the same time line of thought as in paragraph 4.6 can be reapplied in this situation. There, an idea presented with equations (123.) served to maintain the integrity of the circuit. It has been proved, that mode impedance can equivalently be calculated into the standard way with the measurement ports placed in series to the bisections. Than, the division of the circuit was not necessary and the method delivered results from the analysis of the effective sum of the bisections impedance matrix representation. A twin idea has been applied to the admittance description with an appropriate dualism, than forcing a parallel connection of bisections and measurement ports. What is more, simple equations treated as a proof were in agreement with the standard Freitag method assumption of the equal eigenvector sets for bisections. Till this point this arrangement has not changed anything and the original restrictions have stood by. Thus, a simple experiment can be made with the circuit in the measurement configuration – used in the paragraph 4.6.

Let us trace the original idea of the Freitag analysis. For the divided circuit the current vectors were searched for. If the circuit is excited with such current vectors, at each of the circuit's measurement ports equal impedance will be registered. As it was proved by Freitag this vector was equivalent to the eigenvector of impedance description. The impedance value was outlined with eigenvalue associated to this vector. If it happens that the same vector was present for both parts of the divided circuit, the onset of the oscillation could be applied to the sum of the founded equivalent impedances. This summation on the assumption of equal eigenvectors set, is equivalent to the calculation of the eigenvalue from the sum of the impedance matrixes of the bisection. Also, it can be translated to the measurement scheme, where the measurement ports are placed in series to the circuit bisections. Interestingly, such arrangement forces the same current vector to flow through the bisection ports. It is easily observable while the current sources are placed in the measurement ports - Figure 136. In practice, the current vector for which identical ratio of the voltage drops on the current sources to their values, represents eigenvector and the ratio itself represents the circuit's equivalent impedance in that mode. However, stepping back to the matrix description – application of the Freitag method is still possible when the eigenvectors together with appropriate eigenvalues are calculated for the sum of the impedance and the admittance description accordingly. With dualism, similar idea can be applied to the modes equivalent admittance with the measurement

setup presented in the Figure 137. Besides, if the presented measurement setups are compared to the numerically treated Z and Y representations' agreement of the result will be reached.

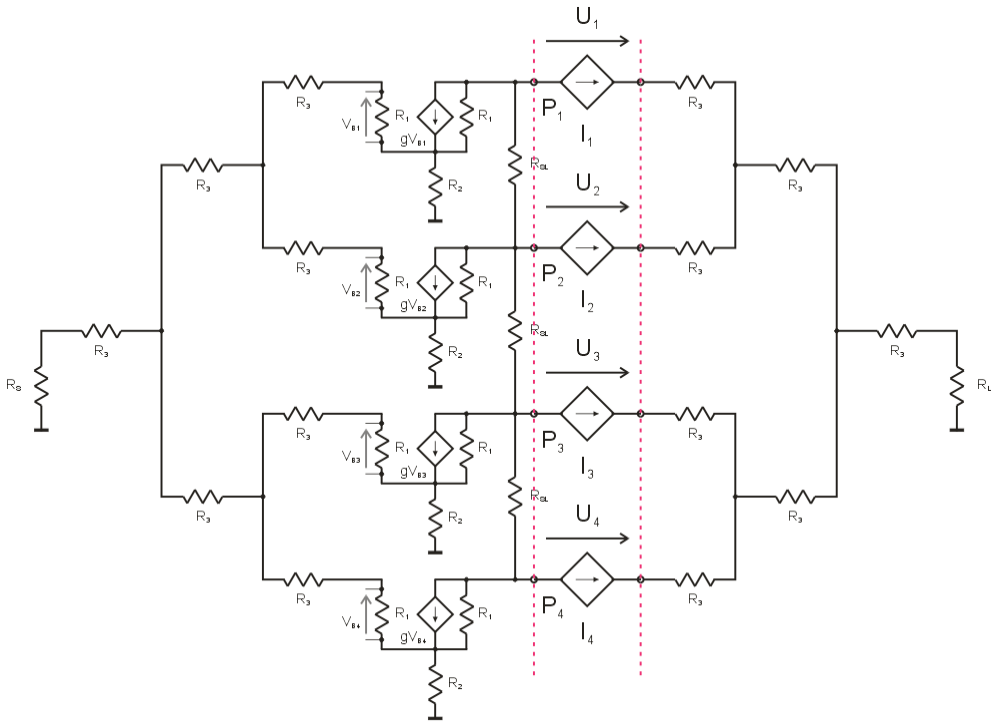

Figure 136 The measurement setup allowing for the ports' impedance $\{Z_1,Z_2,Z_3,Z_4\}$ calculation with the current vector excitation $EV_Z=\{I_1,I_2,I_3,I_4\}$.

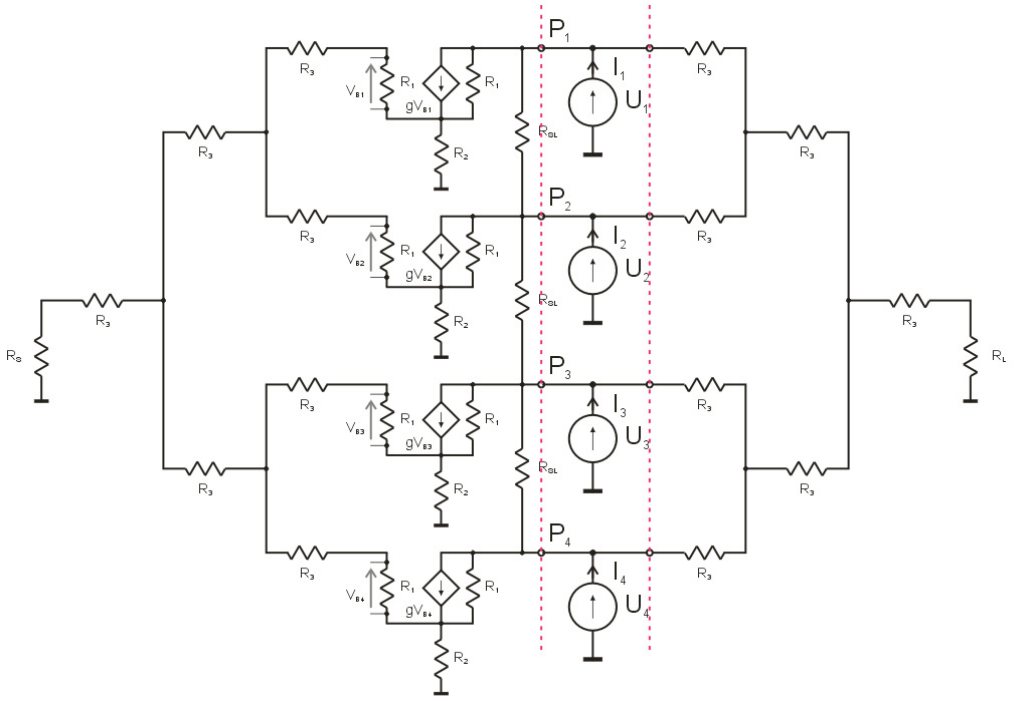

Figure 137 Measurement setup allowing for the ports admittance $\{Y_1,Y_2,Y_3,Y_4\}$ calculation with the voltage vector excitation $EV_Y=\{U_1,U_2,U_3,U_4\}$.

According to the previous statements, the sum of Z and Y matrix descriptions wishes to be considered in eigenvectors/eigenvalues analysis:

$$Z = Z_{in} + Z_{out} = \begin{bmatrix} 140.925 & 76.749 & 54.656 & 49.996 \\ 21.749 & 123.633 & 67.288 & 54.656 \\ 54.656 & 17.288 & 123.633 & 21.749 \\ 49.996 & 54.656 & 76.749 & 140.925 \end{bmatrix}$$

(140.)

$$Y = Y_{in} + Y_{out} = \begin{bmatrix} 0.131 & -0.087 & -0.015 & -0.015 \\ -0.087 & 0.136 & -0.02 & -0.015 \\ -0.015 & -0.02 & 0.136 & -0.087 \\ -0.015 & -0.015 & -0.087 & 0.131 \end{bmatrix}$$

(141.)

Then, due to numerical analysis of the matrixes the following results are obtained:

$$EV_{Z1} = \begin{bmatrix} 1 \\ 1 \\ 1 \\ 1 \end{bmatrix}, EV_{Z2} = \begin{bmatrix} 1.345 \\ 0.655 \\ -0.666 \\ -1.345 \end{bmatrix}, EV_{Z3} = \begin{bmatrix} -1 \\ 1 \\ 1 \\ -1 \end{bmatrix}, EV_{Z4} = \begin{bmatrix} 0.655 \\ -1.345 \\ 1.345 \\ -0.655 \end{bmatrix}, Z_{EV} = \begin{bmatrix} 322.326 \\ 101.693 \\ 59.516 \\ 45.581 \end{bmatrix}$$

(142.)

$$EV_{Y1} = \begin{bmatrix} 1 \\ 1 \\ 1 \\ 1 \end{bmatrix}, EV_{Y2} = \begin{bmatrix} 1.035 \\ 0.965 \\ -0.965 \\ -1.035 \end{bmatrix}, EV_{Y3} = \begin{bmatrix} -1 \\ 1 \\ 1 \\ -1 \end{bmatrix}, EV_{Y4} = \begin{bmatrix} 0.965 \\ -1.035 \\ 1.035 \\ -0.965 \end{bmatrix}, Y_{EV} = \begin{bmatrix} 0.014 \\ 0.08 \\ 0.218 \\ 0.224 \end{bmatrix}$$

(143.)

Y1	Y2	Y3	Y4
0.293715	0.191622	0.191622	0.293715

Z1	Z2	Z3	Z4
45.580527	45.580513	45.580513	45.580527

EVe1	EVe2	EVe3	EVe4
0.655192	-1.344808	1.344808	-0.655192

Figure 138 Impedances and admittances at the test ports for the excitation with eigenvector EV_{Z4}.

Y1	Y2	Y3	Y4
0.223518	0.223517	0.223517	0.223518

Z1	Z2	Z3	Z4
67.238546	35.739789	35.739789	67.238546

EVe1	EVe2	EVe3	EVe4
0.965130	-1.034870	1.034870	-0.965130

Figure 139 Impedances and admittances at the test ports for the excitation with eigenvector EV_{Y4}.

Results of the numerical analysis for the Z matrix (142.) and for the Y (143.) have been applied to the previously introduced measurement setups for Odd mode 2 represented with vectors EV_{Z4} and EV_{Y4}. The Figure 138 presents the outcome for EV_{Z4} and the Figure 139 gather the results for EV_{Y4}. While vector EV_{Z4} has been applied, the values of the impedance at the measurement ports were equal $Z_1=Z_2=Z_3=Z_4$ and equal to the eigenvalue computed from Z matrix. Meanwhile: $Y_1=Y_4\neq Y_3=Y_2$. While vector EV_{Y4} has been applied values of the admittances at the measurement ports were equal $Y_1=Y_2=Y_3=Y_4$ and equal to the eigenvalue computed from Y matrix. Again, $Z_1=Z_4\neq Z_3=Z_2$. These settlements prove that the values of the eigenvector and eigenvalue computation of the sum of the matrix descriptions match the modes equivalent impedances and admittances. Also, it is obvious that eigenvectors for Z and Y matrix can be different for the modes that are described with different eigenvectors for the input and output bisections. When there has been applied EV_{Y1}, which is equal to vector EV_{Z1} - as a consequence the values of the admittances and impedances at the measurement ports were equal $Y_1=Y_2=Y_3=Y_4$, $Z_1=Z_2=Z_3=Z_4$ and also equal to the value computed from Y and Z matrix - Figure 140. This agreement among numerical results and simulations of the simplified example proves the validity of the assumptions and encourages further tests.

Y1	Y2	Y3	Y4
0.013969	0.013969	0.013969	0.013969

Z1	Z2	Z3	Z4
322.325949	322.325949	322.325949	322.325949

EVe1	EVe2	EVe3	EVe4
1.000000	1.000000	1.000000	1.000000

Figure 140 Impedances and admittances at the test ports for excitation with eigenvector $EV_{Z1}= EV_{Y1}$.

Application of the method does not complicate the test procedure and the only difference is that the analysis has to be performed on the sum of the impedance and admittance descriptions of the bisections obtained from the measurements, and not on the bisections individually, as it was done before. In contrast, to perform general eigenvector eigenvalue analysis in CAD environment is quite problematic. This dilemma has been already mentioned in the chapter 4 and it lead to the application of the simplified method. Fortunately, with the assumption of the mirror symmetry and reciprocity of the bisections closed formulas for the eigenvalues have been obtained for N=2 (106.) and N=4 (110.). So that, the method can be applied for the PA.4 example power amplifier, used previously to test the automated Freitag approach.

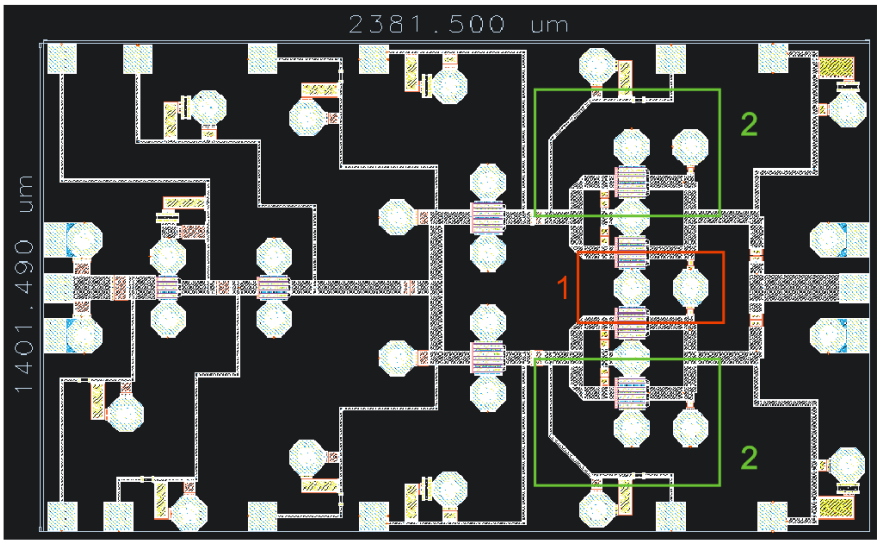

Figure 141 Example power amplifier PA.4 layout.
Marked areas are responsible for the perturbation of the ideal corporate symmetry.

The above amplifier (Figure 141) was designed with attention to maintain its symmetry. However, owing to efficiency of the space usage, the branches of the last stage are not perfectly equal. By studying the area 1- marked with red rectangle it is likely to distinct that the introduction of the alternate pattern of the devices and via holes destroys the ideal corporate combiner symmetry. Moreover, the matching capacitors of the branches B and C are sharing common via hole, while an additional coupling between them is stronger than the one between branches A and D. Simultaneously, in the areas 2, marked with green rectangles, coupling between external branches A, D and gate bias structures of the third stage is stronger. Further, since the analysis is made with the circuital modes, only the influence of the common via holes is taken into account.

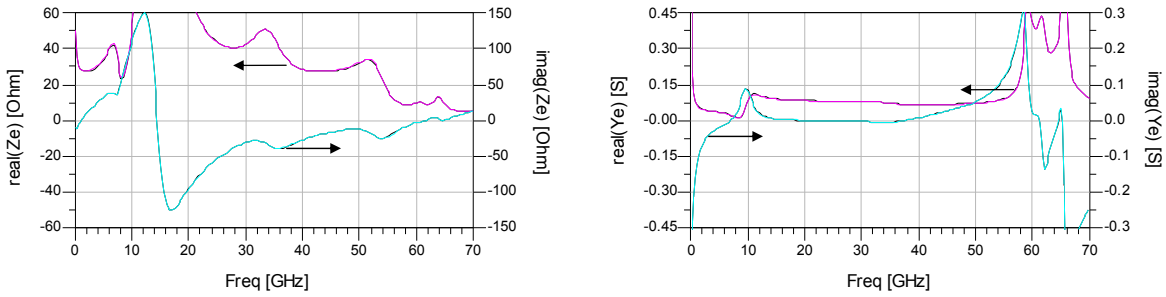

Figure 142 Even mode impedance (Ze) and admittance (Ye) of the example power amplifier PA.4 calculated with generalized and simplified Freitag method (black curves).

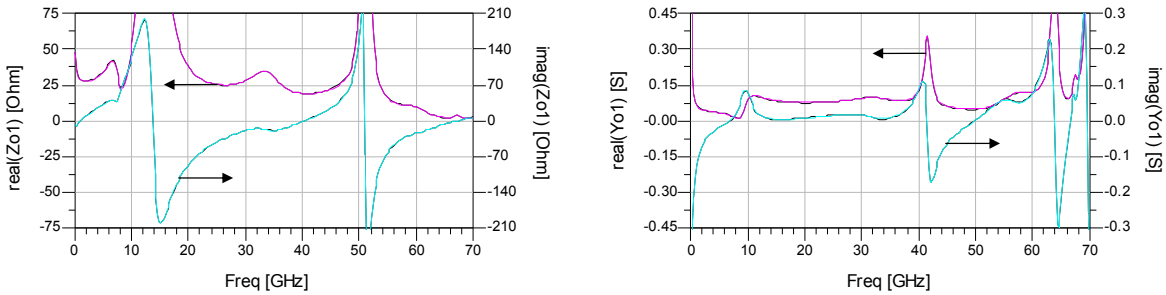

Figure 143 Odd mode 1 impedance (Zo1) and admittance (Yo1) of the example power amplifier PA.4 calculated with generalized and simplified Freitag method (black curves).

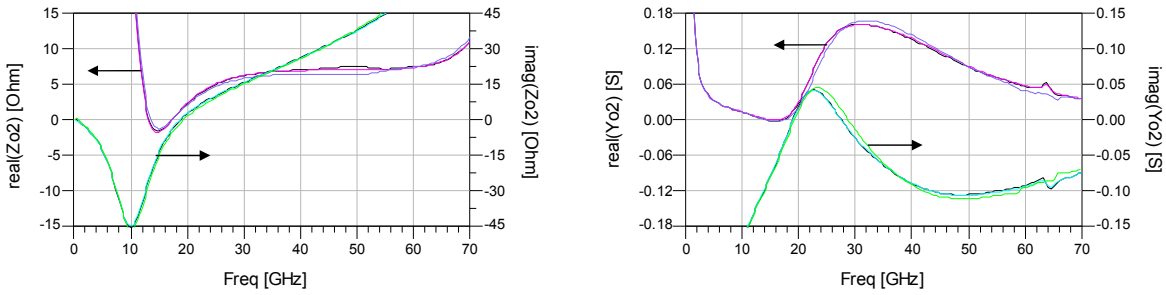

Figure 144 Odd mode 2 a, b, impedances (Ze) and admittances (Ye) of the example power amplifier PA.4 calculated with the generalized and simplified Freitag method (black curves).

While compared to the simplified approach the results of the generalised analysis are almost unchanged. This is positive news since they need a considerably larger amount of effort in comparison to the one required for the simplified method results. The fact that the simplified method produces approximate results with less effort can be used for rapid results, for example in the optimization routines. Moreover simplified method results are very close to the results of the generalized analysis in case of the circuits with small perturbation of the symmetry from the ideal corporate. As a consequence, if given enough margin, the simplified method can be used to stabilize the amplifier in the eventual stabilization process and final validation can be done with either the generalized method or Ohtomo method.

To benefit from the generalized method a more demanding example will be tested. So, the previously used example power amplifier PA.5 will be modified by removal of the resistive components from the lumped elements combiners. To maintain stability, the resistor ladder will be introduced between the branches at the output of the amplification cells PA1 - Figure 145.

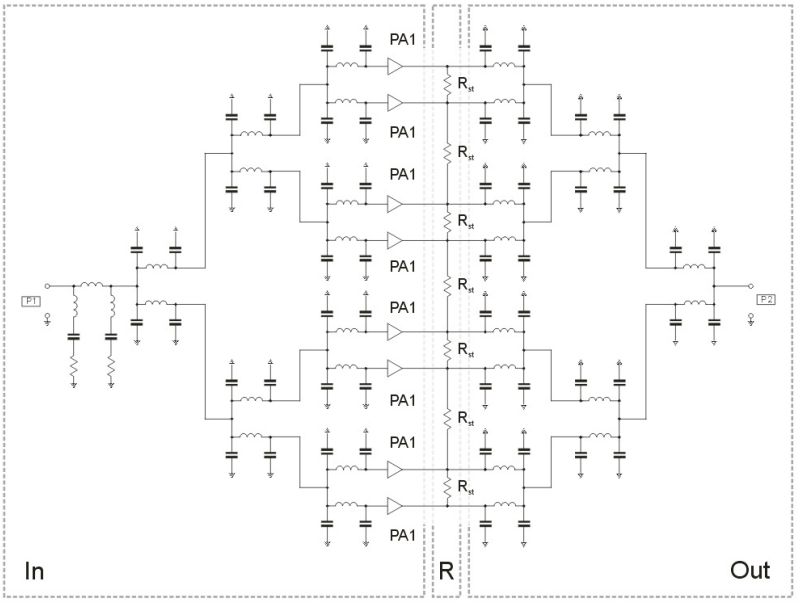

Figure 145 Modified example power amplifier PA.5

If given the presented example, application of the method in the typical CAD environment is not easy due to the computation of the eigenvalues and eigenvectors. To deal with the problem, there is is required an appropriate environment which would allow for uncomplicated data post processing while efficiency in solving eigenvector and eigenvalue problem is essential to create a convenient

stability tool. Sadly, typical CAD environments used in the design process do not provide simple functions to calculate eigenvectors and eigenvalues. On the other hand, the post processing with other environment is not always convenient or possible. For that reason, the iterative Jacobi method along with simple pattern recognition and results filtering functions were implemented into ADS environment as the measurement functions. These tools empowered the appliance of the generalized Freitag method as well the laid out analysis circuit for different values of the stabilizing resistors R_{SL}. Meanwhile, the Original Freitag method may be successfully implemented to the circuit only for the infinitive value of the resistance R_{SL}. In that case, the circuit becomes an ideal corporate amplifier and the simplified method along with the generalized one report identical results. The simulation results for the case in question were presented in the: Figure 146, Figure 147, Figure 148 and Figure 149. Analyzing them it is easy to detect that there are almost no differences between the curves representing equivalent modes impedances and the admittances obtained with the simplified and generalized approaches. Evidently, there are no variations for the modes while the eigenvalues representing different versions of the Odd mode 2 and Odd mode 3 are not distinct. Small differences which were found were caused by the convergence problems of the iterative method. Than, a small error occurs in the result of the generalized Freitag test due to the iterative nature of the algorithm. Moreover, in the extreme cases when the convergence was not reached within maximum iterations, the data points have been replaced by the results filtering algorithm; , changing locally the shape of the curve.

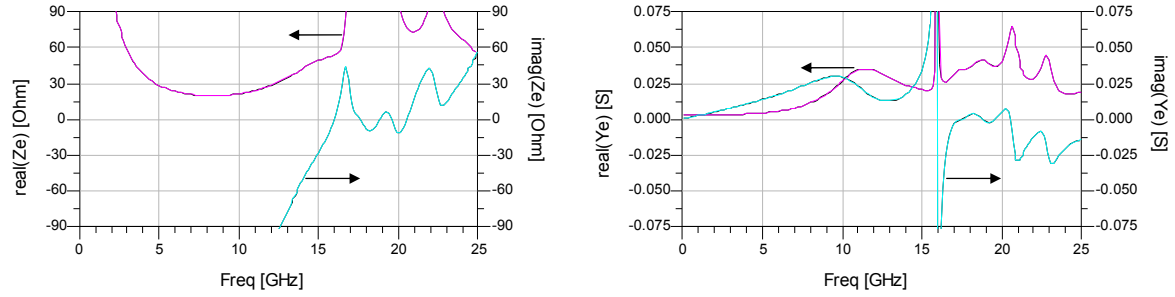

Figure 146 Even mode impedance (Ze) and admittance (Ye) of the modified example power amplifier PA.5 calculated with the generalized and simplified Freitag method (black curves) for the $R_{SL}=\infty$.

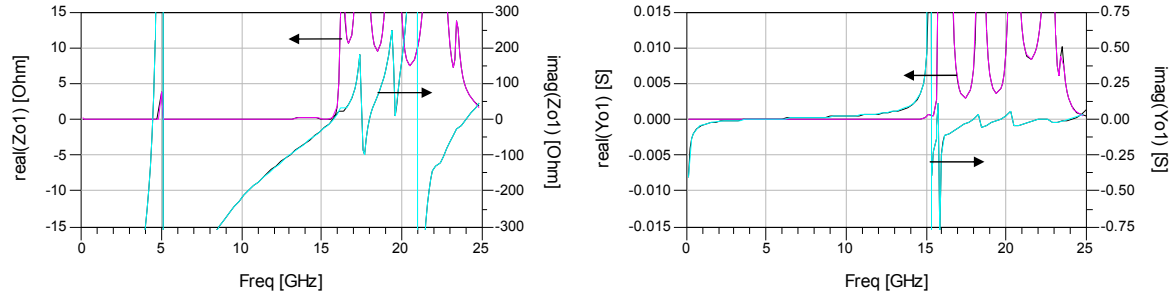

Figure 147 Odd mode 1 impedance (Zo1) and admittance (Yo1) of the modified example power amplifier PA.5 calculated with generalized and simplified Freitag method (black curves) for the RSL=∞.

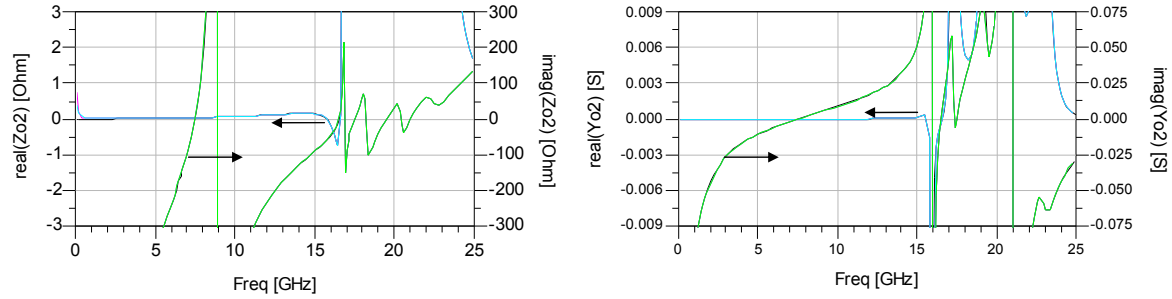

Figure 148 Odd mode 2 impedance (Zo2) and admittance (Yo2) of the modified example power amplifier PA.5 calculated with the generalized and simplified Freitag method (black curves) for the R_{SL}=∞.

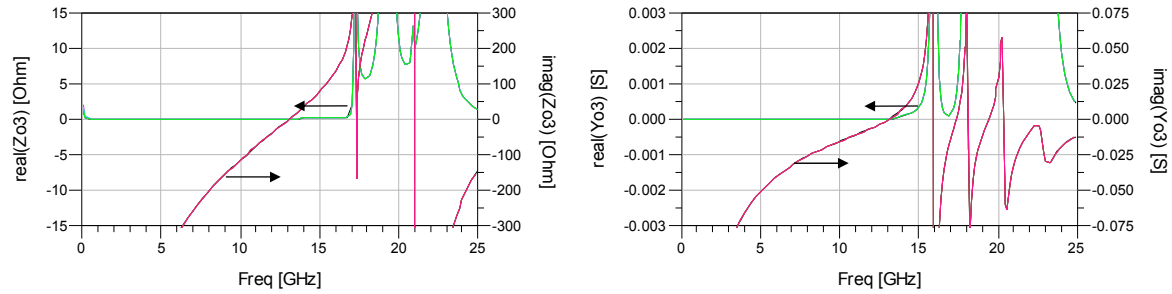

Figure 149 Odd mode 3 impedance (Zo3) and admittance (Yo3) of the modified example power amplifier PA.5 calculated with generalized Freitag method and simplified one(black curves) for the R_{SL}=∞.

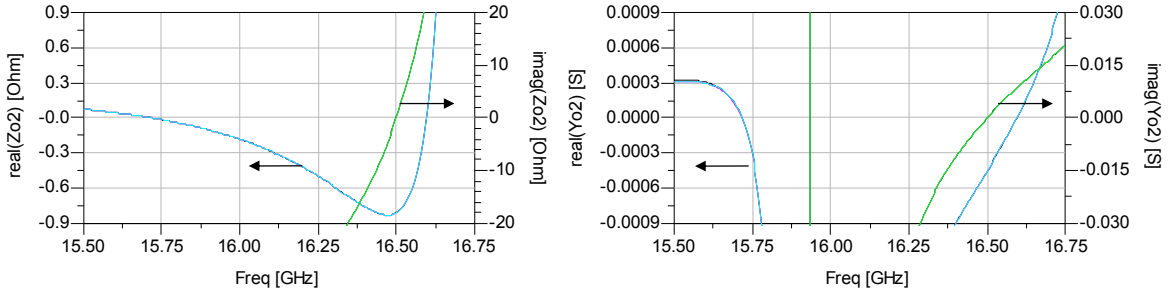

Figure 150 Odd mode 2 impedance (Zo2) and admittance (Yo2) of the modified example power amplifier PA.5 calculated with the generalized Freitag and simplified Freitag method (black curves) for the R_{SL}=∞Ω.

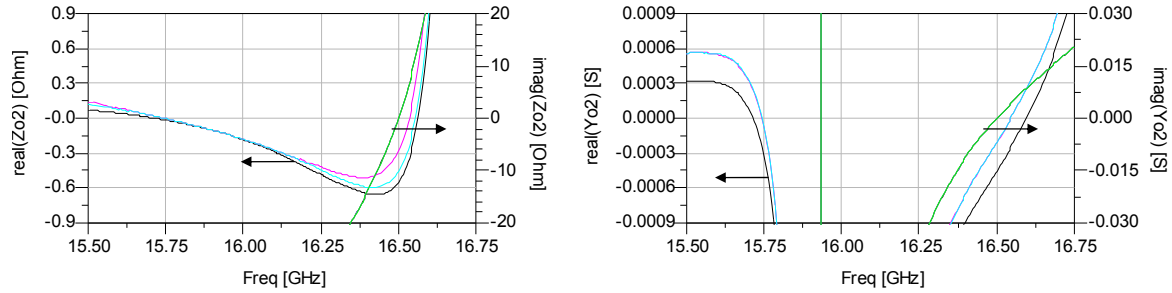

Figure 151 Odd mode 2 impedance (Zo2) and admittance (Yo2) of the modified example power amplifier PA.5 calculated with the generalized and simplified Freitag method (black curves) for the R_{SL}=5kΩ.

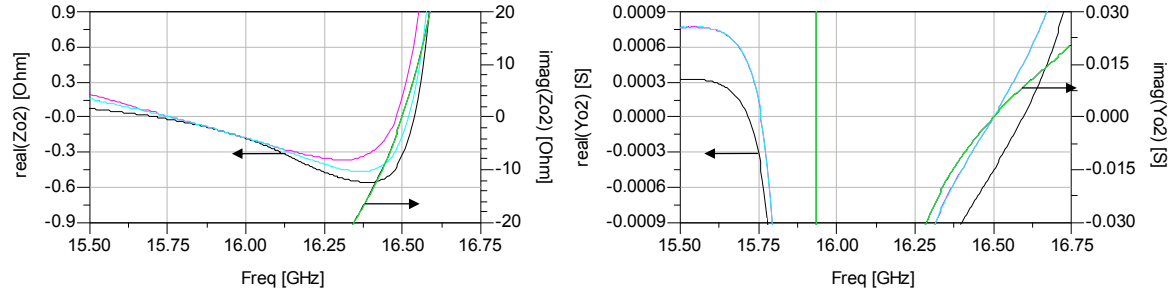

Figure 152 Odd mode 2 impedance (Zo2) and admittance (Yo2) of the modified example power amplifier PA.5 calculated with the generalized and simplified Freitag method (black curves) for the R_{SL}=2.75kΩ.

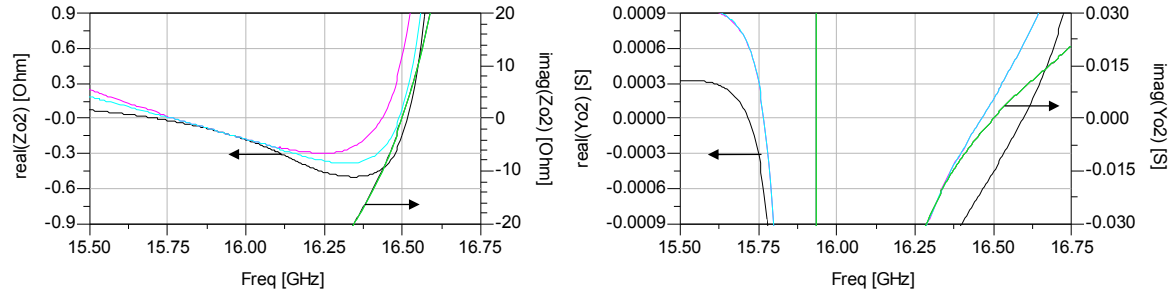

Figure 153 Odd mode 2 impedance (Zo2) and admittance (Yo2) of the modified example power amplifier PA.5 calculated with the generalized and simplified Freitag method (black curves) for the R_{SL}=2kΩ.

The circuit is initially unstable in Odd mode 2 due to impedance and admittance onset of oscillation fulfilment - Figure 150. While large resistors R_{SL}=5kΩ are connected to the circuit, the impedance and admittance curves are slightly shifted upwards to the positive values, but the circuit itself remain unstable - Figure 151. Simultaneously, the difference between the two versions of Odd mode 2 becomes visible and the simplified approach becomes inaccurate. While the resistors are decreased to value of R_{SL}=2.75kΩ the Odd mode 2 b becomes stable while Odd mode 2 a still fulfils the onset of oscillation - Figure 152. Final analysis made for R_{SL}=2kΩ reveals that Odd mode 2 a and b are stable - Figure 153. If the simplified Freitag analysis was performed, the circuit would be still declared unstable.

The Figure 154, Figure 155, Figure 156 and Figure 157 present all modes impedance and admittance analysis for the R_{SL}=2kΩ in wider frequency spectrum. The results confirms full circuit stability. At the same time, the differences between the generalized and the simplified Freitag method for the Odd modes send a clear message that states : differences in the bisection symmetry characters cannot be neglected in this very example.

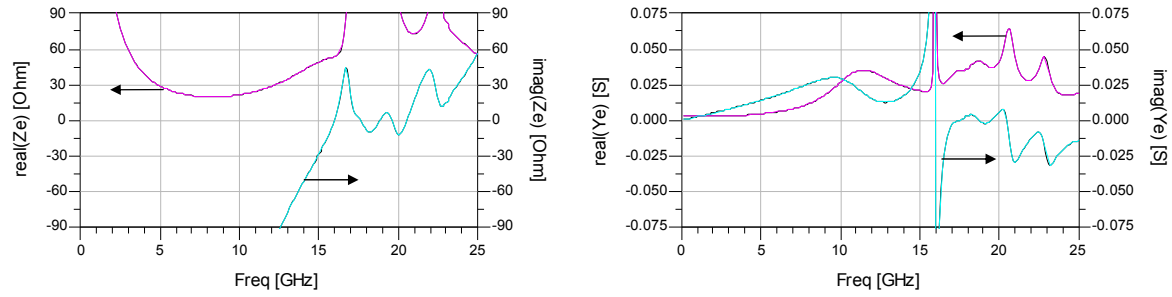

Figure 154 Even mode impedance (Ze) and admittance (Ye) of the modified example power amplifier PA.5 calculated with the generalized and simplified Freitag method (black curves) for the RSL=2kΩ.

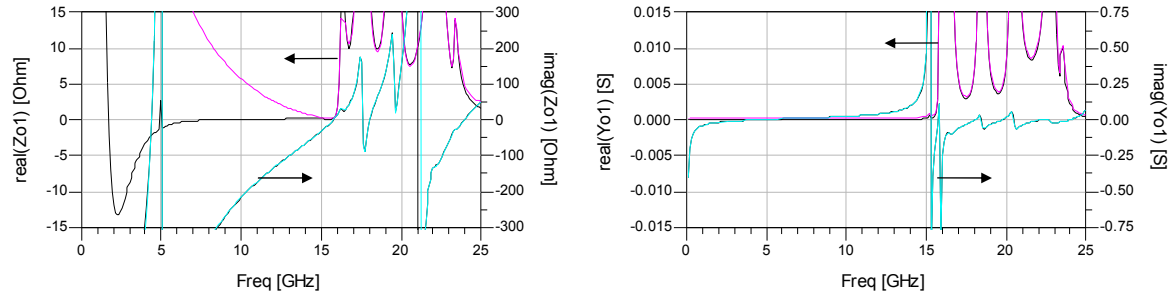

Figure 155 Odd mode 1 impedance (Zo1) and admittance (Yo1) of the modified example power amplifier PA.5 calculated with the generalized and simplified Freitag method (black curves) for the R_{SL}=2kΩ.

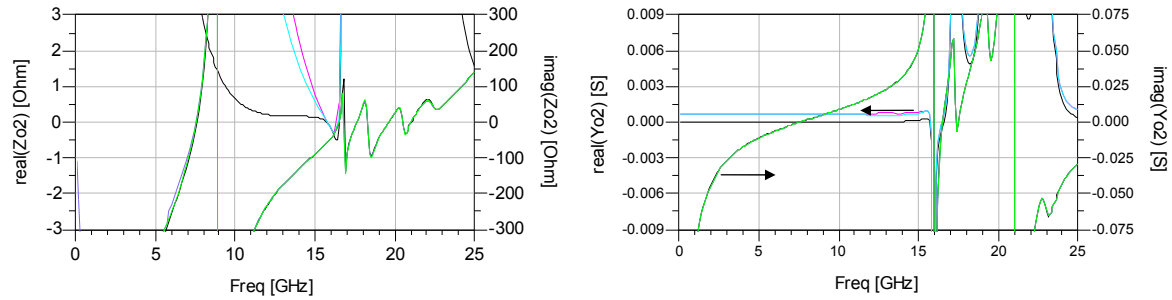

Figure 156 Odd mode 2 impedance (Zo2) and admittance (Yo2) of the modified example power amplifier PA.5 calculated with the generalized and simplified Freitag method (black curves) for the R_{SL}=2kΩ.

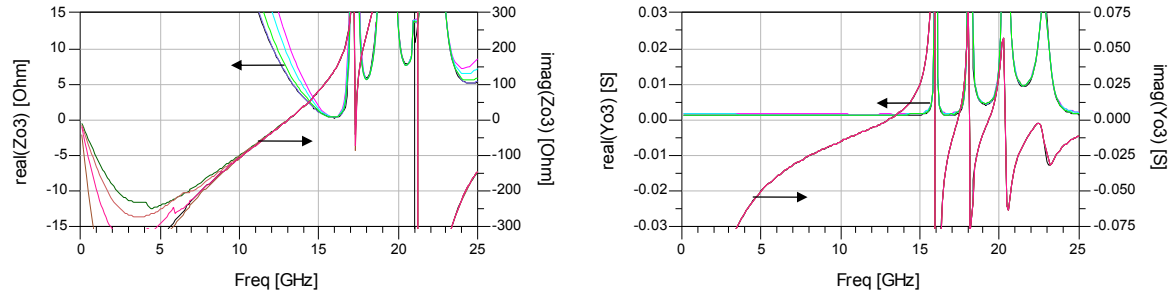

Figure 157 Odd mode 3 impedance (Zo3) and admittance (Yo3) of the modified example power amplifier PA.5 calculated with the generalized and simplified Freitag method (black curves) for the R_{SL}=2kΩ.

For the sake of validating the results of the generalized Freitag method, the Ohtomo method has been applied to the modified example PA.5. The circuit was tested on the part of all previously used values of the R_{SL}. The results were gathered in the Figure 158. Each graph contains all the Ohtomo curves and it is noticeable that only graph d) does not contain any curve that encircles the critical point (1,j0). Ergo, the circuit is stable for the R_{SL}=2kΩ and not stable for the R_{SL}=∞Ω, R_{SL}=5kΩ and R_{SL}=2.75kΩ - in an agreement with the generalized Freitag method results.

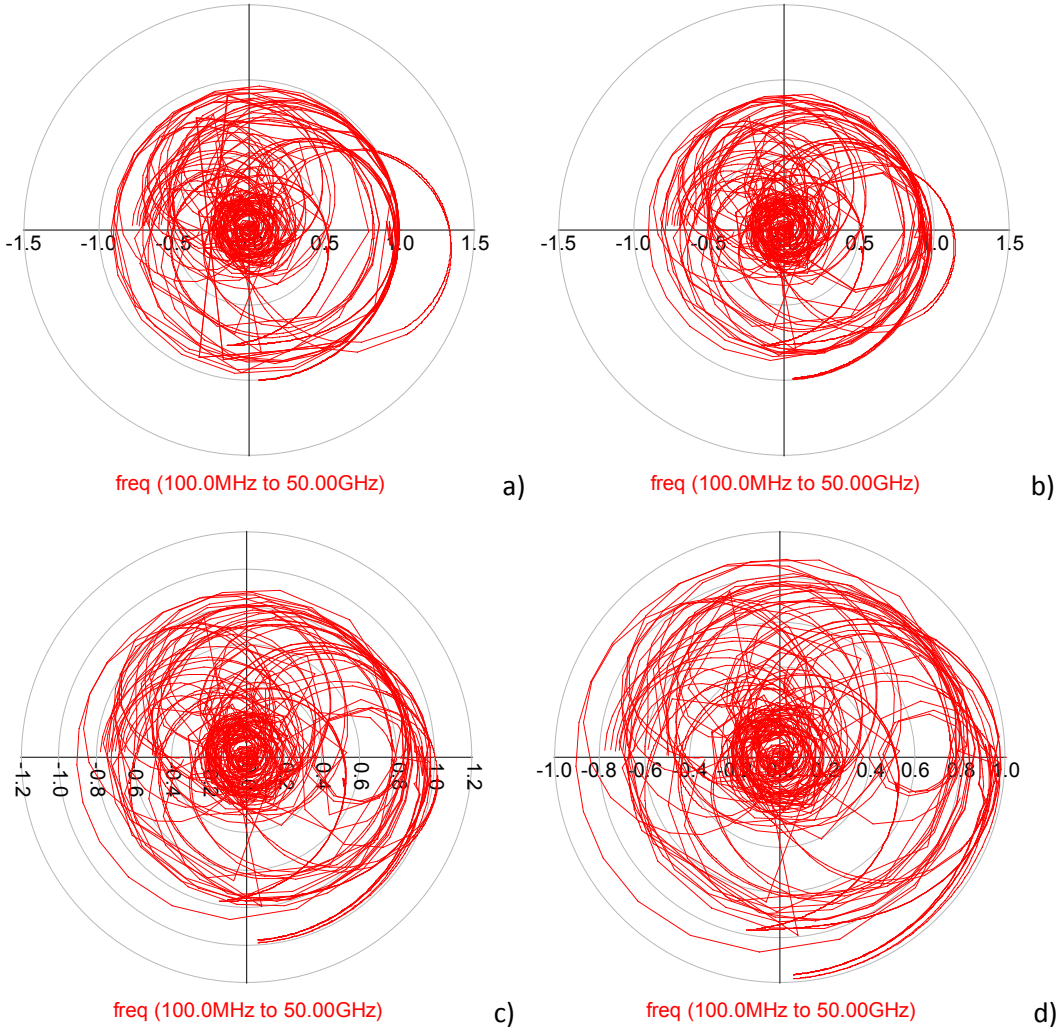

Figure 158 Ohtomo method results for the modified power amplifier example PA.5.
a) $R_{SL}=\infty\Omega$, b) $R_{SL}=5k\Omega$, c) $R_{SL}=2.75k\Omega$, d) $R_{SL}=2k\Omega$.

The presented modification of the original Freitag method extended its usefulness for the particular struggles originated in the design reality where the ideal symmetry and perfect isolation do not exist. The method in its generalized form allows to analyze the circuits which input and output parts are unintentionally or intentionally diverse concerning symmetry point of reference. Thus, nonidealities that result from the coupling, parasitic or are simply introduced due to the layout restrictions do not need to be neglected as this increases risk of the adopted designing approach. All in all, it is achievable to analyze the circuits by involving the input and output structures that possess different symmetry characters due to factors other than stability.

A good example of such a structure is displayed previously buss bar combiner which can now be simulated with the generalized Freitag method. In the end, the method is not restricted to the binary number of the active devices.

CONCLUSIONS

Freitag method contributes significantly in helping the designers to deal with the odd mode stability problems. Treating it as a stability test is an unjustified simplification. This is owing to the fact, that the method provides the designer with indispensable information about the circuit. This information leads to a better understanding of the circuit's behavior. Such knowledge allows to resolve the stability problems by eventual corrective action in a quick and efficient way. The originally presented method was not completed, thus its outcome may not necessarily lead to the stabilizing action or in extreme to not recognized instability. The applied improvement answered the issue and functionality of the improved method has been verified assuredly. To extend the usefulness of the Freitag test further, the simplified scheme addressing the ideal corporate amplifier structures was presented. The implementation of the method for the ideal corporate structure is effortless and efficient. Moreover, the same rule applies to the interpretation of the results. Regrettably, if given more demanding corrective action, there occur problems related to the synchronization of the multiple schematic files. This issue is not only correlated to the designers' comfort but it increases the risk of the random error due to not synchronized schematics. To overcome this shortcoming the automation of the Freitag method was developed, permitting the simultaneous two port simulation and stability test application, given the corporate amplifier circuits. Next, the automation of the method has been implemented in the Agilent ADS and positively confronted with the results of multi-schematic simulation results.

Due to the dissonance between the small signal based test and the power amplifier destiny to work in the large signal condition, an extension of the Freitag method has been proposed. The laid out large-signal/small-signal Freitag method detects the parametric stability problems associated with existence of the desired input signal in the power amplifier under test. Extension of the method has been implemented in the Agilent ADS and the AVR Microwave Office and positively verified by the Time Domain simulations.

To cancel the initial restrictions connected with the symmetry character of the tested circuit generalization of the method was proposed. Furthermore, the approach expands the method's utility for the circuits, for which the bisections possess different symmetry properties. That allows application of the test for the circuits without neglecting the effects of the non intentional symmetry perturbations from the ideal corporate amplifiers symmetry. Moreover, the circuit's bisections designed with the intentionally different symmetry characteristics are no longer excluded from the Freitag method. All in all, the generalized method was implemented in the Agilent ADS and positively confronted with the Ohtomo method.

In the research I tried to present the Freitag method not only as a simple test but as a tool that overcomes the stability problems in the parallel power amplifiers circuits. That is, according to its particular application, the method has evolved from its original form into: the simplified, fast testing tool in case of the ideal corporate structures; the complete, single schematic development tool in case of the automated approach ; the extension to the Large-signal/small-signal regime as to verify the correctness of the assumed at the small signal state stability margins. And finally: the generalized method that permits to verify the impact of non idealities and symmetry perturbations from the stability point of reference. Certainly, this is not yet the border line of the possible applications- just

the consistent interpretation of my researches; handling with different variations of the same tool as with a self-contained whole.

While the work presents various concepts, experiments and their positive results, the path to efficient implementation of the ideas is still open and relies on the will of the CAD producers. Its dependent on them as to provide the users with the math tools or already applied algorithms in order to efficiently compute eigenvalues and eigenvectors, matrix operations as well as the results sorting procedures. Without the above mentioned math tools only such a simplified Freitag approach can be convincing enough for the majority of the engineers to use it.

REFERENCES

[1] William L. Brogan, “Modern Control Theory”, Prentice Hall, 3 edition (October 11, 1990)

[2] Platzker and W. Struble, “Rigorous determination of the stability of linear N-node circuits from network determinants and the appropriate role of the stability factor K of their reduced two-ports,” in 3rd Int. Integr. Nonlinear Microw. Millimeterwave Circuits Workshop, Oct. 1994, pp. 93–107.

[3] J. M. Rollett, “Stability and power-gain invariants of linear twoports,” IRE Trans. Circuit Theory, vol. CT-9, pp. 29-32, Mar. 1962.

[4] M. L. Edwards and J. H. Sinsky, “A new criterion for linear 2-port stability using a single geometrically derived parameter,” IEEE Trans. Microwave Theory Tech., vol. 40, pp. 2303–2311, Dec. 1992.

[5] Robert W. Jackson, “Rollett Proviso In The Stability Of Linear Microwave Circuits—A Tutorial”, IEEE Trans. Microw. Theory Tech., vol. 54, no. 3, pp.993-1000, March 2006

[6] D. Woods, “Reappraisal of the unconditional stability criteria for active 2-port networks in terms of S-parameters,” IEEE Trans. Circuits Syst., vol. CAS-23, no. 2, pp. 73-81, Feb. 1976

[7] Steve C. Cripps, “RF Power Amplifiers for Wireless Communications”, Artech House (31 Mar 1999)

[8] K, J. Russell, “Microwave power combining techniques,” IEEE Trans. Microwave Theo~ Tech.. vol. MTT-27, pp. 472-478, May 1979.

[9] R. L. Ernst, R. L. Camisa, and A. Presser, “Graceful degradation properties of matched N-port power amplifier combiners,” in IEEE MTT-S Int. Microwave Symp. Dig., June 1977, pp. 174–177.

[10] H.-R. Ahn and I. Wolff, “Three-port 3-dB power divider terminated by arbitrary impedances,” in IEEE. MTT-S Symp. Dig., 1998, pp. 781–784.

[11] T. Hirota, A. Minakawa, and M. Muraguchi, “Reduced-Size Branch-Line and Rat-Race Hybrids for Uniplanar MMIC’s,” IEEE Trans. Microwave Theory Tech., vol. 38, pp. 270-275, Mar. 1990.

[12] S.P. Marsh, D.K.Y. Lau, R. Sloan, and L.E. Davis, Design and analysis of an X-band MMIC “bus-bar” power combiner, IEEE Symp High-Perf Electron Dev Microwave Optoelectron Applic, 1999, pp. 164–169.

[13] D. M. Pozar, Microwave Engineering, 2nd ed. New York:Wiley, 1998.

[14] R. G. Freitag, J. E. Degenford, D.C. Boire, M.C. Driver, R.A. Wickstrom, C.D. Chang, ‘‘Wideband 3W Amplifier Employing Cluster Matching,’’ Monolithic Circuit Symp. Dig., May 1983, pp. 62-66.

[15] J. Reed and G. J. Wheeler, “A method of analysis of symmetrical four port networks,” IRE Trans. Microw. Theory Tech., vol. MTT-4, pp. 245–252, Oct. 1956.

[16] R. G. Freitag, “A unified analysis of MMIC power amplifier stability,” in IEEE MTT-S Int. Microw. Symp. Dig., Jun. 1992, pp. 297–300.

[17] M. Ohtomo, ‘‘Stability Analysis and Numerical Simulation of Multidevices Amplifiers,’’ IEEE Trans. Microwa¨e Theory Tech., Vol. MTT-41, 1993, pp. 983]991.

[18] H. Nyquist, “Regeneration Theory”, Bell System Tech. Jouml, vol. 1 1, pp. 126- 147, January 1932

[19] S. Ramberger and T. Merkle, ”A symmetry device to speed up circuit simulation and stability tests”, 2002 IEEE MTT-S Int Microwave Symp Dig 2 (2002), 967–970.

[20] S. A. Maas Nonlinear Microwave and RF Circuits, 2nd ed. Norwood, MA: Artech House, 2003

[21] K. Kurokawa, ‘Some basic characteristics of broadband negative resistance oscillator circuits’, Bell Syst. Tech. J., 48, 1937–1955, 1969.

Appendix 1 POWER COMBINERS

In order to give a deeper look at the power combining subject a previously drafted division of the combining structures was adopted as a base for a more detailed review. As previously, special attention was given to the planar structures and the possibility of planarization in case of the non planar structures. A review is organized into the main two parts. The first has a form of the table containing gathered examples of the combining structures. The order introduced into the table of the gathered examples is a product of previously presented division of the combining structures idea (paragraph 2.2 - Figure 23) and a huge disproportion of the interest in different combiners. The second part contains comments to the most important combiners and techniques developed to extend the original ideas. The comments follow the order introduced in the table.
While the name combiner and the splitter define the mode of use of the power combiner/splitter circuit and could be used interchangeably for clarity of the report, hence all described structures will be named as the combiners.

A1.1 Tabular review of the power combining structures

A1.1.1 Organization of the table

Due to a big difference in quantity of the articles found for each device or approach table will be organized with the use of the following groups:

▪ Junctions	Basics element that is used in almost every following structure but it is able to be a stand-alone power combiner circuit
▪ Wilkinson combiner ▪ Branch-line Coupler ▪ Hybrid Ring ▪ Transmission Line Couplers	The most important approaches extensively examined and studied till nowadays
▪ Lange Coupler	
▪ Tapered line	Using tapered lines of different profiles
▪ Resonant structures	Using resonant techniques
▪ Traveling Wave Combiner	Traveling Wave technique
▪ SIW	Substrate Integrated Waveguide power combiners examples
▪ Others	Other circuits with less amount of examples in the literature

In the following table, the columns gathered the following information:

▪ Type	type or the description of the structure
▪ Bandwidth match/iso.	fractional bandwidth for a defined value of the isolation and reflection coefficient [$(f_{max} - f_{min}) / f_0 * 100\%$]
▪ Bandwidth cup. dff/loss	fractional bandwidth for defined difference or loss in division signals [$(f_{max} - f_{min})/f_0 * 100\%$]
▪ f_0 [GHz]	center frequency [$(f_{max} - f_{min})/2 + f_{min}$]

- Inputs — numbers of inputs – circuit used as combiner
- Planar — field regarding possibility of planar application
- Isolation — value of Isolation in previously given bandwidth
- Size — approximately the size of the structure or impression (explanation bellow)
- RL — Return Losses [RL=-20*$\log_{10}$(Γ) dB]
- Unequal div. — field regarding possibility of an unequal power division
- Phase dif. — phase difference between the outputs (divider point of view)
- Losses — value or impression of the circuit losses
- Reference — reference number regarding structure

It needs to be underlined that the list of the approaches and examples cannot be treated as a completed one, even till the date of the creation of the document. A subject of the power combining is so wide and deeply studied that it is impossible to gather all the results of research in that field. An idea to focus on the planar applicable structures could be also the reason for missing some of the interesting researches results.

A further issue are the missing parameters in the table listed below. It is quite complex to obtain all the parameters that are of interest only from the gathered papers. Some workings were purely theoretical and devoid of the experimental realization. Many authors did not list them in their researches or simply neglected them. If possible they were only determined with errors in the included graphs. The approximate results were than marked with "~". Most authors did not respond to the question of an unequal division possibility in the circuit since the main application of the combiners/dividers is equally split work. So, the following notation for the column responding to this question was used:

- Yes - Authors found possibility of unequal split
- No - Authors found impossibility of unequal split
- No/… - Authors did not respond the question of possibility
- No/Yes - Authors did not respond the question of possibility but it may be assumed that it is possible.

Notation "x/y" in a frequency field regarding multi-frequency operation and meaning that f_1=x GHz and f_2=y GHz. This notation then could be used in the bandwidth field through an analogous way representing B_1=x GHz and B_2=y GHz accordingly.

A1.1.2 Abbreviations

- N.Eq. - not equal
- @fo - at frequency f_0
- Isol. - isolation
- Γ - reflection coefficient
- ±0,2dB - amplitude balance ±0,2 dB
- Δ0,2dB - amplitude balance Δ0,2dB
- Tr. - trade
- n - number of stages in multistage structure
- k - power division ratio
- k dep. - dependent on k value
- TL - transmission line
- Δl - the length difference
- Yes - ! 2L - planar but requests two side processing while the 2nd layer is not for ground plane
- Yes – AB - air bridge needed additionally
- Com. Ord - in comparison to ordinary

- [THEORY] - purely theoretical work
- Des. Dep. - design dependent – in the sense of the trade between other parameters

A1.1.3 The table of gathered examples.

Type	Bandwidth match/iso.	Bandwidth cup. dff/loss	f_0 [GHz]	Inputs	Planar	Isolation	Size	RL	Unequal div.	Phase dif.	Loses	Reference
Junctions												
T,Y junction and multiline conn.	Wide TL-P			2 N	Yes	No	Very Small	1 port.	Yes	Eq. 0^O N=2 Poss. 180^O	Low	[13], [23]
Resistive	Wide TL-P			N	Yes	No	Very Small	Yes	Yes	Eq. 0^O	Large	[12]
Multi-Way Microstrip Power Divider	~90% ~101% ~85%	Δ0.1 dB Δ0.2 dB Δ0.2 dB	4	3 4 9 –Corp	Yes	No	Medium	1 port. ~20 dB	No/Yes	Eq. 0^O	~Low	[24]
Wilkinson combiner												
Wilkinson divider -planar restriction -experiment	 ~20%		 0,5	N 2 8	N<3 Yes Yes No	 ~25dB	~λ/4	 11 dB	No/Yes	Eq. 0^O	Low Negligible	[25]
Wilkinson unequal divider -planar restriction -experiment	~20% ~50%		 3	N 2 2	N<3 Yes Yes Yes	 ~20dB	~2*λ/4	 15 dB	Yes	Eq. 0^O	Low	[26] [10]
Planar N-way	~>30%			N 3	Yes	~20dB	~n*λ/4	~ 20 dB	No/…	Eq. 0^O	n dep.	[27]
Recombinant divider	66%		10	3	Yes	N.Eq. >20dB	~3λ/4	12 dB	Yes	Eq. 0^O	Large	[28]
Radial evolution of Wilkinson -1 stage -2 stages				N	N<3 Yes	N↑ Isol. ↓ N<4 ∞ @f_o N<6 ∞ @f_o	~λ/4 ~2 λ/4	N↑ Γ ↑ N<4 ∞ @f_o N<6 ∞ @f_o	No/	Eq. 0^O		[29]
Fork evolution of Wilkinson -1 stage -2 stages				N	Yes	N↑ Isol. ↓ N<3 ∞ @f_o N<4 ∞ @f_o	~λ/4 ~2 λ/4	N↑ Γ ↑ N<3 ∞ @f_o N<4 ∞ @f_o	No/	Eq. 0^O		[29], [27]
Mod. Luzzato	Trade.	Trade.		3	No	Trade. Match&Loss	π(λ/4)^2	Trade. Isol.&Loss	…	Eq. 0^O	Tr. Low	[30]
Multistage Wilkinson	>=100%			N	N<3 Yes	>19dB and n↑ Isol. ↓	~n*λ/4	> 20 dB	No/Yes	Eq. 0^O	n dep.	[31]
Gysel	~20% for Isol.		1,15	N 2	No Yes	-30dB	Large	~ 20 dB	No/…	Eq. 0^O	Low ~0,3 dB	[32]
Broadband Gysel with 15dB math	44,3%		4	2	Yes	~12 dB	Large	15 dB	No/…	Eq. 0^O	Large	[33]
H.K.Wen (Unequal Gysel)	~35%	~35% Δ0.5 dB	0,85	N 3	2 layers	>~20 dB k dep.	Large	~ 11 dB	Yes	Eq. 0^O	~0,2 +0,5 dB max	[34]
Capacitive Loading miniaturized Wilkinson [λ/5 - λ/12]	TL Δl dep. 40-65%		10	N 2	N<3 Yes	~15 dB	Small -74%	>15 dB	No/Yes	Eq. 0^O	0,55 dB	[35]
Lumped element Wilkinson divider	33%		3,6	2	Yes	~17,5 dB	Small ~ -80%	~17,5 dB	No/Yes	Eq. 0^O	0,3 dB	[40]

Type	Bandwidth match/iso.	Bandwidth cup. dff/loss	f_0 [GHz]	Inputs	Planar	Isolation	Size	RL	Unequal div.	Phase dif.	Loses	Reference
Lumped Wilkinson Power Dividers With Micromachined Technology	25%		8.5 20	2	Yes	14 dB @f_o 9.6 dB @f_o	Small	>15 dB	No/Yes	Eq. 0^O	0.6 dB	[36]
ACPS 180^O Wilkinson	~13%		3	2	Yes Uni	~20 dB	~λ/4	~ 20 dB	No/Yes	Dif. 180^O	0,8 dB	[37]
ACPS 0^O Wilkinson	~30%		3	2	Yes Uni	~20 dB	~λ/4	~ 20 dB	No/Yes	Eq. 0^O	0,4 dB	[37]
Wilkinson above 100GHz	13%	13% ±0,4dB	150	2	Yes	12 dB	0,5x0,5 mm	12 dB	No/Yes	Eq. 0^O	1±0,4dB	[38]
Power Divider Using Parasitic Element	24,4% 15,4%		6	2 3	Yes	12,4 dB 17,1 dB	Large	10 dB	Yes		1.8-2.1 dB ~0-2 dB	[39]
Branch-line Coupler												
Lumped element branch line coupler.	~35		4,25	Corp.	Yes	15 dB	Smal 2x2 mm	10 dB	Yes	90^O	0.4-0.6 dB	[40]
Reduced-Size Branch-Line for Uniplanar MMIC's	~20% ~14%	~20% ±0,5dB	11 25	Corp.	Yes	~10 dB ~15 dB	Small -80%	~10 dB 15 dB	No/Yes	90^O	1,5±0,5dB 2±0,5dB	[11]
Meander multilayer MMIC Quadrature Hybrid (BL)	~15%	~15% ±0,5dB	20	Corp.	MLMMIC	~15 dB	Very Small 0,95x0,91mm	~15 dB	No/Yes	90^O	2,5 dB	[41]
Branchline Coupler using Coupled Rectangular Slotline Ring	~40%	40% Δ1dB	3	Corp.	Yes	~20 dB	~λ/4 x ~λ/4	~20 dB	No/Yes	90^O	0,66 dB@f_o	[42]
Compact Wide-Band Branch-Line Hybrids	~56%		2	Corp.	Yes	~20 dB	~3*λ/4x ~λ/4 -55%	~20 dB	No/…	90^O	0,5 dB	[43]
Double-Sided Branch-Line Coupler	~12- 20%	15-20% Δ1dB	6	Corp.	MLMMIC	~15dB	~λ/4 x ~λ/4	~15 dB	No/Yes	~90^O	1-1,3 dB	[44]
Broadband Impedance Transforming (2-sect)	~30%	~30% Δ0,5 dB	2	Corp.	Yes	~20 dB	~2*λ/4 x ~λ/4	~20 dB	Yes	90^O		[45]
A Reduced Branch-Line Coupler With Eight Stubs	~10%		0,5 1	Corp.	Yes	~20 dB	Small -75%	~20 dB	No/…	90^O	Small	[46]
Folded-Line Branch line Coupler	~10%	~16% Δ0,5 dB	1,5	Corp.	Yes	~20 dB	Small	~20 dB	No/Yes	90^O	Small	[47]
Branch-Line Coupler Using CPW To-Microstrip Transitions	~24%	~24% ±0,5dB	2	Corp.	MLMMIC	~15 dB	~λ/4 x ~λ/4	~15 dB	No/Yes	90^O	0,2±0,5dB	[48]
Multilayer Polyimide Technology	~33% ~28,4%	10,6% 28,4% 0,2dB-AB	30 37	Corp.	MLMMIC		~λ/4 x ~λ/4	~12 dB	No/Yes	90^O	Medium	[49]
Finite-Ground Coplanar-waveguide Branch-Line Coupler	22%	24,8% ±1dB	2	Corp.	Yes Uni	~15 dB	Medium -75%	~15 dB	No/Yes	90^O	~1Δ1dB	[50]
Double band Branch-line coupler using CLR TL	19/16% 27/17%	±0,24/±0,52 ±0,37/±0,46	1/2 1/2.5	Corp.	Yes	~14 dB ~16 dB	Bigger than standard	~13 dB ~14 dB	No/Yes	90^O	Small	[51]
MEMS Branch line coupler using coaxial line with square conductor	20% 10%	20% IL 1,25dB	60	Corp.	MEMS	~14 dB ~18 dB	~λ/4 x ~λ/4	~14 dB ~18 dB	No/Yes	90^O	1,25 dB	[52]
Compact LTCC Branch-Line Coupler	~14%	Δ2,5 dB	2,3	Corp.	LTCC MLMMIC	~15 dB	0.079λ x0.0717λ	~15 dB	No/Yes	90^O	Max 2,1dB Unequal	[53]

Type	Bandwidth match/iso.	Bandwidth cup. dff/loss	f_0 [GHz]	Inputs	Planar	Isolation	Size	RL	Unequal div.	Phase dif.	Loses	Reference
ACPS 90° Branch-line Coupler	10%	10% Δ0,375dB	3	Corp.	Yes Uni	15,3 dB	~3 λ/4 x ~λ/4	17,1	No/Yes	90 ^{O}	0,5dB@f_o	[54]
N-Way Branch Line Directional Coupler (two poss. structures)	~5% -		2,4 -	N=3 / 4 N / 2(N-1)	Yes N<4 / 5 Yes	~12 dB -	2~λ/4 x ~λ/4 3D	~19 dB	Yes	Not equal. 90 ^{O}, 0 ^{O}		[55]
Planar, Multiport, Quadrature-Like Power Dividers/Combiners	5~10%		2,9 -	N=4 N	Yes	~14 dB Des. Dep.	3~λ/4 x ~λ/4 (N-1)λ/4x ~λ/4	~17 dB Des. Dep.	No	n90 ^{O} nπ/N		[56]
Branch-Line Hybrid with Coupled Lines	~12%	~28% Δ0.5 dB	3	Corp.	Yes	~20 dB	Medium	~20 dB	No/…	~90 ^{O}	Large (from neq.)	[57]
Compact-Size Branch-Line Coupler (-55%)	8% 20%	~15% Δ1 dB	2,4	Corp.	Yes	~20 dB	-55%	~20 dB	No/…	90 ^{O}	~Medium ~0,5@f_o	[58], [59]
Hybrid ring and Magic-T												
The hybrid Ring with the coupled Lines	~28%	~28% Δ0.5 dB	3	Corp	Yes	~20 dB	Medium	~20 dB	No/…	180 ^{O}/0 ^{O}	Medium	[57]
A Broad-Band Printed Circuit Hybrid Ring Power Divider	~45%		18	Corp.	Yes	~10 dB	Large	~10 dB	Yes	0 ^{O}	Low	[60]
Broad-Band Design of Improved Hybrid-Ring	45,3%	45,3% Δ1 dB	6	Corp.	Yes	~20 dB	Large	~20 dB	Yes	180 ^{O}/0 ^{O}	Medium 0.5±0.5dB	[61]
Lumped element miniaturized Hybrid Ring	~14%	14% Δ0,75dB	25	Corp.	Yes Uni	~20 dB	Small ~ -80%	~15 dB	No/Yes	180 ^{O}/0 ^{O}	3,75±0,75 dB	[11]
ACPS 180^{O} Hybrid Ring	~25%	~25 ±0,4dB	3	Corp.	Yes Uni	21 dB	Large	23 dB	No/Yes	180 ^{O}/0 ^{O}	3,5±0,4dB	[54]
180 Reverse-Phase Hybrid-Ring Coupler (Magic-T)	~60%	66.6% ±0.4 dB	3	Corp.	Yes Uni	23 dB	Large	15 dB	No/…	180 ^{O}/0 ^{O}	3,95±0,45 dB	[54]
0.8 λ - 180 Reverse-Phase Hybrid-Ring Coupler (Magic-T)	~60%	66.6% ±0.3 dB	3	Corp.	Yes Uni	29,8 dB	Medium	15 dB	No/…	180 ^{O}/0 ^{O}	3,5±0,4dB	[54]
Hybrid-Ring Directional Coupler Using λ/8 or λ/6 Sections	~15%	~>10% Δ1 dB	9,4	Corp.	Yes	~15 dB	Medium	~ 15 dB	No/…	180 ^{O}/0 ^{O}	Low / Medium	[62]
Slotline hybrid ring coupler.	~26%	26% ±0.3 dB	3	Corp.	Yes - ! 2L	20 dB	Large	…	No/…	180 ^{O}/0 ^{O}	Medium	[63]
Slotline crossover hybrid ring coupler	~80%	80% ±0.2 dB	3	Corp.	Yes - ! 2L	35 dB	Large	…	No/…	180 ^{O}/0 ^{O}	Medium	[63]
CPW-slotline hybrid ring coupler	~30%	18.6% ±0.3 dB	3	Corp.	Yes Uni	20 dB	Large		No/…	180 ^{O}/0 ^{O}		[64]
CPW-slotline reverse-phase hybrid-ring coupler			3	Corp.	Yes Uni		Medium		No/…	180 ^{O}/0 ^{O}		[64]
Crossover hybrid-ring coupler (Magic-T)	~30%	66.6% ±0.3 dB	3	Corp.	Yes Uni	20 dB	Medium			180 ^{O}/0 ^{O}		[64]
Crossover λ/6 hybrid-ring coupler (Magic-T)	~68%	68% ±0.4 dB	6,85	Corp.	Yes Uni	23 dB	Medium	10 dB	No/…	180 ^{O}/0 ^{O}	3,5-4 dB	[65]

Type	Bandwidth match/iso.	Bandwidth cup. dff/loss	f_0 [GHz]	Inputs	Planar	Isolation	Size	RL	Unequal div.	Phase dif.	Loses	Reference
Rat Race Coupler With High Isolation [THEORY]	~65%	~70% ±0.3 dB	10	Corp.	Yes	25 dB	Medium	20 dB	No/…	180 ^{O}/0 ^{O}	Low [THEORY]	[66]
Broadband Uni-planar MMIC Ring Coupler	~28,5%	~28,5% ±0.3 dB	35	Corp.	Yes Uni	16 dB	Medium	13 dB	No/Yes	180 ^{O}/0 ^{O}	Large ~1,3 dB	[67]
Cascadable Hybrid-Ring Couplers	1sect 2 sect	~25% ~54%	2	Corp.	Yes AB	~15 dB	Medium	~15 dB	Yes	180 ^{O}/0 ^{O}	0,4 dB (?) 0,8 dB (?)	[68]
Enhanced-Bandwidth Hybrid Ring using a Left-Handed TL Section	>78%	~45,5% ±0.25dB	2	Corp.	Yes	20 dB	Medium -67%	15 dB	No/Yes	180 ^{O}/0 ^{O}	Medium 0,53dB	[69]
Coupled-line 180 hybrid rings with frequency independent characteristics	25 %	~30% IL<1 dB	1	Corp.	Yes	30 dB	Medium	~12 dB	No/…	180 ^{O}/0 ^{O}	Medium <1 dB	[70]
180 hybrid ring using dielectric-supported air-gapped microstriplines	~30% ~21%	~21%IL	60 95	Corp.	MEMS	20 dB ~13 dB	Large	~12 dB ~17 dB	No/…	180 ^{O}/0 ^{O}	0,31/0,580 ~0.9 @ f_0	[71]
Slow-wave EBG microstrip rat-race hybrid ring	~24%	~18 IL<1 dB	1,65	Corp.	Yes	~15 dB	Small 11%	~17 dB	No/…	180 ^{O}/0 ^{O}	~3,75±0.75 dB	[72]
Double Frequency 180° Lumped-Element Hybrid	~>10%		2/5	Corp.	Yes	~25 dB	Small 2.9x1.9mm	~15 dB	No/…	180 ^{O}/0 ^{O}	Large	[73]
A Size-Reduced CPW MMIC Rat Race Coupler	90%		5,5	Corp.	Yes	20 dB	Smal 1x0.8mm	~16 dB	No/…	180 ^{O}/0 ^{O}	Large 2 dB	[74]
Coupled line coupler												
MMIC Quadrature coupler using a braided microstrip structure	~100%		6	Corp.	Yes AB	~11 dB	~λ/4	~17 dB	No/…	90 ^{O}	Large	[75]
Ultra-Wide-Band Nonuniform Quadrature Directional Coupler	Meas. range	158% ±1,75dB	9,5	2	Yes AB	~15 dB	Large	16 dB	Yes	90 ^{O}		[76], [77]
Multiway uniform combline directional couplers	Meas. range	66,6% ±1,75dB	2,4	2-9 Meas. 5	Yes	> 24 dB	Large (L=163.2mm)	>~18 dB	Yes	n90 ^{O}		[78]
MMIC Compatible Coupled Line Structure		123% ±1,5dB	13	Corp.	Yes	10 dB	~λ/4	15 dB	Yes	90 ^{O}	Large	[79]
Broadside-Offset-Coupled Coplanar-Microstrip	100%		30	Corp.	MLMMIC		~λ/4		Yes 3 - 30 dB	90 ^{O}		[80]
Floating conductor coupler	0-30 GHz	20% ±0,2dB	20	Corp.	MLMMIC	26 dB	~λ/4	22 dB	Yes	90 ^{O}	Medium 0,7±0,2dB	[81]
Structure of Tightly Coupled Lines	~64%	~64% 4±1dB	~13	Corp.	Yes AB	~14 dB	~λ/4 0.45x1.9mm	~11 dB	No/…	90 ^{O}	~Large	[82]
Air-Gap Stacked Microstrip Coupled Lines	~76%	66%	33	Corp.	Yes AB	10 dB	~λ/4	15 dB	No/…	90 ^{O}	0.33±0.46dB 0.73±0.43dB	[83]
Wide-Band Lumped-Element Quadrature 3-dB Couplers in Microstrip		100% Δ1,7dB	2	Corp.	2 Layer	25 dB	>~λ/4	21,5 dB	No/...	90 ^{O}	0,4Δ1,7 dB	[84]

Type	Bandwidth match/iso.	Bandwidth cup. dff/loss	f_0 [GHz]	Inputs	Planar	Isolation	Size	RL	Unequal div.	Phase dif.	Loses	Reference
Broadband Left-Handed (LH) Coupled-Line Backward Coupler	37%	37% ±0,4dB	3,8	Corp.	Yes	20 dB	Large ~0,4λ	18 dB	Yes	90 ^{O}	0,3±0,4dB	[85]
High Directivity CPW Directional Coupler Using DGS	Meas range.	50%	2	Corp.	2 Layer	~30 dB 47 dB @ f_0	~λ/4	20 dB	No/Yes	90 ^{O}	0,21 dB	[86]
Coupler Based on the Coupled Artificial Transmission Lines	8%	8% ±0,5dB	0,57	Corp.	Yes	23 dB	14% of ~λ/4	23 dB	No/...	90 ^{O}		[87]
Lange												
The original Lange coupler	58%	60% ±0,25dB	3	Corp.	Yes AB	~30 dB	~λ/4	25 dB	No/Yes	90 ^{O}	0.13 dB	[88]
High-Performance Lange Coupler	120%	120% ±0,6dB	5	Corp.	MLMMIC	20 dB	~λ/4	20 dB	No/Yes	90 ^{O}	Medium 0.6±0.6 dB	[89]
Lange Unfolded Lange	73 68	±0,5dB	6,5	Corp	Yes AB	18 dB 17,5 dB	~λ/4	17 dB 18,5 dB	No/Yes	90 ^{O}	0.43 0.3	[90]
Tapered line												
Tapered line planar combiners	~20%		60 44	3 5 N	Yes	>16 dB (dif.) >15 dB (dif.) N↑ Isol. ↓	~2λ	10 dB 15 dB	No/…	Eq. 0^{O}	0,6 dB	[91]
Integrated Planar Spatial Power Combiner [Theory]	14,8%	14,8% ~Δ2dB	27	4 N	Yes		Medium	16 dB	No/… ~Equal	~Eq. 0^{O}	0,4-0,8 dB	[93]
Broadband Tapered-Line Power Divider with Several Strip Resistors	116%		1,2	2 3	Yes	22 dB	Large	19 dB 20 dB	Yes No/…	Eq. 0^{O}		[94], [95]
N-Way Broadband Planar Power Combiner	113%	113% ±0.5 dB	11,5	5 N	Yes	15 dB	Large	16,5 dB	No/…	Eq. 0^{O}	0,2 dB	[96]
Resonant structures												
Planar Disk Quadrature Hybrid	~3T ~6,8E		6-8	Corp.	Yes	~14 dB	Large	Yes ~20 dB	No/…	90 ^{O}	Large	[97]
Improved Circular Disc 3 dB Coupler	~20%		1,5 3	Corp.	Yes	~16 dB	Large	Yes ~20 dB	No/…	90 ^{O}	Low	[98]
Rectangular disk Quadrature Hybrid	~25%		3 8 12	Corp.	Yes	~20 dB	Large	Yes ~20 dB	No/…	90 ^{O}	~Low	[99]
A Quadrature-Hybrid Design Using a Four-Port Elliptic Patch	~25%		3,5 14,4	Corp.	Yes	~20 dB	Large	Yes ~20 dB	No/…	90 ^{O}	~Low	[100]
Broad-Band Symmetrical Five-Port Circuit based on ring	57%	57% ~Δ3dB	7,4	4	Yes	no	Large	~17 dB	No	Δ120 ^{O}	Large – from uneq.	[101]
Microstrip disc circuits	41% 44%		9,5 12	3 4	Yes		Large	~14 dB	-3,-6,-6 dB ~Equal	No. eq.		[102]

Type	Bandwidth match/iso.	Bandwidth cup. dff/loss	f_0 [GHz]	Inputs	Planar	Isolation	Size	RL	Unequal div.	Phase dif.	Loses	Reference
Microstrip Sector components	~22%	~22% ±0.6 dB 1st band	9/17	4 5	Yes	5 - 25 dB Dep. Port. location	Large	12 dB	Yes		0,7 dB	[103]
Microstrip Sector components For an unequal power split	~>40%		~7,5	4	Yes		Large	14 dB	Yes			[104]
Sinusoidally Taped Power Combiner Including Compensation Hole	5%		14,5	3 N	Yes			15 dB	No/…	Eq. 0^O	Large 1,6 dB	[92]
Multiple-Port Power Combiner Circuits Using Circular Microstrip Disk Configurations	28,5%		17,5	3 … 10	No Coax. Output	9 dB	Large	12,6 dB	Yes		0,23 dB 1 dB	[105]
Three-Port Rectangular Microstrip Unequal Power Combiner	k dep.	k dep.	1,5	2	Yes	no	Small	1 port.	Yes			[106]
Travelling Wave												
Travelling Wave Power Combiner	70%	82% ±0,5dB	8,5	4 N	Yes	14 dB	Large (N-1) Uneq. Wilkinson	14 dB	No/Yes	Const. dif. nΦ	0,25±0,5 dB	[107]
Travelling Wave Power Combiner for High-Density Packages	~60%	60% IL<1,1dB	11,5	4 N	Yes		Large (N-1) Uneq. Wilkinson	12 dB	No/Yes	Const. dif. nΦ	1,1 dB max	[108]
Travelling Wave Power Combiner 6-Way		28% IL<1dB	35	6 N	Yes		Large (N-1) Uneq. Wilkinson		No/Yes	Const. dif. nΦ	1,1 dB max	[109]
Lumped Elements Traveling Wave Power Combiner			0,437	4 N	Yes				No/Yes	Const. dif. nΦ		[110]
Substrate Integrated Waveguide												
Quadrature Directional couplers	16%		25	Corp.	Yes	15 dB		12 dB	Yes	90^O	0,9-1,2 dB	[111]
180^O Narrowwall Directional Coupler	5,4%	5,4% ±0.3dB	11	Corp.	Yes	20 dB		12 dB	No/…	180^O	~1,5 dB max	[112]
H-plane T-junction H-plane Y-junction	10,2% 25,2%		29,5 29,75	2	Yes	no	Small	19 dB 18,5 dB	No/Yes	Eq. 0^O	0,3-1 dB 0,3-2 dB	[113]
Others												
3-Way Power Divider with Various Output Power Ratios				2 3	Yes		~λ/2 * ~λ/2		Yes			[114]
Extended resonance Broadband Extended resonance	~5-12% ~85%		0,9-33 7	N	Yes	No	Small ~NxL	1 port.	…	Const. dif. nΦ	Small	[115] [116]
Bus bar			10-17	2,4,8 $N=2^n$	Yes	No	Small	1 port.	No	Eq. 0^O	Small	[12]

Type	Bandwidth match/iso.	Bandwidth cup. dff/loss	f_0 [GHz]	Inputs	Planar	Isolation	Size	RL	Unequal div.	Phase dif.	Loses	Reference
Broadband Series Power Divider Using 0° Phase-Shifting Lines	36%	Not equal -3dB 16-71%	1,92	4	Yes	No	Smal Com. Ord.	1 port. 10 dB	No/Yes	Eq. 0^O	Not Equal ~0,6-2,1dB	[117]
Uniplanar Wheatstone bridge	~8%		4	Corp.	Yes Uni	~19 dB	~λ/4	Yes ~13 dB	No/…	90^O	Large	[118]
Bailey divider	k dep.	k dep.	1,413	2	Yes	>6 dB [Theory]	Large	In. Yes Out k dep	Yes	Eq. 0^O		[119]
MEMS switched evolution of Bailey concept divider [theory]			11,75	2	MEMS	20 dB	Large	25 dB	Yes	Eq. 0^O		[120]
Extend Bailey divider (Page)			2	2	Yes		Large	In. Yes Out - No	Yes	Arbitrary		[121]
Composite Coupler		~30% k±0,1dB	0,5	2	Yes		Large 3xUneq. Wilkinson		Yes	Eq. 0^O		[122]
Miniaturization of 3- and 5- way Bagley Polygon power dividers				3 5 N=(2n-1)	Yes	N↑ Isol. ↑	Large	1 port.	No/…	Not Equal		[123]

Table 1 Reviev of the most important power combining structures examples.

A1.2 Commentary to the table's examples.

A1.2.1 Junctions

Junctions are extremely important building blocks used as stand-alone power combiners or as parts of the bigger combining structures. If lack of isolation or matching at the output/input ports can be accepted, they may offer a wide bandwidth, the benefit of the simple and small size.

A1.2.1.1 T, Y, multi-line connection

T and Y junction are the simplest elements to be used as power combiners. They consist of the parallel or a serial connection of the transmission lines. A basic form of T junction resembles the letter T, with two arms as an inputs and one as the output, when treated as the power combiner. If T junction contains no anisotropic material it is a passive, reciprocal component. As a three -port device in basic form it cannot be simultaneously lossless and matched at all the ports. T junction can be implemented in every kind of transmission line technology. Depending on a connected transmission lines, parallel or series type connection could be obtained.

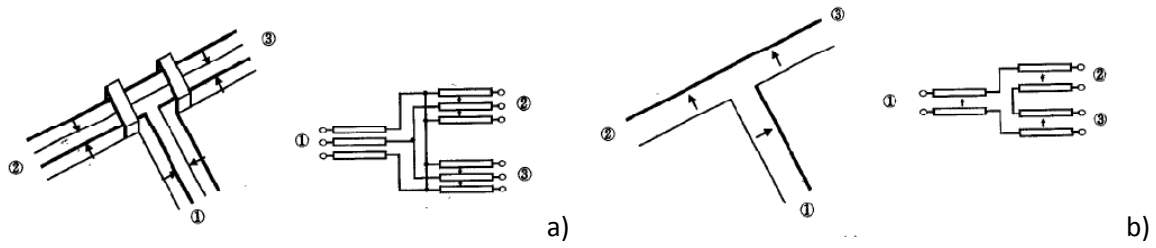

Figure 159 Parallel and serial connection

While coplanar waveguide central connector forms the T junction (like in the Figure 159 a), in result the transmission lines form the parallel connection. While the slot lines are arranged into T structure like in the Figure 159 b), series connection of the transmission lines is obtained. Basically, T junction treated as a power combiner splits the signal with ratio equal to the impedance or admittance ratio of the output ports, depending on the type of connection. For appropriately chosen output impedance values it is possible to obtain simultaneous input match and assumed power split ratio. Unfortunately, the output ports will be mismatched. Also, the lossless T junction did not provide isolation between the output ports. Three port T junction idea could be easily extended for a multi-line junction. To overcome a lack of simultaneous match at all ports, the losses have to be introduced to the combiner.

A1.2.1.2 Resistive divider

By means of the resistive divider the preferred power splits between the output ports and a simultaneous match at each port is possible. Obviously, such network is reciprocal and lossy, which severely restricts its usefulness.

A1.2.1.3 Combination of parallel and serial connection.

An interesting approach, taking advantage of the complementarities of the serial and parallel T junction is presented in [124] by Nakatsugawa and Nishikawa. The authors present how to build the corporate structure without the matching sections - Figure 160. Combiner of this type can be used to combine $N=4^n$ sources and in case of the presented example requests two layers to be built.

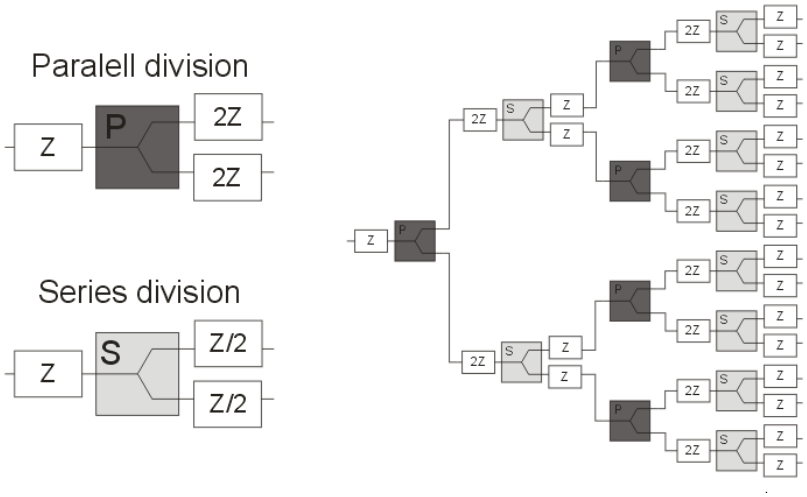

Figure 160 Combination of the parallel and serial connection.

A1.2.2 Wilkinson combiner

Combiner introduced by E. J. Wilkinson in [25] is one of the most important passive component in the microwave engineering. Originally presented as "A N-way power divider" it is the most useful for planar implementation when N=2. For more than two inputs structure it is three dimensional and its planar implementation is impossible without modifications.

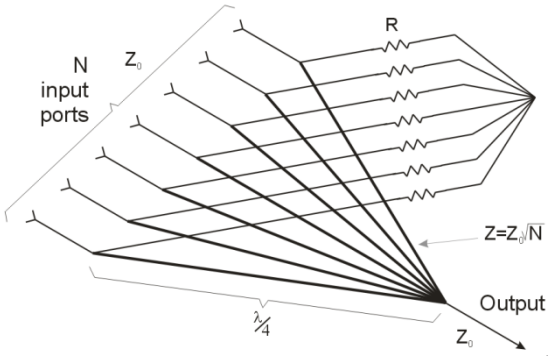

Figure 161 Wilkinson combiner.

The basic concept of the combiner is shown in the Figure 161. It incorporates N input ports for the characteristic impedance Z_0 connected with the utilizing the quarterwave transformers of the characteristic impedance $Z=Z_0*\sqrt{N}$. This transformation assures equal division and matches with the common output port of the impedance Z_0. Each of N input is connected with a floating node by the means of resistor $R=Z_0$ which provides isolation between the inputs. Originally Wilkinson analyzes the circuit containing N inputs with the ordinary circuit equations, an assumption of the equal power split and same characteristic impedance of the inputs and output. The author provides an analytic equation for the value of quarterwave transformer impedance and a resistance of the isolating resistors.

When N=2 is assumed, planar and symmetrical circuit is obtained, moreover even and odd excitation method [15] could be used to analyze it [12]. The analysis is based on finding scattering matrixes values for two bisection circuits which are obtained by application of the electric or magnetic wall in axis of circuit symmetry. Procedure of the Wilkinson combiner division into bisections is shown in the

Figure 162. The equations expressing relations between the scattering matrix of the divider and scattering parameters of the bisections circuits are also summarized there.

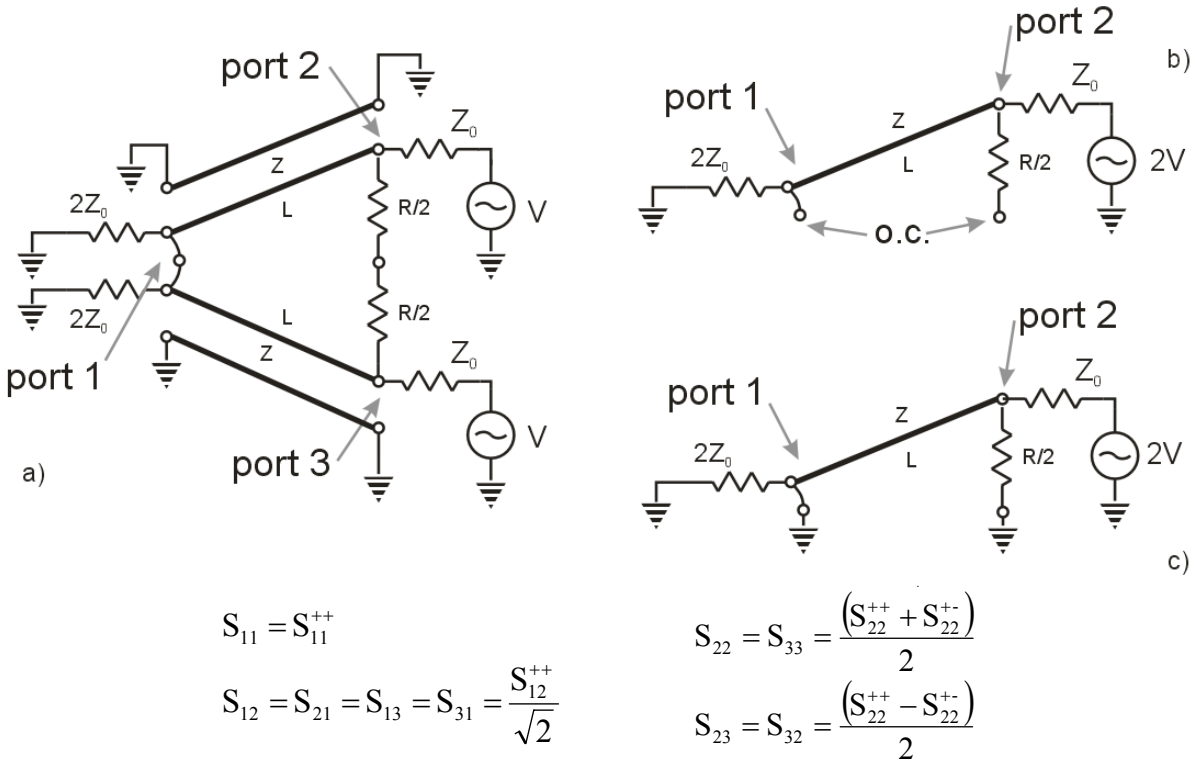

$$S_{11} = S_{11}^{++}$$

$$S_{12} = S_{21} = S_{13} = S_{31} = \frac{S_{12}^{++}}{\sqrt{2}}$$

$$S_{22} = S_{33} = \frac{\left(S_{22}^{++} + S_{22}^{+-}\right)}{2}$$

$$S_{23} = S_{32} = \frac{\left(S_{22}^{++} - S_{22}^{+-}\right)}{2}$$

Figure 162 Even and odd analysis of N=2 equal Wilkinson combiner
a) circuit prepared for analysis b) even excitation c) odd excitation d) equations

Wilkinson combiner is as a lossy network and even for N=2 (three port network) it can be matched at all the ports. It has an advantage of being lossless when all the inputs are matched. Only the reflected power is dissipated in the isolating resistors network. Input ports are perfectly isolated at the center frequency. In general, the form combiner possesses circular symmetry and maintain the equal phase at the inputs. Circular symmetry leads to problems of planar implementation when N>2. The structure needs to be modified or multi layer realization needs to be involved, however it is very difficult to maintain the symmetry. For high values of N or for higher division ratios in unequal power combiner the problems with the realization and losses of transmission lines can be observed. Performances of the combiner depend on the technology of realization. A perfect isolation is maintained only at center frequency and decreases rapidly. A bandwidth of divider was determined as B~20% for simultaneously matched and isolated outputs for an ideal structure at -25dB. A position of resistors and their connections causes problems in the high power application. Additionally, to treat resistor as a lumped one at a higher frequency, it requests for the resistor to be especially small. That, in turn, leads to the troubles with a dissipation energy, positioning of the resistor and coupling between the arms. At a higher frequency the problems of discontinuity in T junctions used in divider as well as an isolation branch non-idealities are distinguished.

A1.2.2.1 Unequal dividing and arbitrary chosen impedances

It is achievable to design a Wilkinson power combiner for unequal power splitting [26]. What is more, it is also possible to design a circuit for the arbitrary chosen impedances [10]. These important features open the way to a miniaturization and a circuit size and loss reduction by eliminating the

matching networks. Additionally, unequal splitting could be used to build more complicated combining structures like recombinant divider; corporate divider or travelling wave divider.

A1.2.2.2 Widening bandwidth

Insufficient bandwidth for a wide bandwidth application results in evolution of the Wilkinson combiner. Most successful technique was introduced by S. B. Cohn in [31]. His approach relies on exchanging one stage quarterwave transformer with an isolating network for the multistage transforming network with isolating resistors between each section. This change in the topology as illustrated in Figure 163 for N=2.

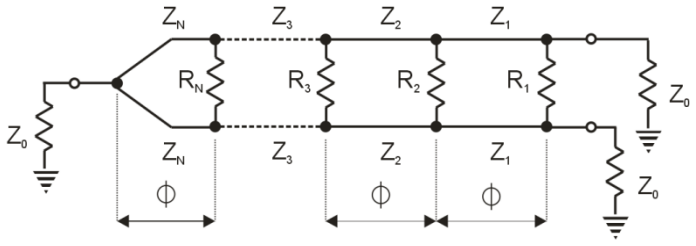

Figure 163 Multistage N=2 Wilkinson equal divider.

Approach leads to great improvement of the input match and isolation bandwidth but in exchange of the size and a loss of structure. Other techniques: the use of less dispersive transmission lines like CPW, ACPS [36], compensation techniques [125], incorporating baluns into the isolation network [126].

A1.2.2.3 Multi-frequency operation

Another approach to overcome the problem of the finite bandwidth is a multi-frequency Wilkinson divider. If continuous, the wide bandwidth is not necessary but separate smaller bands are sufficient, there exist dual [127] and triple frequency band dividers [128]. The designs are based on the replacement of quarterwave transformers with the multistage transformers.

A1.2.2.4 Miniaturization

In order to save precious space in the integrated circuit designs lot of effort was devoted to miniaturize Wilkinson divider, especially in the lower frequencies where λ_0 is large. The natural approach is the replacement of transmission lines with the lumped element equivalent circuits. This may be very effective but only at lower frequencies. The technique suffers from very lossy inductors which could also resonate at higher frequencies. The capacitors are usually in tolerances from 10 to 20% which is too small for the narrow-band applications. To defeat a low Q of inductors, the micro-machined technology had to be incorporated, the successful lumped design was reported for this approach at 8.5 and 20 GHz [36]. As to avoid the inductors capacitive loading of the quarter wave, the transmission lines are used what in turn results in the shortened versions the combiner. An effective design utilizing $\lambda_0/5$ and $\lambda_0/12$ at 10 GHz was demonstrated [35]. In order to entirely evade the risky lumped elements, it is achievable to use the full-planar approach, incorporating shunt and series stub loading transmission lines. The design based on this approach was shown at 22,5 GHz [129]. The usage of the 1-D PBG slow-wave TL structure was demonstrated in [130] as to reduce the line lengths at 2 GHz without additional losses. Another equally effective method serving to fold the transmission lines into a meander coupled line with an inductive slit what has been prepared in

[131]. Unfortunately, the ratio of width to the length of transmission line increases along with the frequency, what makes this particular approach hard to realize. The designs using multilayer approaches [132], [133]; active inductors [134]; stepped impedances as well as large inductance through the application of transverse slits were also reported.

A1.2.2.5 Planarization for N>2

As it has been mentioned before, the Wilkinson combiner holds circular symmetry. This characteristic makes the planar realization impossible when N>2 for the classic structures. To overcome this limitation a few approaches were undertaken. Obviously, it is likely to use a multilayer design like in [135] but if a realization is restricted to one layer or uniplanar approach, the choice is exceedingly limited. The trials of planarization conserving symmetry with applying the air-bridges were portrayed in [136] at 1,9 GHz. Unluckily, this approach may be pleasing only at relatively low frequencies. To use a structure that is closer to corporate divider than to a stand-alone Wilkinson is one alternative. The design of the N=3 combiner circuit was demonstrated along with the making use of the three traditional Wilkinson combiners [28]. By extending this approach it is potential to construct any N combiner and the only constrain in that approach would be the loss of the network. As a result, there appears an identical situation as in the case of the corporate combining/dividing network, where each next level of the network decreases the power combining efficiency.

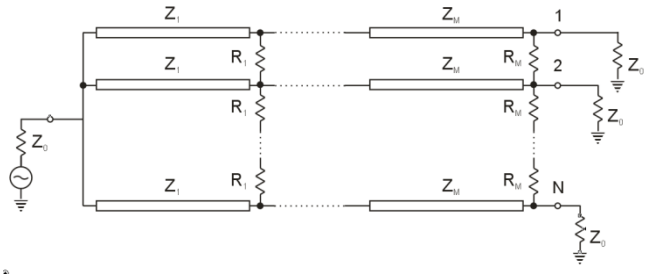

Figure 164 "Fork" Wilkinson divider.

Finally, the last but at the same time the most promising technique was shown in [27] and [29]. The topology of the combiner is introduced in the Figure 164. The isolating resistors are no longer connected by the floating node, nevertheless they do connect each adjacent transmission line with each other. It was exposed that by the means of N-1 stages it is likely to obtain similar behavior in the narrow bandwidth around the center frequency as in the case of N-way Wilkinson combiner. Alas, this implies that the circuit will have to be longer and more lossy. What is more, if this approach will be compared with the corporate structure in case of example N=4 it will be evident that the combining tree needs two stages what also indicates that any combining patch will consist of the two λ/4 transmission line transformers. In the case of Wilkinson's "fork" each patch will consist of the three λ/4 transmission line transformers. When N is increased it not only complicates the structure of combiner but it also leads to the linear increase of the losses. On the other hand, approach have the advantage of arbitrary N while the combining tree only allows $N=2^M$ inputs.

A1.2.2.6 High power capabilities

The troubles regarding the use of Wilkinson combiner in the high power applications are related to the internal isolating resistor network. If a perfect isolation between the inputs needs to be obtained,

pure resistance has to be introduced as an isolating element. This stands for a requirement to use a lumped element resistor with the size no less than few times smaller than the wavelength. From another perspective, the power handling capabilities of the Wilkinson's power combiner are determined by the power capacity of its isolating resistor network, what implies large size of the resistor. It makes two key issues in opposition. An approach to overcome this shortcoming may well change the structure of the combiner, what was actually proposed by Gysel in [32]. Such a changed version of the combiner is often called "Gysel divider". In this very design each resistor in a star configuration was replaced by the circuit consisting of the two transmission lines and shunted resistance. Consequently, the resistors can be connected externally and their size is no longer an issue. This happens at the cost of a bigger size and a little more complicated structure. That approach is valid for any N outputs and could be planar for N=2. For N>2 it is possible to place the design on the two layers [34]. In [137], Eyring proposed to design a combiner with lowered value of the resistance.

A1.2.2.7 High frequency problems

As it was mentioned earlier, at a millimeter wave, the region isolating resistor becomes very small. That means that the branches of the combiner will need to be placed there very closely. To minimize the coupling transmission, the lines are arranged into the circular shape. Unfortunately, in the case of high frequency transmission lines, the ratio of their width to length rises with the frequency, and gets especially high for low impedance lines, what limits the radius of the bend. Another important issue is the placement of the resistor between the branches. A response of the divider is strongly dependent on this fact, making the fabrication of the device tricky. In order to relax this constrains, Antsos et al. proposed a modified circuit [138]. Its design is optimum for the highly asymmetric power-split ratios. Chip-resistor placement is easier and a process is more deterministic here than in the standard design. However, one drawback of this approach is an expanded circuit size and a reduced bandwidth. Nevertheless, there were also found some examples of the integrated Wilkinson's combiner circuits designed so carefully, that they use the ordinary techniques with exceptionally good performances [38]. This confirms the usefulness of Wilkinson's divider even at such high frequencies.

A1.2.2.8 Techniques to overcome the difficulties of the technology of realization

A wide and important topic in case of the Wilkinson's combiner as well as others is the technology of realization. A power division ratio for Wilkinson's combiner is strictly connected with impedance ratio of transmission lines in T junctions. This in turn leads to the limitation on the value of that ratio. A different range of realizable impedances are possible, depending on a kind of transmission line and parameters of technology used. Few techniques were invented to rise above this obstacle. From simple search for the best transmission line technologies that will suit combiner needs, being aware of new interesting opportunities [37]. Alternatively, using techniques which would allow to change the used impedance by shortening and loading transmission line with lumped [35], as well as distributed elements [129]. Utilising techniques such as defected ground structure [139] or electromagnetic bandgap [140]; [130] is also possible. A multilayer approach offers some possibilities as well [133].

A1.2.2.9 Technologies for special purposes

There are various ideas such as this of incorporating filtration capability into the combiner structure [141], [142] or suppression of harmonics [143]; [144]. In [39] there was shown that it is potential to create Wilkinson-like circuit through parasitic.

A1.2.3 Branch-line Coupler

A basic branch line coupler is constructed by using four transmission lines connected in a way as shown in Figure 165. The circuit could be analyzed by means of even and odd mode method with one (b-b) [12] or two (a-a and b-b) [22] axis of symmetry. When the quarterwave length transmission lines of the impedance $Z_1=Z_0/\sqrt{2}$ and $Z_2=Z_0$ are used, 3 dB coupler with 90° phase difference at output ports: 2,3 will be obtained. A simultaneous perfect isolation of port no. 4 and match at all ports at center frequency is also obtained. Bandwidth of the coupler is limited to 10~20% and it is connected with the quarterwave transformers bandwidth. Branch-line coupler is planar, corporate structure in basic form restricted to N=2. An isolated port along with other ports lays on the edge of the circuit, thus it is possible to connect any kind of matched load making the circuit useful for the high power applications.

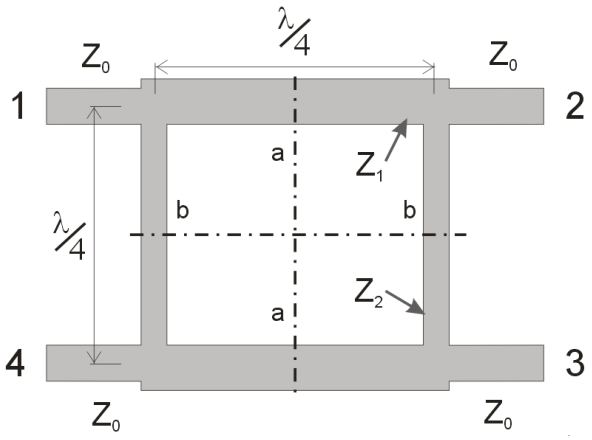

Figure 165 Branch line coupler.

Due to the restrictions in realizable impedances values the coupler is most suitable for coupling ratios from 3-6 dB, except for it is possible to extend this range through various techniques. In basic form the branches of the coupler are quarterwave transmission lines and their impedances came from the desired value of coupling. Therefore, the coupler is determined by the coupling factor and there is not much freedom in the design process. Owing to the properties of transmission line it can be expected that the circuit will operate on each odd harmonic. In higher frequency region, where ratio of width to length becomes high, the problems of mutual coupling between the arms of the coupler arise. Also, the discontinuities in the junctions become stronger, deteriorating the circuit performances. Utilising the coplanar transmission line technology leads to problems of an isolated island in the center of the circuit what may become a source of the ground resonant modes and discontinuities.

A1.2.3.1 Unequal dividing and arbitrary chosen impedances

The only restriction in a design of the unequal divider in a basic structure of a Branch-line coupler is the realization of the transmission lines with appropriate characteristic impedance. As it was shown in [45] the circuit can also provide impedance transformation without any degradation of performance for the limited range impedances ratio. It is achievable to design a coupler with freedom of arbitrary impedance at each port and arbitrary power division - [145].

A1.2.3.2 Widening the bandwidth

Theoretically, the most successful technique for widening the bandwidth is a multistage extension of branch-line coupler [146]. Regrettably, it is very complex to use it in the case of the planar circuit, since the planar transmission lines do not give so much autonomy in choice of impedance as the waveguides or coaxial lines. The Zolotarev design [147] has this advantage over the standard Butterworth and Chebyshev branch-line couplers, as it reduces the needed impedance range. Moreover, further reduction were introduced using general form of the Chebyshev function in [148], and computer aided design [149].

An additional approach is to use the transmission lines which are less dispersive and use less sensitive to frequency junctions like CPW-slotline T-junction. The experimental results were delivered in [42]. Besides, it was shown that it is possible to connect this very approach with the previous one, creating uniplanar multi-section branch-line coupler. In [50], authors used a compensation network to improve bandwidth for bent finite-ground coplanar-waveguide branch-Line coupler.

A1.2.3.3 N-band dividers

On condition of multi-frequency operation of branch-line coupler several approaches were found for double the frequency work: usage of Composite Right Left Handed Transmission Lines (CLRH TL) of basic [51], [150], along with the improved structure [151] and design of the coupler with non equal transmission lines lengths and impedances [152], plus improved structure with shortened and stub loaded transmission lines [153]; in addition to modified coupler with third branch [154] or cross coupling branches [155].

A1.2.3.4 Miniaturization of the structure

To obtain very compact designs it is achievable to use a lumped element circuit like in [40], or a modified multilayer vertical version [53]. Other possibilities are to use various types of the loading: capacitive [11], series and shunt uniplanar stubs [129], wide asymmetric stubs [59], eight two step stubs [46], artificial transmission line stub (quasi lumped approach) [58] as well as multiple shunt stubs [43]. Replacement of the transmission line with an artificial transmission line has been portrayed in [157]. Further, it is potential to use various Photonic Band Gap techniques, like DGS, Compact Microstrip Resonant Cell (CMRC) or Compensated Spiral Compact Microstrip Resonant Cell (CSCMRC) [156]. It is also possible to fold the transmission line in meander coupled line structure [47] or avoid the coupling between the adjacent lines of the meander line using MEMS square coaxial line [158]. Usage of the fractal shape lines for folding was demonstrated in [159]. A multilayer version of the circuit shown in [41] uses the meander line structure for the branches and a ground plane to separate orthogonal pairs of them. In [57] the authors flattened originally square structure of the branch-line coupler and took into account the coupling between the transmission lines.

A1.2.3.5 N-Way dividing with a Branch-line Coupler

Two examples of N-way extension for Branch-line Coupler have been found In [55], two kinds of multi-port branch-line couplers with N and with 2(N-1) outputs are described. They are based on the same structure of N parallel and 2(N-1) shunt quarter wavelength transmission lines except for different choice of impedances and location of the isolated ports (port in case of the second structure). According to the type of structure the planar cases are for N=3 and N=4. In general, the structure is appropriate for equal and unequal power division with non equal phase distribution. The two groups of the outputs with 90° phase difference between the groups and equal phase outputs in each group at the center frequency are distinguished. The second approach is described in [56]. It is likely to divide the power for arbitrary number of reflective outputs maintaining the input match. Basically, N outputs structure resembles N branches coupler but has N+2 ports. The most important feature is full planarity of the basic approach. In case of the improved isolation the evolution structure requires crossovers.

A1.2.3.6 Technology of realization, specific aspects

Problems of the isolated ground island have been overcome in [48] by the usage of the multilayer structure or ACPS transmission lines [54]. Troubles of not reachable impedances were risen in [160] and improved by applying not equal branches lengths. In [161], there was demonstrated an ability to obtain the phase compensation at the coupled port (0 phase shift with respect to the input) along with a choice of either a positive or a negative phase quadrature (±90° phase shift) at the through port. How to overpower the millimeter wave region implementation difficulties in a microstrip technology was shown in [162] through 3/4λ transmission line segment, elliptic shape of coupler and orthogonal inputs. Even higher frequency implementation was laid out in [52] by means of the square coaxial transmission lines. In [49], the authors proposed a branch-line coupler based on the silicon/metal/polyimide (SIMPOL) structure which reduced the noise crosstalk, and provided a very low line loss, even at the millimeter-wave regime.

A1.2.4 Hybrid Ring

A basic structure of hybrid ring was shown in the Figure 166 The simplest way to the analysis circuit is to use even and odd mode method with the usage of the a-a axis of symmetry [12].

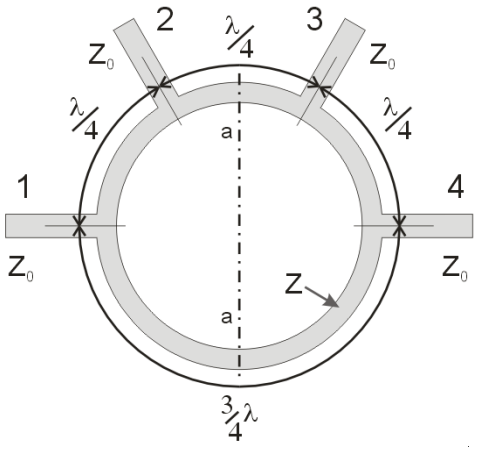

Figure 166 Hybrid ring.

When $Z_1=\sqrt{2}\,Z_0$, all the ports will be matched and the circuit will behave like 3 dB directional coupler. A scattering matrix of the circuit is the same as the one of the Magic-T, except for different port numeration and choice of the input reference planes. The circuit may be used as a divider along with in or out of phase division dependent on the chosen input port. When used as a combiner, it delivers the sum and difference signal to the individual output ports. The bandwidth of the circuit is limited to 20-25% by frequency dependence of the ring lengths.
The hybrid ring coupler is planar, the corporate structure in a basic form restricted to N=2. An isolated port as well as other ports lays on the edge of the circuit. It is achievable to connect any kind of the matched load for that port, making this circuit useful for high power applications. As in the case of the branch-line couple using the coplanar transmission line technology leads to problems of the isolated island in the center of the circuit what may be a source for the ground resonant modes and discontinuities. When modified for non equal power split, the circuit requires impracticably high-impedance line sections for the large power-split ratios. The size of the circuit is large. A mixer application suffers from fixed and not really suitable port positions.

A1.2.4.1 Widening bandwidth

The most successful technique that overcomes a limited bandwidth in case of the hybrid ring structure is a replacement of relatively long 3/4λ transmission line section with equivalent structures providing a wider bandwidth. An idea proposed originally in [163] evolved in several applicable approaches. One of them is to use the crossovers in different transmission line technologies, as in: [65], [54], [63], [64], [67], [74]. Next, by means of the coupled transmission line section as an inverter and compensation network of the two quarter-wave shunt short-circuit stubs [66]. Then, usage of the coupled transmission line section instead each transmission line, where only one of them with the phase inversion characteristic [70]. Beside, through the artificial lumped-element left handed transmission line section [69]. In [63], the authors proposed the usage of the slotline transmission line ring and for further increase of bandwidth an incorporation of the crossover junction. Unfortunately, this approach involved two layer structure. In [64] and [54] the authors used uniplanar transmission lines only for improving the circuit performances.
The widening bandwidth is to be obtained by adding additional isolated port when the circuit works as an in-phase combiner [60]. In [61] 3/4λ the transmission line was divided and diversified in an impedance value what improved the bandwidth. By using the crossovers it is possible to rearrange the structure of hybrid ring and cascade it into a two stage structure. That leads to improvement in the bandwidth as shown in [68].

A1.2.4.2 N-band dividers

Within the domain of the multi-frequency operation, the lumped element approach for a double band structure was found [73].

A1.2.4.3 The miniaturization of structure

The miniaturization of the structure may be obtained while using the lumped element approach [164]. Loading, connected with lumped element approach leads to a small size and freedom in the port rearrangement, sufficient especially for the mixer application [11]. It is also probable to use alternative structures to 3/4λ transmission line sections like crossovers: [63], [64], [67] or the coupled lines: [163], [81]. Beside, different transmission line lengths for the coupler segments like

λ/6 or λ/8 can be employed [62]. In the [54], [65] connection of these two above techniques was shown. What is more, the phase inverting structure with the spiral slot lines and shunt capacitance was presented in [74]. Further, the way to fold transmission line into the meander coupled line structure was shown in [165] as well as use of the fractal shape lines for the folding was shown in [159]. In addition, applying the artificial transmission lines was presented in [157]. Using the compact microstrip resonant cells (CMPC) has been introduced in [166] and with a modified structure of cell in [72]. In order to be much more compact as when using the crossovers it is possible to rearrange the coupler [68].

A1.2.4.4 Technology of the realization; specific aspects

The multi-section design presented in [68] overcomes the impractical high-value of the impedance needed to design a large power split-ratio. An application of the dielectric-supported airgapped microstrip lines (DAMLs) structure in design of hybrid ring coupler was shown in [71]. Signal lines were elevated from the ground plates, to reduce the substrate dielectric loss and obtain low losses in the millimeter-wave frequency band with a wide impedance range.

A1.2.5 The transmission Line Couplers

A coupled transmission line or three-wire line is able to propagate two TEM types of waves. Each of that type we call the mode of propagation. As was shown in [12], with assumption of TEM type of propagation, electrical properties of line for each mode may be found by utilizing effective capacitance between the lines and velocity of the propagation. This leads to two impedances and two velocities of the propagation for the coupled transmission lines. They will be named: even and odd accordingly to the way they are excited in the coupled lines. In an ideal case it is expected that the propagation velocities are equal what leads to directivity of the circuit. At the same time it is expected that even and odd characteristic impedances are of different values which will introduce the coupling. Coupling coefficient for that element will depend on difference between the values of the impedance in each mode and length of the coupled line section. If the impedances are chosen so that $Z_0=\sqrt{Z_{0e} Z_{0o}}$ we will obtain the match at all ports. The coupled line structure is best suited for the weak coupling due to of problems with physical realization of the impedances in the tight coupling cases. This difficulty arises also in the microstrip version owing to different velocities of propagation derived from different electrical constants in even and odd mode of operation.

If a tighter coupling or wider bandwidth is needed, the most straightforward way is to apply multi-section coupler or tandem version. There is range of approaches to overcome problems of the couplers with very tight coupling. These are: utilizing the embedded microstrip in MMIC technology [79], braided structure [75], Broadside-Offset-Coupled Coplanar-Microstrip [80], multilayer MMIC using thin dielectric layers and floating conductor [81], a periodic structure of loosely and strong coupling sections [82], air-gap stacked microstrip lines [83], lumped-element quadrature hybrid [84], Composite Right-/Left-Handed Coupled-Line [85], Broadside Coupled Coplanar Waveguide lines with Defected Ground Structure [86], Broad-Side Coupler with a Symmetric Structure [167], Coupled Artificial Transmission Lines [87].

Due to the gathered examples the ones worth underlining are as follows. In the case of the Broadside Coupled Coplanar Waveguide lines with a Defected Ground Structure [86] fine performance of the isolation was obtained. The usefulness of wiggly geometry results in improved isolation and increased effective dielectric constant what provides a shorter coupler length in [76], [77]. An

application of the Composite Right-/Left-Handed Coupled-Line [85] as to easily obtain the arbitrary coupling factor, even 0 dB.
It is within reach to miniaturize the structure through applying Artificial Transmission Lines [87], or folding into the meander line [167], or by using the lumped-element quadrature hybrid [84].
Moreover, it is possible to us coupled line structure of more than two coupled transmission lines. In [78] the authors present a multi-way uniform forward combline directional couplers.

A1.2.6 The Lange Coupler

Without additional techniques coupled, the transmission lines couplers are not able to provide the tight coupling. One idea not mentioned before is to employ the multiple coupled alternated lines in the way shown in Figure 167. Than, an increased coupling comes from application of fringing field between the adjacent inner coupled transmission lines. This leads to a significant increase in odd mode lines capacitance, thus lowers the odd mode impedance. This topology is called Lange coupler [88] Figure 167a, and rearranged structure is called “unfolded” Lange coupler Figure 167b [90].

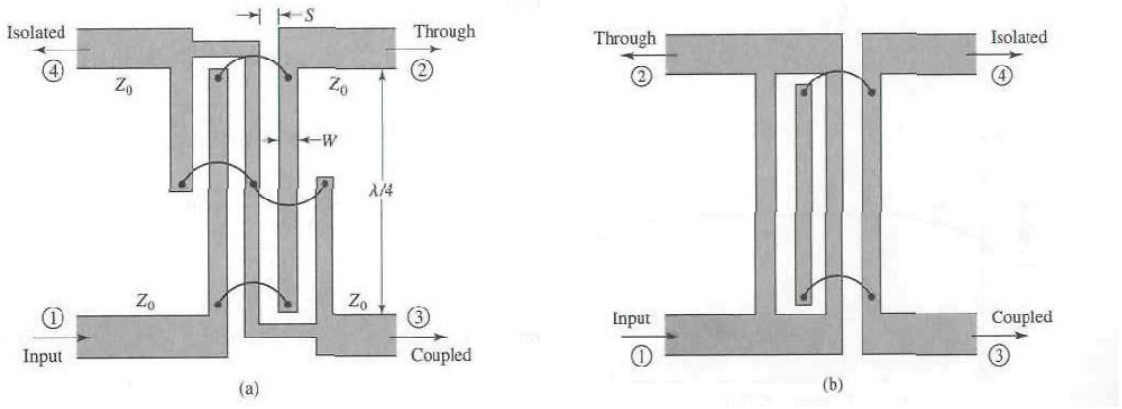

Figure 167 Lange couplers. (a) traditional microstrip form (b) unfolded structure

The structure works well over an octave bandwidth as a consequence of the interdigital coupling section which compensates for even- and odd-mode phase velocity dispersion over the wide frequency range. Main drawback of the Lange coupler is a difficulty of manufacturing derived from very thin transmission lines, as well as small gaps in interdigital section and a need for wire-bonding. The circuit is very sensitive to the change in gaps dimensions and a metallization thickness. The unfolded version enables the easiest circuit analysis and gives designers flexibility in designing bigger systems.
Thin lines in the coupler are problematic not only from the manufacturing point of view. They could increase losses of structure. In [168], the author suggests a design of the coupler by means of lower characteristic impedance which in turn results in lower losses and less problematic manufacturing. Also, it is more convincing in a multi-stage balanced amplifier design resulting in smaller matching circuits.
Use of the multilayer structure in [169] leads to wider and of less losses lines and to evading the wire-bonding in [89].
The one and only example of the miniaturization is folding the structure but care must be taken not to destroy the symmetry of the circuit.

A1.2.7 The tapered line

Tapered lines are transmission lines with continuously changing characteristic impedance. They are alternative to multi-section matching transformer, especially in higher frequency, when each step in impedance leads to a rise in discontinuity by deteriorating the circuit performance. It is accessible to use shape and the properties of the tapered line with other techniques to design the power combiners. An implementation of the tapered lines with Wilkinson's power divider were shown in [91]. For small N they are used as transformer circuits, when N is higher additional tapered line transform input impedance before splitting. An evolution of this idea lead to nonuniform transmission lines power divider with a distributed isolation. Theoretically, this kind of the circuit has no upper boundary of the operating frequency range in a single-wave approximation [170]. Unfortunately, distributed resistance filling area between the lines causes attenuation due to the current flow through the resistive material in the direction of the tapered line. This situation in turn leads to approaches utilizing multiple resistors in form of the ladder network, that resembles "fork" evolution of Wilkinson. In such circuits the forward currents are suppressed and the insertion losses are decreased [94], [95]. In [96] Dolph-Tchebycheff taper is used as optimum in the sense that it has the minimum length for a specified maximum reflection coefficient magnitude in the pass-band.
An appliance of the tapered line transformers leads to usefulness of Wilkinson's "fork" approach in high frequency minimizing the problems of discontinuity in an isolating network. Other approach is to use tapered line with an optical diffraction theory [93]. In presented structure; power combining functions are simply realized by the transition between an oversized microstrip line and as a set of parallel multiport microstrip lines.

A1.2.8 Resonant structures

Using particular shape of conductor with the size compared to the wavelength leads to a frequency dependent particular field pattern. With properly chosen port positions and width the power combining is within reach. In high frequency applications, the resonant combiners might avoid problems of the transmission line circuit such as: parasitic reactances introduced to the circuit associated with junctions; increasing width to length ration and physically non realizable impedance values of the transmission lines,; unwanted coupling between the transmission lines forming the device.
The approaches utilizing different shapes of patches with a few additional techniques are found in literature. In [105] the microstrip circular disc together with central coaxial feed are analyzed. The authors show that introducing additional shortened ports within the structure could improve the performances. Alas, this structure is not uniplanar and requires the multilayer implementation. Fully planar version for N=3,4 was shown in [102]. Design 3dB quadrature hybrid with appliance of the circular patch with additional tuning elements in the form of the impedance steps and reactive stubs were demonstrated in [97] and in [98]. The modification preventing from submerging the open circuit stubs by the fringing fields of the disk was to use an elliptic patch [100].
Finally, good results were obtained with rectangular path and concaves, convexes, and short-circuited stubs added symmetrically at the periphery of the disk, with the four ports connected diagonally at the four corners, or perpendicularly in the center of each side of the disk [99]. By inserting the impedance steps between each port and the disk itself, a very flat coupling was realized along with a wide-band matching. By placing the symmetrical hole, the circular path was transformed

into annual ring for which it is possible to gain various power combining structures [101]. By applying a three-port rectangular microstrip power divider [106], an arbitrary power division between the two ports can be created. The structure avoid problems of physically unrealizable impedances for either tight or loose coupling factors. A very useful feature of the power combiner is the opposite location of the input-output ports. Sadly, the multi-output versions of the previously mentioned circuits do not posses this feature. A more appropriate element in that case will be the sector component [103] and a modified sector component for unequal division [104]. They are more suitable for corporate connection but the output is still placed in a radial manner. In some application this could be disadvantageous and became a reason for a development of the tapered power combiner along with compensation holes responsible for the phase equalization and a straight line output arrangement [92].

A1.2.9 Travelling Wave Combiner

The Travelling Wave divider is a circuit that incorporates Wilkinson dividers in a serial combining manner. The schematic of the structure is shown in Figure 168.The circuit incorporates N-1 combiners of the various power-spilt ratio from 3 to $10\log_{10}(N)$ dB and delays lines responsible for the in phase power combining.

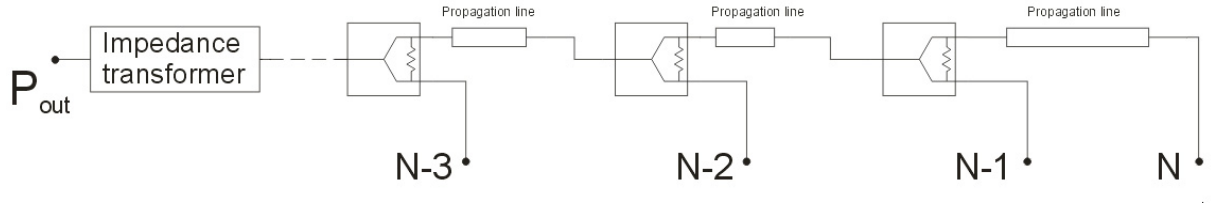

Figure 168 Travelling wave combiner schematic.

In a corporate approach utilizing the Wilkinson's divider the connection of the equal mismatched loads will degrade the input match. This happens as the Wilkinson's divider is not able to dissipate the even backward waves. However, when the dividers are connected in the serial manner with the proper phase delay, lines it is possible to cancel the backward travelling wave in their isolating network.

The combiner is attractive for the monolithic implementation due to its planar structure and an inherent broad-band inter-port isolation characteristics. In the higher frequency region apart from problems of design each designer structure is very suitable for amplifiers design [109]. In [108], the design with the near wall of package was simulated as a way to minimize the circuit size. In [110], the low frequency implementation of the combiner with the lumped approach was shown. The lumped approach causes structure to loss wideband characteristic.

A1.2.10 SIW

The rectangular waveguides are important building blocks due to their power handling capability and low losses. Their biggest disadvantage is their size and troubles of integration with other components. Most of the approaches to integrate them into the microwave substrates as Substrate Integrate Waveguides (SIW) can be found in literature. A structure of this kind possesses advantages

of waveguides and in addition is small, so that allows an effortless integration and uncomplicated fabrication.
Basic building blocks like T or Y junctions created in that technology maybe used as stand-alone power dividers [113], or exploited in more complicated structures like 6 port junction [172] or other concepts like corporate N=16 network [171]. Slot SIW quadrature coupler [111] and a modified structure incorporating slow wave effect to became 180° coupler [112] were reported. Moreover, it is also possible to create resonant cavities and use them in the function of the power combiners [173].

A1.2.11 Other approaches

A few other interesting approaches with fewer publications will be described shortly below.

A1.2.11.1 3-way power divider with various output power ratios

Structure of the circuit proposed in [114] is presented in Figure 169. This circuit is a planar transmission line structure and does not need any resistors to be built. It could be used as a three way or two way divider/combiner circuit with a perfect match and isolation at the center frequency for all the ports. It is achievable to obtain an arbitrary power division by changing the values of the five characteristic impedances used in the circuit.

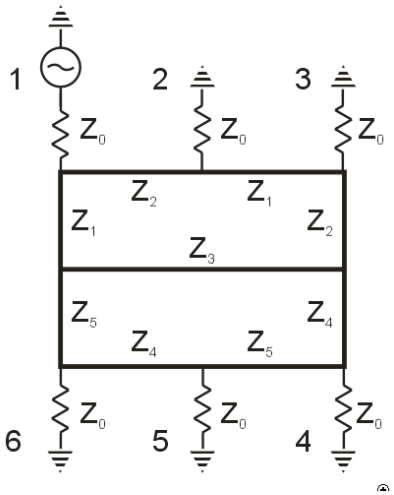

Figure 169 Structure of the 3-way power divider.

The proposed circuit is very flexible in design, offering very interesting features; for example a change in the input port location has given different split power ratio for the same circuit. The circuit can be expanded to N way combiner. Using this circuit the authors built a balanced amplifier [174], an interesting phenomenon is that they need only one combiner for that purpose and it served simultaneously as a combiner and a divider with an input and output in ports: 2, 5 and amplifiers connected to the pairs of ports: 1,6 and 3,4. In that configuration the circuit showed relatively wide-bandwidth behaviour.

A1.2.11.2 Extended resonance

The proposed power combining technique is similar to the construction of the direct coupled waveguide cavity filters. The extended resonance technique can be used to build multiple devices

oscillators and amplifiers, the phased array. This technique is suitable for the planar connection on N devices, without individual matching circuits providing a very compact structure. Extended resonance places the devices in shunt to combine the power, the magnitude of the voltage at each of them is than of the same value.

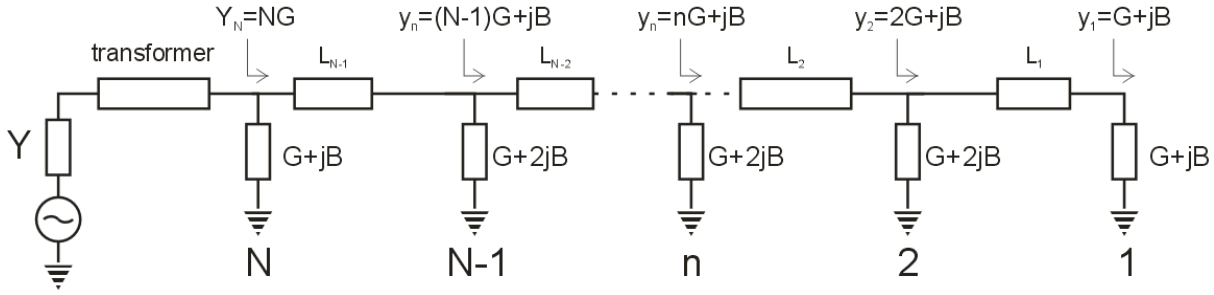

Figure 170 Extended resonance concept – N divider example.

In the Figure 170, the concept of the extended resonance technique has been presented in the example of N way power divider. The source of the admittance Y is connected with N loads. Admittances are normalized to a characteristic admittance of the transmission lines. The first and the last device admittance is G+jB and admittances of the internal devices are G+j2B. The first length L_1 is chosen to transform the admittance G+jB into its conjugate value G-jB. Then, looking at the circuit in a right direction from the second node - we notice that it consists of the second as well as the transformed by L_1 the first device – therefore the admittance y_2=2G+jB is observed. Next, the length of the next transmission line L_2 is chosen again to conjugate the load seen and the third device again see load of 2G-jB. After the summation with the third device +jB of the imaginary part of the admittance is obtained again. Each next step repeats the procedure until the last stage, when addition of N-th admittance cancels the imaginary part. The very last step is to match the Y_N=NG admittance distinguished when looking into N devices network to the source admittance Y along with an arbitrary matching circuit.

The extended resonant technique is narrowband due to the resonant nature, in case of the amplifier application 3-dB bandwidth it is limited to ~ 5%. In response to that shortcoming the broadband extended resonance was introduced in [116]. An amplifier utilizing this technique was designed as to show the broadband performance. A main difference between the approaches is the way the admittances have been transformed. This time, the loaded complex admittance $G_k(f)+jB_k(f)$ has been converted to its conjugate value $G_{k+1}(f)-jB_{k+1}(f)$ by the network N as distinct from a simple transmission line in an original approach.

A1.2.11.3 Broadband Series Power Divider Using 0° Phase-Shifting Lines

The serial power combiners are attractive replacements of the corporate combining networks offering smaller area occupied and lower losses. However, they exhibit varying power split ratios with frequency. Another problem is to obtain an equal-phase combiner. A standard approach is to put meander like λ_g long delay lines between the single combiners. Although, this leads to a big size and narrow bandwidth connected with the delay line length. One of the solution is to use artificial 0° phase shifting line. Metamaterial (MM) phase-shifting lines are particularly suitable in this case, since they can incur a zero insertion phase over a large bandwidth; maintaining a compact length at the same time. Usage of this line given the serial combiner transforms it into a parallel combiner.

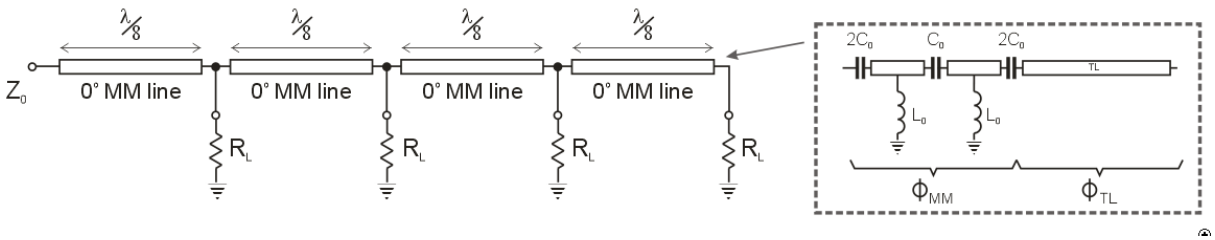

Figure 171 Metamaterial serial N=4 combiner.

In the Figure 171, a basic structure of the combiner and 0° phase shifting transmission line structure from [117] was shown. A parallel connection of the lines implies the use of additional transforming network for the equal input-output impedances.

This metamaterial series power combiner offers the broadband in-phase power combining, maintaining the small size in comparison to a conventional transmission line series power divider. It offers a compact and planar structure in which ports can be spaced arbitrarily apart. This technique can be extended to arbitrary number of ports.

A1.2.11.4 The uniplanar Wheatstone bridge

This particular approach was designed in order to overcome difficulties of very narrow gaps in Lange coupler at lower frequencies. 90° hybrid coupler shown in Figure 172 a), where it was implemented with the use of the Wheatstone bridge Figure 172 b). An inductive reactance was realized using a short circuited slotline stub and in order to achieve a capacitive reactance an open-circuited coplanar waveguide stub was employed.

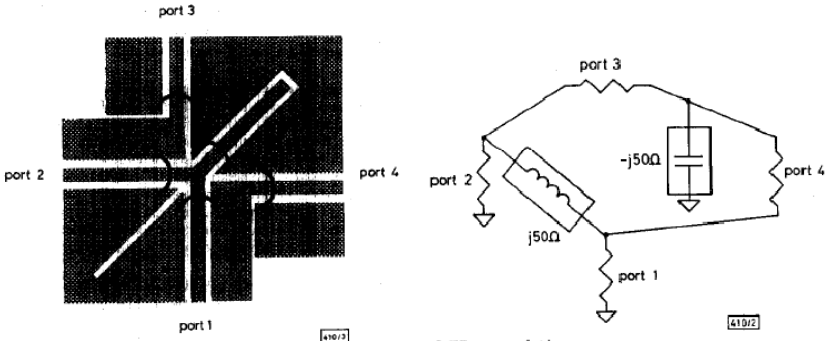

Figure 172 90° hybrid coupler a), Wheatstone bridge b).

Its total length is λ/4, in contrast to the Lange coupler, the structure does not require narrow strips and gaps. The bandwidth is narrow (8%).

A1.2.11.5 Bailey's divider concept and evolution

A dilemma of the necessity for a wide range power-split ratio combiners concerns many applications. It derives from the fact that most useful approaches in domain of the transmission line circuits control the power-split ratio along with impedances of the used transmission lines. The difficulty is especially important in a planar implementation, when range of available values of characteristic impedance is narrower than in coaxial, the waveguide or even in the multilayer implementation. In [119] there was presented an approach in which ratio of the in-phase power division is separately controlled from the values of the impedances of the transmission lines. The structure comprises

from: T-junction with a quarterwave transformer, delay section as well as branch-line hybrid coupler as it was shown in the Figure 173.

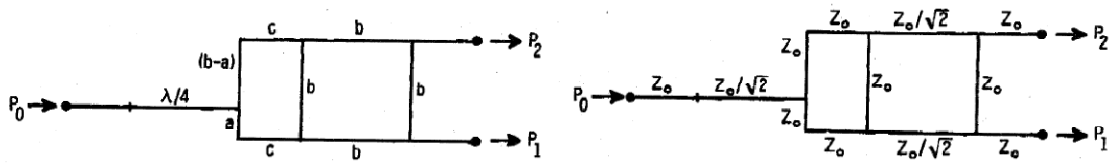

Figure 173 Bailey's divider: a) lines' length details b) lines' impedances details.

Further, unequal amplitude and equal phase splitting is assured by exciting both inputs of branch-line hybrid coupler with equal amplitude and different phase. Than, the output signal will be a superposition of the response for these two excitations and a proper split power-ratio may be obtained through choosing different length of the line in a delay section: a; b-a. For a structure defined in such a way the delay changes with a position of T-junction in the vertical line comprised of a and (b-a) sections. Thereby, the position of T-junction controls the division ratio. Unfortunately, the relation between the power split and a length of transmission line denotes automatically that the power split will vary with frequency; making this approach a narrow bandwidth.

A slightly different approach was presented in [120]. Input T-junction was exchanged for another branch-line hybrid coupler; and a delay section was replaced for a programmable phase shifter. The circuit works in the same manner, allowing different power-split ratios for a different phase shift, but according to a chosen input for the signal: in or out of the phase power division at the output is likely to obtain. This in turn lead to another degree of freedom in reconfigurability of the circuit.

A diverse evolution of that approach was proposed in [121]. The structure used in this very concept is basically the same as the one proposed originally by Bailey. However, on these conditions the power-split ratio for either input T-junction or output branch-line coupler has been determined as variable. By this procedure in the design exist three degrees of freedom, thus it is achievable to either chose an arbitrary power-split ratio or the phase relation. For the specific output power ratio plus phase difference two variables need to be determined so that the third one can be fixed. It is an incredibly precious property leading to a great deal of freedom in the design of this structure. Finally, a narrowband behaviour of the combiner might be improved by means of the wideband combiner circuits such as the tapered matching sections in T-junction or multi-branch coupler.

A1.2.11.6 The Composite Coupler

An additional way to rise the possible value of the power-split ratio in planar dividers is to employ a composite approach shown in [122]. A practical limitation on that ratio may be extended by incorporating the same types of couplers into a network shown in the Figure 174.

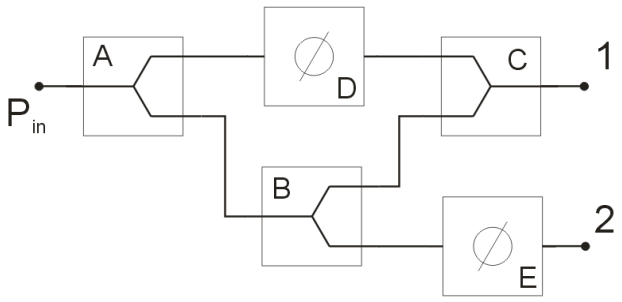

Figure 174 The structure of the composite divider

The indicated method uses three dividers to split and recombine the power in order to achieve greater power-split ratio. Performances of the circuit are dependent on the characteristics of the divider used to build the network. Output power handling, phase tracking along with the reflection coefficient will be similar to individual divider performances, however maximal power-split ratio will be improved. It will happen so at the expense of the expanded circuit size and an increase in the amount of the components required.

A1.2.11.7 The Bagley Polygon power dividers

Some other interesting approach for N-way transmission power combiner is to apply the Bagley polygon.

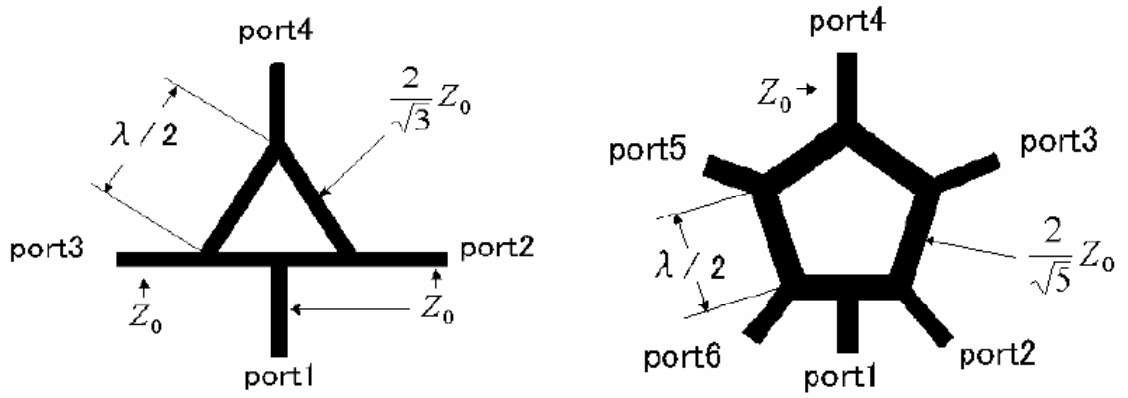

Figure 175 Bagley polygon power dividers (a) N=3, (b) N=5.

It is obtainable to combine odd number of the sources maintaining the input match and isolation between the outputs at the center frequency. Shapes for N=3 and N=5 are shown in the Figure 175. Regrettably, the circuits are large since the polygons' sides are λ/2 long. They expand with a growing number of the inputs/outputs. Moreover, the position of the input/output ports is not proper for the planar applications. The circuit properties are in connection with the transmission line length, thus the wide-bandwidth behaviour is not expected. For the sake of reducing the combiner structure , the stub loading was proposed in [123].

A1.3 References

[22] R. E. Collin, Foundations for Microwave Engineering, 2nd Ed., McGraw-Hill 1992.

[23] T. Hirota, Y. Tarusawa, and H. Ogawa, “Uniplanar MMIC hybrids- A proposed new MMIC structure,” IEEE Trans. Microwave Theory Tech., vol. MTT-35, pp. 576-581, June 1987.

[24] M. Kishihara, K. Yamane, I. Ohta, .T. Kawai, “A Design of Multi-Stage, Multi-Way Microstrip Power Dividers with Broadband Properties”,

[25] E. J. Wilkinson, “An n-way hybrid power divider: IRE Trans. Microwave Theory Tech., vol. MTT-8, pp. 116-118, Jan. 1960.

[26] L. Parad and R. Moynihan, “Split-tee power divider”, IEEE Trans. Microwave Theory Tech., vol. MTT-13, pp. 91-95, Jan. 1965.

[27] N. Nagai et al., “New N-way hybrid power dividers”, IEEE Trans. Microwave Theory Tech., vol. MT”l’-25, p. 1008, Dec. 1977.

[28] Marc E. Goldfarb, “A Recombinant, In-Phase Power Divider”, IEEE Trans. Microwave Theory Tech., vol. 39, No. 8, Aug. 1991

[29] A. A. M. Saleh, “Planar, Electrically-Symmetric, N-Way, Hybrid Power Dividers/Combiners”, IEEE Trans. Microwave Theory Tech., vol. MTT-28, pp. 555-563, June 1980.

[30] H. R. Mgombelo and J. G. Gardiner, “Three-way power dividers and combiners constructed on the basis of a three-way Luzzato divider,” Proc. IEE Colloq. RF Combining, pp. 4/1–410, Apr. 12, 1990.

[31] S.B. Cohn, "A class of broadband three-port TEM-mode hybrids," IEEE Trans. MTT, vol. MTT-16,pp. 110-116, Feb.1968

[32] U. Gysel, “A new N-way power divider/combiner suitable for high power applications,” in 1975 MT Symp. Dig., pp.116-118.

[33] B. Ooi, W. Paler, and M. S. Leong, "Broad-banding technique for in-phase hybrid ring equal power divider, " IEEE Trans. Microwave Theory and Tech., vol. 50, no. 7, pp. 1790-1794, Jul. 2002.

[34] G. Ge, H.K.Wen, ” Research on microstrip multiway unequal power divider/combiner”, IEE Proceedings - Microwaves, Antennas and Propagation, Volume: 143, Issue: 5 pp. 437-440, Oct 1996

[35] M. C. Scardelletti, G. E. Ponchak, and T. M. Weller, “Miniaturized Wilkinson power dividers utilizing capacitive loading,” IEEE Microw. Wireless Compon. Lett., vol. 12, no. 1, pp. 6–8, Jan. 2002.

[36] Liang-Hung Lu, Pallab Bhattacharya, Linda P. B. Katehi, “X-Band And K-Band Lumped Wilkinson Power Dividers With A Micromachined Technology”, Microwave Symposium Digest, 2000 IEEE MTT-S International

[37] L. Fan and K. Chang, “Uniplanar power dividers using coupled CPW and asymmetrical CPS for MIC’s and MMIC’s,” IEEE Trans. Microwave Theory Tech., vol. 44, pp. 2411–2419, Dec. 1996.

[38] C.Y. Ng, I.D. Robertson, “A 140 GHz Wilkinson power divider/combiner”, High Frequency Postgraduate Student Colloquium, 2002.7th IEEE

[39] Hajime Izumi, Hiroyuki Arai, “Electromagnetic Coupled Power Divider Using Parasitic Element”, Microwave Conference, 2000 Asia-Pacific, pp. 233-236

[40] R. K. Gupta, and W. J. Getsinger, “Quasi-lumped-element 3- and 4-port networks for MIC and MMIC applications,” in IEEE MTT-S Int. Microwave Symp. Dig., 1984, pp. 409-411.

[41] S.Banba, T.Hasegawa and H.Ogawa, "Multilayer MMIC branch-line hybrid using thin dielectric layers," IEEE Microwave and guided wave letters, Vol.1, pp.346-347, 1991.

[42] C. H. Ho, L. Fan, and K. Chang, “A broad-band uniplanar branch-line coupler using a coupled rectangular slotline ring,” IEEE Microwave Guided Wave Lett., vol. 3, pp. 175–176, June 1993.

[43] Young-Hoon Chun, Jia-Sheng Hong, “Compact Wide-Band Branch-Line Hybrids” IEEE Trans. Microwave Theory Tech., vol. 54, no. 2, February 2006

[44] C.-Y. Lee, and T. Itoh, “Full-wave analysis and design of a new double-sided branch-Line coupler and its complementary structure,” IEEE Trans. Microwave Theory Tech., vol. MTT-43, pp. 1895-1901, Aug. 1995

[45] S. Kumar, C. Tannous, and T. Danshin, “A multisection broadband impedance transforming branch-line hybrid,” IEEE Trans. Microwave Theory Tech., vol. 43, pp. 2517–2523, Nov. 1995.

[46] I. Sakagami, M.Haga and T.Munehiro, “Reduced branch-line coupler using eight two- step stubs”, IEE Pro.- Microw.Antennas Propag., vol. 146, pp455-460, 1999.

[47] R. K. Settaluri, A. Weisshaar, C. Lim, and V. K. Tripathi, “Design of compact multilevel folded-line RF couplers,” IEEE Trans. Microwave Theory Tech., vol. 47, pp.2331 – 2339, Dec. 1999.

[48] J. H. Lee and H. Y. Lee, “Novel quadrature branch-line coupler using CPW-to-microstrip transitions,” in IEEE MTT-S Int. Microwave Symp., 2000, pp. 621–624.

[49] Juno Kim, Yongxi Qian, Guojin Feng, Pingxi Ma, M. Frank Chang, Tatsuo Itoh, ”Millimeter-Wave Silicon MMIC Interconnect and Coupler Using Multilayer Polyimide Technology”, ,” IEEE Trans. Microwave Theory Tech., vol. 48, no. 9, pp.1482-1487, Sep. 2000

[50] C. T. Lin, C. L. Liao, and C. H. Chen, “Finite-ground coplanar-waveguide branch-line couplers,” IEEE Trans. Microw. Wireless Compon. Lett., vol. 11, no. 3, pp. 127–129, Mar. 2001.

[51] ZHANG Yu, HU Li, HE Sai-ling, “A tunable dual-broad-band branch-line coupler utilizing composite right/left-handed transmission lines”, Journal of Zhejiang University SCIENCE 2005 Vol. 6A No. 6

[52] J.R. Reid, R.T. Webster, “A 60 GHz Branch Line Coupler Fabricated Using Integrated Rectangular Coaxial Lines”, Microwave Symposium Digest, 2004 IEEE MTT-S International, vol. 2, pp. 441- 444

[53] Tsung-Nan Kuo, Yo-Shen Lin, Chi-Hsueh Wang, Chun Hsiung Chen,”A Compact LTCC Branch-Line Coupler Using Modified-T Equivalent-Circuit Model for Transmission Line”, IEEE Microw. Wireless Compon. Lett., vol. 16, no. 2, pp. 90–92, Feb. 2006.

[54] B. Heimer, L. Fan, and K. Chang, “Uniplanar hybrid couplers using asymmetrical coplanar striplines,” IEEE Trans. Microw. Theory Tech., vol. 45, no. 12, pp. 2234–2240, Dec. 1997.

[55] L. C. Chao, “N-way branch line directional couplers,” in IEEE MTT-S Int. Microwave Symp. Dig., vol. 74, Jun. 1974, pp. 93–96.

[56] ADEL A. M. SALEH, “Planar Multiport Quadrature-Like Power Dividers/Combiners”, IEEE Trans. Microwave Theory Tech., vol. MTT-29, no. 4, April 1981

[57] V. K. Tripathi, H. B. Lunden, and J. P. Starski, “Analysis and design of branch–line hybrids with coupled lines,” IEEE Trans. Microwave Theory Tech., vol. MTT-32, pp. 427–432, Apr. 1984.

[58] Shry-Sann Liao, Jen-Ti Peng, “Compact Planar Microstrip Branch-Line Couplers Using the Quasi-Lumped Elements Approach With Nonsymmetrical and Symmetrical T-Shaped Structure”, IEEE Trans. Microwave Theory Tech., vol. 54, no. 9, Sept. 2006

[59] S. S. Liao, P. T. Sun, N. C. Chin, and J. T. Peng, “A novel compact-size branch-line coupler,” IEEE Microw. Wireless Compon. Lett., vol. 15, no. 9, pp. 588–590, Sep. 2005.

[60] G. F. Mikucki and A. K. Agrawal, “A broad-band printed circuit hybrid-ring power divider,” IEEE Trans. Microwave Theory Tech., vol. 37, pp. 112-117, Jan. 1989.

[61] D. I. Kim and Y. Naito, “Broad-Band design of improved hybrid-ring 3-dB directional couplers,” IEEE Trans, Microwave Theory Tech., vol. M’IT-30, pp. 2040-2046, Nov. 1982.

[62] KIM, D.I., and YANG. G.s.: “Design of new hybrid-ring directional coupler using λ/8 or λ/6 sections”, IEEE Trans. Microwave Theory Tech., 1991, MlT-39, pp. 1179-1783

[63] C. H. Ho, L. Fan, and K. Chang, “Ultra wide band slotline hybrid-ring couplers,” in IEEE MTT-S Int. Microwave Symp. Dig., Albuquerque, NM, June 1992, pp. 1175–1178.

[64] C. H. Ho, L. Fan, and K. Chang, “Broad-band uniplanar hybrid-ring and branch-line couplers,” IEEE Trans. Microwave Theory Tech., vol. MTT-4 1, pp. 2116-2125, Dec. 1993.

[65] M. H. Murgulescu, E. Moisan, P. Legaud, E. Penard, and I. Zaquine, “New wideband, 0.67 wavelength circumference 180° hybrid coupler,” Electronics Letters, Vol. 30, No. 4, pp. 299-300, Feb. 1994.

[66] J.L.B. Walker, “Improvements to the design of the 0–180° rat-race coupler and its application to the design of balanced mixers with high LO to RF isolation”. IEEE MTT-S Int Microwave Symp Dig 1997, pp. 747–750.

[67] H. An, T. Wang, E Cardinal, A. Scott, K. Wu, A. Harrison, “A Novel Broadband Uni-planar MMIC Ring Coupler for Wireless LANs Applications”, Wireless Communications Conference, 1997., Proceedings, pp. 198-200

[68] Kian Sen Ang, Yoke Choy Leong, Chee How Lee, “A New Class of Multisection 180 Hybrids Based on Cascadable Hybrid-Ring Couplers”, IEEE Trans. Microwave Theory Tech., vol. 50, no. 9, Sept. 2002

[69] H. Okabe, C. Caloz, and T. Itoh, “A compact enhanced-bandwidth hybrid ring using a left-handed transmission line,” IEEE Trans. Microw. Theory Tech., vol. 52, no. 3, pp. 798–804, Mar. 2004.

[70] Kian Sen Ang, Yoke Choy Leong, Chee How Lee, “Impedance-transforming, coupled-line 180° hybrid rings with frequency independent characteristics”, Microwave Symposium Digest, 2003 IEEE MTT-S International, Volume: 2 8-13 June 2003 pp. 1239- 1242

[71] B.S. Ko, T.J. Baek, D.H. Shin, S.C. Kim, B.O. Lim, H.S. Lee, S.K. Kim, H.C. Park, Y.H. Chun, J.K. Rhee, “Design and fabrication of 180° hybrid ring coupler for applications of MMICs using dielectric-supported air-gapped microstriplines”, ELECTRONICS LETTERS 27th May 2004 Vol. 40 No. 11 pp. 675 - 676

[72] D. Esic, ” Slow-wave EBG microstrip rat-race hybrid ring”, ELECTRONICS LETTERS 13th October 2005 Vol. 41 No. 21, pp. 1181 - 1183

[73] F. Giannini and L. Scucchia, “A double frequency 180 lumped-element hybrid,” Microwave Optical Technol. Lett., vol. 33, no. 4, pp. 247–251, May 2002.

[74] Sanghyo Lee, Wooyeol Choi, Sungwon Kim, Kwang-Seok Seo, Youngwoo Kwon, ” A Size-Reduced CPW MMIC Rat Race Coupler”,

[75] D. A. Willems, “A Broadband MMIC Quadrature coupler using a braided microstrip structure”, Microwave Symposium Digest, 1994., IEEE MTT-S International, 23-27 May 1994, pp. 899-902 vol.2

[76] UYSAL, S., and AGHVAMI, H.: ‘Synthesis, design, and construction of ultrawide-band nonuniform quadrature directional couplers in inhomogeneous media’, IEEE Trans. Microw. Theory Tech., 1989, 37, (6), pp. 969–976

[77] Jia-Liang Chen, Sheng-Fuh Chang, Yng-Huey Jeng, Chun-Yo Lin, “Wiggly technique for broadband non-uniform line couplers”, ELECTRONICS LETTERS 2nd October 2003 Vol. 39 No. 20

[78] Saiful Islam, ”Multiway Uniform Combline Directional Couplers for Microwave Frequencies” IEEE Trans. Microwave Theory Tech., vol. 36. no. 6, June 1988

[79] D. Willems and I. Bahl, “A MMIC compatible coupled line structure that uses embedded microstrip to achieve extremely tight couplings,” in 1993 IEEE MTT-S Dig., pp. 581–584.

[80] F. Mernyei, I. Aoki, H. Matsuura, “A novel MMIC coupler-measured and simulated data”, Microwave Symposium Digest, 1994., IEEE MTT-S International, 23-27 May 1994, 229-232 vol.1

[81] S. Banba and H. Ogawa, “Multilayer MMIC directional couplers using thin dielectric layers,” IEEE Trans. Microwave Theory Tech., vol. 43, pp. 1270-1275, June 1995.

[82] Yansheng Xu, Renato G. Bosisio, “A Novel Structure of Tightly Coupled Lines forMMIC/MHMIC Couplers and Phase Shifters”, IEEE Trans. Microwave Theory Tech., vol. 45, no. 9, Sept. 1997

[83] G.-H. Ryu, D.-H. Kim, J.-H. Lee, and K.-S. Seo, “A novel 3-dB coupler for MMIC using air-gap stacked microstrip lines,” IEEE Microw. Wireless Compon. Lett., vol. 10, no. 1, pp. 1–3, Jan. 2000.

[84] D. P. Andrews and C. S. Aitchison, “Wide-band lumped-element quadrature 3-dB coupler in microstrip,” IEEE Trans. Microw. Theory Tech., vol. 48, no. 12, pp. 2424–2431, Dec. 2000.

[85] Christophe Caloz, Atsushi Sanada, Tatsuo Itoh, “A Novel Composite Right-/Left-Handed Coupled-Line Directional Coupler With Arbitrary Coupling Level and Broad Bandwidth”, IEEE Trans. Microw. Theory Tech., vol. 52, no. 3, March 2004

[86] Dong-Joo Kim, Yongwoo Jeong, Jung-Hoon Kang, Jong-Hwa Kim, Chul-Soo Kim, Jong-Sik Lim, Dal Ahn, “A Novel Design of High Directivity CPW Directional Coupler Design by Using DGS”, Microwave Symposium Digest, 2005 IEEE MTT-S International, 12-17 June 2005, pp. 4

[87] Zhiyang Liu, Robert M. Weikle, “A Compact Quadrature Coupler Based on Coupled Artificial Transmission Lines”, IEEE Trans. Microw. Theory Tech., vol. 15, no. 12, Dec. 2005

[88] J. Lange, “Interdigitated stripline quadrature hybrid,” IEEE Trans. Microwave Theory Tech., vol. MTT-17, pp. 1150–1151, Dec. 1969.

[89] D. Bourreau, B. Della, E. Daniel, C. Person, S. Toutain, “High-Performance Lange Coupler”, ELECTRONICS LETTERS 8th October 1992 Vol. 28 No. 21, pp. 1997-1998

[90] R. Waugh, D. LaCombe, “Unfolding the Lange Coupler (Short Papers)”, ”, IEEE Trans. Microw. Theory Tech., vol. 20, issue. 11, Nov. 1972

[91] D. I. Stones and D. Chow, "Q- and V- Band Planar Combiners," IEEE MlT-S Int. Microwave Symposium Dig., June 1991, pp. 1049-1052.

[92] J. Benbrahim, H. Kobeissi, and K.Wu, “CAD and electrical performance of new compact power divider suitable for use in M(H)MIC’s,” in IEEE MTT-S Inter. Microwave Symp., Denver, CO, June 1997, pp. 1595–1598.

[93] Lin Li, Ke Wu, “Integrated Planar Spatial Power Combiner”, IEEE Trans. Microwave Theory Tech., vol. 54, no. 4, April 2006

[94] Yukihiro Tahara, Hideyuki Oh-hashi, Moriyasu Miyazaki, Shigeru Makino, “A Broadband Three-Way Tapered-Line Power Divider with Several Strip Resistors”, 2005 European Microwave Conference, 4-6 Oct. 2005, vol. 1, pp. 4

[95] Yukihiro Taharat, Hideyuki Oh-hashit, Araki Ohnot, Moriyasu Miyazakit, Shuji Urasakitt, “A Broadband Asymmetric Tapered-Line Power Divider with Several Strip Resistors”, Microwave Conference, 2004. 34th European, 13 Oct. 2004, vol. 2, pp. 601-604

[96] W. Yau, J. M. Schellenberg, Y. C. Shih, “A New N-Way Broadband Planar Power Combiner/Divider”, Microwave Symposium Digest, MTT-S International, 2 Jun 1986, vol. 86, issue 1, pp. 147- 149

[97] M. J. Page and S. R Judah, “A microstrip planar disk 3-dB quadrature hybrid,” IEEE MTT-S Dig., 1989, pp. 247-250

[98] M. E. Bialkowski and S. T. Jellett, “Analysis and design of a circular disc 3-dB coupler,” IEEE Trans. Microwave Theory Tech., vol. 42, pp. 1437–1442, Aug. 1994.

[99] Tadashi Kawai, Isao Ohta, “Planar-Circuit-Type 3 -dB Quadrature Hybrids”, IEEE Trans. Microw. Theory Tech., vol. 42, no. 12. Dec. 1994

[100] Kin-Lung Chan, Fayez A. Alhargan, Sunil R. Judah, “A Quadrature-Hybrid Design Using a Four-Port Elliptic Patch”, IEEE Trans. Microw. Theory Tech., vol. 45, no. 3, Mar.1997

[101] Faton Tefiku, Eikichi Yamashita, “Improved Analysis Method for Multiport Microstrip Annular-Ring Power-Dividers”, IEEE Trans. Microw. Theory Tech., vol. 42, no. 3, Mar.1994

[102] K. C. Grpta and M. D. Abouzahra, “Analysis and design of four-port and five-port microstrip disc circttits,” IEEE Trans. Microwave Theory Tech., vol. MTT-33, pp. 1422–1427, Dec. 1985

[103] M. D. Abouzahra and K.C. Gupta, "Multiport Power Divider-Combiner Circuits Using Circular-Sector-Shaped Planar Components", IEEE Transactions on Microwave Theory and Techniques Vol. 36, No.12, pp 1747-1751, Dec. 1988

[104] F. A. Abouzahra and K. C. Gupta, “Multi-way unequal power divider circuits using sector-shaped planar components,” in IEEE MTT-S Int. Dig., Jun. 1989, vol. 1, pp. 321–324.

[105] M.D. Abouzahra and K.C. Gupta, Multiport power divider/combiner circuits using circular microstrip disk configurations, IEEE Trans Microwave Theory Tech MTT-35 (1987), 1296-1301.

[106] Sudhabindu Ray, Girish Kumar, “Three-Port Rectangular Microstrip Unequal Power Divider And Coupler”, Microwave And Optical Technology Letters vol. 29, no. 4, May 20 2001
[107] A. G. Bert and D. Kaminsky, “The traveling-wave power divider/combiner”, IEEE MTT-S Inr. Microwave. Symp. Dig., I980, pp. 487-489.
[108] Willems, D.; Bahl, I.; Kruger, B., “A Quazi-Microstrip Travelling-Wave Power Divider/Combiner for use in High-Density Packages,” IEEE Microwave Guided Wave Letters, vol. 3, pp. 148-149, May 1993.
[109] B. Kim, N. Camilleri, H.-D. Shih, H.Q. Tserng, M. Wurtele, “35 GHz GaAs power MESFETs and monolithic amplifiers”, IEEE Trans. Microw. Theory Tech., vol. 37. no. 9, Sept. 1989, pp. 1327-1333
[110] C.W. Cheung, Y.O. Yam, “Travelling-wave power combiner/divider implemented by lumped elements”, ELECTRONICS LETTERS 28th April 1994 Vol. 30 No. 9, pp. 713-715
[111] Z.C. Hao, W. Hong, J.X. Chen, H.X. Zhou, K. Wu, “Single-layer substrate integrated waveguide directional couplers”, IEE Proc.-Microw. Antennas Propag., vol. 153, no. 5, October 2006
[112] Bing Liu, Wei Hong, ZhangCheng Hao, Ke Wu, “Substrate Integrated Waveguide 180-degree Narrowwall Directional Coupler”, Microwave Conference Proceedings, 2005. APMC 2005. Asia-Pacific Conference Proceedings, 4-7 Dec. 2005, vol. 1, pp. 3
[113] Simon Germain, Dominic Deslandes, Ke Wu, “Development of Substrate Integrated Waveguide Power Dividers”, Electrical and Computer Engineering, 2003. IEEE CCECE 2003. 4-7 May 2003, vol.3, pp. 1921- 1924
[114] Jong-Sik Lim, Soon-Young Eom, “A New 3-Way Power Divider with Various Output Power Ratios”, Microwave Symposium Digest, 1996., IEEE MTT-S International, pp. 785-788 vol.2
[115] A. Martin, A. Mortazawi, and B. C. De Loach, Jr., “A power amplifier based on an extended resonance technique,” IEEE Microwave Guided Wave Lett., vol. 5, pp. 329–331, Oct. 1995.
[116] Xin Jiang, Amir Mortazawi, “A broadband power amplifier design based on the extended resonance power combining technique”, Microwave Symposium Digest, 2005 IEEE MTT-S International, 12-17 June 2005, pp. 4
[117] Marco A. Antoniades, George V. Eleftheriades, “A Broadband Series Power Divider Using Zero-Degree Metamaterial Phase-Shifting Lines”, IEEE Microwave And Wireless Components Letters, Vol. 15, No. 11, November 2005
[118] M.-H. Murgulescu, P. Legaud, E. Penard, I. Zaquine, “New small 90° hybrid coupler”, ELECTRONICS LETTERS 4th August 1994 Vol. 30 No. 76, pp. 1289-1290
[119] M.C. Bailey, ” Simple stripline design for uneven power split”, NASA Technical Memorandum, August 1980
[120] A.Ocera, R.Vincenti Gatti, P.Mezzanotte, P.Farinelli, R.Sorrentino, “A MEMS Programmable Power Divider / Combiner for Reconfigurable Antenna Systems”, 2005 European Microwave Conference, 4-6 Oct. 2005, vol. 1 pp. 4
[121] Juan E. Page, ”Power dividers with prescribed amplitude and phase balance”, COMITE Conference on Microwave Technique 2005,
[122] Thomas C. Choinski, “Composite Coupler Design”, IEEE Trans. Microw. Theory Tech., vol. MTT-32, NO. 6, June 1984
[123] Tuya Wuren, Keiiti Taniya, Iwata Sakagami, Minoru Tahara, “Miniaturization of 3- and 5- way Bagley Polygon power dividers”, APMC2005 Proceedings
[124] Nakatsugawa, M. Nishikawa, K., “A novel configuration for 1:N multiport power dividers using series/parallel transmission-line division and apolyimide/alumina-ceramic structure for HPA module implementation”, IEEE Trans. Microwave Theory Tech., Vol.: 49, Issue: 6, Part 2
[125] Arie Shor, “Broadbandings techniques for TEM N-way power dividers”, Microwave Symposium Digest, 1988 IEEE MTT-S International
[126] Qingxin Guo,Yanjun Ma and Jilong Ju, “A Novel Broadband High-Power Combiner”, APMC 2005 Proceedings

[127] L.Wu and Z. Sun, H. Yilmaz, M. Berroth, “A dual-frequency Wilkinson power divider,” IEEE Trans. Microw. Theory Tech., vol. 54, no. 1, pp. 278–284, Jan. 2006.
[128] Mitchai Chongcheawchamnan, Sumongkol Patisang, Monai Krairiksh, Ian D. Robertson, “Tri-Band Wilkinson Power Divider Using a Three-Section Transmission-Line Transformer”, IEEE Trans. Microw. Theory Tech., vol. 16, no. 8, pp. 452-454, Aug. 2006
[129] Khelifa Hettak, Gilbert A. Morin, Malcolm G. Stubbs, “Compact MMIC CPW and Asymmetric CPS Branch-Line Couplers and Wilkinson Dividers Using Shunt and Series Stub Loading”, IEEE Trans. Microw. Theory Tech., vol. 53, no. 5, May 2005
[130] Kam Mam Shum, Quan Xue, Wing Nam Chau, Chi Hou Chan, “A Compact Wilkinson Power Divider With Curved Pbg Cells”, MICROWAVE AND OPTICAL TECHNOLOGY LETTERS / Vol. 31, No. 2, October 20 2001
[131] Young-Soon Lee, Ikmo Park, Chull-Chai Shin, “A miniaturized Wilkinson power divider”, Precedings of APMC2001, Taipei, Taiwan
[132] Yi Sun, A. P. Freundorfer, “Broadband Folded Wilkinson Power Combiner/Splitter”, IEEE Trans. Microw. Theory Tech., vol. 14, no. 6, June 2004
[133] K. Nishikawa, T. Tokumitsu, and I. Toyoda, “Miniaturized Wilkinson power divider using three-dimensional MMIC technology,” IEEE Microwave and Guided Wave Letters, vol. 6, pp, 372-374, Oct. 1996.
[134] Kenjiro Nishikawa, Associate Member, Tsuneo Tokumitsu, Member, Ichihiko Toyoda, Liang-Hung Lu, Yu-Te Liao, Chung-Ru Wu, “A Miniaturized Wilkinson Power Divider With CMOS Active Inductors”, IEEE Microwave And Wireless Components Letters, vol. 15, no. 11, Nov. 2005
[135] Ali Darwish, Amin Ezzeddine, Ho C. Huang, K. Bumman, L. Joonyoul, Y. Sungwhan, M. Mah, J. Cook, “Vertical Balun and Wilkinson Divider”, Microwave Symposium Digest, 2002 IEEE MTT-S International
[136] David Maurin, Ke Wu, “A compact 1.7-2.1 GHz tree-way power combiner using microstrip technology with better than 93.8% combining efficiency”, IEEE Microwave and guided wave letters, vol. 6, no. 2, Feb. 1996
[137] Paul Eyring, ”New High-Power Wilkinson Power Divider Design Utilizing An Aluminium Nitride Substrate And An Optimally Chosen Isolation Resistors”, Antenna and Propagation Society International Symposium, 1991 AP-S. Digest
[138] D. Antsos, R. Crist, and L. Sukamto, “A novel Wilkinson power divider with predictable performance at K- and Ka-band,” in IEEE MTT-S Int. Microwave Symp. Dig., 1994, pp. 907–910.
[139] Jong-Sik Lim, Sung-Won Lee, Chul-Soo Kim, Jun-Seok Park, Dal Ahn, and Sangwook Nam, “A 4 : 1 Unequal Wilkinson Power Divider”, IEEE Microwave And Wireless Components Letters, vol. 11, no. 3, March 2001
[140] Young-Joon Ko, Jae-Yeong Park, Jong-Uk Bu, “Fully Integrated Unequal Wilkinson Power Divider With EBG CPW”, IEEE Microwave And Wireless Components Letters, vol. 13, no. 7, July 2003
[141] S. Avrillon, A. Chousseaud, and S. Toutain, “Dividing and filtering function integration for the development of a band-pass filtering power amplifier,” in IEEE MTT-S Int. Dig., Jun. 2–7, 2002, vol. 2, pp. 1173–1176.
[142] S. Avrillon, I. Pele, A. Chousseaud, and S. Toutain, “Dual-band power divider based on semiloop stepped-impedance resonators,” IEEE Trans. Microw. Theory Tech., vol. 51, no. 4, pp. 1269–1273, Apr. 2003.
[143] D. Woo, T. Lee, “Suppression of Harmonics in Wilkinson Power Divider by using Asymmetric Spiral DGS,” European Microwave Conference Proc., pp. 467-470, 2004.
[144] Kun-Hui Yi, Bongkoo Kang, “Modified Wilkinson Power Divider for nth Harmonic Suppression” IEEE Microwave And Wireless Components Letters, vol. 13, no. 5, May 2003

[145] H.-R. Ahn, I. Wolff, “Arbitrary power division branch-line hybrid terminated by arbitrary impedances”, ELECTRONICS LETTERS 1st April 1999 Vol. 35 No. 7
[146] R. Levy and L. Lind, “Synthesis of symmetrical branch-guide directional couplers,” IEEE Trans. Microwave Theory Tech., vol. MTT-16, pp. 80-89,Feb. 1968.
[147] R. Levy, “ Zolotarev branch-guide couplers,” IEEE Trans. Microwave Theory Tech., vol. MTT-21, pp. 95-99, Feb. 1973.
[148] R. Levy and J. Helszajn, “Specific equations for one and two section quarter-wave matching networks for stub-resistor loads”, IEEE Trans. Microwave Theory Tech., vol. MTT-30, pp. 55–62, Jan. 1982.
[149] M. Muraguchi, T. Yukitake, and Y. Naito, “Optimum design of 3-dB branch-line couplers using microstrip lines,” IEEE Trans. Microwave Theory Tech., vol. MTT-31, pp. 674–678, Aug. 1983.
[150] I. H. Lin, C. Caloz, and T. Itoh, “A branch-line coupler with two arbitrary operating frequencies using left-handed transmission lines,” in IEEE MTT-S Dig., vol. 1, June 2003, pp. 325–328.
[151] X. Q. Lin, R. P. Liu, X. M. Yang, J. X. Chen, X. X. Yin, Q. Cheng, T. J. Cui, “Arbitrarily Dual-Band Components Using Simplified Structures of Conventional CRLH TLs”, IEEE Trans. Microw. Theory Tech., vol. 54, no. 7, pp. 2902-2909, July 2006.
[152] F. L.Wong and K. K. M. Cheng, “A novel planar branch-line coupler design for dual-band applications,” in IEEE MTT-S Int. Microwave Symp. Dig., June 2004, pp. 903–906.
[153] K. K. M. Cheng and F. L. Wong, “A novel approach to the design and implementation of dual-band compact planar 90 branch line coupler,”IEEE Trans. Microw. Theory Tech., vol. 52, no. 11, pp. 2458–2462, Nov. 2004.
[154] C. Collado, A. Grau, and F. D. Flaviis, “A dual-band planar quadrature hybrid with enhanced bandwidth,” Microwave Theory and Techniques, IEEE Transactions on, 2004, submitted.
[155] Myun-Joo Park, Byungje Lee, “Dual-Band, Cross Coupled Branch Line Coupler”, IEEE Microwave And Wireless Components Letters, vol. 15, no. 10, pp. 655-657, Oct. 2005
[156] J. Gu and X. Sun, “Miniaturization and harmonic suppression of branch-line and rat-race hybrid coupler using compensating spiral compact microstrip resonant cell,” in IEEE MTT-S Int. Microw. Symp. Dig., Jun. 2005, pp. 1211–1214.
[157] K. W. Eccleston and S. H. M. Ong, “Compact planar microstripline branch-line and rat-race coupler,” IEEE Trans. Microwave Theory Tech., vol. 51, pp. 2119–2125, Oct. 2003.
[158] R. T. Chen, E. R. Brown, R. S. Singh, “A Compact 30 GHz Low Loss Balanced Hybrid Coupler Fabricated Using Micromachined Integrated Coax”, Radio and Wireless Conference, 2004 IEEE
[159] H. Ghali, and T. A. Moselhy, “Miniaturized Fractal Rat-Race, Branch-Line, and Coupled-Line Hybrids,” IEEE Trans. Microwave Theory Tech., vol. 52, pp. 2513–2520, Nov. 2004.
[160] C. Toker, M. Saglam, M. Ozme, and N. Gunalp, “Branch-Line Couplers Using Unequal Line Lengths,” IEEE Trans. Microwave Theory Tech., Vol. 49, No.4, pp.718-721, Apr. 2001.
[161] Islam, R., and Eleftheriades, G.V.: ‘Phase-agile branch-line couplers using metamaterial lines’, IEEE Microw. Wirel. Compon. Lett., 2004, 14, (7), pp. 340–342
[162] P. Meaney, “A novel branch-line coupler design for millimeter-wave applications,” in IEEE MTT-S Int. Microwave Symp. Dig., vol. 1, May 1990, pp. 585–588.
[163] S. March, “A wideband stripline hybrid ring,” IEEE Trans. Microwave Theory Tech., vol. MTT-16, p. 361, 1968.
[164] S. J. Parisi, “180 lumped element hybrid,” in IEEE MTT-S Int. Dig.,1989, pp. 1243–1246.
[165] Settaluri, R.K., Sundberg, G., Weisshaar, A., and Tripathi, V.K.: ‘Compact folded line rat-race hybrid couplers’, IEEE Microw. Guid. Wave Lett., 2000, 10, (2), pp. 61–63
[166] Xue, Q., Shum, K.M., and Chan, C.H.: ‘A novel microstrip ring hybrid incorporating a PBG cell’, IEEE Microw. Wirel. Compon. Lett., 2001, 11, (6), pp. 258–260
[167] H. OKAZAKI, T. HIROTA, “Multilayer MMIC broad-side coupler with a symmetric structure”, IEEE Microw. Guid. Wave Lett., 1997, MGWL-7, (6), pp. 145-146

[168] M. Kumar et al., “Monolithic GaAs interdigitated 90° hybrids with 50 and 25 ohm impedances”, IEEE Int Microwave and Millimeter Wave Monolithic Circuits Symp Dig 1982, pp. 50-53.
[169] Inder J. Bahl, “Six-Finger Lange Coupler On 3 Mil GaAs Substrate Using Multilayer Mmic Technology”, MICROWAVE AND OPTICAL TECHNOLOGY LETTERS / Vol. 30, No. 5, September 5 2001, pp. 322-327.
[170] S.V. Drusin, IN. Saliy, “Dissipative canonical nonuniform transmission lines as basic components of power dividers with distributed isolation impedance”, Electronics and Radiophysics of Ultra-High Frequencies, 1999 International University Conference
[171] ZhangCheng Hao, Wei HongMember, Hao Li, Hua Zhang, Ke Wu, “Multiway Broadband Substrate Integrated Waveguide (SIW) Power Divider”, Antennas and Propagation Society International Symposium, 2005 IEEE
[172] X. Xu, R. G. Bosisio, and K.Wu, “A new six-port junction based on substrate integrated waveguide technology,” IEEE Trans. Microw. Theory Tech., vol. 53, no. 7, pp. 2267–2273, Jul. 2004.
[173] K. Song, Y. Fan and Y. Zhang, “Radial cavity power divider based on substrate integrated waveguide technology”, Electronics Letters, Sept. 2006, vol. 42, issue 19, pp. 1100- 1101
[174] Jong-Sik Lim, Soon-Young Eom, Jae-Hee Han, Seong-Hun Kim, Deok-Hee Lee, Sangwook Nam, “A new balanced amplifier using 6-port power divider”, Microwave Symposium Digest, 2001 IEEE MTT-S International

Appendix 2 NYQUIST CRITERIA FOR THE MICROWAVE STABILITY

As it was previously pointed in the paragraph 1.1.5, by investigating the roots of the circuit determinant it is likely to determine the stability of the circuit. Sadly, it is a complicated and laborious process. What is more, the analysis does not give clear guidelines as how to correct the system to make it stable. Such was a motivation of Nyquist in search for more efficient way to analyze the stability of the circuits. His analysis focused on the closed loop systems, therefore a simple feedback amplifier will be introduced as a base for his theory.

A2.1 Nyquist criteria

For a circuit in the Figure 176 there is defined an amplifier characterized with ratio A, independent from the frequency finite amplifying along with the feedback network characterized by the ratio *J(jω)*, independent from the gain of the amplifier.

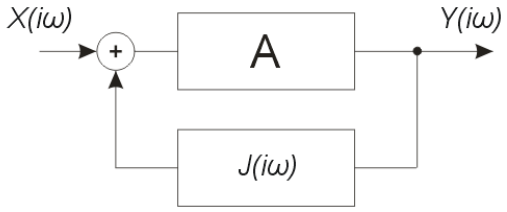

Figure 176 Amplifier with single feedback loop.

Then, the closed loop transfer function is as follows:

$$H(i\omega)=\frac{X(i\omega)}{Y(i\omega)}=\frac{A}{1\text{-}AJ(i\omega)} \tag{144.}$$

Before Nyquist published his work a typical stability analysis was based on the roots of the characteristic equation. Nyquist took a different starting point, by investigating the frequency domain criteria for the stability [18]. He introduced quantity *AJ(jω)*, today called Open Loop Transfer Function. He described it in these words: "Let the complex quantity *AJ(jω)* represent the ratio by which the amplifier and feedback circuit modify the current in one round trip". To assume that oscillations could be maintained at ω_0 while $AJ(j\,\omega_0)=1$ is intuitively reasonable. The same way it can be expected, that the system will be stable when $|AJ(i\omega)|<1$ and $|A|<\infty$. Nyquist shows that the stability criteria could be developed by analyzing the graph of the function *AJ(jω)* and the encirclements of the critical point. A placement of the critical point of the amplifier is (1,*i*0) on the complex plane, which is evident in a light of the previous observations and inspection of the equation (144.). The rule of the stability given by Nyquist says: "Plot plus and minus imaginary part of $AJ(i\omega_0)$ against the real part for all frequencies from 0 to ∞. If the point (1,i0) lies completely outside this

curve the system is stable; if not it is unstable."The original analysis was fairly complicated [18], however, it was later shown that the result can be easily obtained from a theorem of Cauchy, *Argument Principle* of the complex analysis. Which states that if Z is the number of zeros and P is the number of poles in the region D of the function *f(s),* than:

$$N = Z - P = \frac{1}{2\pi i}\int_D \frac{f'(s)}{f(s)} ds = \frac{1}{2\pi}\Delta_R \arg f(s)$$

(145.)

Theorem were graphically explained in the Figure 177- in the area D of the *s-plane* there are two zeros and four poles of the function *f(s)*. If the contour of that area is mapped through function *f(s)* it will encircle origin on *f(s)-plane* N times in the same direction as the original contour. *N=Z-P=*-2 meant for this example, results in turn in two encirclements in opposite direction.

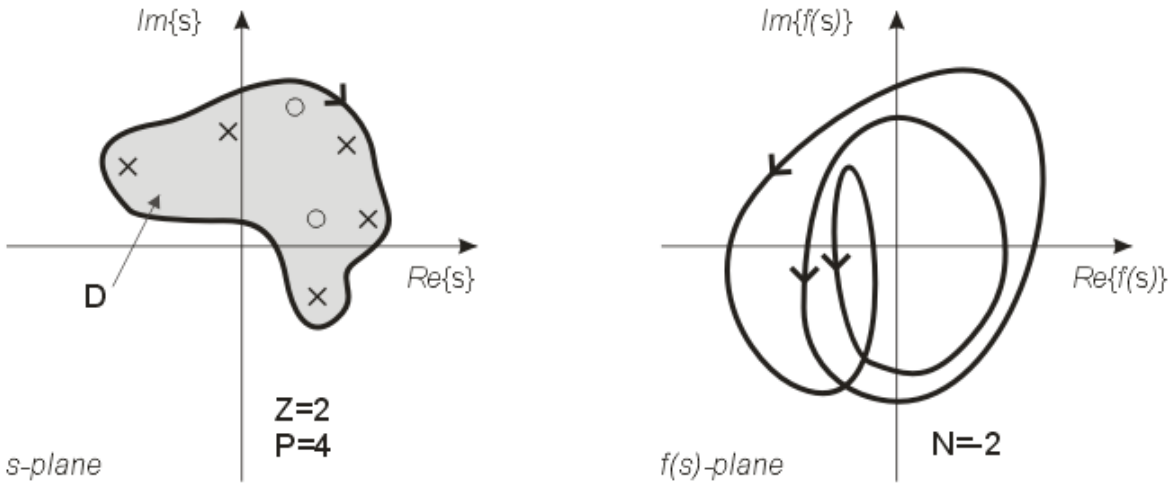

Figure 177 Graphical explanation of Cauchy's Argument Principle.

Let us remind that any Laplace domain transfer function can be expressed as the ratio of the two polynomials:

$$T(s) = \frac{N(s)}{D(s)}$$

(146.)

Than zeros of the T(s) are the roots of the N(s)=0 and poles of the T(s) are the roots of the D(s)=0. At the beginning, the stable system will be defined, as one without poles of T(s) in the right half of the complex plane. As a result, the Open Loop Transfer Function may be defined as:

$$F(s) = \frac{N_{OL}(s)}{D_{OL}(s)}$$

(147.)

After closing it can be observed that the poles of characteristic equation are zeros of the 1-F(s) which in fact means they are roots of the $D_{OL}(s)$-$N_{OL}(s)$=0.

To use Cauchy Argument of the principle for the Right Half of Complex Plane, zeros and poles check a contour that encircles that area is required. It will be referred as the Nyquist Contour. It composes of the path travelling up the $i\omega$ from (0,-$i\infty$) to (0,$i\infty$), and semicircular arc with radius r→∞ that starts (0,$i\infty$) and travels clockwise to (0,-$i\infty$) - Figure 178.
The Nyquist Contour mapped through the open loop-transfer function F(s) yields the Nyquist plot for F(s). According to the Argument Principle, the number of clock-wise encirclements of the origin must be the number of zeros of F(s) in the right-half complex plane minus the poles of F(s) in the right-half complex plane. If the contour's encirclements of the (1,i0) point will be considered instead of the origin, the difference between the number of poles and zeros in the right-half complex plane of 1 - F(s) will be found. Recalling that the zeros of the 1 - F(s) are the poles of the close-loop system, and noting that the poles of 1 - F(s) are same as the poles of F(s),The Nyquist Criterion is stated:
For Nyquist Contour Γ_s, P is the number of the poles of F(s) encircled by Γ_s, and Z is the number of zeros of 1-F(s) encircled by Γ_s - therefore the number of poles of T(s). The resultant contour in the F(s)-plane, $\Gamma_{F(s)}$ shall encircle (clock-wise) the point (1 + i0) N times, so that $N = Z - P$.
For stability of the system, Z = 0, ie. the number of closed loop poles in the right half of s-plane must be zero. Hence, the number of anticlockwise encirclements about (1 + i0) must be equal to P, the number of the open loop poles in the right half plane [175].

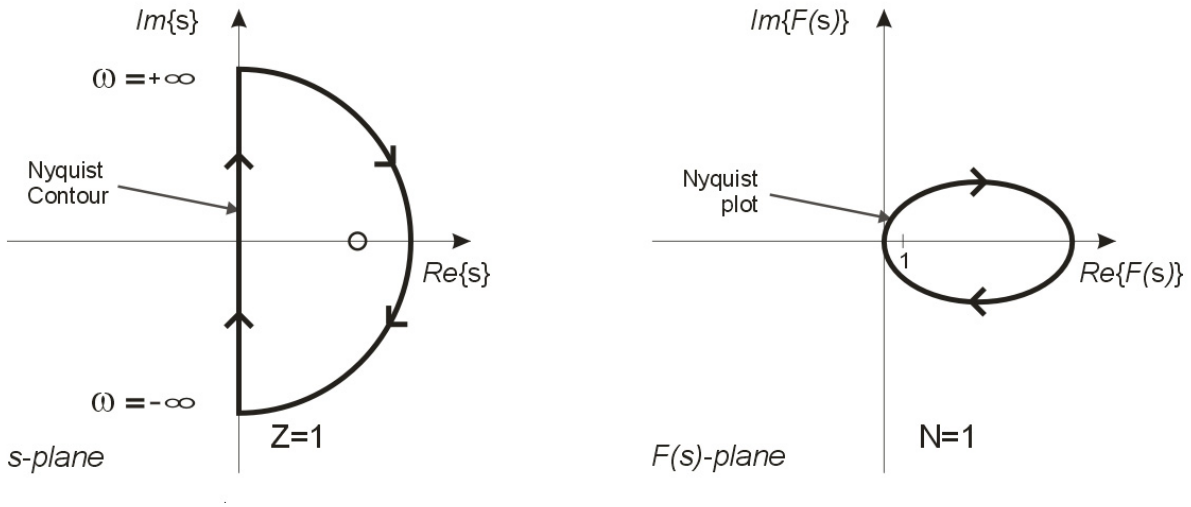

Figure 178 Nyquist Contour on s-plane and resulting Nyquist plot on H(s)-plane (example).

This theorem allows us to check the numbers of the Right Half Complex Plane zeros quickly as to avoid an analytic analysis of the open loop function or the poles of the determinant of the closed loop transfer function. It is a lot more convenient, as in a simple test it checks the existence of the poles rather than the computation of their values. Inspection of the locus of the open loop transfer function is to a great extent less laborious in examples other than the basic ones.

6.1.1 Nyquist criteria as a stability test- example

Firstly, the criteria will be demonstrated by the means of an undemanding example. Although easy examples are not the kind that would force Nyquist to search a new method, they certainly are an opportunity to test and validate the idea practically. The circuit in the Figure 179 a) can by simplified with a block representation as it was shown in Figure 179 b). If the loop is broken in a position

indicated by the cross, Open Loop Transfer Function H_{OLTF} can be computed - (148.). The Nyquist plot was computed and presented in the Figure 180.

$$H_{OLTF}(s) = F(s) = \frac{V_{2`}}{V_1} = A \cdot \frac{1}{s \cdot C \cdot R + 1} = \frac{A}{R \cdot C \cdot \left(s + \frac{1}{R \cdot C} \right)} \tag{148.}$$

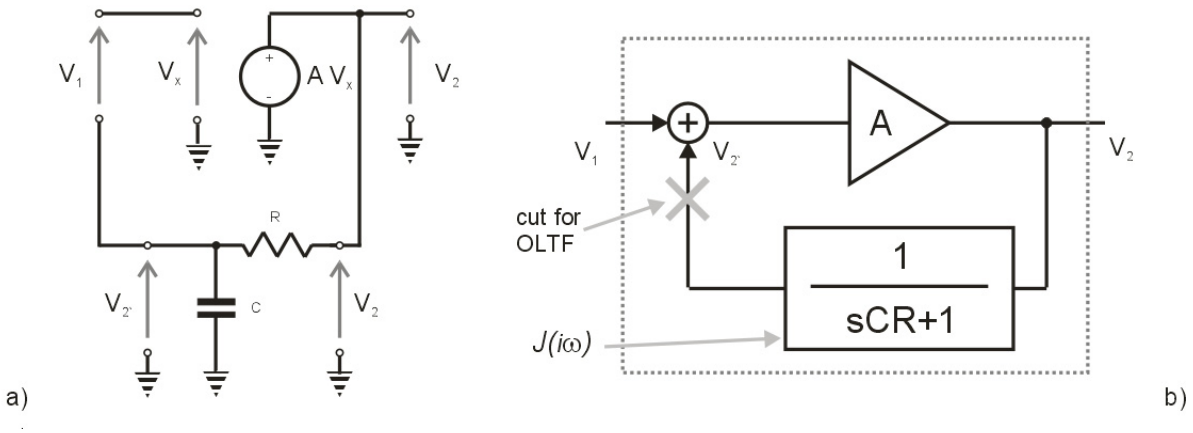

Figure 179 Example of the feedback system analyzed through Nyquist theorem.

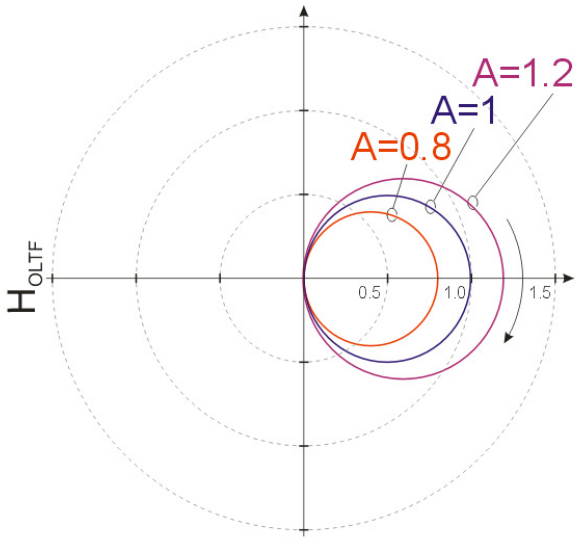

Figure 180 Nyquist plot of example H_{OLTF}.

Without a doubt, with A>1 the Nyquist plot encircles the critical point indicating instability. If the closed loop transfer function is computed and examined (149.) ,it is clear that Nyquist theorem results are in agreement. Sign of the pole of the transfer function depends on the (1-A) term value. If A=1, than the pole is in origin, if A>1 it moves to Right Half of the Complex Plane.

$$H(s)=\frac{V_2}{V_1}=\frac{A}{1-A\cdot J(s)}=\frac{A}{1-\dfrac{A}{R\cdot C\cdot\left(s+\dfrac{1}{R\cdot C}\right)}}=\frac{A\cdot\left(s+\dfrac{1}{R\cdot C}\right)}{s+\dfrac{1-A}{R\cdot C}}$$

(149.)

If the inverse Laplace transform transfers function to the Time Domain impulse there is obtained the response:

$$H(t)=L^{-1}\{H(s)\}=A\cdot\delta(t)+\frac{A^2}{R\cdot C}e^{-\left(\frac{1-A}{R\cdot C}\right)\cdot t}\ \text{for t}\geq 0$$, where δ(t) is Dirac function.

(150.)

As a result, two elements in the response of the system (150.) can be found. The first is responsible for the steady state response and the second is a term of the transient response. If the pole of system will be placed in the Right Half of Complex Plane this term will rise with time to infinity and clearly, the system will be unstable.

A2.2 Nyquist criterion in the microwave circuits.

In the scope of the field of this research arises the question: How to apply the Nyquist criteria in the stability analysis of the microwave circuits? Let us consider a plain example of the two one port devices connected together in a manner shown in a graph form in the Figure 181 a).

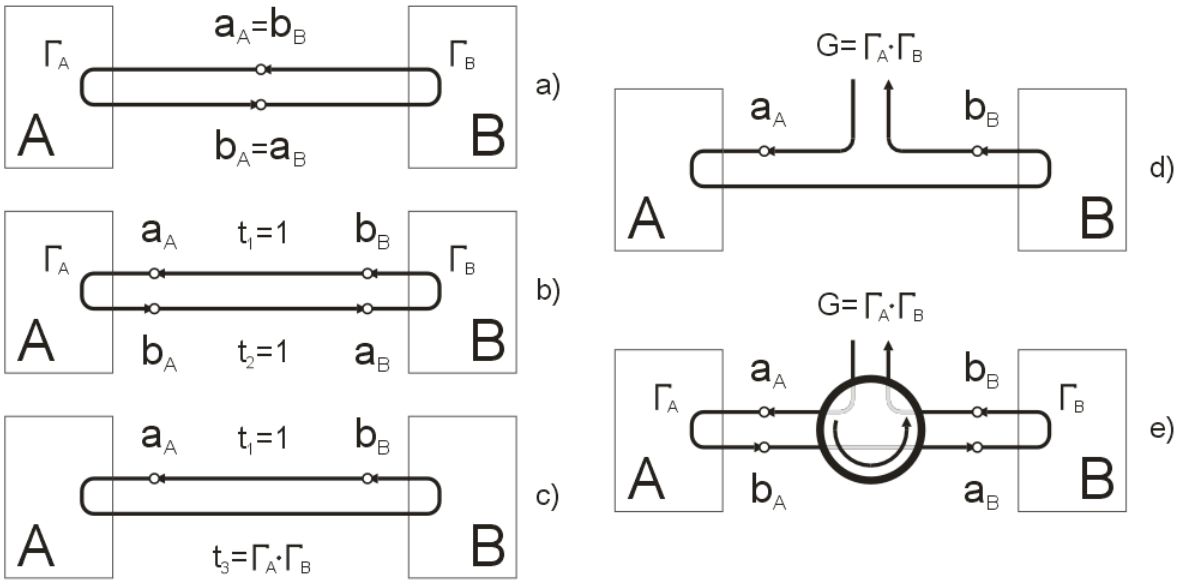

Figure 181 Implementation of Nyquist criterion in microwave circuit stability analysis.

Each device is characterized with the reflection coefficient, accordingly: Γ_A and Γ_B. They are connected directly, so it can be noticed that $a_A= b_B$ and $b_A= a_B$. If the graph nodes will be separated, paths t_1 and t_2 are inserted - Figure 181 b). While a relation between the voltage waves a_A and b_B is of the interest,

the graph can be modified to the form presented in the Figure 181 c). Clearly, it is a system with a feedback loop. If a_A will be treated as a signal source, than the system can be descried through the Open Loop Transfer Function G(s) as:

$$H(s)=\frac{b_B(s)}{a_A(s)}=\frac{G(s)}{1\text{-}G(s)} \tag{151.}$$

Where *G*(s) -, describes modifications to the voltage wave, introduced by the forward and the feedback path in one round trip (Figure 181 d):

$$G(s)=t_1\cdot t_3(s)=\Gamma_A(s)\cdot\Gamma_B(s) \tag{152.}$$

Path t_1 was broken to measure G(s). To enable this operation in the microwave circuits a nonreciprocal device like the circulator - Figure 181 e) may be used. It is possible than to implement measurement of *G*(s) in any CAD or in the real measurement environment. Having knowledge of the Open Loop Transfer Function, an advantage of the Nyquist criterion is taken in order to check the stability of the network. An important issue is to remember that analysis of the locus of the Nyquist Plot informs about the difference between the number of zeros and poles in Right Half of Complex Plane region. Therefore, to be certain about the test results and the stability of the circuit none of the bisections can possess Right Half Complex Planes poles.

Nyquist criteria applied this way is very useful in order to check the circuits stability. In [176], Jackson shows that this method is more convenient than the criterion of the onset of oscillation defined as:

$$|\Gamma_A||\Gamma_B|>0 \text{ and } \Phi_A+\Phi_B=0 \tag{153.}$$

(153.) may lead to false conclusions sometimes. Jackson's examples are quoted below:

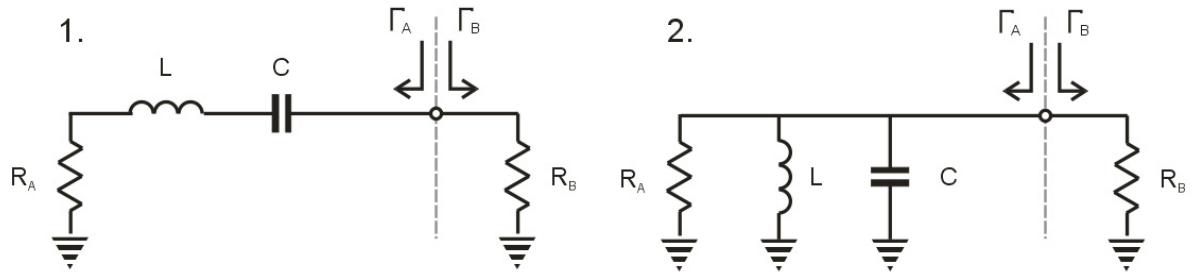

Figure 182 Circuit tested by the Nyquist criterion of stability.

The two circuits with additional numbering are shown in the Figure 182: 1,2. In each case R_A=60Ω and R_B=-70Ω and the circuit is divided between passive –A, and active –B. The Open Loop Transfer Functions versus frequency for both of them are than plotted at the polar plot - Figure 183.

Critical point of the system is (1,j*0). Each locus circulates in a clockwise direction. It is traceable that only G_1(s) encircles the critical point, what denotes instability of the circuit no. 1.

The results of Nyquist's analysis are in contrast to the criterion stated previously (153.) which indicated stability of the both circuits in resonance, as $|\Gamma_A|*|\Gamma_B|$= 0,091*6=0,545. This value is easily

observable in the Figure 183, as a point shared for G_1 and G_2. However, on this very assumption in relation to this point the circles lay on the opposite parts of the plot and G_1 encircles (1,j*0).
Nyquist criteria is a very important tool and its usefulness is not limited only to simple cases but could be useful in analysis of more complicated circuits. Special concern should be given to ensure there are no right poles present in the tested Open Loop Transfer Function as they may lead to some false conclusions.

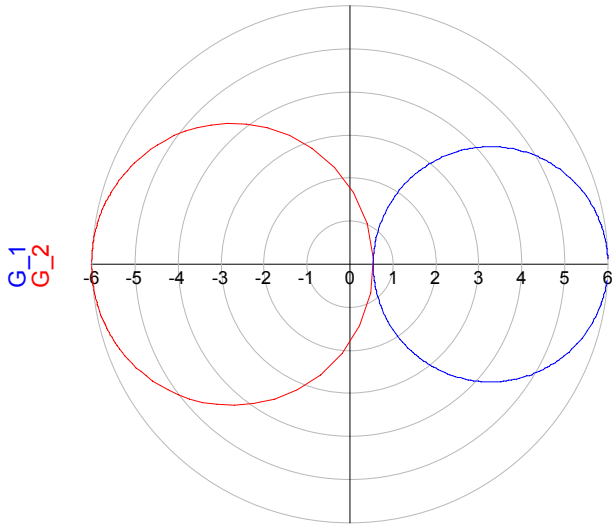

Figure 183 Polar plot of the Open Loop Transfer Functions of the examples used in Nyquist criteria for the stability test.

A2.3 References

[175] http://en.wikipedia.org - Nyquist stability criterion.
[176] R. W. Jackson, “Criteria for the Onset of Oscillation In Microwave Circuits”, IEEE Trans. Microwave Theory Tech., vol. 40, no. 3, pp. 566-568, Mar. 1992.